جمهورية العراق
وزارة التعليم العالي
والبحث العلمي
جامعة بابل
كلية الهندسة
قسم الهندسة المدنية

السلوك الإنشائي للأعمدة الخرسانية المسلحة ذات القلب المجوف و المحصورة بالملاط المقوى بالنسيج البوليمر (TRM) و / أو السترات المقوى بالألياف (FRP)

أطروحة
مقدمه لكلية الهندسة جامعة بابل
في استيفاء جزئي لمتطلبات الدرجة
دكتوراه الفلسفة في الهندسة المدنية
(الانشاءات)

وليد خليل نايل

(بكلوريوس هندسه مدني 2005)

(ماجستير هندسه انشاءات 2017)

المشرف

الاستاذ المساعد الدكتور محمد جواد كاظم

2022

Abstract

As a result of their low ductility, insufficient shear or flexural strength, and inadequate reinforcing anchorage, columns built to obsolete design codes may sustain catastrophic damage during seismic events. There are a number of factors that can affect the hollow column's overall performance, including its shape and cross-section thickness, the quantity of longitudinal and transverse reinforcing, and the axial load. Square hollow parts are the focus of this study. The specimen had a dimension (150 x 150 x 900) mm with an internal hole of (50 x 50 x 600) mm. Main reinforcement bars of 8 mm in diameter and 6 mm for stirrups. It investigates the behavior of columns under a state of compression with a concentric and eccentric load. The experiments are conducted to examine the behavior of a hollow column using carbon fibre polymer (CFRP) or textile reinforced mortar (TRM) composite materials to improve cross-section performance in terms of ductility and flexural strength. Thirty-two hollow concrete columns were tested, divided into specimens without strengthening (control specimens) composed of eight specimens, and the remaining specimens (24 specimens) are strengthening externally by CFRP or TRM was employed. The strengthening by CFRP consist of five specimens with concentric loading. The same as for the TRM, also study the behavior of strengthened specimens by CFRP or TRM under eccentric loading.

This study has two parts: the first part focuses on the structural performance of square hollow columns, while the second part examines FRP-strengthened hollow columns under similar loading conditions and investigates the resulting changes in failure mode and ductility. In this study, experimental results compare advances in axial strength and ductility. The columns' ability to withstand axial loads has increased.

For the specimens with concentric loading, the maximum load reached (749.2) kN for the specimen have (one vertical) CFRP laminate on each column side and (2X-shape) of CFRP at the top and bottom, with an increase of about (22.8) % compared with the control specimen under concentric load (CC-CO-H) (610) kN. The maximum ductility is equal to the (1.9) of the specimen having the (one vertical) CFRP laminate on each column side. For the specimens under eccentric loading, the maximum. Load reached (94.8) kN for the specimen confining by (one vertical) laminate at the tension side and (three) hoop laminate, one at the middle height of the column and another two top and bottom, with an increase of about (39.4) % compared with the control specimen under eccentric load (CC-ECC-H) of (68.03) kN. In addition, the maximum ductility value obtained from the case confining by the X-configuration at two areas, one at the top and one at the bottom, is (5.4). For specimen has side openings, when the specimens are subjected to concentric loading, the load decreases by about (-9) % for specimens with the circular side opening. For specimens with square side openings, the decreasing percentage increased to (29.5) %. These decreased in compression load compared with the control specimen (CC-CO-H). The max ductility equals (1.5) when the specimen has a circular opening. Moreover, for the specimen with circular side openings and strengthened by (one vertical) CFRP laminate on each column side and (2X-shape) of CFRP at the top and bottom, this specimen failed at the compression load reached (660) kN, an increase of approximately (18.9) % over the control specimen. Furthermore, for the specimen has square side openings at the top and bottom, also strengthened by (one vertical) CFRP laminate on each column side and (2X-shape) of CFRP at the top and bottom, the maximum load capacity is equal to the (560.3) kN with an additional capacity of 30.3% compared with the control specimen. The circular side opening increases the ductility by a value of about (2.1). For the specimen with circular side opening and under eccentric loading, the max. load capacity reached the value of 65.8 kN. The specimen has a square side opening, the maximum. load capacity equals to

the (64.8) kN. The maximum ductility equal to (2.5). For the specimen with a circular side opening and strengthened by (one vertical) laminate at the tension side and (three) hoop laminate, one at the middle height of the column and another two top and bottom, and under eccentric loading, the maximum, load capacity reached the value of (80.1) kN, and for the specimen with a square side opening with the same configuration of strengthened, the load was equal to (75.38) kN. The increase in load capacity obtained from the case has the circular side openings is equal to the (21.73%) compared with control specimen, and the increase is equal to the (16.32%) % with the specimen for the specimen has the square side openings**.** and also for the case has the circular side opening and strengthening by CFRP, the maximum value for strain in concrete via the SGC is obtained from SGC1 = 0.0085, where the SGC1 located in the compression face near the circular opening at the top. the experimental work was simulated in the ABAQUS software and had a good result.

الخلاصه

نتيجة لقابليتها المنخفضـــة ، وقوة القص أو الانثناء غير الكافية ، وعدم كفاية التثبيت المقوى ، قد تتعرض الأعمدة المصـــممة لمدونات التصـــميم المتقادمة لأضـــرار كارثية أثناء الأحداث الزلزالية. هناك عدد من العوامل التي يمكن أن تؤثر على الأداء العام للعمود المجوف ، بما في ذلك شكله وسمك المقطع العرضي ، وكمية التعزيز الطولي والعرضـــي ، ونسـبة الحمل المحوري. الأجزاء المجوفة المربعة هي محور هذه الدراسة. كان للعينة أبعاد (150 × 150 × 900) مم مع ثقب داخلي و (50 × 50 × 600) ملم. قضبان التسليح الرئيسية بقطر 8 مم و 6 مم للافقيه . حيث يبحث في سلوك الأعمدة تحت حالة ضـغط مع حمولة متحدة المركز وغريبة الأطوار. أجريت التجارب لفحص سـلوك العمود المجوف باسـتخدام بوليمر ألياف الكربون (CFRP) أو مواد مركبة من الملاط المقوى بالنسـيج (TRM) لتحسـين أداء المقطع العرضـي من حيث المطيليه وقوة الانثناء. تم اختبار 32 عمودًا خرســـانيًا مجوفًا ، وتم تقســـيمها إلى عينات بدون تقوية (عينات تحكم) تتكون من ثماني عينات ، والعينات المتبقية (24 عينة) للتقوية ، حيث تم اســـتخدام التعزيز الخارجي عبر CFRP أو .TRM يحتوي التعزيز بواســـطة CFRP على خمس عينات ذات تحميل متحد المركز ، ومثلما هو الحال بالنسبة لـ TRM ، أيضًا بدراسة سلوك العينات المعززة بواسطة CFRPأو TRM تحت تحميل غريب الأطوار.

تتكون هذه الدراســـة من جزأين: الجزء الأول يركز على الأداء للأعمدة المجوفة المربعة ، بينما يفحص الجزء الثاني الأعمدة المجوفة المعززة بـ FRP في ظل ظروف تحميل مماثلة ويفحص التغييرات الناتجة في نمط الفشـــل والمطيليه. في هذه الدراســـة ، تم اســـتخدام النتائج التجريبية لمقارنة التطورات في القوة المحورية والمطيليه. حيث زادت قدرة الأعمدة على تحمل الأحمال المحورية.

-بالنســـبة للعينات ذات التحميل المتحد المركز ، يكون اكبرحمل بلغ (749.2) كيلو نيوتن للعينة تحتوي على (صـفائح CFRP رأسـية واحدة) على كل جانب من العمود و CFRP 2(X) في الأعلى والأسـفل. بزيادة قدرها حوالي (22.8)٪ مقارنة بعينة التحكم .KN (610) (CC-CO-H) أقصـــى ليونة تســـاوي (1.9) للعينة التي تحتوي على صفائح (CFRP رأسية واحدة) على كل جانب من جوانب العمود. بالنسبة للعينات تحت تحميل غريب الأطوار ، يكون الحد الأقصـــى. وصـــل الحمل إلى (94.8) كيلو نيوتن للعينة المحصورة بواسطة صفائح (رأسية واحدة) في جانب الشد و (ثلاثة) صفائح دائرية ، أحدهما في منتصف ارتفاع العمود والآخران أعلى وأسفل.

بزيادة قدرها حوالي (39.4)٪ مقارنة بعينة التحكم (CC-ECC-H) البالغة (68.03) كيلو نيوتن. وفيما يتعلق بالليونة ، فإن القيمة القصوى للمطيليه التي تم الحصول عليها من العينه المحصورة بالتكوين X في منطقتين ، واحدة في الأعلى والأخرى في الأسفل هي.(5.4)

بالنسبة للعينة التي تحتوي على فتحات جانبية ، عندما تخضع العينات لتحميل متحد المركز ، ينخفض الحمل بنحو (9) ٪ للعينات ذات الفتحة الجانبية الدائرية. بالنسبة للعينات ذات الفتحات الجانبية المربعة ، زادت نسبة التناقص إلى (29.5)٪. انخفضت هذه في حمل الضغط مقارنة بعينة التحكم .(CC-CO-H) أقصى مطيليه تساوي (1.5) عندما يكون للعينة فتحة دائرية. وبالنسبة للعينة ذات الفتحات الجانبية الدائرية والمدعومة (عموديًا واحدًا) بصفائح CFRP على كل جانب عمود و-2X) شكل (من CFRP في أعلى وأسفل ، فشلت هذه العينة عند وصول الضغط إلى (660) كيلو نيوتن ،حققت زيادة حوالي (18.9)٪ بالمقارنه مع عينة التحكم. وبالنسبة للعينة التي تحتوي على فتحات جانبية مربعة في الأعلى والأسفل ، تم تقويتها أيضًا (رأسيًا واحدًا) بصفائح CFRP على كل جانب عمود و (شكل 2 Xمن CFRP) في الأعلى والأسفل ، فإن أقصى سعة تحميل تساوي (560.3) كيلو نيوتن بسعة إضافية 30.3٪ مقارنة بعينة التحكم. يزيد الفتح الجانبي الدائري من المطيليه بقيمة تقارب (2.1). بالنسبة للعينة ذات الفتحة الجانبية الدائرية وتحت التحميل اللامركزي ، يكون الحد الأقصى. بلغت سعة الحمولة 65.8 كيلو نيوتن. العينة لها فتحة جانبية مربعة ، الحد الأقصى. سعة الحمولة تساوي (64.8) كيلو نيوتن. المطيليه القصوى تساوي (2.5). بالنسبة للعينة ذات الفتحة الجانبية الدائرية والمدعومة برقائق (رأسية واحدة) في جانب الشد و (ثلاثة) صفائح دائرية ، واحدة في منتصف ارتفاع العمود واثنان آخران أعلى وأسفل ، وتحت تحميل غريب الأطوار ، الحد الأقصى ، وصلت سعة الحمولة إلى قيمة (80.1) كيلو نيوتن ، وبالنسبة للعينة ذات الفتحة الجانبية المربعة بنفس التكوين المعزز كانت الحمولة تساوي (75.38) كيلو نيوتن. الزيادة في سعة الحمولة التي تم الحصول عليها من العينه لها فتحات جانبية دائرية تساوي (21.73٪) مقارنة بعينة التحكم ، والزيادة تساوي (16.32٪) مع العينة للفتحات الجانبية المربعة . وأيضًا بالنسبة للحالة ذات الفتحة الجانبية الدائرية والتقوية بواسطة CFRP ، يتم الحصول على القيمة القصوى للانفعال في الخرسانة عبر مقياس الضغط الخرساني SGC من 0.0085 = SGC1 ، حيث تم تثبيت الSGC1 في وجه الانضغاط بالقرب من الفتحة الدائرية في الأعلى. تمت محاكاة العمل التجريبي في برنامج ABAQUS وكانت النتيجة جيدة.

Introduction

1.1. General

Worldwide application and vast experience for the last 100 years, reinforced concrete (RC) technology has shown that correctly constructed RC structures are dependable and long-lasting., built and maintained. It is possible that existing RC constructions may be deficient due to porosity and cracking of concrete and corrosion of steel reinforcement under harsh and hostile climatic conditions as well as high loads. Design errors, increased load bearing requirements, a change in the structure's purpose, and failure to implement more severe design rules, particularly in high-effective seismic zones, are other reasons for structural inadequacy. as shown in Fig. (1-1). To maintain the infrastructure of a nation, it is necessary to either destroy and construct new buildings or rehabilitate the existing ones to satisfy current criteria for the continuance of contemporary civilization, which is well-known. The deterioration of long-established structures is unavoidable in nations with well-established structural infrastructure. Iraq’s Highway bridges, in particular, were found to be in critical need of strengthening, according to the evaluation of the infrastructure as the plate (1-1). There is, however, no estimate of how much the restoration will cost. Increasing costs of construction materials and labor.

It is increasingly difficult for even the most developed nations to deal with this expensive issue because of financial difficulty. Since creating a new structure is more expensive than repairing or upgrading an existing one, today's engineers must come up with innovative repair and upgrade methods and materials that are more cost-efficient and effective.

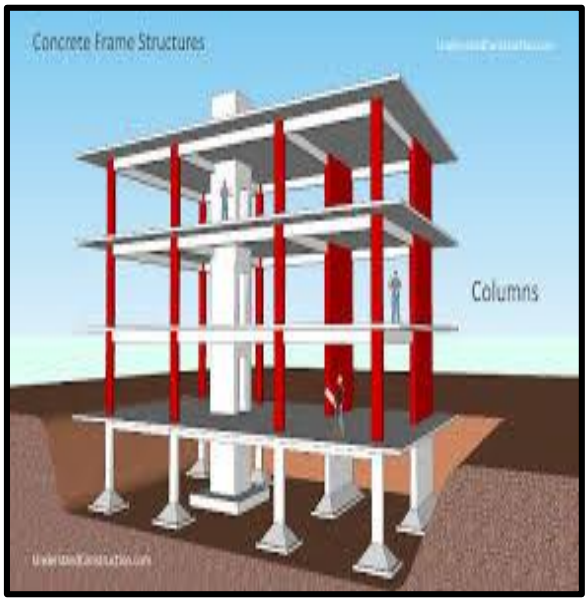

Fig (1-1): Columns and shear wall to carry the loads[1]

Plate (1-1): Basra bridge under constructions [2]

1.1.1 RC Columns in Structures

Many structures are erected on RC columns. The entire behavior of structures is greatly influenced by the strength, ductility, and durability of RC columns, thus understanding how each column responds to a variety of loading scenarios is of great importance[1][2]–[7]. Strengthening by Fiber-reinforced polymer (FRP) or textile-reinforced mortar (TRM) is the subject of this research. Vertical load-carrying structural components are often known as RC columns. Nevertheless, in reality, columns can sustain shear and bending stresses depending on their placement in the structure, and this category is only an idealization, uneven settlements, craftsmanship flaws and seismic stresses. As highway bridge peers, vertical load-carrying components in structures, or subterranean piles, RC columns are built to suit your needs. Depending on structural requirements and material availability, they may be built with a wide variety of cross-sectional geometries and heights and several options kinds and concrete and steel reinforcing amounts. Fig (1-2) illustrate the cross-section of a solid concrete column.

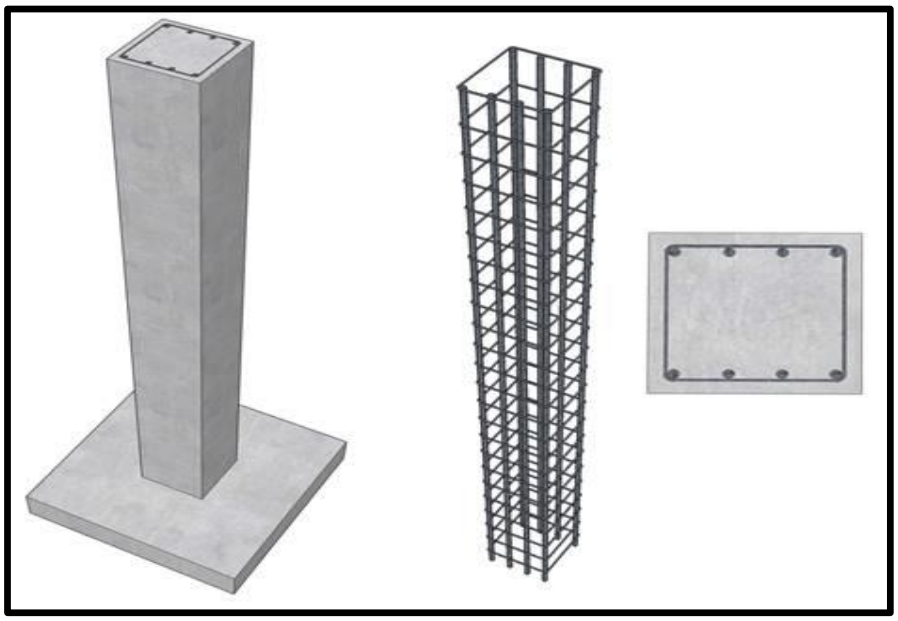

Fig (1-2): Solid concrete column [1]

1.1.1 Hollow RC Columns in Structures

Hollow concrete column structures can be one option for enhancing strength-mass and stiffness-mass ratios, and lessen the effect of weight on structures that will gradually reduce the total spending of the structure. In many existing bridge piers, Hollow structural members have already been used[8] [9], [10],and[11]. In order to avoid the columns' delicate shear failure, special care must be given to the plastic hinges. Shear strength of RC columns drops dramatically when the lateral displacement ductility rises. The circular column of hollow reinforced concrete is widely used in earthquake areas [8][12] , hollow segment piers made of reinforced concrete (RC) are ubiquitous the structural approach, commercially desirable for bridge systems for a variety of factors like a greater moment- inertia as solid parts of equivalent size [13] . Shear resistance mechanisms characteristic of hollow RC columns are quite similar to those typical of tube sections, relying mostly on the aspect ratio of the webs, in order to avoid catastrophic collapse of bridge piers during

a shear failure. The low thickness of the deterioration processes limits the confined concrete core, which is critical for seismic energy dissipation. [13].

Hollow-core columns with circular columns the holes showed better performance compared to the columns non-circular hole [14]

If the concrete layer spills off, the longitudinal bars between the transverse reinf orcement become exposed and are thus vulnerable to buckling,

Resulting in a weak collapse, if the section is not properly confined in a hollow column, the inside face of the column may implode due to the high axial strain levels. Therefore, it is also important to have a lateral reinforcement along the inside of the column, as the plate (1-2)

Plate (1-2): Hollow concrete column [14]

1.1.2 Confinement of RC Columns

Special transverse reinforcement strongly intersperses the concrete in directions perpendicular to the stress applied. The behavior in circular columns of fiber-reinforced polymer (FRP) confined concrete has been extensively studied[2], but in FRP square columns it is far less known that the concrete is non-stringed and the containment efficiency has been reduced considerably as the fig. (1-3) [15]. The report shows the existence of an inner space reduces the effect.

of external FRP confinement, but this reduction of confinement effects could be adjusted by using an appropriate cylindrical tube as the interior confinement [12][16].fig(1-4) explain the stress vs. strain curve for the stress-strain curve for confined and unconfined concrete.

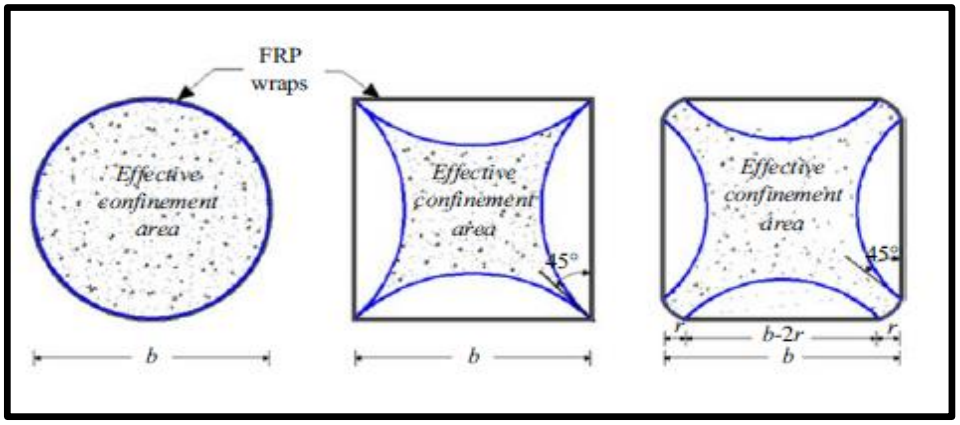

Fig. (1-3): Effective confinement of concrete column [15]

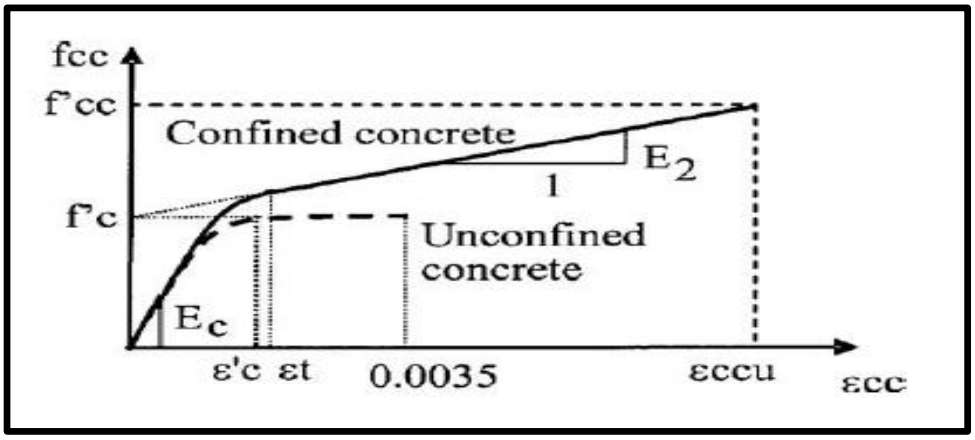

Fig. (1-4): Stress-strain curve for confined and unconfined concrete [16]

FRP-confined concrete models for analyzing the increase in concrete strength and peak axial strain produced experimentally are the most often used. As stated in equation (1-1),[17][18]:

$$f'_{cc} = f'_c\left[2.25\sqrt{1+7.9\frac{f_l}{f'_c}}-2\frac{f_l}{f'_c}-1.25\right] \quad \text{----------} \quad (1\text{-}1)$$

The strength and ductility of reinforced concrete are enhanced when it is surrounded by a rigid base, such as in concrete-filled tubular steel columns. In this case, the concrete is called confined concrete, and the mechanical properties of this concrete improve considerably compared to unconfined concrete, based on the yield stress and the geometries of the outer stiffness substrate [19],as the Fig.(1-5) With circular columns, this process is considerably more efficient than with square or rectangular columns. It is because the latter also concentrates the restricting action at the corners [19].

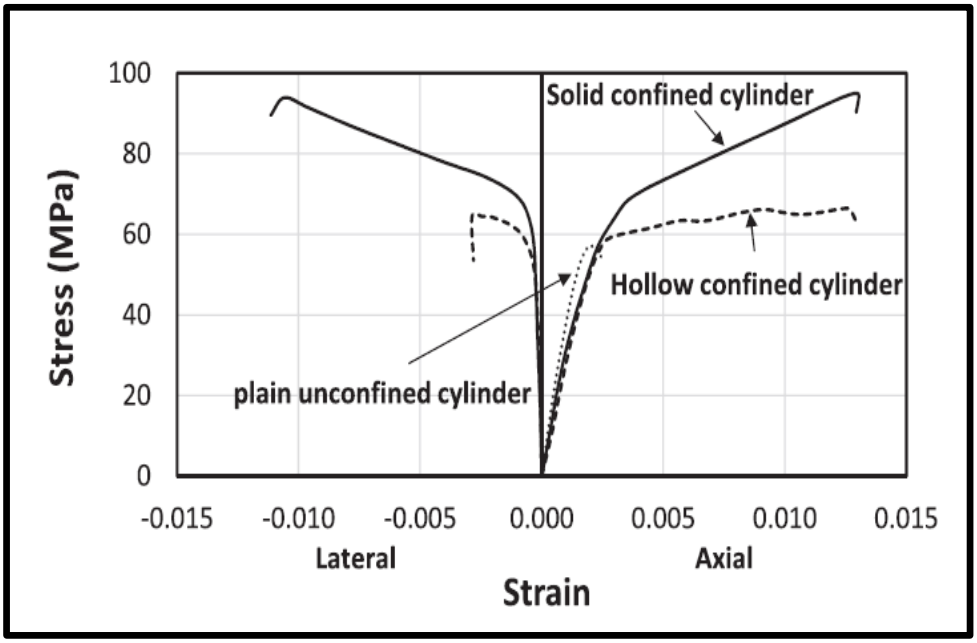

Fig. (1-5): Comparison confinement for solid and hollow columns [19]

When is it important to strengthen a R.C. column?

1- Either an increase in the number of floors or a blunder in the design increases the column's load.

2- There is a problem with the concrete's compressive strength or the percentage and type of reinforcing.

3-The column's inclination is higher than permitted.

4-The foundation has settled longer than intended.

5- a structure that has been shaken by an earthquake.

Reinforced concrete columns may be strengthened in a variety of ways, including the following: -

* steel jacketing.
* reinforced concrete jacketing.
*TRM confining.
*FRP jacketing.

1.1.2.1 Textile reinforced mortar (TRM)

With an open-mesh design, a natural fiber reinforced with an inorganic matrix is used in TRM., as well as hydraulic lime-based grout or mortars. Fire retardant, easy to apply by hand, and may be treated to wet or small surfaces, TRM is a low-cost, manual-friendly, and can be used to wet or low-temperature surfaces, [20]–[23]. TRM is becoming increasingly popular as an alternative to FRP in the reinforcement of internal systems for all of these reasons, as seen in the figure (1-7) improved conditions of bonding between fibers and matrix in a mortar once continuous fiber sheets were made of composite materials Textiles were removed. At first, the modern composite made of textiles Materials called silk reinforced concrete (in Europe) (TRC) or coated woven mortar (TRM) [24][25].

In applications where the force is mostly linear, TRM wrapping may be used in columns to assist a multiaxial stress condition to benefit from the commensurate improvement in constrained concrete strength and deformation efficiency. [26] ,as the fig (1-6) and fig (1-7).

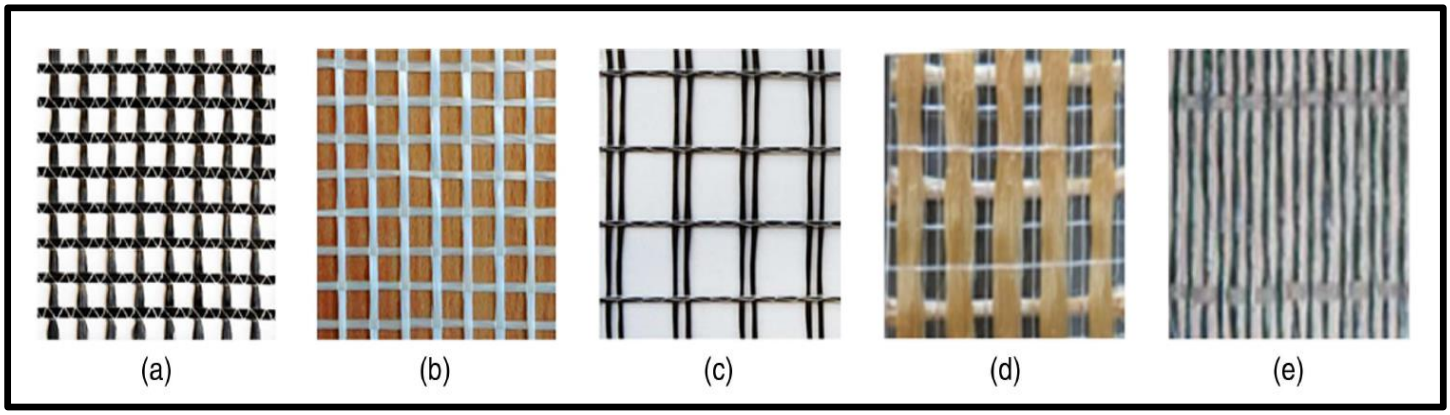

Fig. (1-6): Textile fiber reinforcements

(a) Textile made from carbon fiber. (b) glass fiber textile. (c) basalt fiber textile. (d) polyphenylene bezobisoxazole (PBO)fiber textile. (e) steel fiber textile [26].

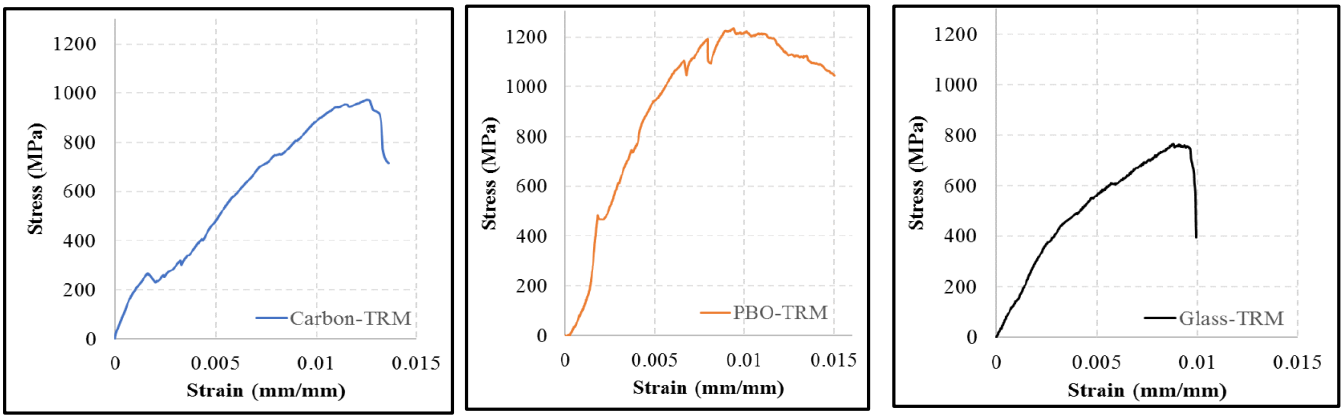

Fig. (1-7): Stress-strain curves for the (a) Carbon-TRM, (b) PBO-TRM, and (c) Glass-TRM[26]

Plate (1-2) show the tensile test for TRM

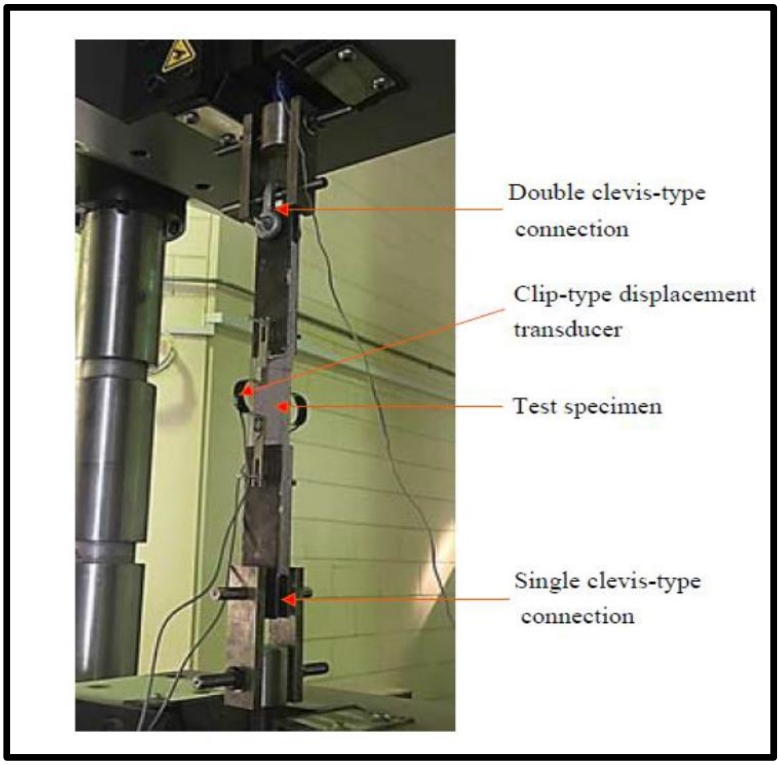

Plate (1-2):test setup and instrument for TRM tensile test

1.1.2.2 Polymer with fiber reinforcement (FRP)

Polymer reinforced with fibers (FRP) materials possess continuous carbon (c), glass (g), or aramid (a) as the fig. (1-8), fibers tied together in an epoxy matrix, vinyl ester, or polyester materials, containing excellent properties such as high tensile strength, high rigidity, corrosion-resistant, and lightweight. Composite structures are widely used in engineering applications, owing to their high performance.[25]–[29]

Products from Fiber Reinforced Polymer (FPR) are used to enhance flexural strength, shear strength, and ductility of current sub-standard structures [30][31]. A good example is concrete structures reinforced by FRP sheets at the stress point.

FPRs improve concrete's tensile strength. Also improve column capability. Fiber-reinforced polymer bonding (FRP) composites with suitable parts

The epoxy adhesive is one of the commonly used methods for fixing rigid concrete beams. For general, a beam may be bonded to an FRP sheet on either the soffit or the web, soffit bonding is used for flexural beam strengthening, while web bonding is used for shear strengthening.

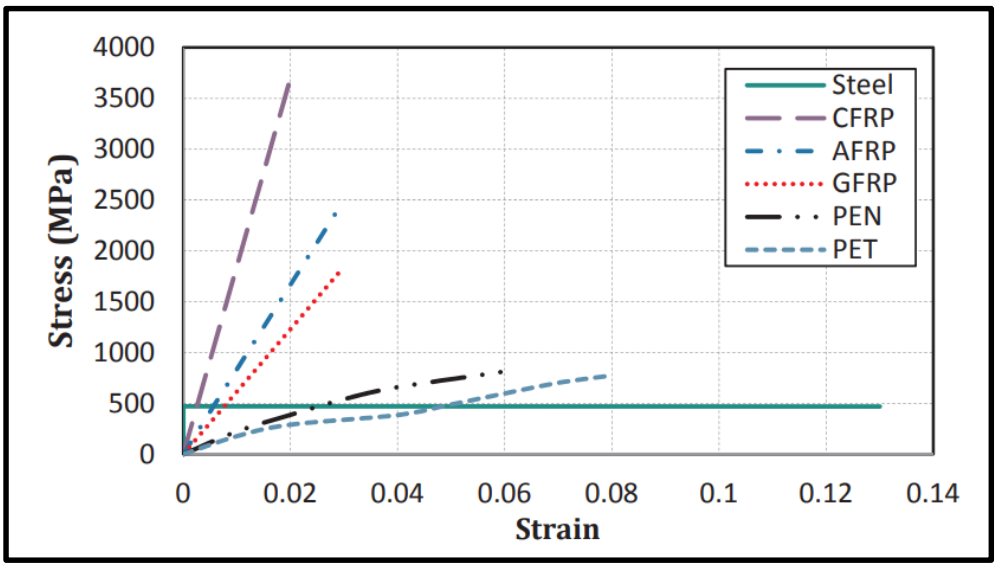

Fig. (1-8): Stress vs. strain curve for steel and FRP[29]

Since of its ease of deployment and less time consumption compared to concrete or steel jacket reinforcing, CFRP reinforcement has been one of the key solutions in structural reinforcement [12].

Full CFRP containment encountered an eruption of unexpected collapse without early notice, when no original crack or spalling could be seen [12].

The moderately confined CFRP specimens were able to provide proper lateral mitigation which reduced concrete dilation and further decreased column failure [32]. It was observed that the mode of strength, ductility, and failure CFRP wrapping direction of enclosed cylinders focuses on and thickness to laminate Wrap [4].

The application of FRP in the construction industry can reduce specific harmful concrete properties, such as high-strength concrete's brittle behavior. FRP is particularly useful for reinforcing columns and other irregular types [4].

Due to compressive stresses in the concrete, the fibers in the direction of the hoop resist lateral expansion. This results in confining stress to the core, delaying concrete fracture and thus increasing the compressive strength and ultimate concrete compressive strain [12], [33]–[41].

Reported that both ductility and shear strength improved significantly with FRP jacket thickness, eliminating all shear cracks and changing the pattern of failure of the specimen from shear to bending [42] [43] [44]. Plate (1-3) shows the multi types of FRP materials used in strengthening.

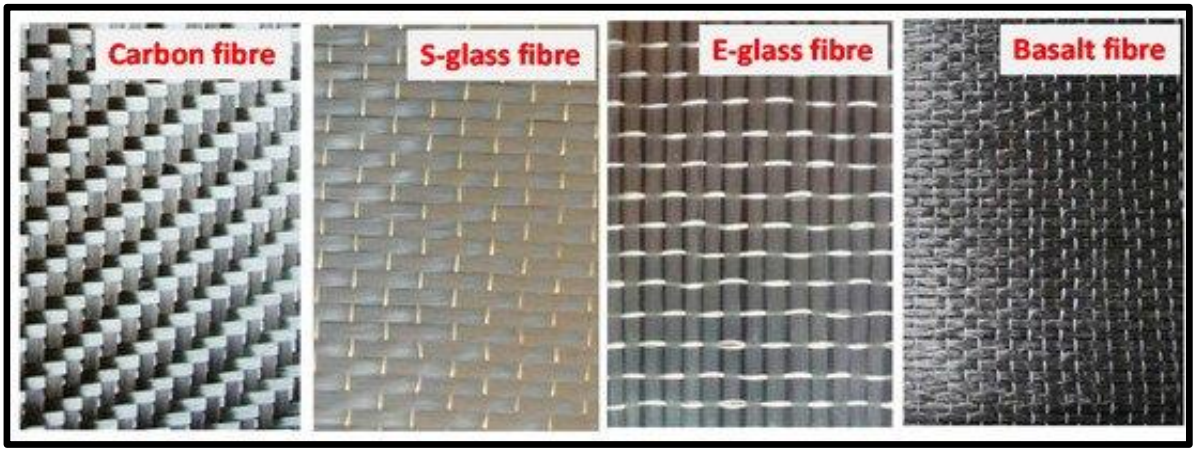

Plate (1-3): multi types of FRP materials [41]

Fig. (1-9) explain the effect of the FRP wrap with use different column cross-section shape

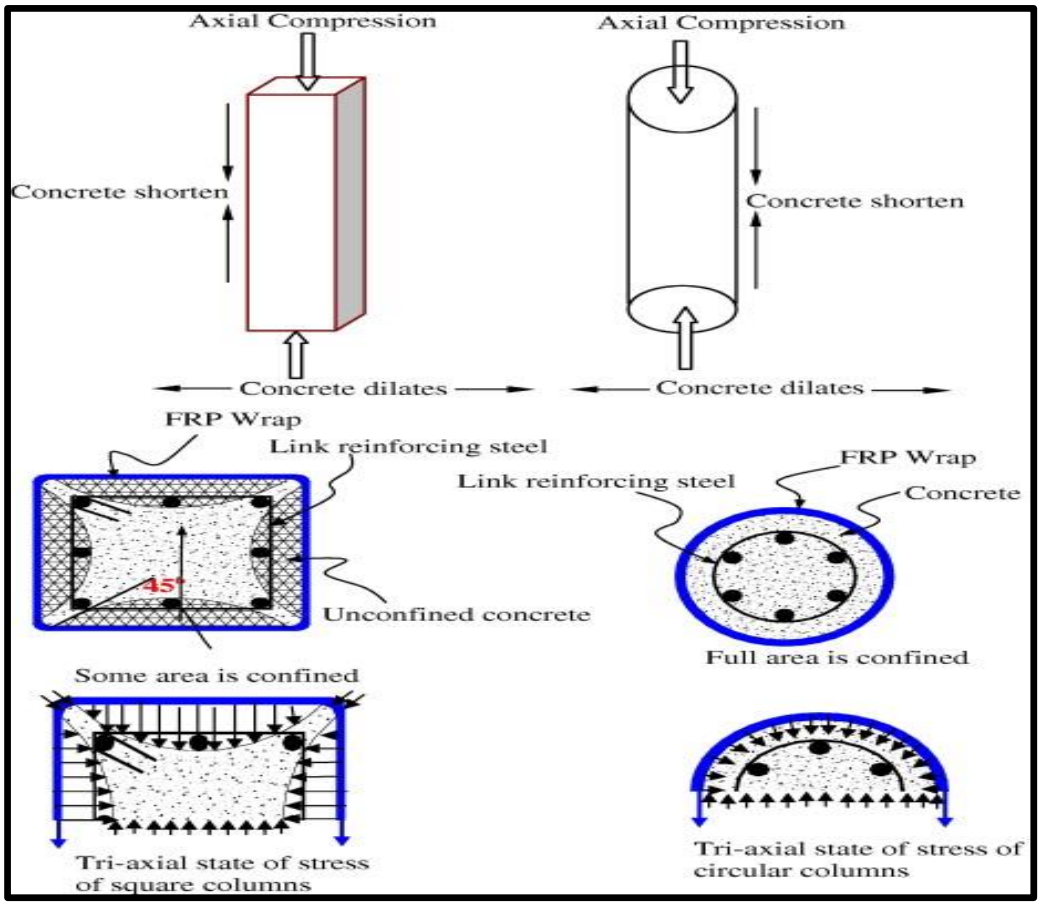

Fig. (1-9): Comparing between the circular and noncircular effect with use FRP [42]

1.2 The aim of the study

* Study the compressive strength of solid concrete column and hollow concrete column and comparing between the results.

* Investigate at hollow-core reinforced concrete columns with textile reinforced mortar (TRM).

* Investigate at hollow-core reinforced concrete columns with carbon fibre reinforced polymer (CFRP).

*Study the five confinement of external strengthened for hollow concrete column by (CFRP or TRM) under concentric loading.

*Study the five confinement of external strengthened for hollow concrete column by (CFRP or TRM) under eccentric loading.

*Comparing the results obtained from the test for the specimens subjected to concentric or eccentric load and strengthened by (CFRP or TRM), these comparisons according to the: compressive strength, load vs. displacement curve, ductility, mode of failure, and stress vs. strain curve.

Originality: * Study the side opening in the hollow concrete column with two shapes circular and square holes and also comparing the results.

Originality: * Strengthening the specimens with side opening (circular or square) by two CFRP forms.

* Improve the capacity of the hollow concrete column by using FRP or TRM within conditions such as locations and configurations of each of them.

1.3 The Design of the Thesis

The current study is divided into six chapters, which are as follows:

The Present chapter (**chapter one**) provides an overview of column behavior and applications.

Chapter two: provides a review of past research (experimental and theoretical) relevant to the current subject.

Chapter three: provides the experimental details of thirty-two (32) similar RC columns with similar reinforcements and strengthening partially by (CFRP or TRM).

Chapter four: includes the outcomes of experiments and their discussion.

Chapter five: presents the finite element modeling of the present problem using ABAQUS.

Chapter six: presents conclusions and recommendations for future works.

Chapter Two

2.1: Introduction

One of the essential topics in constructing buildings and other structures such as bridges is the problem of concrete column failure. The column is important in the structures, as the loads move from the roof to the foundations using the column. Rehabilitation and strengthening of concrete columns are often very significant, and the materials and methods used are varied and various. For example, (steel jacketing, cementitious materials, steel fibers, fiber-reinforced polymer).

2.2: Concrete column with solid section

(Doran et al., 2009),Theoretical study for the purpose of knowing the behavior of a concrete column has the (square and rectangular) cross-section and with using fiber-reinforced polymer (FRP) by the (non-linear finite element by using the (NLFEA) where the proposed model was represented under the central load. Where it was simulated 33 models short and long column with the slender column. The columns have been the subject of much earlier research, but they have been constrained by his limitations (FRP). Also, the maximum load on the square or rectangular column is unpredictable without taking into account the confined load due to the effect of the shape. Various angles as well as a modest influence on the flat sides are used to designate non-circular columns. Therefore, find it difficult to use the assumptions of regular pressure, as is the case for the column with a cylindrical shape. Columns in this scheme are made of steel and concrete by using concrete to damage plasticity (CDP). When compared to circular section models, the non-circular specimens had a serious implication on confinement. The less constriction there is at the flat side's midpoints**[48].**

(Micelli & Modarelli, 2013), A practical study analyzing the properties of concrete columns used by carbon fiber (CFRP) and (GFRP) sheets, and these columns have different sections and lengths the sections are circular and non-circular, and some of the columns have a hole along the column. The loads on the columns were monophasic. Instead of the (89) models constrained by (CFRP) and (GFRP), 128 specimens were constructed from concrete columns that were separated into (33) models without confines. Use the fiber-reinforced polymer in the circular sections more than effect than the non-circular sections. To test the non-circular columns, researchers used 3000 kN for the short specimens (150x300 mm) and 1500 kN for the mid-sized specimens (400x600 mm). The results indicated that failures occurred around the column's edges and corners, even in the specimens that had not been strengthened. An increase in the hollow core causes an increase in the sudden failure of the inner part due to the separation of the concrete from the inner part of the column. Plate (2-1) show the failure in the specimen**[49]**.

Plate (2-1): Concrete crushing of unconfined prismatic concrete column [49]

(Afifi et al., 2014), Study the circular concrete bars, using a (GFRP) bars and spirals and with subjected to axial force effect, where 12 models of reinforced concrete columns were implemented with a circular cross-section, the dimensions (300*1500) mm, where are these models divided to three parts, nine models are GFRP, two steel reinforcement, one plain column without reinforcement. The research aims at assessing the GFRP concrete columns, also studied are several variables, including longitudinal reinforcement, the proportion of reinforcement, the diameter of the reinforcement, and the distances of the transverse reinforcement. In the laboratory a pressure device was used with axial capacity (11400 kN), also was used the (SG) to Record the strain in the rebar and used the (LVDTs). To avoid a major event at the column's ends, employ steel plates with a thickness of 12.7mm and a diameter of 250 mm. And work small concrete layers have high compressive strength grouting to insure good distribution for an axial load. The results of the examination showed that the unreinforced model (plain). This model fails due to brittle failure caused by a lack of reinforcing steel, which gives the member ductility. A fracture develops along the column as a result of this failure. The failure occurred after reaching the maximum load by 2468 kN. The GFRP and steel reinforcement specimens had the same initial behavior. Where crack hairs are generated, he has 85% to 95% of the axial load. The load on the strengthened specimens (GFRP) varies from 2804 to 3019 kN. In contrast, the axial loads of the steel specimens have increased by 8% to 3159 kN. When using transverse reinforcement at wide distances or the percentage of less than (0.7%) of failure, a result occurs when the longitudinal bar buckling outside. While specimens have good confinement, failure occurs due to the concrete reaching its maximum. plate (2-2) showed the test machine **[50]**.

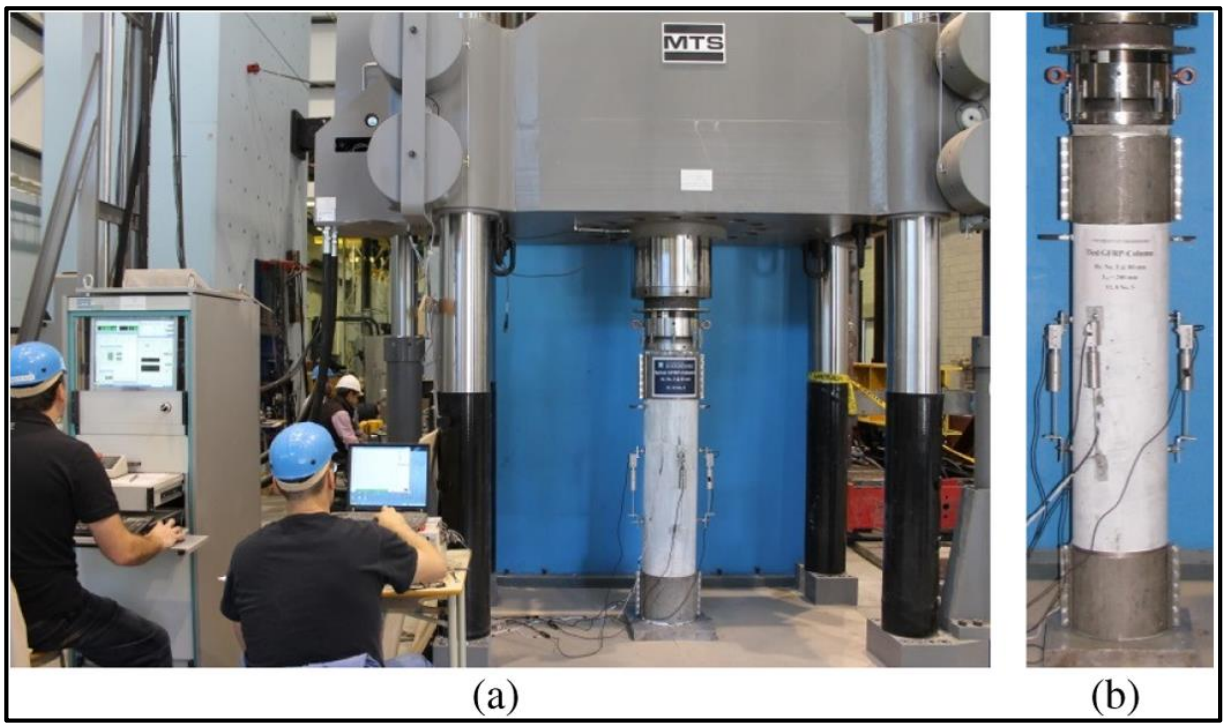

Plate (2-2) (a) MTS loading machine and data-acquisition system; (b) LVDTs and steel collars [50]

(Fitzwilliam and Bisby, 2020), in this paper, a study of strengthening concrete long columns by using carbon fiber polymer (FRP). Where previous studies focused on the short columns. Research is being conducted to compare the performance of a carbon fiber-reinforced polymer composite (FRP)-encased circular concrete column to that of a control column. In the laboratory implementation of 18 circular concrete columns with different slenderness ratios which had diameter (152) mm and height (300, 600, 900, 1200) with strengthening by (CFRP) where this group labeled (C) or without strengthening (U). In this study, the ratio of longitudinal bars based on the Canadian code was equal to (0.7%). The longitudinal direction of the carbon fibers is unaffected by the 100 mm hoop-to-hoop overlap of the fibers. For the purpose of strengthening to flexural, carbon fiber (CFRP) should be placed longitudinally before the hoop direction. The number of layers used (0, 1, 2) for axial strength and (0, 2, 4) for flexural. The result showed, using a single carbon-fiber tape increases strength capacity by 18%.

Whereas the strength of the two-layer tape has enhanced about 65%. The test occurred with a 20mm eccentric load. Also the hoop direction in (CFRP) increase the carry load in the column for the axial and flexural. For the unstrengthen column, the failure started in the part above the middle of the column height. For the strengthened column, the failure was observed in the middle height of the column. when the slenderness ratio is reduced the ultimate load increase and the lateral deflection failure is reduced. Plate (2-3) showed the test setup and scheme of test **[51]**.

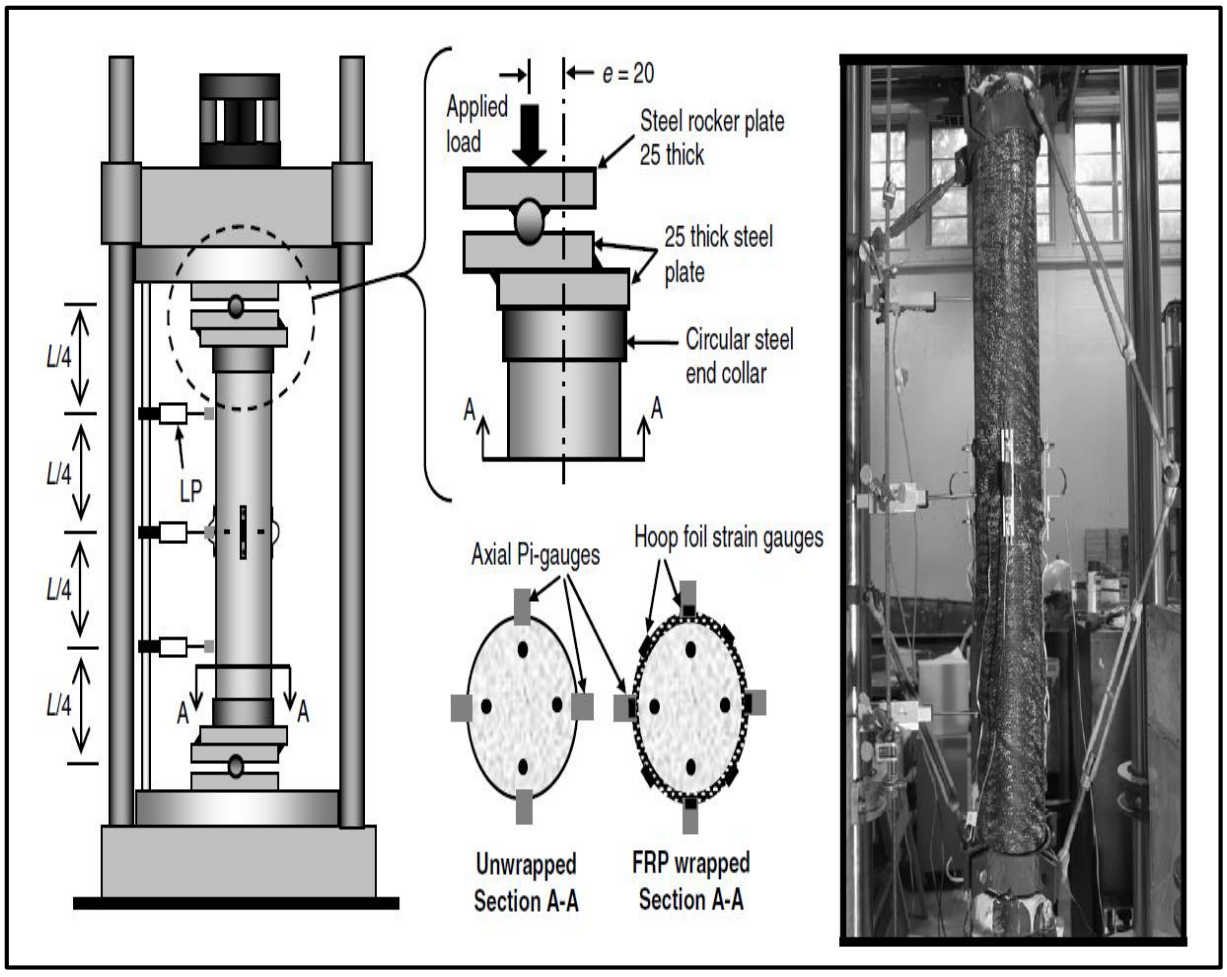

Plate (2-3) Schematic and photo !1200C-1-0-A" of test setup and selected instrumentation! dimensions in millimeters"[51]

2.3: Hollow concrete columns

(Congress, 2006), A carbon fiber reinforcement has been used in this work to investigate the hollow column's bending behavior and improve its structural integrity (CFRP), When a lateral force is applied to a hollow column, a plastic hinge is generated, making hollow columns ideal for seismically active places. study the effect of using carbon fibers on non the circular columns, and study the effect of steel reinforcement (transverse reinforcement), also study the location of neutral axis forces, the models used were in dimensions (360x360x1300) mm and hole (310x310) mm, as shown plate (2-4).

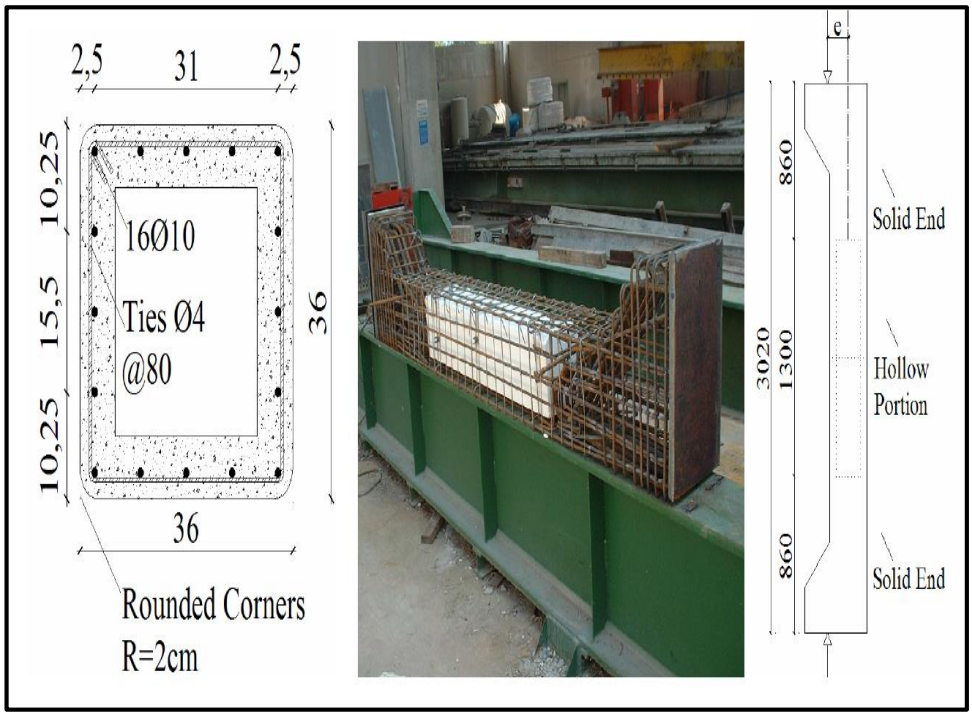

Plate (2-4) Geometry of specimen [52]

Where six specimens were completed, and one specimen was used as a control, see table (2-1) below and the (U-unstrengthen, S-strengthened) Results showed the: specimens (U1, U3, S2) failure occurred in the base of the column. specimens (U2, S3, S1) failure occurred in the mid-span of the column.

the specimens without CFRP had brittle failure mode. The greater the distance of eccentricity (e) the axial load reduced and the buckling in the main bar reduced - CFRP delays the failure in the concrete then changes the mode of failure from brittle to ductile **[52]**.

Table (2-1) Test Matrix

Specimen Code		Loading Condition	e (mm)
UnStrengthened	With FRP		
U0	---	Pure Compression	0
U1	S1	Compression and Flexure	50
U2	S2	Compression and Flexure	200
U3	S3	Compression and Flexure	300

(Kusumawardaningsih and Hadi, 2010),this research was for the study of the effect the shape of cross-section and the shape of the inner hole of the concrete column in a circular or square under the influence of a central force, Where casting 12 specimens of RC of the column with the use of high strength concrete (HSC), with compressive strength about 72MPa .and had the short concrete column to prevent lateral bending due to long Some models had been added Carbon fiber reinforced CFRP and other specimens without CFRP use as control specimens. The result showed concrete specimens non-container CFRP Failure gets out brittle deformations, while models containing carbon-reinforced fibers are ductile deformation. Circular models and contain circular holes had higher carrying capacity than the Circular specimens containing square holes. Also, the specimens are found Square specimens with circular holes are better than square specimens with square holes. In the case of circular holes, this behavior provides a more suitable distribution of strength force. Plate (2-5) represented the failure for specimens **[53].**

Plate (2-5) Typical failure behavior of circular and square columns [53].

(Units et al., 2020),experimental study on the hollow rectangular column under the influence of axial and cyclic bilateral forces, Where five columns were executed with dimensions (500x360x1440)mm and inside dimensions (260x120) as the plate (2-6), where the results showed that failure occurs due to flexural, this failure was generated as a result of buckling for the main bar reinforcement at the base of the column, also, the cyclic force showed a deterioration in hardness and strength significantly. Hollow columns with add configurations lateral reinforcement had a good efficacy against earthquake The pattern of failure in two short sides same also for the long sides. At the (1/6) of the height column, a hinge made of plastic was produced **[54]**.

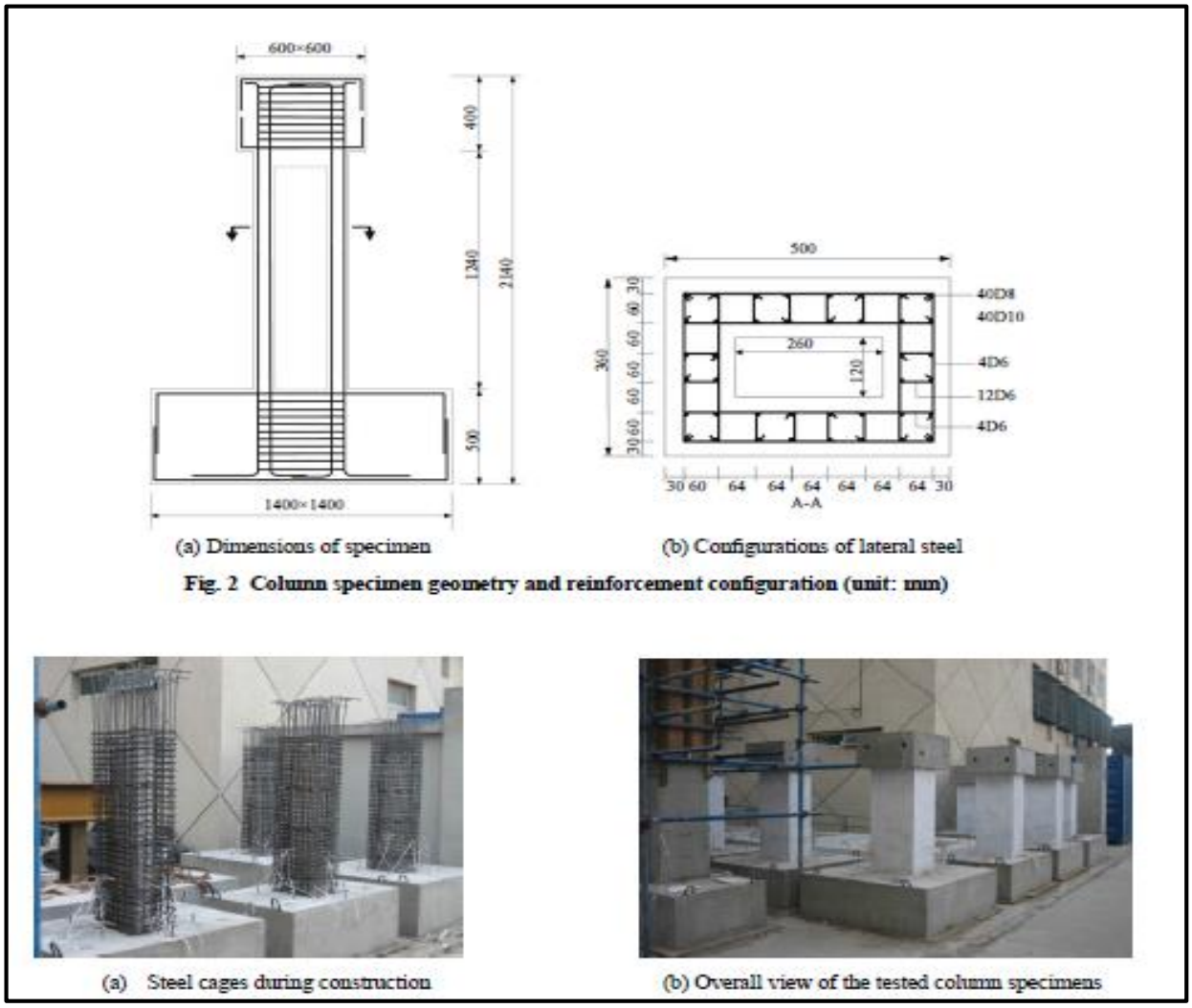

plate (2-6) Construction of specimens [54]

(Cassese et al., 2017), studied hollow concrete columns of bridged concrete with rectangular cross-section, where the search includes looking at bridges Implemented before 1980 where the details of reinforcement against seismic load not required. where it was worked out 4 hollow concrete columns with a different aspect ratio(Lv/H) and the dimensions (600x400x1500) mm and (400x600x900) mm, as the plate (2-7). The primary goal of the practical research is to determine the influence of various transverse reinforcement forms and amounts, as well as the effect of aspect ratio. Laboratory results showed the flexural failure occurred in the tall columns, while the shear failure occurred after flexural yield in the short columns. Shear failure occurs in columns with an aspect ratio under 2.5, whereas flexural failure occurs in columns with an aspect ratio greater than 2.5 **[55]**.

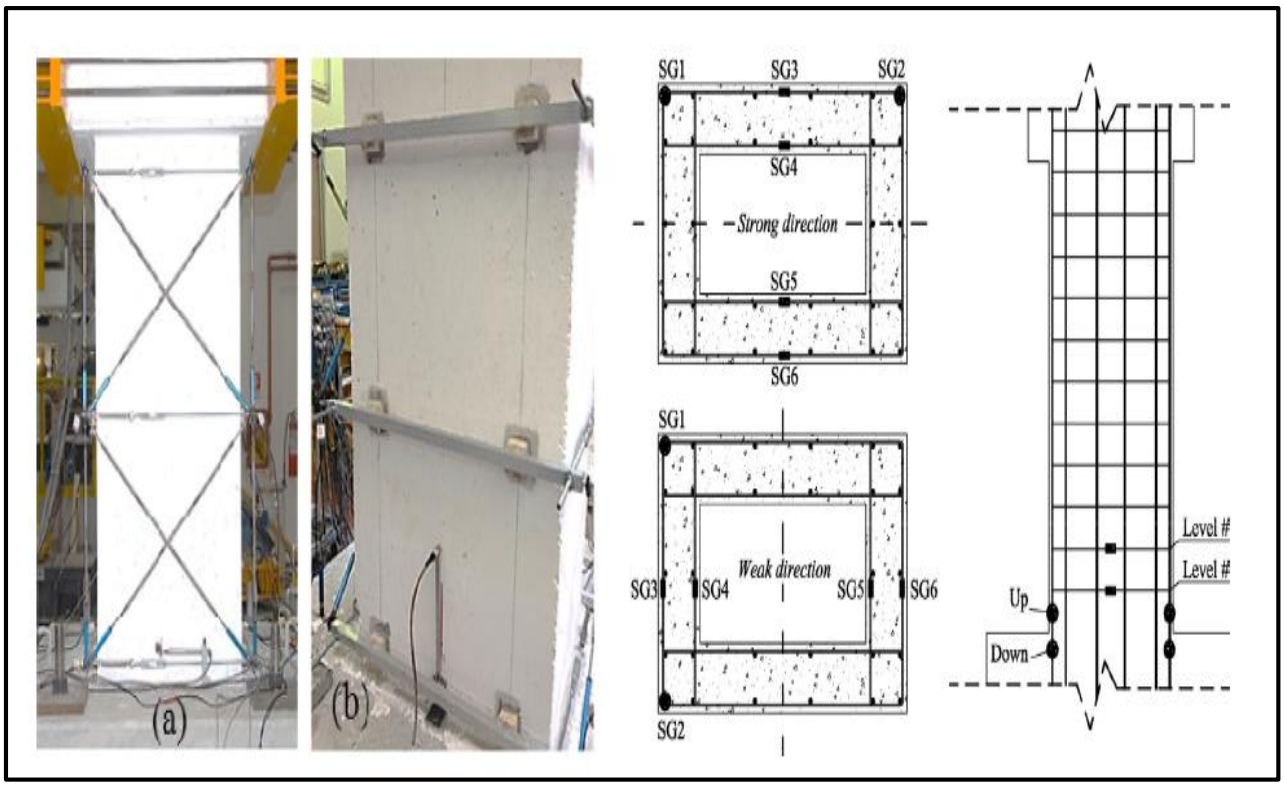

Plate (2-7) Instrumentation scheme: LPs (a), Base LVDTs (b) and Strain Gauges (SGs) (c) [55]

(Ismail et al., 2019), In this study the study was partially strengthened for Hollow cylinder concrete column by using (CFRP) Where six models of hollow columns were built with dimension (250x2000) mm and hole dimension (110) mm, strengthened of the columns using carbon fiber(CFRP) better than conventional method like steel plate because this method ease in work and installation, where research has proven The use of carbon fiber (CFRP)increases the strength and ductility of the concrete column. to measure strain in rebar use SG by three locations along the height column, (CFRP) had thickness (o.165 mm\ply) and area (300 g\mm2) and epoxy with ratio 4:1. The load on the specimens about (1500 kN), where the load applied by adding 10 kN, with a five-minute pause, to avoid sudden failure. The results of the investigation revealed Instead of the top of the column failing due to a failure of the concrete cover as it did when CFRP was not used to strengthen it, the rapture in CFRP laminates at the top was caused by the column failing due to a failure of the concrete cover, and this was the first crack recorded at axial force when CFRP was used (160 kN). Compared to specimens lacking partial CFRP, the axial load of specimens having partial CFRP rose by about 38%, as the fig (2-1) **[56]**.

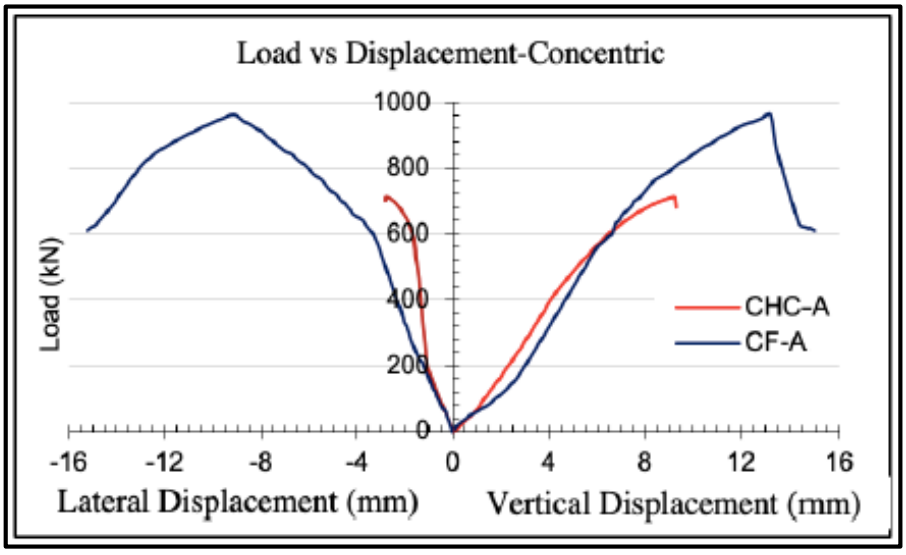

Fig. (2-1) Load vs Displacement Behavior [56]

(Jamatia and Deb, 2020), in this research using a theoretical study By simulation in the Aba*q*us software program Compare the results with the practical research was studying the effect of cohesion forces, when hollow concrete columns are used. A quasi-brittle failure in concrete columns occurs when carbon fiber is not used, but when central works on concrete columns are used and carbon fiber is used, the endurance period increases for tiny columns. Is this study the consistency between concrete and carbon fiber? Concrete expansion is the primary cause of failure, whereas shear banding growth is the primary cause of failure for big columns. concrete damage plasticity was employed in the Abaqus software application The Druker-Prager yield criterion for evaluating confinement sites necessitates the implementation of two different types of tests. To analyze failure sites, the second type of carbon fiber (CFRP) is utilized in place of the first type, which has a higher ultimate strength of 1825.5MPa, while the first type has an E=80.1 GPa and an ultimate strength of 1825.5MPa. With a large number of layers of carbon fiber. When the number of layers is four or more, we see a high-stress strain in the material. In order to verify this, the average confining pressure throughout a 35-mm-high cylindrical zone on the concrete surface positioned 800 mm from the fixed end was measured. as depicted in the following figure (2-2) **[57]** .

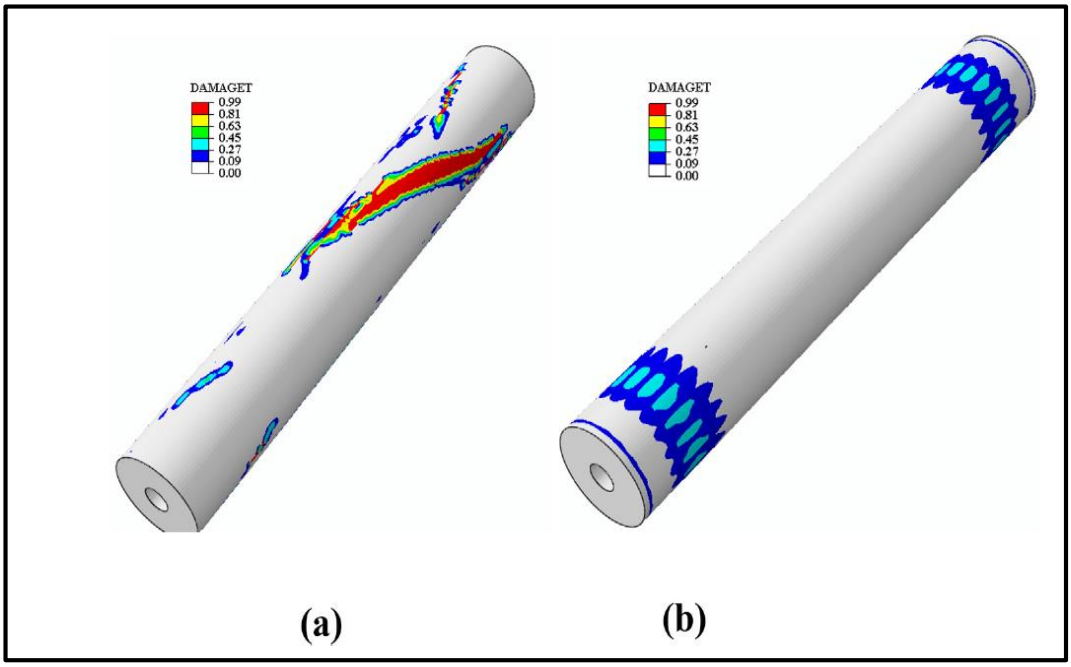

Fig. (2-2) Damage contour at applied stress of 34 MPa in (a) 2 layers and (b) 4 layers GFRP confined hollow circular column, respectively [57] .

2.4: Strengthening by using steel jacketing

(Calderón et al., 2009), Reinforcement of RC columns can be accomplished using one of three major methods: jacketing in concrete, steel, and lightweight materials (FRP).Steel caging is a variant of the technique of steel jacketing and is known as being easy to use and fairly cheap. When designing a steel caged RC column, the ultimate load can be determined using this novel design suggestion. An experimental and computational analysis of specimens on a large scale is used in the creation of the current proposal to understand the mechanisms of failure. When an RC column is loaded axially with steel caging, it is possible to measure the final load. For a cage-strengthened RC column, the transfer of loads between the column and cage necessitates a series of steps. Plates 2-8 of the RC column show how steel caging can be used to strengthen the structure **[58]**.

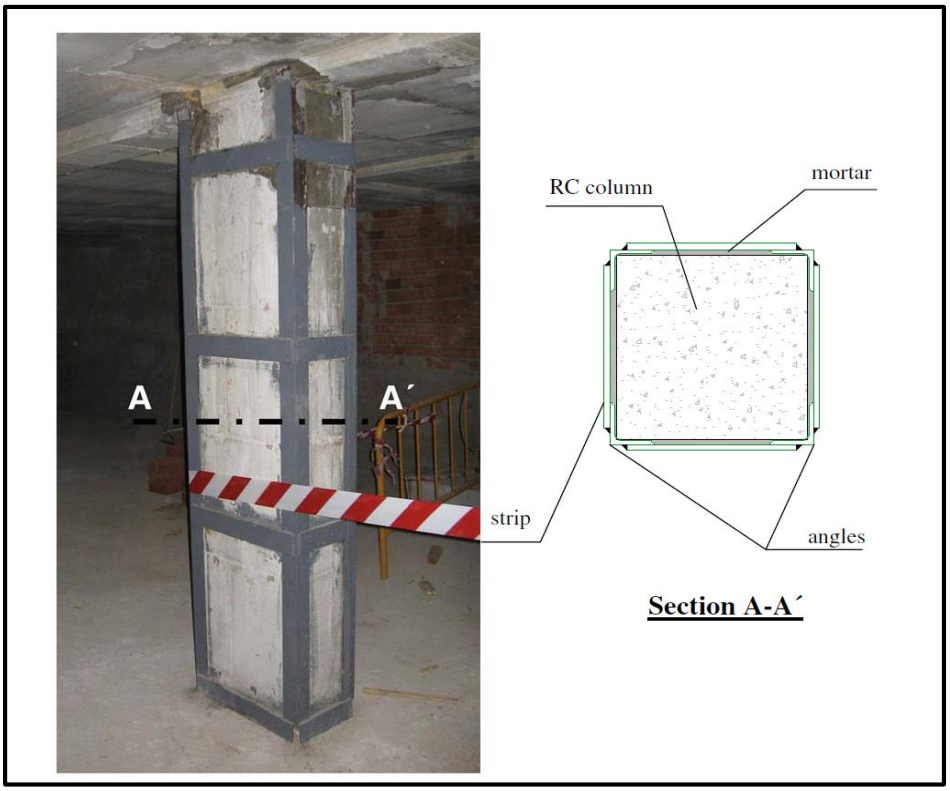

Plate (2-8) RC column strengthened by steel caging (without additional elements at the ends of the cage) [58].

(Kusuma and Suprobo, 2011), For the containment of concrete using typical rectilinear connections and welted wire cloth, there are several analytical models available. The reinforced concrete column's strength and ductility are considerably enhanced if the column's core is restrained by lateral armor. Fig. (2-3) show how the Welded Wire Fabric WWF, in addition to typical links, can be stacked transversely in the concrete column's middle, with a regular longitudinal spacing, or it can be wrapped around the column. Researchers created each and every one of the available models to fit their unique set of data. These models, as shown in table (2-2), took into account a variety of influencing factors, such as the lateral reinforcement's breadth, spacing, and yield strength, as well as the distribution of longitudinal steel and the consequent connection design. The ability of various containment models to avoid the actual experiments is tested in a comparative analysis. The investigation has been completed. According to the findings, nearly all models can accurately predict the stress-strain curve's rising

portion. It is common for models to underestimate or overestimate the test results when attempting to estimate the post-peak stress-strain curve. That's what the current analysis concludes: none of the currently known analytical models are able to effectively forecast the resulting stress-strain curve **[59]**.

Table (2-2) details Authors' and other researcher's specimens [59].

Reference	Section dimension (mm)	Number	Height (mm)	Gauge length (mm)	f'_c (MPa)	Transverse reinforcement			
						s (mm)	ρ_s (%)	f_{yh} (MPa)	Grid arrangement*
Holland (1995)	127 x 127	62	381	152.4	42.6-46.9	12.7-50.8	0.80-3.40	288-576	A, B, C
Hong (1997)	127 x 127	24	381	152.4	50.6-56.4	12.70-31.75	1.23-4.30	288-490	D, E , F
	356 x 356	6	1524	610	52.6-59.4	25.4-50.8	2.40-3.80	490	E, G
Lambert-Aikhionbare (1999)	356 x 356	10	1524	610	62-76	44-95	3.50-5.00	490	E, F
Authors (2010)	180 x 180	18	720	320	43.4	30-120	1.20-4.80	500	D, E, H, I

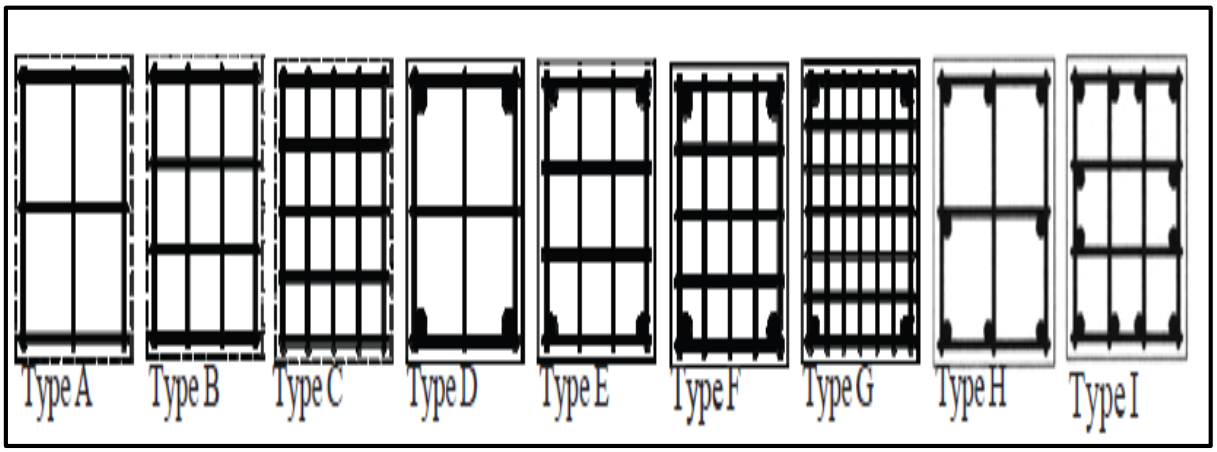

Fig (2-3) arrangements of WWF [59].

(El-kholy and Dahish, 2015), This paper presents work for the use of single expanded metal mesh layers combined in realistic configuration with specific volumetric relations as lateral reinforcement for short square reinforced concrete columns, in addition to standard tie reinforcement, this paper introduces a functional configuration consisting of a single extended metal mesh (EMM) sheet. When used as an extra lateral reinforcement for column specimens with a volumetric bond ratio q = 0.2714 percent, the findings showed that one Expanded Metal Mesh Sheet raised the ultimate load of Phase 2 by 11.02 percent and 18.55 percent compared to Phase 1 for Groups 1 and 2 as the plate (2-9). Expanded Metal Mesh (EMM) sheet combinations in functional configurations are explored in this research. By distorting more EMM layers and employing EMM with stronger mechanical characteristics, it is possible to obtain high ultimate load potential, improved ductility, larger volumetric reduction of the ties, and greater energy dissipation. Table (2-1) and figure (2-3) illustrated it **[60]**.

Plate (2-9) Reinforcement of column specimens [60]

(Khun et al., 2016), According to the most recent RC structure design guidelines, strong but ductile columns are preferred because they can tolerate large deformations without cracking. Segmental analysis of slender steel strapping, technically constrained columns subjected to eccentric stresses yielded novel parameters. It has been suggested that a new equivalent stress system and system depth factor equation be developed. This research proposed new criteria for the practical design of columns utilizing an enhanced Steel Strapping Tensioning Technique (SSTT) for circular high-strength concrete using a nominal curvature technique (HSC) as the fig. (2-4). Segmental analyses of thin, SSTT-confined columns subjected to eccentric loads yielded the new parameters. For SSTT-confined HSC columns, the nominal curvature technique yields conservative estimates of maximum axial load and small-scale column flexural resistance. Given the suitable stress-strain model, the suggested design approach may be used to columns of rectangular or square sections **[61]**.

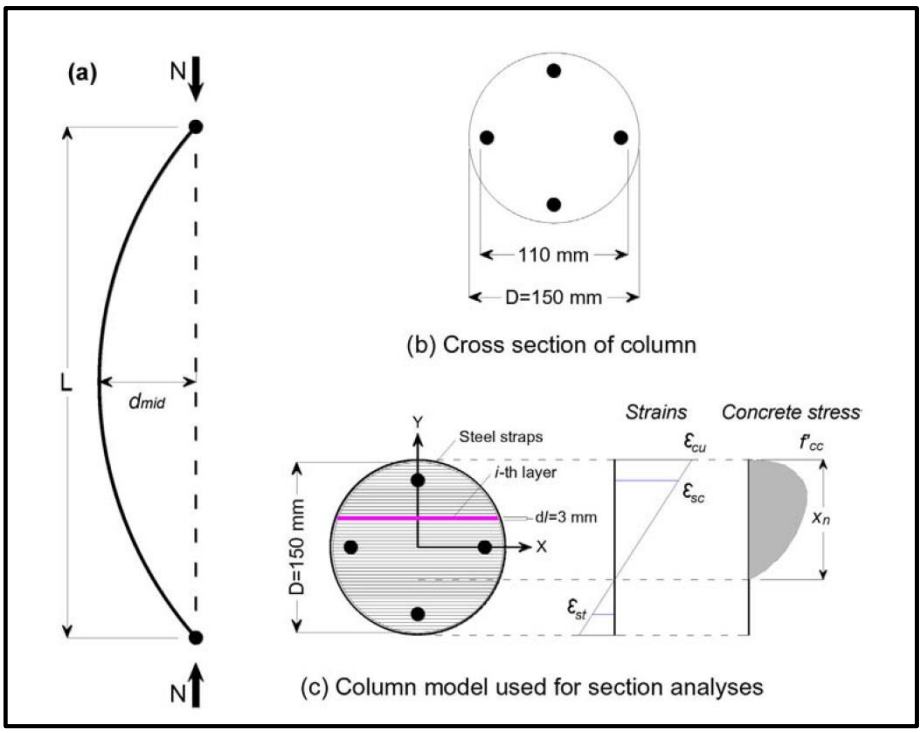

Fig (2-4) (a)This model has hinged ends, (b–c) and a theoretical segmented column model [61].

(Fatehi, 2018), Many buildings have to have their reinforced concrete (RC) columns rehabilitated, either as a result of structural defects requiring the columns to carry more loads than originally planned or as a result of natural wear and tear. Many nations throughout the globe currently employ steel caging for this purpose. Experiments to study the behavior of reinforced concrete columns under axial stresses with a steel jacket are reported in this research. Twelve identical (120x120) mm cross-section square reinforced concrete columns with a height of 1000 mm make up this research project. Steel angles and steel plates are increasingly being used in the construction sector to support reinforced concrete columns. experimenting The major goal of the test program is to gather data and information on the structural behavior and ultimate strength of reinforced concrete columns with steel jackets under axial compressive load in a series of twelve columns. Various theoretical models have been used to study axially constrained and unconfined systems. The study's main results are: Using an external steel jacket consisting of steel angles and plates in addition to horizontal battens to reinforce RC columns is legitimate and can raise the total load for all reinforcement instances from (42.2-121.7 percent) compared to unreinforced columns. In the first case of reinforcement utilizing an external steel jacket consisting of (4 steel angles of various sizes as [(1"x1"x1/8), "(1.25"x1.25"x3/16") and (1.5"x1.5"x3/16)] "at column corners connected by horizontal battens of dimensions (1") with a thickNess of 3 mm, the ultimate load is increased. Plate (2-10) showed the failure if the strengthened specimen **[62]**.

Plate (2-10) The failure pattern of strengthened column [62]

2.5: Strengthening by using TRM and FRP

(Colombo et al., 2011), study the behavior of the TRM material subjected to high temperatures. TRM material was used and a substance was composed of a mixture of (glass fabric and grind matrix). The purpose of the TRM sheets is to place the material in the direction of the driving force and also do not need to use a concrete cover of wear extent to get a lightweight member. One of the important things presented by the research was the time-dependent on the loss of strength in the case (AR-glass embedded cement base), as well as a good explanation about the behavior of the TRM with high temperatures. The Dimensions used equaled to (400x70x6) mm and two-dimensional with temperatures increase gradually (20,200,400,and600), then analyzed the residual mechanical properties after applied tensile strength and temperature. The outcomes of a 30 kN device carrying

capacity laboratory test. Depending on the(stress-strain) diagram of the examined specimens, the fig. (2-5) Showed it, at temperatures (20 and 200), the same curve is made up of three sections (non-linear response), Whereas at (600) temperatures the behavior of specimen brittle (linear). The first crack occurred at a temperature (20 and 200), These cracks occurred as a result of the shrinkage in the mortar. but at the (600) Sliding mortar **[63]**.

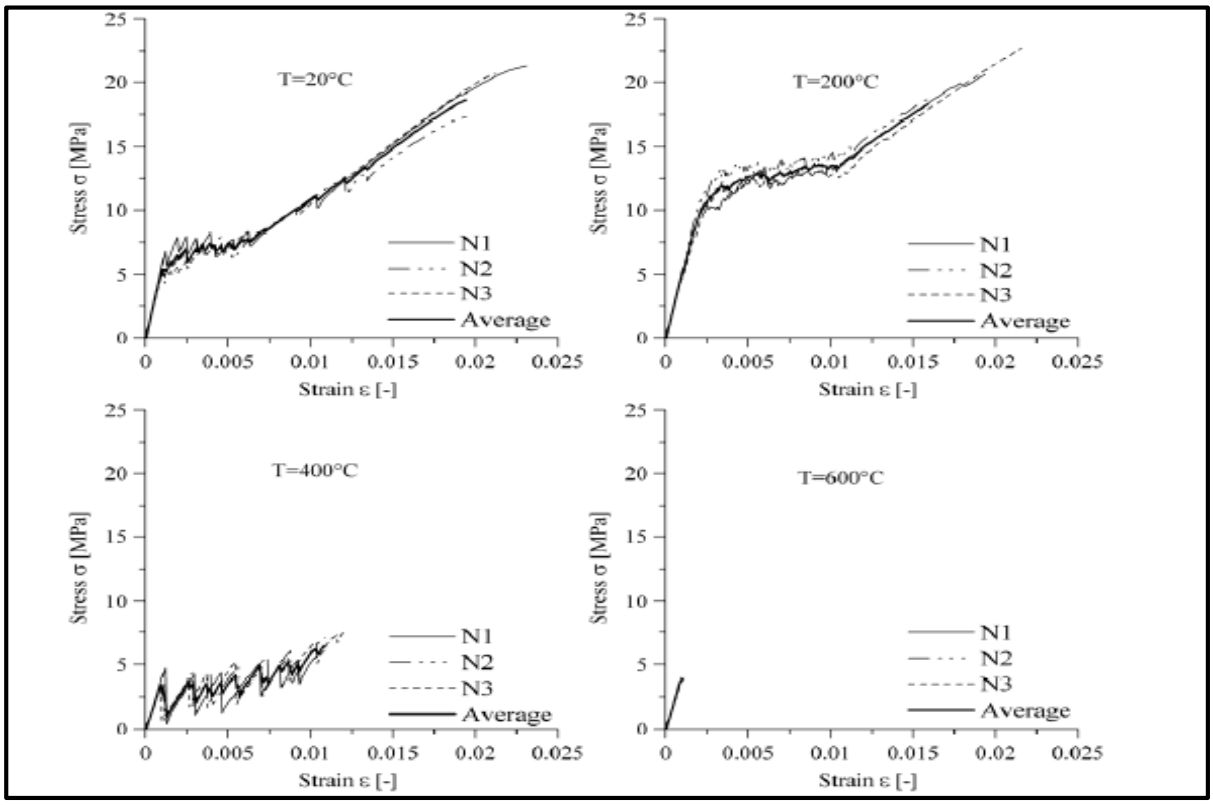

Fig (2-5) Load vs displacement curve in uniaxial tension at different temperatures[63]

(Raoof et al., 2016), a practical study on the cohesion between the TRM and concrete column, Where was used from (1-4)layers of TRM. When the concrete and TRM are bonded together, the bonding distance is around (50-450) mm. The laboratory equipment supplied a pressure to the concrete column equivalent to (15-30) MPa, which was measured in millimeters per second. The aim of the study was interconnectivity and cohesion between TRM and concrete columns. 80

models were created from square section and prism with dimensions (100x250) mm and the width of cohesion 80mm. Used the Carbon Textile with thickness about (0.095) mm for one layer, it was used TRM and covered with mortar. The laboratory examination was performed after completing the treatment of the specimens for a period of six weeks. Some of the previous studies have focused on the cohesion between (single-lap) shear tests. Whereas, the use of the (double-lap) is important in the case of using more than one layer. After the laboratory examination, the following was obtained. The effect of the cohesion length and the number of layers on the load carriers of the model, as in the use of the FRP. In the case of using (1-4) layers, the bonding length will be L_{eff}= (200-300) mm and for users (1-2) Adhesion increases with limits (450) mm Increasing the number of layers changes the shape of failure. As the specimens containing (1-2) layers of TRM failed with reason slippage textile fiber from the mortar. The specimens having three to four layers, on the other hand, failed due to the deboning of TRM from concrete. Plate (2-11) explained the method of application the TRM,**[64]**.

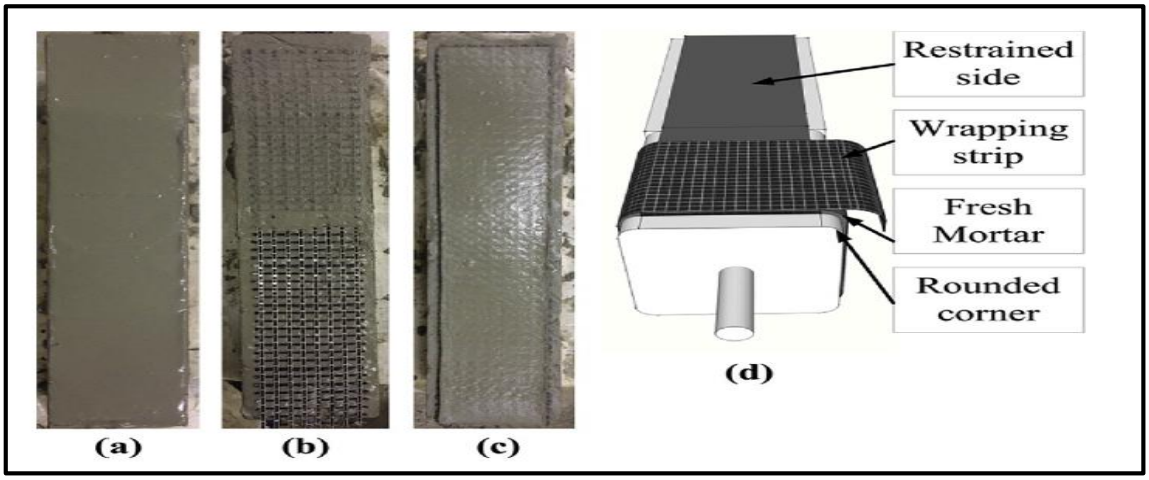

Plate (2-11) (a) Application of the first layer of mortar; (b) application of the first layer of textile layer into the mortar; (c) application of the final layer of mortar; and (d) wrapping with TRM jacket at the side of specimen under examination Test [64].

(Younis et al., 2017), A look into TRM's physical and chemical properties. This property is tensile strength. The use of a substance that is common in strengthening and improving the walls of the floors and the concrete structural members. The TRM was tested in the laboratory as the plate (2-12). 15 specimens were used from TRM of V with dimensions 410 mm length and 50 mm width and thickness of 10 mm. Three different types of this substance are also used (carbon, glass, polyparaphenylene). The research aims to add some data on the properties of TRM for the purpose of future use in repairing concrete installations. Code AC 434 was used to analyze the specimens. By using a stress-strain diagram for each TRM model as below. The results of the examination showed that (polyparaphenylene PBO) gives more cracks than others that is meant the failure in this type of more ductility **[65]**.

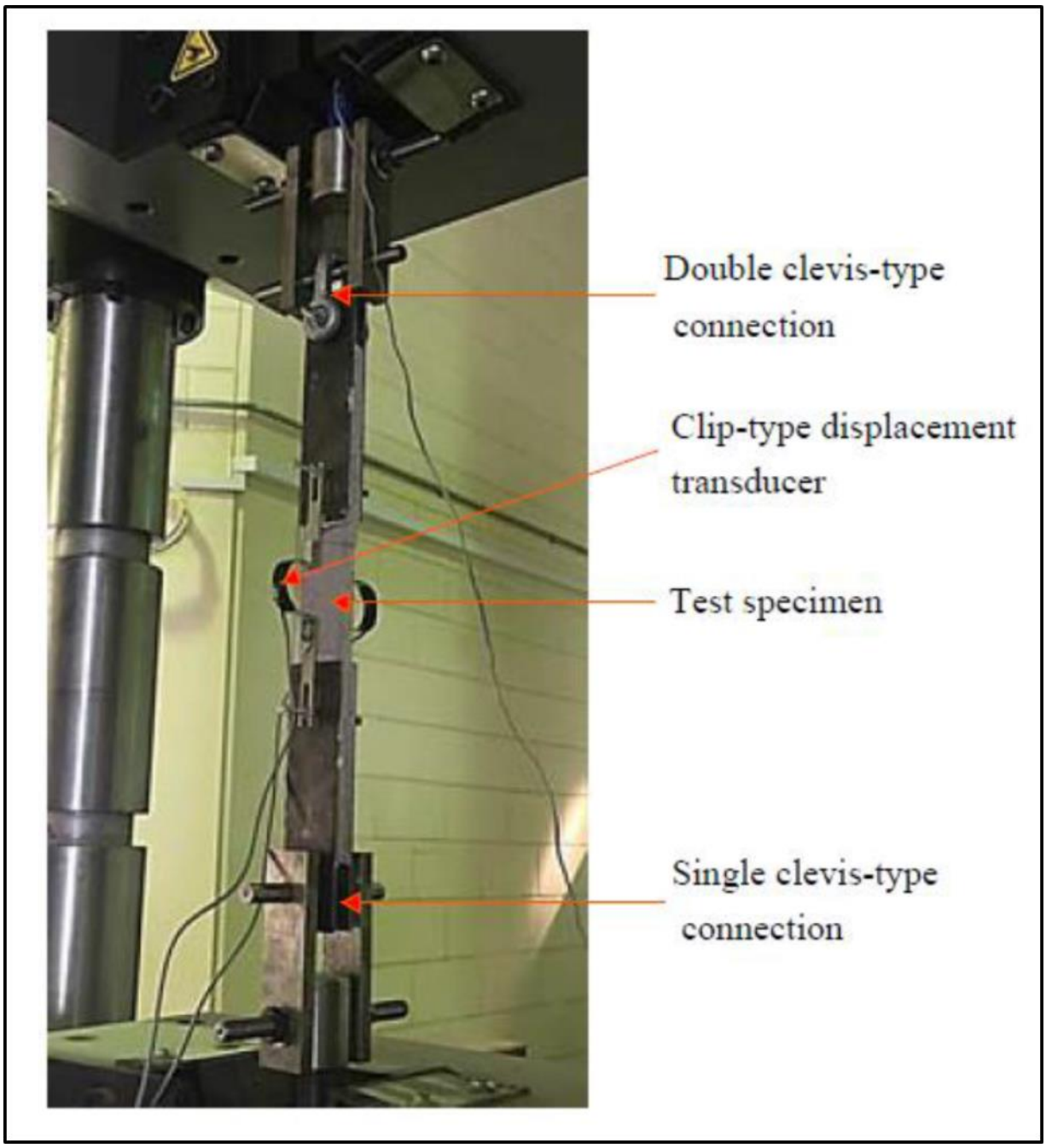

Plate (2-12) Test setup and instrumentation for the TRM tensile characterization test [65].

(Yin et al., 2019),The study of the behavior of the concrete columns under the influence of the eccentric pressure force with the use of a substance of TRM and PVA where TRM was textile reinforced mortar and PVA as polyvinyl alcohol. In this study, 9 specimens of concrete columns are used with the presence of corboles at the ends of columns. Concrete facilities often need to be reinforced, for many

reasons, including construction, environmental, or others., TRM is one of the suitable options for strengthening the concrete column. Where the columns were used concrete with dimensions (120x150x800) mm and corboles (120x250x200) mm, the testing device used applied a force of (7000) kN Where the column had to be loaded 35 mm eccentricity. With the use of a steel plate with a thickness of (10) to avoid failure at the ends. Also, the use of three layers of FRP at the corboles. Used 40 MPa as a compression concrete load for concrete. In contrast, the specimens with three to four layers failed because the TRM was deboned from the concrete. When the loads are increased, the load reaches the maximum the longitudinal cracks appeared at the edges of the sides and when you continue to increase the loading more effect, transverse cracks appear which were far from the load machine area. At the side loaded with compression stress, the specimen (C0) immediately collapsed. The specimens with strengthening by TRM in the initial loading stage, conduct the columns similar to the corresponding specimens without TRM. When the load reached (90%) of the maximum load, there were fewer cracks on one side. Continuing to applied loads caused failure TRM at the edges of the column. Textile reinforcements at mid-height have strengthened the column by (1-2) layers. During the compressive loads, concrete was removed from the fabric. The exhibited side cracks appeared on was tension stress, Reinforcement of the column with fabric textile causes delays in the concrete column, as well as improving the column deformations. In the event that the column is reinforced with three layers of TRM, the failure appeared at the upper edge of the TRM and the side cracks appeared at the side upper column as the plate (2-13). PVA had led to little improvement compared to TRM **[66]**.

Plate (2-13) Failure modes of columns [66]

2.6: Side opening

(Son et al., 2006), a research study that aims to know the amount of loss by resistance in the event of a side opening in the concrete column, as a result of the need for electrical and other services. If the side openings are not taken, in other words, there are openings during the design phase, or upon implementation, this may cause the building to collapse, as it clearly affects the resistance and hardness, due to a redistribution of the internal strength and

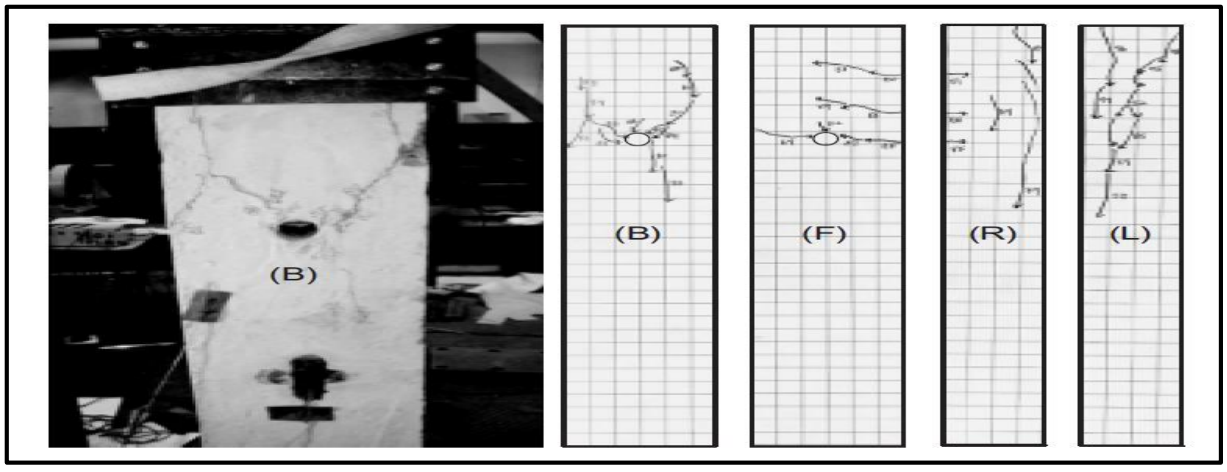

Plate (2-14) Typical cracking pattern for column [67]

bending. Where the nine columns were implemented, one from them as a control specimen and the dimension (200x300x1600) mm. The opening on the side was easily spotted. Due to the side opening's existence, the long columns become more unstable. The presence of the side opening reduced the column resistance and was proportional to the lost space. To avoid brittle failure, the column at the aperture on the side must be strengthened. Plate (2-14) showed the failure for the specimen **[67]**.

(Alsalim et al., 2017),investigate the behavior of structural concrete columns and subjected to axial loads and unidirectional bending, with a circular side opening in the column at the mid-height of the column. Where 20 columns were implemented in the laboratory with dimensions (150x150x900) mm as the fig (2-6). According to the specifications of the ACI 2014 code, the percentage of the side opening is no more than 4% in the cross-section Metal plates have been installed at the column's ends to protect the column from collapsing suddenly. The work was divided into two groups (A-B), where group (A) the eccentricity indirection parallel to the L-open, and group (B) the eccentricity indirection normal to the L-open. The sizes of the side aperture were (0,15,20, and 25). There was a 2000 kN. The machine is weighed down. The percentage of side opening under axial stress and eccentric (45-120mm) mm on specimens in group A was determined to be (0,10,13.33,16.67). As the results showed that the resistance is reduced due to reduced part exposed to compression. Also in the eccentric (45) mm the results showed when the eccentric ratio was (e/h=0.3) the column fail due to concrete reach to the ultimate strength, whereas the results with (120) mm showed the fail in the column due to bending stress. group (A) findings revealed a significant impact of the side opening due to the presence of all of the side opening in the compression zone. When the eccentric load was parallel to the side opening the column behaves better than the load was normal. The presence of the

side opening in the structural part, which was considered a weak area, affects its strength and stiffness **[68]**.

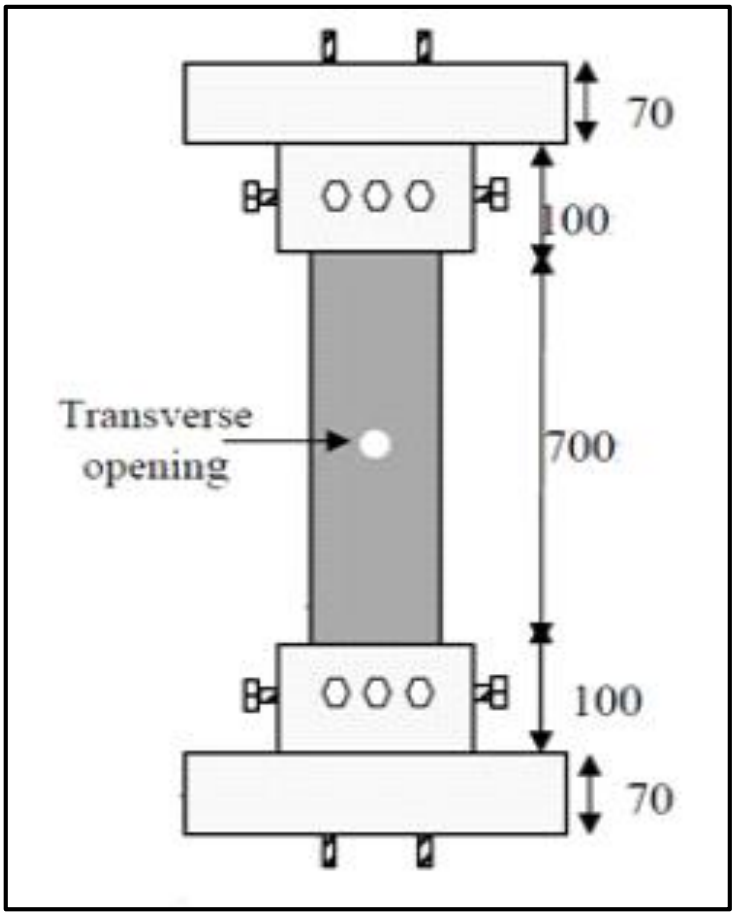

Fig (2-6) Specimen details and dimensions [68].

(Tahir et al., 2019), A look at the impact of columns with side apertures made of concrete. Where seven models of concrete columns were used, as the number of reference specimens reached two. Put the side hole in the third upper of the column. As the area of the side opening reached about 15% of the area of the side cross-section of the column, the axial force of the concrete columns was subjected to the purpose of examination. The implemented specimens were with dimensions of the square section (203 x 203) mm except for the specimen in CHS they were

with dimensions of (229 x 229) mm and that all models with a height of 1000 mm. also the result depicted below:

Column Nomenclature Detail of Options

- **CC Controlled Column without hole**
- **CH Standard Column with a hole**
- **CHS Column with a hole with an increased cross-sectional area**
- **CHA Column with a hole with an increased area of steel**
- **CHF Column with a hole with the increased strength of concrete**
- **CHFA Column with a hole with increased strength and steel**
- **CHP Column with a hole with MS Pipe**

Laboratory results indicated that the rise in column contact area or the increase in the concrete compression pressure did not have a clear effect on column ductility. The reference specimen ***(CC)*** showed the first cracking and longitudinally due to the split of the concrete at the corners of the column, with the continue of load the cracks reach to the middle of the specimen and the buckling of steel occurred before failure in the column. The reference specimen showed the first cracking and longitudinally due to the split of the concrete at the corners of the column, with the continuous load the cracks reach the middle of the specimen and the buckling of steel occurred before they fail in the column. The specimen ***(CH)*** showed the cracks formed as (X) shape around the opening as the plate (2-15). The horizontal crack occurred in the first stage of loading and the quarter of the upper column. Because of the increased stress in the side opening area, this region is more exposed to failure. Fig (2-7) illustrated the comparison between the strengthened specimens and the control **[69]**.

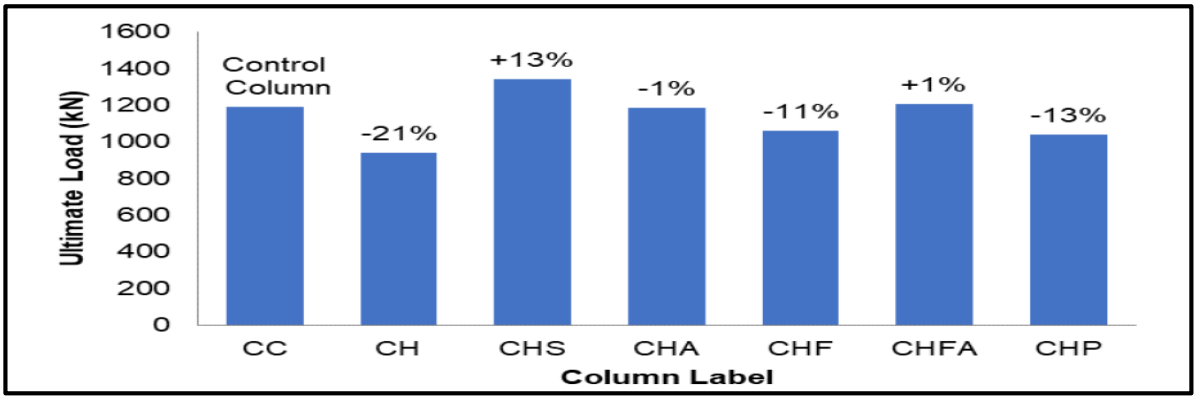

Fig (2-7) Comparison of average ultimate strengths of specimens with control [69].

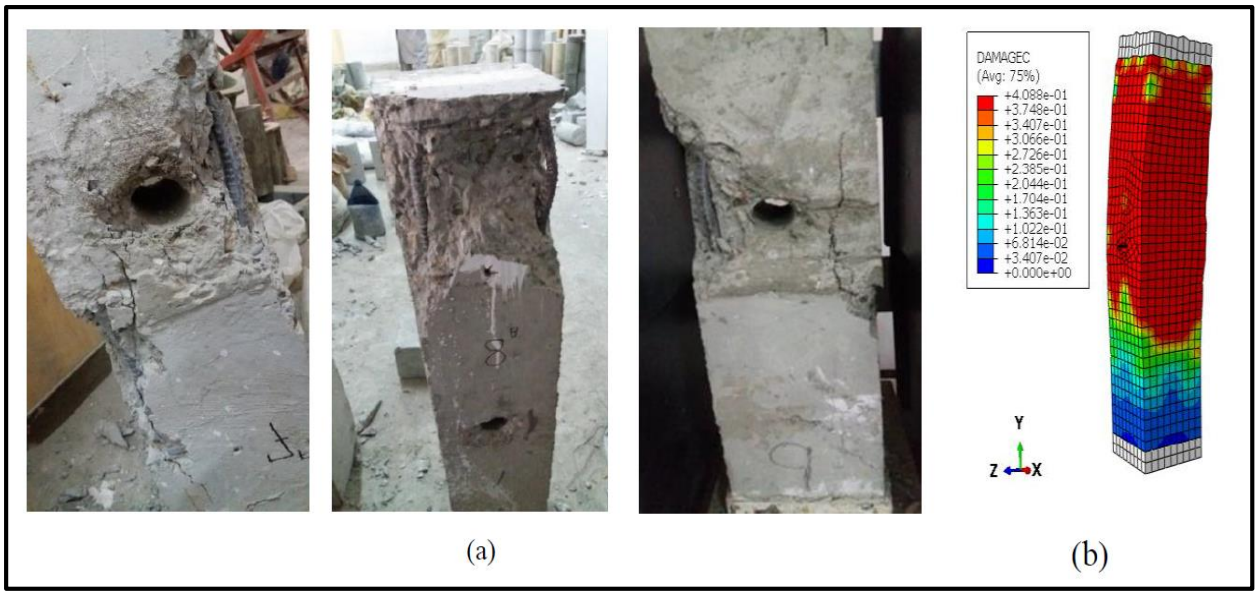

Plate (2-15) (a) Cracks pattern of three specimens of CH Columns after testing and (b) ABAQUS Cracks pattern [69].

References

[1] D. Liu, H. Huang, J. Zuo, K. Duan, Y. Xue, and Y. Li, "Experimental and numerical study on short eccentric columns strengthened by textile-reinforced concrete under sustaining load," 2017, doi: 10.1177/0731684417725396.

[2] H. Al-nimry and A. Soman, "Performance of FRP-Jacketed RC Columns under Axial-Flexural Loading," no. May 2019, pp. 1–5, 2018, doi: 10.15224/978-1-63248-150-4-45.

[3] M. N. S. Hadi, F. Asce, H. Karim, and M. N. Sheikh, "Experimental Investigations on Circular Concrete Columns Reinforced with GFRP Bars and Helices under Different Loading Conditions," pp. 1–12, 2011, doi: 10.1061/(ASCE)CC.1943-5614.0000670.

[4] M. N. S. Hadi, F. Asce, M. T. Jameel, and M. N. Sheikh, "Behavior of Circularized Hollow RC Columns under Different Loading Conditions," no. 1995, 2014, doi: 10.1061/(ASCE)CC.1943-5614.0000808.

[5] H. Qiang, D. Xiuli, Y. Zhou, and G. C. Lee, "Experimental study of hollow rectangular bridge column performance under vertical and cyclically bilateral loads," vol. 12, no. 3, pp. 433–445, 2013.

[6] F. Micelli and R. Modarelli, "Experimental and analytical study on properties affecting the behaviour of FRP-confined concrete," *Compos. Part B Eng.*, vol. 45, no. 1, pp. 1420–1431, 2013, doi: 10.1016/j.compositesb.2012.09.055.

[7] A. M. El-kholy and H. A. Dahish, "Improved confinement of reinforced concrete columns," *AIN SHAMS Eng. J.*, 2015, doi: 10.1016/j.asej.2015.06.002.

[8] M. N. S. Hadi, M. T. Jameel, and M. N. Sheikh, "Behavior of Circularized Hollow RC Columns under Different Loading Conditions," *J. Compos. Constr.*, vol. 21, no. 5, p. 04017025, 2017, doi: 10.1061/(asce)cc.1943-5614.0000808.

[9] I. A. S. Al- Shaarbaf, M. J. H. Al-zubaidi, and E. A. A. Al- Zaidy, "Effect of Hollowing Ratio on the Behavior of Hollow Self-Compacting Reinforced Concrete Slender Column Under Eccentric Loading," *Int. J. Eng. Technol.*, vol. 7, no. 4.20, p. 390, 2018, doi: 10.14419/ijet.v7i4.20.26141.

[10] A. M. Sahi and M. S. A. Ali, “Experimental Study of Hollow Slender Reinforced Concrete Columns Subjected to Eccentric Loads,” *Civ. Environ. Eng.*, vol. 17, no. 1, pp. 303–317, 2021, doi: 10.2478/cee-2021-0032.

[11] Y. Kusumawardaningsih and M. N. S. Hadi, “Comparative behaviour of hollow columns confined with FRP composites,” *Compos. Struct.*, vol. 93, no. 1, pp. 198–205, 2010, doi: 10.1016/j.compstruct.2010.05.020.

[12] R. Ismail, R. S. M. Rashid, F. A. A. Zakwan, and F. Hejazi, “Experimental study of circular hollow reinforced concrete column strengthened with partial Carbon Fibre Reinforced Polymer (CFRP) confinement,” *IOP Conf. Ser. Mater. Sci. Eng.*, vol. 615, no. 1, 2019, doi: 10.1088/1757-899X/615/1/012075.

[13] P. Cassese, P. Ricci, and G. M. Verderame, “Experimental study on the seismic performance of existing reinforced concrete bridge piers with hollow rectangular section,” *Eng. Struct.*, vol. 144, pp. 88–106, 2017, doi: 10.1016/j.engstruct.2017.04.047.

[14] M. N. S. Hadi and T. D. Le, “Behaviour of hollow core square reinforced concrete columns wrapped with CFRP with different fibre orientations,” *Constr. Build. Mater.*, vol. 50, pp. 62–73, 2014, doi: 10.1016/j.conbuildmat.2013.08.080.

[15] T. H. Han, N. H. Lim, S. Y. Han, J. S. Park, and Y. J. Kang, “Nonlinear concrete model for an internally confined hollow reinforced concrete column,” vol. 9831, no. 6, pp. 429–440, 2008, doi: 10.1680/macr.2008.60.6.429.

[16] He, Chunbao, and Jun-Jie Zeng. "Fiber-Reinforced Polymer-Confined Non-Circular Columns with Shape Modification: A Comprehensive Review." Polymers 14.3 (2022): 564.

[17] M. N. S. Hadi and T. D. Le, “Behaviour of hollow core square reinforced concrete columns wrapped with CFRP with different fibre orientations,” vol. 50, pp. 62–73, 2014, doi: 10.1016/j.conbuildmat.2013.08.080.

[18] M. Nematzadeh, M. Mousavimehr, J. Shayanfar, and M. Omidalizadeh, “Eccentric compressive behavior of steel fiber-reinforced RC columns strengthened with CFRP wraps: Experimental investigation and analytical modeling,” *Eng. Struct.*, vol. 226, no. April 2020, p. 111389, 2021, doi: 10.1016/j.engstruct.2020.111389.

[19] Z. C. Tetta, L. N. Koutas, and D. A. Bournas, “Shear strengthening of full-scale RC T-beams using textile-reinforced mortar and textile-based anchors,” *Compos. Part B*, 2016, doi: 10.1016/j.compositesb.2016.03.076.

[20] A. Younis, U. A. Ebead, and K. C. Shrestha, “Tensile Characterization of Textile Reinforced Mortar Tensile Characterization of Textile Reinforced Mortar,” no. July, 2017, doi: 10.14455/ISEC.res.2017.155.

[21] S. P. Yin, X. Q. Hu, and Y. T. Hua, “Compression performance and bearing capacity calculation model of small-eccentricity columns strengthened with textile-reinforced mortar (TRM),” vol. 69, no. 335, pp. 1–11, 2019.

[22] Y. Hou, “Impact damage assessment in orthotropic CFRP laminates using nonlinear Lamb wave : Experimental and numerical investigations Impact damage assessment in orthotropic CFRP laminates using nonlinear Lamb wave : Experimental and numerical investigations,” no. January, 2020, doi: 10.1016/j.compstruct.2020.111869.

[23] M. Fossetti, F. Basone, G. D. Arenzo, G. Macaluso, and A. F. Siciliano, “FRP-Confined Concrete Columns : A New Procedure for Evaluating the Performance of Square and Circular Sections,” vol. 2018, 2018.

[24] L. N. Koutas, Z. Tetta, D. A. Bournas, T. C. Triantafillou, and M. Asce, “Strengthening of Concrete Structures with Textile Reinforced Mortars : State-of- Strengthening of Concrete Structures with Textile Reinforced Mortars : State-of-the-Art Review,” no. October 2018, 2019, doi: 10.1061/(ASCE)CC.1943-5614.0000882.

[25] S. M. Raoof, L. N. Koutas, and D. A. Bournas, “Bond between textile-reinforced mortar (TRM) and concrete substrates : Experimental investigation Bond between textile-reinforced mortar (TRM) and concrete substrates : Experimental investigation,” *Compos. Part B*, vol. 98, no. May, pp. 350–361, 2016, doi: 10.1016/j.compositesb.2016.05.041.

[26] T. C. Triantafillou, C. G. Papanicolaou, and P. Zissimopoulos, “Concrete Confinement with Textile-Reinforced Mortar Jackets Concrete Confinement with Textile-Reinforced Mortar Jackets,” no. January 2006, 2018.

[27] A. Kazemnadi, “Predicting the Compressive Stress–Strain Curve of FRP-Confined Concrete Column Considering the Variation of Poisson’s Ratio,” *Int. J. Civ. Eng.*, doi: 10.1007/s40999-020-00550-3.

[28] J. Park, S. K. Park, and S. Hong, “Experimental Study of Flexural Behavior of Reinforced Concrete Beam Strengthened with Prestressed Textile - Reinforced

Mortar," 2020, doi: 10.3390/ma13051137.

[29] Othman, Zrar Sedeeq, and Ahmed Heidayet Mohammad. "Behaviour of eccentric concrete columns reinforced with carbon fibre-reinforced polymer bars." Advances in Civil Engineering 2019 (2019).

[30] J. J. Zeng, W. Y. Gao, Z. J. Duan, Y. L. Bai, Y. C. Guo, and L. J. Ouyang, "Axial compressive behavior of polyethylene terephthalate/carbon FRP-confined seawater sea-sand concrete in circular columns," *Constr. Build. Mater.*, vol. 234, 2020, doi: 10.1016/j.conbuildmat.2019.117383.

[31] Y. Guo, W. Gao, J. Zeng, Z. Duan, X. Ni, and K. Peng, "Compressive behavior of FRP ring-confined concrete in circular columns : Effects of specimen size and a new design-oriented stress-strain model," *Constr. Build. Mater.*, vol. 201, pp. 350–368, 2019, doi: 10.1016/j.conbuildmat.2018.12.183.

[32] X. Li, H. Xie, M. Yan, H. Gou, G. Zhao, and Y. Bao, "Eccentric Compressive Behavior of Reinforced Concrete Columns Strengthened Using Steel Mesh Reinforced Resin Concrete," pp. 1–22, 2018, doi: 10.3390/app8101827.

[33] X. Liang, D. Ph, S. Sritharan, D. Ph, and M. Asce, "Effects of Confinement in Circular Hollow Concrete Columns," vol. 144, no. 9, pp. 1–13, 2018, doi: 10.1061/(ASCE)ST.1943-541X.0002151.

[34] S. S. Khamees, M. M. Kadhum, and N. A. Alwash, "Experimental and numerical investigation on the axial behavior of solid and hollow SIFCON columns," *SN Appl. Sci.*, vol. 2, no. 6, 2020, doi: 10.1007/s42452-020-2907-9.

[35] O. S. Alajarmeh, A. C. Manalo, B. Benmokrane, W. Karunasena, W. Ferdous, and P. Mendis, "TECHNICAL PAPER A New Design-Oriented Model of Glass Fiber-Reinforced Polymer-Reinforced Hollow Concrete Columns," no. 117, 2020, doi: 10.14359/51720204.

[36] Y. L. Suku and E. Flores, "Modeling and Analysis of the Effect of Holes in Reinforced Concrete Column Structures Modeling and Analysis of the Effect of Holes in Reinforced Concrete Column Structures," no. January, 2020, doi: 10.22146/jcef.48722.

[37] S. İpek and E. Mete, "Nonlinear finite element analysis of double skin composite columns subjected to axial loading," 2020, doi: 10.1007/s43452-020-0012-x.

[38] P. Cassese, P. Ricci, and G. M. Verderame, "Experimental study on the seismic

performance of existing reinforced concrete bridge piers with hollow rectangular section," vol. 144, pp. 88–106, 2017, doi: 10.1016/j.engstruct.2017.04.047.

[39] G. Kalogeropoulos and A. Tsonos, "Cyclic Performance of RC Columns with Inadequate Lap Splices Strengthened with CFRP Jackets," 2020.

[40] P. Cassese, A. Bonati, M. T. De Risi, and G. M. Ver-, "Which capacity models for shear-critical reinforced concrete hollow piers ? Which capacity models for shear-critical reinforced concrete hollow piers ?," no. January 2020, 2019.

[41] O. S. Alajarmeh, A. C. Manalo, B. Benmokrane, K. Karunasena, W. Ferdous, and P. Mendis, "Hollow concrete columns : Review of structural behavior and new designs using GFRP reinforcement," vol. 203, no. October 2019, 2020.

[42] Q. Han, J. Wen, X. Du, and J. Jia, "Journal of Reinforced Plastics and Composites," 2014, doi: 10.1177/0731684414557716.

[43] S. Review, S. Raza, M. K. I. Khan, S. J. Menegon, and H. Tsang, "Strengthening and Repair of Reinforced Concrete Columns by Jacketing : sustainability Strengthening and Repair of Reinforced Concrete Columns by Jacketing : State-of-the-Art Review," no. June, 2019, doi: 10.3390/su11113208.

[44] F. Colomb, H. Tobbi, E. Ferrier, and P. Hamelin, "Seismic retrofit of reinforced concrete short columns by CFRP materials," *Compos. Struct.*, vol. 82, no. 4, pp. 475–487, 2008, doi: 10.1016/j.compstruct.2007.01.028.

[45] Freberg, Laura A. An Introduction to Applied Behavioral Neuroscience: Biological Psychology in Everyday Life. Taylor & Francis, 2022.

[46] Kadid, A., and A. Boumrkik. "Pushover analysis of reinforced concrete frame structures." (2008): 47-59.

[47] M. Z. Naser, R. A. Hawileh, and J. A. Abdalla, "Fiber-reinforced polymer composites in strengthening reinforced concrete structures : A critical review," *Eng. Struct.*, vol. 198, no. June, p. 109542, 2019, doi: 10.1016/j.engstruct.2019.109542.

[48] B. Doran, H. O. Koksal, and T. Turgay, "Nonlinear finite element modeling of rectangular / square concrete columns confined with FRP," *Mater. Des.*, vol. 30, no. 8, pp. 3066–3075, 2009, doi: 10.1016/j.matdes.2008.12.007.

[49] F. Micelli and R. Modarelli, "Experimental and analytical study on properties affecting the behaviour of FRP-confined concrete," *Compos. Part B Eng.*, vol. 45, no. 1, pp. 1420–1431, 2013, doi: 10.1016/j.compositesb.2012.09.055.

[50] M. Z. Afifi, H. M. Mohamed, and B. Benmokrane, "Axial Capacity of Circular Concrete Columns Reinforced with GFRP Bars and Spirals," *J. Compos. Constr.*, vol. 18, no. 1, p. 04013017, 2014, doi: 10.1061/(asce)cc.1943-5614.0000438.

[51] J. Fitzwilliam and L. Bisby, "Slenderness effects on circular FRP-wrapped reinforced concrete columns," *Compos. Civ. Eng. CICE 2006*, vol. 14, no. June, pp. 499–502, 2020.

[52] I. Congress, "Flexural Behaviour of RC Hollow Columns Confined with," *Test*, no. January, pp. 1–12, 2006.

[53] Y. Kusumawardaningsih and M. N. S. Hadi, "Comparative behaviour of hollow columns confined with FRP composites," *Compos. Struct.*, vol. 93, no. 1, pp. 198–205, 2010, doi: 10.1016/j.compstruct.2010.05.020.

[54] H. Qiang, D. Xiuli, Y. Zhou, and G. C. Lee, "Experimental study of hollow rectangular bridge column performance under vertical and cyclically bilateral loads," vol. 12, no. 3, pp. 433–445, 2013.

[55] P. Cassese, P. Ricci, and G. M. Verderame, "Experimental study on the seismic performance of existing reinforced concrete bridge piers with hollow rectangular section," *Eng. Struct.*, vol. 144, pp. 88–106, 2017, doi: 10.1016/j.engstruct.2017.04.047.

[56] R. Ismail, R. S. M. Rashid, F. A. A. Zakwan, and F. Hejazi, "Experimental study of circular hollow reinforced concrete column strengthened with partial Carbon Fibre Reinforced Polymer (CFRP) confinement," *IOP Conf. Ser. Mater. Sci. Eng.*, vol. 615, no. 1, 2019, doi: 10.1088/1757-899X/615/1/012075.

[57] R. Jamatia and A. Deb, "FRP confined hollow concrete columns under axial compression: A comparative assessment," *Compos. Struct.*, vol. 236, no. July 2019, 2020, doi: 10.1016/j.compstruct.2020.111857.

[58] P. A. Calderón, J. M. Adam, S. Ivorra, F. J. Pallarés, and E. Giménez, "Design strength of axially loaded RC columns strengthened by steel caging," *Mater. Des.*, vol. 30, no. 10, pp. 4069–4080, 2009, doi: 10.1016/j.matdes.2009.05.014.

[59] B. Kusuma and P. Suprobo, "The Twelfth East Asia-Pacific Conference on

Structural Engineering and Construction INVESTIGATION OF STRESS-STRAIN MODELS FOR CONFINEMENT OF CONCRETE BY Welded Wire FABRIC," vol. 14, pp. 2031–2038, 2011, doi: 10.1016/j.proeng.2011.07.255.

[60] A. M. El-kholy and H. A. Dahish, "Improved confinement of reinforced concrete columns," *AIN SHAMS Eng. J.*, 2015, doi: 10.1016/j.asej.2015.06.002.

[61] C. Khun, A. Zawawi, R. Garcia, W. Omar, K. Pilakoutas, and M. Azimi, "Nominal Curvature Design of Circular HSC Columns Con fi ned with Post-tensioned Steel Straps," *ISTRUC*, vol. 7, pp. 25–32, 2016, doi: 10.1016/j.istruc.2016.04.002.

[62] Makki, Ragheed Fatehi, and Salah Talib Nimnim. "Rehabilitation of structural columns by using steel angles." International Journal of Scientific and Engineering Research 1.6 (2015): 981-987.

[63] I. Colombo, M. Colombo, A. Magri, and G. Zani, "Textile Reinforced Mortar at High Temperatures Textile Reinforced Mortar at High Temperatures," no. May 2014, 2011, doi: 10.4028/www.scientific.net/AMM.82.202.

[64] S. M. Raoof, L. N. Koutas, and D. A. Bournas, "Bond between textile-reinforced mortar (TRM) and concrete substrates : Experimental investigation Bond between textile-reinforced mortar (TRM) and concrete substrates : Experimental investigation," *Compos. Part B*, vol. 98, no. May, pp. 350–361, 2016, doi: 10.1016/j.compositesb.2016.05.041.

[65] A. Younis, U. A. Ebead, and K. C. Shrestha, "Tensile Characterization of Textile Reinforced Mortar Tensile Characterization of Textile Reinforced Mortar," no. July, 2017, doi: 10.14455/ISEC.res.2017.155.

[66] S. P. Yin, X. Q. Hu, and Y. T. Hua, "Compression performance and bearing capacity calculation model of small-eccentricity columns strengthened with textile-reinforced mortar (TRM)," vol. 69, no. 335, pp. 1–11, 2019.

[67] K. Son, K. Pilakoutas, and K. Neocleous, "Behaviour of concrete columns with drilled holes," vol. 9831, no. 7, pp. 411–419, 2006.

[68] AL-Shaarbaf, Ihsan AS, Abbas AbdulMajeed Allawi, and Nabeel H. AlSalim. "Strength of Reinforced Concrete Columns with Transverse Openings." Journal of Engineering 23.10 (2017): 114-133.

[69] M. F. Tahir, F. Shabbir, and A. Ahmad, “Experimental and Numerical Investigation of Opening on Load Carrying Capacity of RC Columns Iranian Journal of Science and Technology , Transactions of Civil Engineering Experimental and Numerical Investigation of Opening on Load Carrying Capacity of RC C,” no. December, 2019.

[70] ACI COMMITTEE. Building code requirements for structural concrete (ACI 318-08) and commentary.

[71] R. Abokwiek, J. A. Abdalla, R. A. Hawileh, and T. El Maaddawy, “RC Columns Strengthened with NSM-CFRP Strips and CFRP Wraps under Axial and Uniaxial Bending: Experimental Investigation and Capacity Models,” J. Compos. Constr., vol. 25, no. 2, p. 04021009, 2021, doi: 10.1061/(asce)cc.1943-5614.0001117.

[72] ASTM E8, “ASTM E8/E8M standard test methods for tension testing of metallic materials 1,” Annu. B. ASTM Stand. 4, no. C, pp. 1–27, 2010, doi: 10.1520/E0008.

[73] X. Li, H. Xie, M. Yan, H. Gou, G. Zhao, and Y. Bao, “applied sciences Eccentric Compressive Behavior of Reinforced Concrete Columns Strengthened Using Steel Mesh Reinforced Resin Concrete,” 2018, doi: 10.3390/app8101827.

[74] EFNARC, “The European Guidelines for Self-Compacting Concrete,” Eur. Guidel. Self Compact. Concr., no. May, p. 63, 2005, [Online]. Available: http://www.efnarc.org/pdf/SCCGuidelinesMay2005.pdf.

[75] BS EN 12350-2: 2009. "Testing fresh concrete. Slump-test." National Standards Authority of Ireland (2009).

[76] British Standard, “Testing Concrete,” Constr. Stand., vol. 2, no. 2, pp. 1–14, 1983.

[77] C. C. Test, T. Drilled, and C. Concrete, “Standard Test Method for Flexural Strength of Concrete (Using Simple Beam with Third-Point Loading) 1,” Hand, vol. C78-02, no. C, pp. 1–4, 2010, doi: 10.1520/C0078.

[78] ASTM C469-02, “Standard Test Method for Static Modulus of Elasticity and Poisson’s Ratio of Concrete in Compression,” ASTM Stand. B., vol. 04, pp. 1–5, 2002, [Online]. Available: http://portales.puj.edu.co/wjfajardo/mecanica de solidos/laboratorios/astm/C469.pdf.

[79] Y. Wei, Y. Xu, G. Wang, X. Cheng, and G. Li, “Influence of the Cross-Sectional Shape and Corner Radius on the Compressive Behaviour of Concrete Columns Confined by,” 2022.

[80] M. Usman, M. Yaqub, A. Ahmad, and M. Usman, “Advance repairing technique for enhancement of stiffness of post - heated concrete cylinders,” Asian J. Civ. Eng., vol. 22, no. 4, pp. 689–700, 2021, doi: 10.1007/s42107-020-00340-1.

[81] J. J. Zeng, G. Lin, J. G. Teng, and L. J. Li, “Behavior of large-scale FRP-con fi ned rectangular RC columns under axial compression,” vol. 174, no. November 2017, pp. 629–645, 2018, doi: 10.1016/j.engstruct.2018.07.086.

[82] Test, Mortar. "For each mix required, according to ASTM C 109/C 109M for compressive strength." ASTM C 1506.

[83] Soudki, K., and T. Alkhrdaji. "Guide for the design and construction of externally bonded FRP systems for strengthening concrete structures (ACI 440.2 R-02)." Structures Congress 2005: Metropolis and Beyond. 2005.

[84] A. Kumar et al., “Prediction of FRCM – Concrete Bond Strength with Machine Learning Approach,” pp. 1–25, 2022.

[85] J. Zhou, W. Lin, S. Guo, J. Zeng, and Y. Bai, “Behavior of FRP-confined FRP spiral reinforced concrete square columns (FCFRCs) under axial compression,” J. Build. Eng., vol. 45, no. October 2021, p. 103452, 2022, doi: 10.1016/j.jobe.2021.103452.

[86] M. H. Hameed et al., “Enhancing the strength of reinforced concrete columns using steel embedded tubes,” Mech. Adv. Mater. Struct., vol. 0, no. 0, pp. 1–16, 2020, doi: 10.1080/15376494.2020.1847373.

[87] J. Y. Zhu et al., “FRP-Confined Square Concrete Columns with Section Curvilinearization under Axial Compression,” vol. 24, no. 1993, pp. 1–13, 2020, doi: 10.1061/(ASCE)CC.1943-5614.0000999.

[88] M. H. Lai, M. T. Chen, F. M. Ren, and J. C. M. Ho, “Thin-Walled Structures Uni-axial behaviour of externally confined UHSCFST columns,” vol. 142, no. January, pp. 19–36, 2019, doi: 10.1016/j.tws.2019.04.047.

[89] H. Suliman, A. Nimry, R. Amer, and A. Rabadi, “Axial – Flexural Interaction in FRP - Wrapped RC Columns,” Int. J. Concr. Struct. Mater., 2019, doi: 10.1186/s40069-019-0366-8.

[90] A. M. Sahi and M. S. A. Ali, “Experimental Study of Hollow Slender Reinforced Concrete Columns Subjected to Eccentric Loads,” *Civ. Environ. Eng.*, vol. 17, no. 1, pp. 303–317, 2021, doi: 10.2478/cee-2021-0032.

Republic of Iraq
Ministry of Higher Education and Scientific Research
University of Babylon
College of Engineering
Civil Engineering Department

Structural behavior of hollow core reinforced concrete columns confined with textile reinforced mortar (TRM) and /or fiber reinforced polymer (FRP) jackets

A Dissertation
Submitted to the College of Engineering of the University of Babylon
in Partial Fulfillment of the Requirements for the Degree of Doctor of Philosophy in Civil Engineering
(Structure)

By

Waleed Khaleel Nayel

(B.Sc. in Civil Engineering 2005)

(M.Sc. in Civil Engineering 2017)

Supervised by

Assist.Prof. Dr. Muhammad Jawad Kadhim

2022

اللَّهُ الَّذِي رَفَعَ السَّمَاوَاتِ بِغَيْرِ عَمَدٍ تَرَوْنَهَا ۖ ثُمَّ اسْتَوَىٰ عَلَى
الْعَرْشِ ۖ وَسَخَّرَ الشَّمْسَ وَالْقَمَرَ ۖ كُلٌّ يَجْرِي لِأَجَلٍ مُسَمًّى ۚ
يُدَبِّرُ الْأَمْرَ يُفَصِّلُ الْآيَاتِ لَعَلَّكُم بِلِقَاءِ رَبِّكُمْ تُوقِنُونَ

صدق الله العلي العظيم

سورة الرعد (الآية2)

ACKNOWLEDGMENTS

It is with great pleasure that I express my deepest sense of gratitude to my Asst Prof**. Dr. Muhammad Jawad Kadhim** for his expert guidance and support for the research. His encouraging attitude and help was very valuable.

I would also like to express my thanks to faculty members, my classmates and all my friends for their support.

Nothing would have been possible without the support of my family members, who have been backing me throughout my life. Special thanks are given to my father and the spirit of my mother my Lord forgives her and dwell her in Paradise, who was a constant sense of inspiration and whose blessing made me achieve what I aspired. All thanks are given to my wonderful wife, children, brothers, and dear sister, all thanks to the people who supported me.

I would like to express my gratitude to all people behind the screen who helped me.

All thanks are given to people who supported me.

TABLE OF CONTENTS

LIST OF FIGURES

LIST OF PLATES

LIST OF TABLES

Abbreviations

Abbreviation	Description
2D	Two dimensions
3D	Three dimensions
ABAQUS	Finite element package
ACI	American Concrete Institute
AEUDRL	Actual uniformly distributed repeated load
ASTM	American Society for Testing and Materials
BS	British Standard
BSI	British Standard Institute
c/c	Center to center
CFRP	Carbon fiber reinforced polymer
TRM	Textile reinforced mortar
e.g	For example
Eq.	Equation
et al.	And others
etc.	To the end
Exp.	Experimental
FEA	Finite element analysis
FEM	Finite element method
GPa	Giga Pascal (equal to $1000\times N/mm^2$ (MPa))
HRWRA	High range water reducing admixture
i.e	In other word
IQS	Iraqi Quality Standardization
kg	Kilogram
m	Meter
max.	Maximum
min.	Minimum
mm	Millimeter
MPa	Mega Pascal (MN/m^2)
No.	Number (issue)
NSC	Normal strength concrete
SCC	Self-compacted concrete
SGC	Concrete strain gauge
SGS	Steel strain gauge

CHAPTER 3-EXPERIMENTAL WORK

3.1 Introduction

In this chapter , the behavior of hollow concrete column subjected to concentric and eccentric loading with using external strengthening by using (CFRP or TRM). At first, preparing and testing, the necessary equipment and materials composed in this research such as (cement, sand, gravel, steel rebars, and admixture) and manufacturing the molds (steel plate and plywood), as well as the strain gauge for concrete and rebars reinforcement. In this study, two different types of concrete columns are employed, depending on the type of loading (concentric or eccentric) as the plates (3.1) and (3.2). The steel reinforcement configuration conventional design, which met the basic criteria. When developing an RC column, the ACI 318 standard is used. There are 32 columns in this group. divided into three groups according to the type of loading (concentric loading or eccentric loading) and the strengthening by (CFRP or TRM), which had the same features the outside of each column's cross section was (150 x 150) mm, and its height was 900 mm.

Furthermore, the interior hole (50mm x 50mm), the level of the hole established in the middle zone of the column, is equal to (600mm). According to the minimum specifications of the ACI 318[70], 4 rebars of (Dia. 8mm) were obtained to apply as it refers to the main column rebar, and (Dia. 6mm) spaced at 100mm was used as the stirrups reinforcements excluding top and bottom the transverse in this zone near to the 50mm to avoid sudden failure at the ends of columns. So that could estimate the column's theoretical load, an analysis is performed to determine how much load may be applied to an unconfined concrete column. The theoretical load was calculated using the ACI 318 code and the following equation Eq(3-1)[71]:

$$P_{no} = \begin{cases} f'_c(A_g - A_{st}) + A_{st}f_{so} & \text{Unconfined} \\ f'_{cc}(A_g - A_{st}) + A_{st}f_{sc} & \text{CFRP Confined} \end{cases} \quad \ldots\ldots\ldots (3.1)$$

In Equation (3.1), there is a 25 MPa limit for concrete compression after treatment time of 4 weeks, and also a 22500 mm^2 cross-sectional area (Ag), that was a total of 200.96 mm^2 for 4 rebars with diameter #8. The steel rebar has a diameter (8) mm and (6) mm the yield strength is measured to be (507) N/mm^2 and (486.5) N/mm^2, respectively and with elongation about (24.9) mm , and (11.2) mm, respectively. The column's failure load was calculated using these parameters. There is a load of (610) kN recorded.

Plate (3.1) specimens subjected to concentric loading

Plate (3.2) specimens subjected to eccentric loading

3.2 Proposed Matrix

There are 32 hollow concrete columns arranged in three groups in the proposed matrix. Control columns are used in the first set of (8) unconfined columns, these eight models containing the same concrete property has the type of self-compacted concrete (SCC) divided as the table (3.1) below: -

Table (3.1) control specimen

Control specimens	
CC-CO-S	CC-CON-Cir.O
CC-CO-H	CC-CON-Squ.O
CC-ECC-90	CC-ECC-Cir.O
CC-ECC-60	CC-ECC-Squ.O

The specimen with the label (CC-CO-S) defines as a control column with concentric loading for a solid column, the specimen with the label (CC-CO-H), define as a control column with concentric loading for a hollow column, the specimen with the label (CC-ECC-90) define as an control column with eccentric loading (0.9h) have the eccentricity distance equal to (135)mm for the hollow column, the specimen with the label (CC-ECC-60) define as control column with eccentric load (0.6h) have the eccentricity distance equal to (90)mm for a hollow column. And the (CC-CON-Cir.O) defines as a control column with concentric loading have circular side opening, (CC-CO- Squ.O) defines as a control column with concentric loading have square side opening(CC-ECC-Squ.O) defines as a control column with eccentric loading has a square side opening and the (CC-ECC-Cir.O) defined as control column with eccentric loading has circular side opening.

The second group comprises 10 columns of confined with (CFRP) have two types of loading (concentric and eccentric). The third group same as the second group but the confinement by use (TRM). All strengthening models tabulated as below (Table (3.2))

Table (3.2) specimen labels under concentric and eccentric loading

Strengthening by CFRP under concentric force	Strengthening by CFRP under Eccentric force	Strengthening by TRM under concentric force	Strengthening by TRM under Eccentric force
C.F.1	E.F.1	C.T.1	E.T.1
C.F.2	E.F.2	C.T.2	E.T.2
C.F.3	E.F.3	C.T.3	E.T.3
C.F.4	E.F.4	C.T.4	E.T.4
C.F.5	E.F.5	C.T.5	E.T.5

These specimens are defined as (C.F) concentric specimen confinement with (CFRP) (E.F) eccentric specimens confinement with (CFRP) (C.T) concentric specimens confinement with (TRM) (E.T) eccentric specimens confinement with (TRM).

The numbering (1,2,3,4, and 5) is according to the strengthening shape, as shown in the figures (3.1) below.

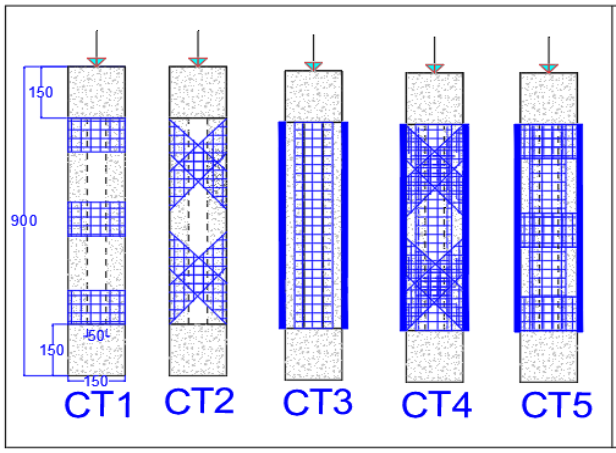

Fig. (3.1.a) strengthening by TRM for concentric loading

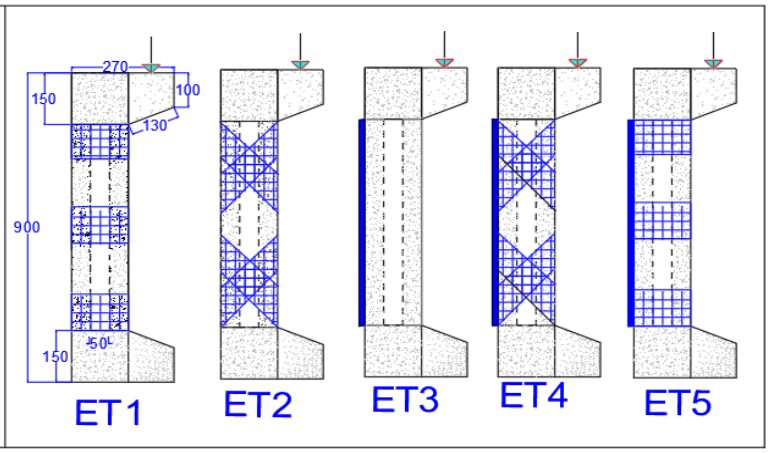

Fig. (3.1.b) strengthening by TRM for eccentric loading

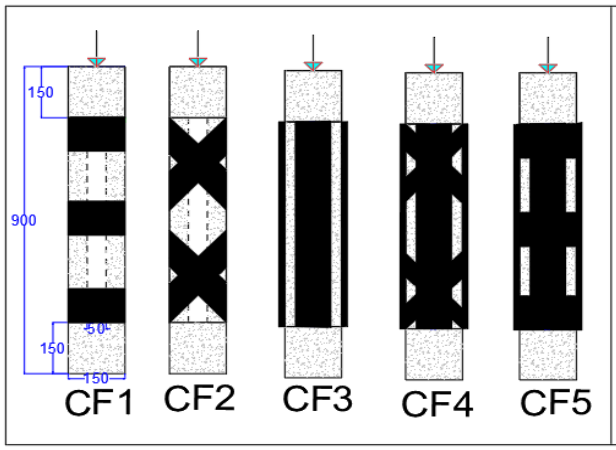

Fig. (3.1.c) strengthening by CFRP for concentric loading

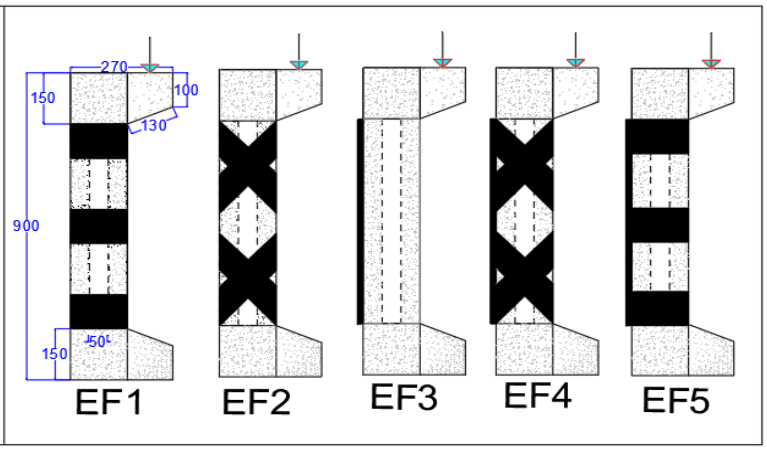

Fig. (3.1.d) strengthening by CFRP for eccentric loading

Fig. (3.1) strengthening by CFRP or TRM for concentric and eccentric specimens

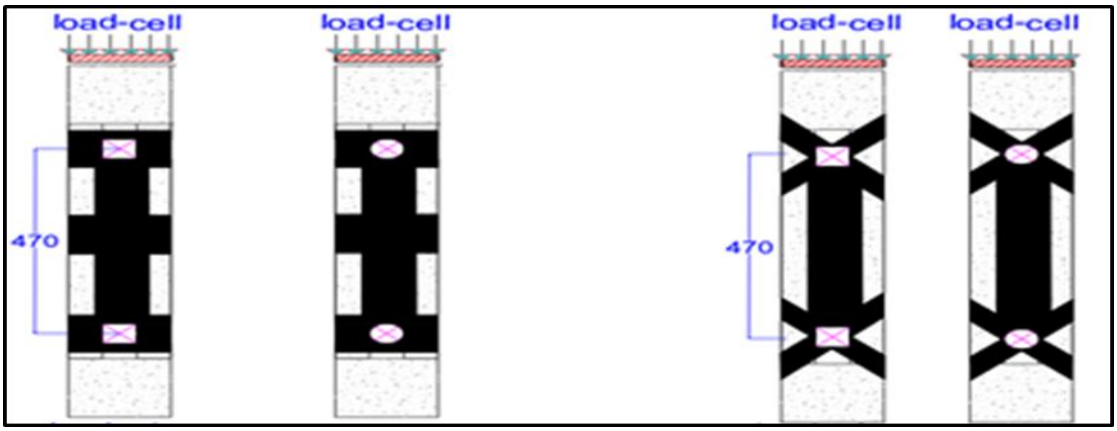

Fig. (3.2) strengthening by CFRP for concentric and eccentric specimens with side openings

3.3 Parameters Considered

The parameters considered in this research, study the effect of loading on the hollow concrete column as (concentric and eccentric) loading, also the type of external strengthening by Carbon Fiber Reinforced Polymer and Textile reinforced mortar (CFRP and TRM), and study the effect of shape and the position of two side opening (circular or square).

3.4 Materials properties (Implementation of Experiments)

All materials are provided before initiating this work. Appendix (A), (B) provided the results of the test.

3.4.1 Cement

All specimens were cast with ordinary Portland cement (type I) produced at KARBALA under the trade name (karasta). In Appendix A, Tables A-1 and A-2 detail its chemical components and physical characteristics. The results of the tests indicated that the cement conforms to Iraq standard No. (5)-1984. All of these tests were done at the factory directly.

3.4.2 Coarse aggregate

Crushed gravel from (Al-Niba'ee) area was used as coarse aggregate in this research. A sieve (10mm) separated the coarse aggregate from the larger aggregate particles, which were then thoroughly cleaned to remove any dust and fine material remaining in the air before being placed into nylon bags with a saturated dry surface condition.

3.4.3 Fine aggregate

The sand used in this project came from the (Al-Ukhaider) Karbala city region, and the sand was washed clean. In the end, the air-dried everything out, and it was ready to use. A variety of scales and physical characteristics have been examined. Sulfate content and grade conformed to Iraqi Specification No.45/ 1984 Zone2 as indicated in Appendix A of the results of the test.

3.4.4 Chemical admixture

As a third-generation HRWRA, Sika ViscoCrete® 5930-L was utilized in the production of SCC. Use the manufacturer's suggested dosage (1.2 to 2) percent by weight of cement) to get the best results. According to ASTM C494/C494M-13[72], Sika ViscoCrete® 5930-L satisfies the criteria for SP. Listed in Appendix A is the product's datasheet from the manufacturer's website.

3.4.5 Water mixing

The water mixing use in this research is a tap water.

3.4.6 Steel bar reinforcement (8 and 6) mm

In KARBALA LAB, they were evaluating the strength of 8- and 6-mm steel rebar reinforcement. Machine testing is used as a plate in this experiment (3.3). Steel rebars were tested according to the ASTM E8 code[73], which specifies how they should be tested. The yield and ultimate strength of a No. 8 steel rebar specimen were measured. The specimen measured (400) millimeters in length. Using the yield strength and area of the steel (Ast) of four #8 mm rebars (50.24 mm2), as well as the yield strength of the steel (486.5MPa) and the elongation of about 24.9 mm (11.2 mm), the test results shown in the figures, the column was examined and the load at which the column fails was calculated (3.2)

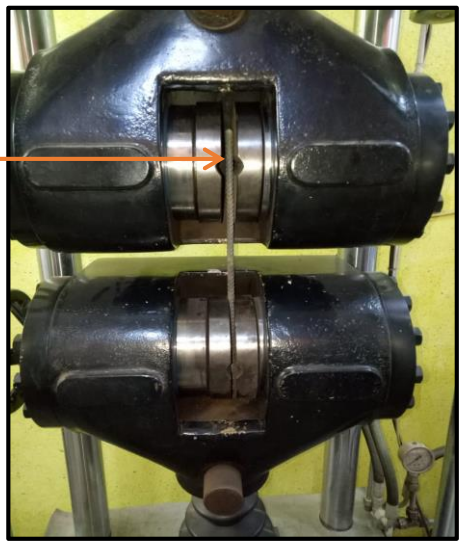

Plate. (3.3.a) **Plate. (3.3.b)**

Plate (3.3) a. rebar testing, b. rebar testing

Plate (3.4.a)

Plate (3.4.b)

Plate (3.4) rebar after testing a. (6mm), b. (8mm)

Plate (3.4) show the behavior of steel rebar after reach the yielding stress. Where figure. (3.4.a) represents the steel cutting in rebar (6mm), While figure. (3.4.b) showed the failure mode in rebar (8mm).

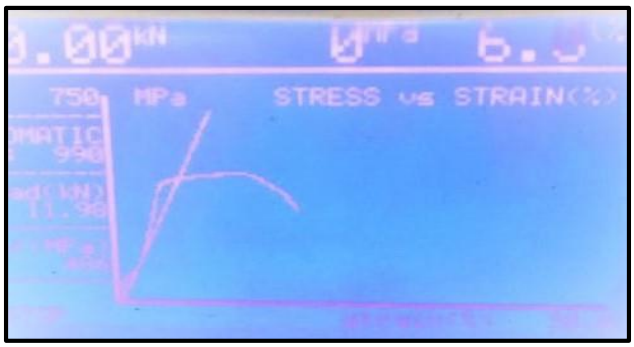

Fig. (3.2.a) rebar test (6mm) **Fig. (3.2.b) rebar test (8mm)**

Fig. (2) Stress-strain curve for rebars (6 and 8)

From figure (3.2) above, the stress-strain curves for the steel rebar test showed that the ductility for steel bar (8mm) is more than (6mm).

3.5 Steel rebar configuration

This research used two steel rebars with dimensions (8 and 6) mm, where the rebar with diameter (8) mm use in main reinforcement in the concrete column while the rebar has the diameter (6) mm work as the transverse rebar. The configuration of the steel rebar represents studying the stresses on the column when the concrete column is subject to concentric or eccentric loading. To make the hollow section

in the concrete column use the foam-polystyrene. with dimensions (50*50) mm and the height equal to the (600) mm, as below plate (3.5).

Plate (3.5.a) steel rebar configuration

Plate (3.5.b) steel rebar inside the mold

Plate (3.5) a. steel rebar configuration, b. rebar in the mould

3.6 Framework

The dimensions of molds (150 x 150 x 900)mm for columns concerning concentric loading and (270 x 270 x 900)mm for columns subjected to eccentric loading. Were the molds casting from steel plate and plywood, plywood used in the cases of sideopening (circular and square), as the plate (3.6)

Plate (3.6) steel molds and plywood molds

In addition, a number of steel mold types were used for the determination of the strength of experimental concrete (as seen in the plate (3.7)). For the molding of concrete specimens for tensile tests, three cylinders of the size 150 x 300 mm were used. For concrete moulding specimens for flexural testing, three (100x100 x500) mm prismatic steel shapes are used. Three cubic steel molds have dimensions of (150x150x150) mm for compression testing. All specimens have the same concrete properties as the self-compacting concrete (SCC).

Plate (3.7) molds for hardened concrete

3.7 Installing steel rebar strain gauges

Before starting the concrete casting in molds need to install (steel strain gauge) on the steel rebars[74]. This research has conducted a Japanese-imported strain gauge (SGS) to measure the column's steel rebar's strain. By using the (FLAB-6-11-3LGC-F) with a length equal to (6) mm for the steel rebar strain gauge (SGS). For the measurement of steel rebar strain, stirrups and main rebars are used in both directions. To ensure a flat surface for the strain gauges, the steel rebar should be flattened off by about 10 cm before installation. When applying the (SGS) and then put the glue type (CN-E) on the surface of (SGS), then use the white sheet paper and press on the (SGS) for one minute approximate after

this processing use the (wax) and covering the (SGS) to prevent the effects of concrete on it. The (SGS) was put in the control specimens only as a plate (3.8).

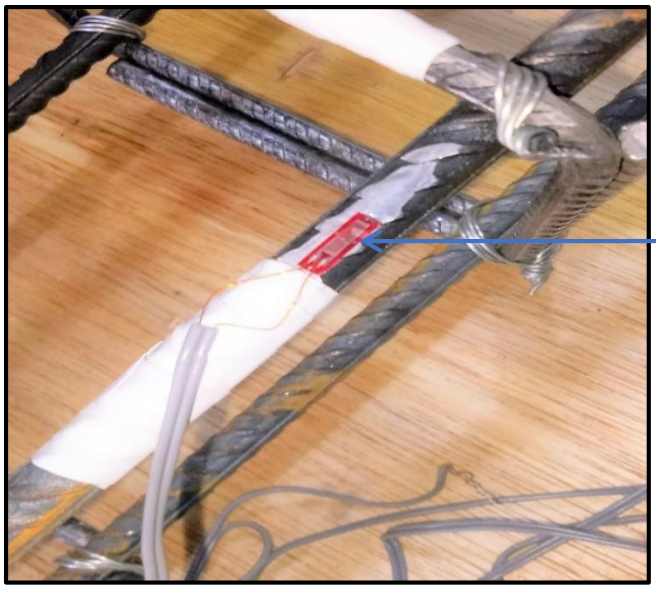

Plate (3.8.a) SGS for steel rebar

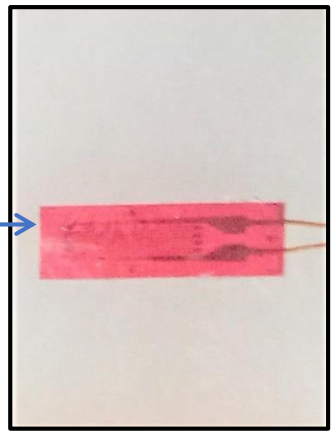

Plate (3.8.b) SGS FLAB-6-11-3LGC-F

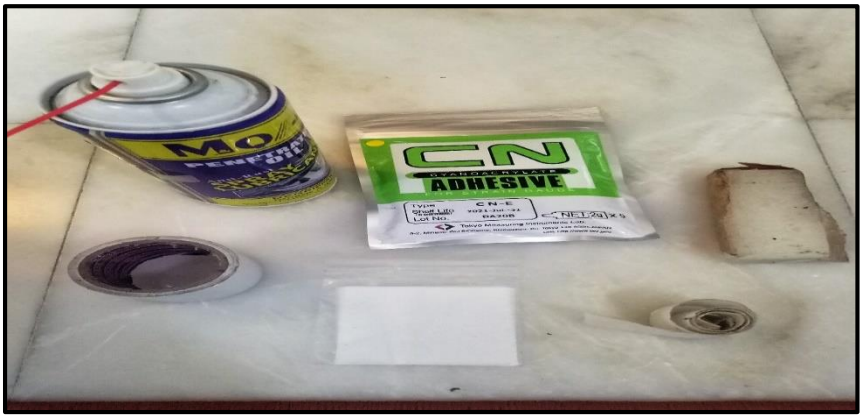

Plate (3.8.c) SGS accessories

Plate (3.8): (a) SGS for steel rebar, (b) SGS FLAB-6-11-3LGC-F, and (c) SGS

3.8 Concrete Mix Design

A self-compacted concrete mix (SCC) is designed according to EFNARC[75]. Also in this research dependent on a trail mixing suggested from[76], the concrete is made of normal concrete with self-compacting concrete to ensure the molds fully with concrete without using the vibrator or handshaking in order not to cause damage to the hole inside the column. The

mixing is composed of cement, water, coarse aggregate, fine aggregate, superplasticizer(SP)5930L, and limestone (powder) as the plate (3.9). The concrete mix is designed with compressive strength of about 25MPa. The materials are mixing by the electrical mixer machine, were at first put the fine aggregate (FA), and then put coarse aggregate (CA) and mixing the component by electrical machine with time near to (1.5) min. After that put the cement and repeat the electrical machine with time near to (2) min, and then put the water, after that put the (SP)5930L, these part of mixing takes time about the (7) min. The proportions of materials are tabulated as below:

Plate (3.9): materials using in SCC

The proportions of materials mixing as the table (3.3) below: -

Table (3.3): materials proportions of the SCC

Material	Cement (kg)	Water (kg)	C.A (kg)	F. A (kg)	SP(5930L) (kg)	Limestone\powder (kg)
Specimen	13.3	6.65	28	28	0.2	5.6

Steel plate moulds were used to cast the columns vertically as the plate (3.10). Prior to it, the concrete was uniformly spread using tiny containers. Following this, the specimens is flattened with a metal piece that is used for this purpose to ensure have a smooth surface at the top end of the columns as possible. For the specimens with lateral opening, use plywood. Put the wooden moulds in the horizontal, as the plate (3.11).

Plate (3.10): cast the columns by using the steel molds

Plate (3.11): cast the columns by using the plywood molds

3.9 Test of fresh concrete properties

The self-compacted concrete SCC mixture was examined with ordinary fresh properties to ensuring that the SCC requirements were accomplished, in this

research atrial mix suggested by. It will be investigated the viscosity, flowability, and passing ability of the fresh mixture. Various evaluation procedures, such as Slump-flow, J-ring, V-funnel, and L-box.

3.9.1. Slump Flow Diameter & T50cm Tests

The slump test measurements are commonly used in conventional concrete to calculate the followability and viscosity of fresh concrete when the effect of bleeding and segregation can be interpreted. The diameter is a fluidity measurement for the SCC, while the time required by the SCC mix is a viscosity measurement to achieve 500 mm (T500). Truncated cone, conforming to EN12350-2 (2010)[77]. The test has the cone consist with the top diameter of 100 mm, the bottom 200 mm, and the height of 300 mm. The cone is set on square thick plywood with a diameter of at least 800 mm. After that, draw two rings with a diameter of 200mm for inside and 500mm for outside. After a short period, the cone was filled with normal concrete without a rode. Following that, the cone was smoothly pushed upward via one motion, and with its own gravity, the material started to flow outward. After the halted concrete flows, the concrete spreads via two perpendicular diameters, and the mean value is indicated. Estimated T500 is based on measuring how long it takes the cone's tip to reach a diameter of 500mm.

Plate (3.12) shows the performed test, the dimensions of the slump cone, and the base plate.

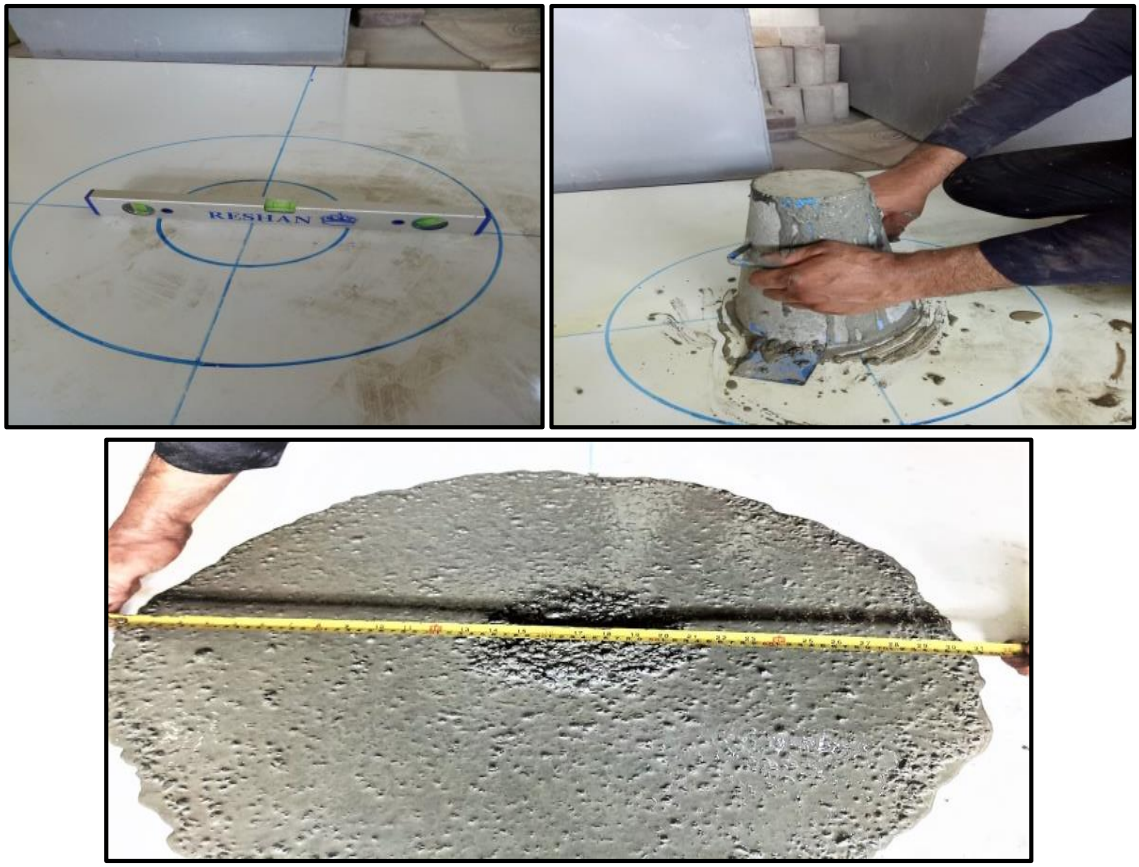

Plate (3.12): Slump flow and T500 test

3.9.2 V-funnel test

To see how well it filled up and how much viscosity and ability it had, with a maximum aggregate size of 10 (mm). (BS EN 12350-9 (2010)[78] plate (3.13) shows the v-test funnel's and dimension. The normal concrete was put into the device without using the shaker. The flow rate was recorded as the amount of time it took for it to pass through it. Because of the nature of the equipment, a large volume of coarse material or a viscous combination might cause a blockage. Because paste viscosity and inter-particle friction are low, reduced flow time and high filling ability can be connected. This plate depicts the results of the test and the V- funnel.

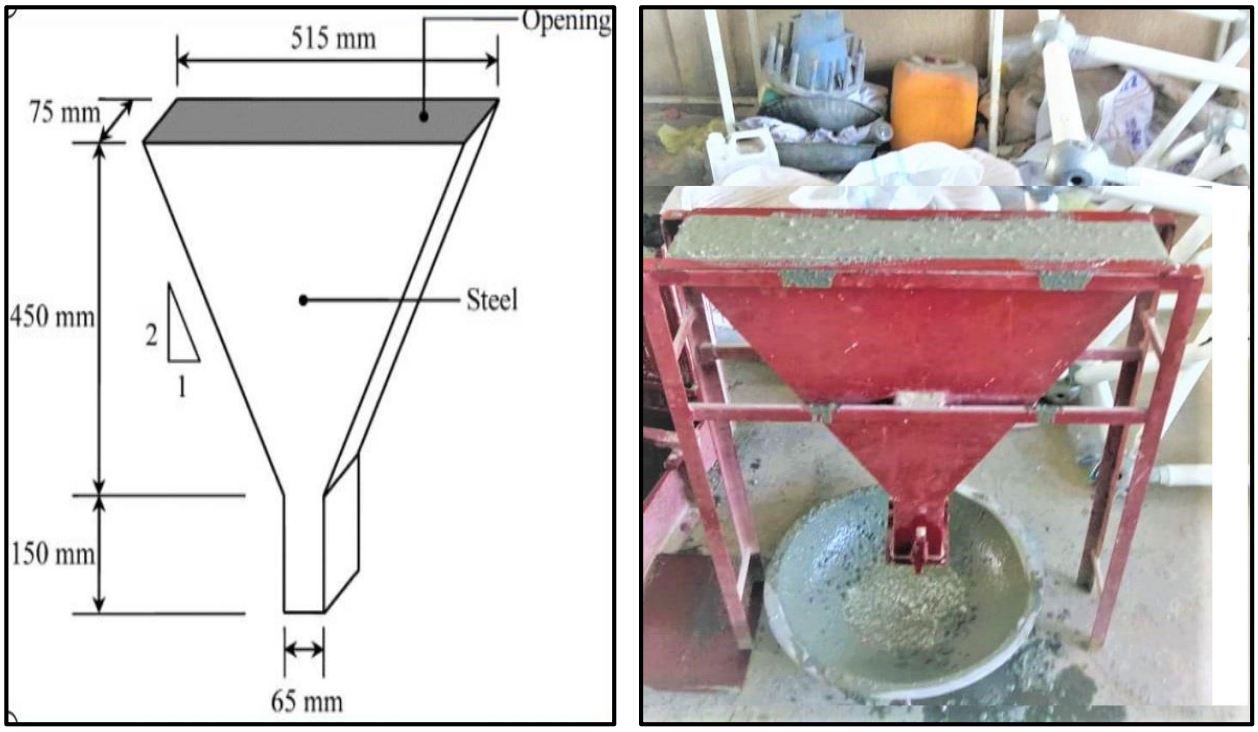

Plate (3.13): V-Funnel test

3.9.3 L-Box Test

As part of this test, the filling capacity of SCC is evaluated and the ability to pass through enclosed openings without segregation is assessed. The apparatus of L-Box with the horizontal and vertical channels are shown in plate (3.14). A movable gate made of steel bars separates the vertical and horizontal channels. The vertical portion was filled with concrete after leveling the L-Box horizontally. In order to establish the passing ability factor, the heights H1 and H2 were measured after the gate was opened, and the concrete was allowed to flow into the horizontal channel under its weight.

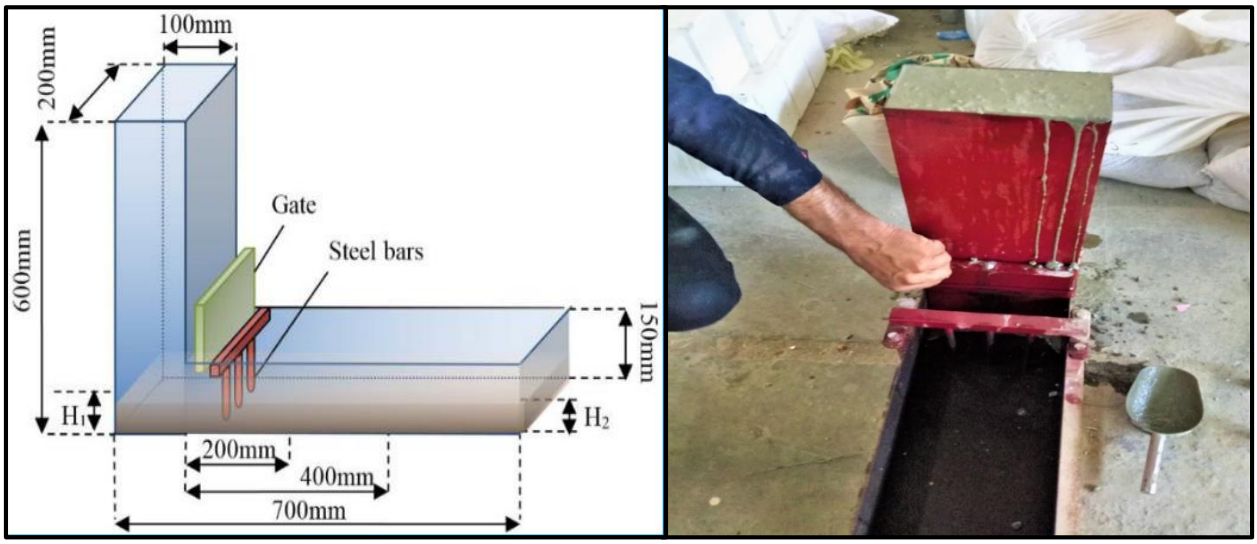

Plate (3.14): L-box test

The readings from all of the above tests are reported in table (3.4).

Table (3.4): results of SCC testing

Test Methods	The Characteristic	Measured Value	Limitations
Slump flow	Flowability, filling ability	**(765) mm**	*SF (640 - 800) mm*
T500	Viscosity, flowability	**(4.5) Sec**	*>2 sec*
V-funnel	Viscosity, flowability	**(10.10) Sec**	*VF (7 - 27) sec*
L-box	Passing ability	**0.8**	*≥ 0.75*

3.10 Hardened concrete properties

3.10.1 Compressive strength

According to BS.1881: Part116 (1989), the concrete compressive strength of each patch was determined. At the same time as molding the columns, three (150*150*150) mm cubes and (150*300) mm cylinders were formed to assess the compressive strength. The molds were also testing after 28 days, and they passed. It is shown in plate (3.15). It's listed in table (3-4).

3.10.1.1 Cubical and cylindrical Compression test

The cubical compression test is directed following BS 1881-Part 116 [79], using concrete cubes of 150 mm length (for NSC). Concrete specimens were cured and prepared, as described previously in section 3.3. This test was carried out by using 2000 kN applying compression a hydraulic machine, as shown in Plate (3.15). the stress calculate using Eq(3-2)

$$f'_c = \frac{P}{A} \quad \text{..... (3-2)}$$

where:

f'_c = compression strength (MPa),

P = peak load (N) and

A = specimen cross-sectional area (mm^2).

Plate (3.15.a): Cubic compression test

Plate (3.15.b): cylinder compression test

Plate (3.15): hardened compression test

3.10.2. Modulus of rupture (f_r)

Standard test methods such as ASTM C78-02 [80], are used to determine the rupture modulus. For each group, three 100 x 100 x 500 mm prisms were also cast at the same time as the columns. The prisms were put to the test at the same day as the columns for each group. The four-point bending test was used to conduct the testing. Modulus of rupture test results is shown on Plate (3.16) and founded by apply equation(3-3)

$f_r = 3PL/bd^2$ …….. (3-3)

where:

f_r = modulus of rupture (MPa).

P = peak load (N).

d = average depth of specimen (mm).

b: average width of specimen (mm).

L= span length (mm).

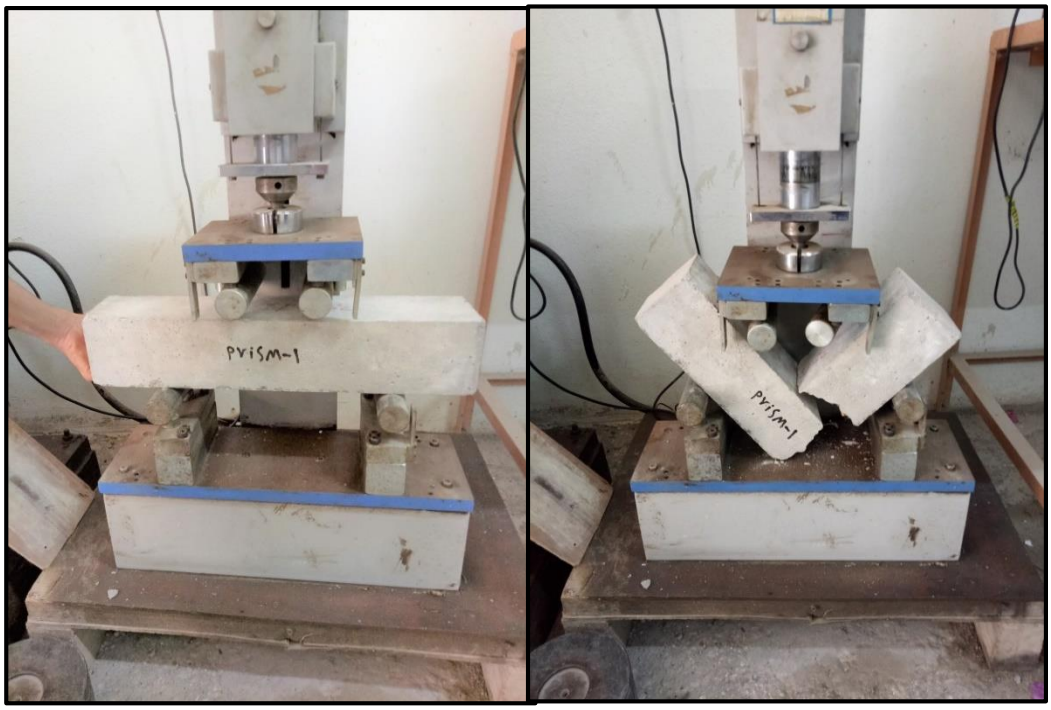

Plate (3.16): Flexure test

3.10.3 The static-modulus of elasticity test

The static-modulus of elasticity test was performed for concrete specimens in accordance with ASTM C469 / C469M – 14[81]. The stress-strain relationships as shown in Figure (3-3) along with the modulus of elasticity and the Poisson's ratio were investigated using cylindrical specimens at the age of 28 days. To prepare specimens after curing, an electrical steel grinder was used to level the top of the concrete cylinders, as shown in Plate (3.17.a), and then fixation the concrete strain gauge (SGC) on the middle height of the cylinder concrete specimen and also connect the specimen with computer by using (LVDT) laser as the plate (3.17.b). This test was done using a hydraulic machine of a capacity equal to 2000 kN, as shown in Plate (3.17.c).

Plate (3.17.a): grinded the top surface

Plate (3.17.b): (LVDT) liser

Plate (3.17.c): machine test

Plate (3.17): static-modulus of elasticity test

The modulus of elasticity along with a Poisson's ratio was calculated for each mixture of SCCs as the average of three cylindrical specimens using Eq. 3-4 and Eq. 3-5.

$$E = \frac{S_2 - S_1}{\varepsilon_2 - 0.00005} \quad \ldots\ldots\ldots\ldots\ldots \quad (3\text{-}4)$$

where:

E = the modulus of elasticity (MPa),

S_1 = the stress corresponding to a longitudinal strain equal to 0.00005 (MPa),

S_2 = the stress corresponding to 40% ultimate load (MPa) and

ε_2 = the longitudinal strain produced by stress S_2.

$$\mu = \frac{\varepsilon_{t2} - \varepsilon_{t1}}{\varepsilon_2 - 0.00005} \ldots\ldots\ldots\ldots\ldots\ldots\ldots\ldots \quad (3\text{-}5)$$

where:

μ = Poisson's ratio,

ε_{t1} = transverse strain produced by stress at mid-height of the specimen corresponding to S_1 and

ε_{t2}= transverse strain produced by stress at mid-height of the specimen corresponding to S_2.

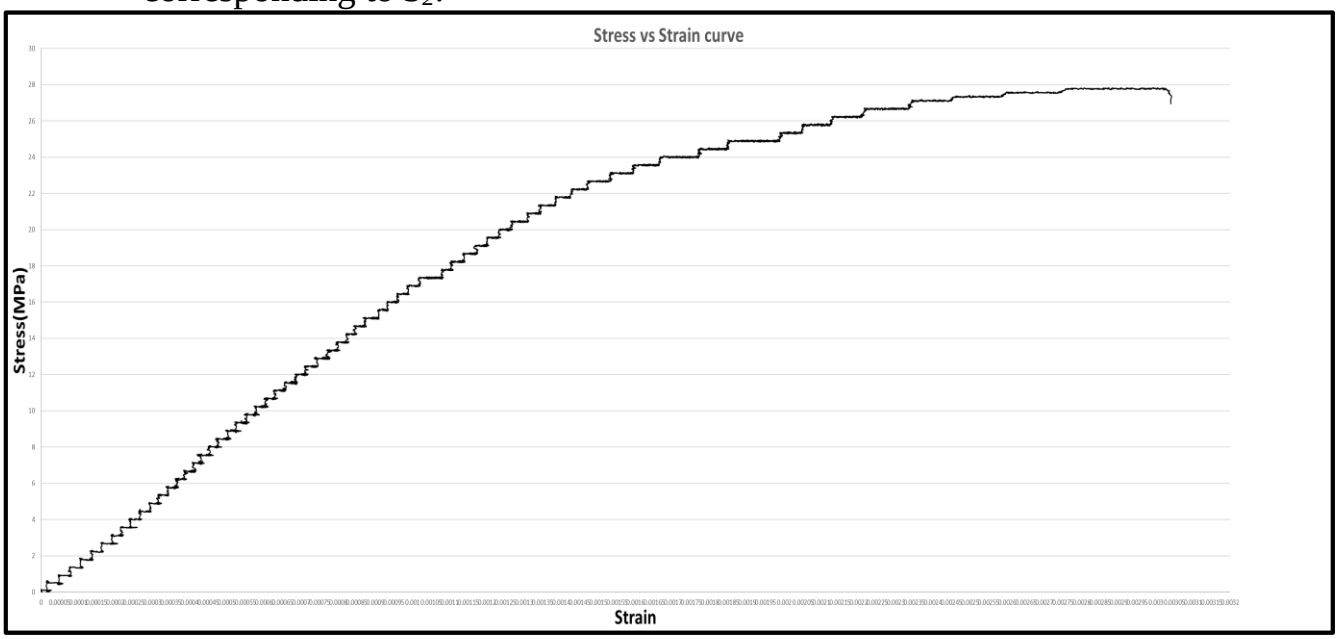

Fig (3.3): Stress-Strain curve to calculate (E) value

3.11 Curing

After completing the concrete casting, the curing of concrete starts during the 24hr until the 28 days, using a thermometer to measure the temperature of the water used in the curing process. Where the full submerge method is used as shown in a plate (3.18) below.

Plate (3.18): Curing basins

3.12 Columns Preparation

Before testing specimens and also before the use of external strengthening by (CFRP and TRM), All exterior edges columns will be rounded with the radius equal to (20-30) mm [82], in the longitudinal direction as shown in the plate (3.19). All specimens rounded by the (small machine for grinded) to prevent the failure in the (CFRP and TRM), Because of the concentrated loads at sharp corners, shapes were adapted to have round corners.

Plate (3.19.a): Sharpe edges specimens

Plate (3.19.b): Rounded edges specimens

Plate (3.19): rounded edges specimens

3.13 Strengthening by CFRP and TEM

CFRP and TRM were both utilized as exterior strengthening materials.

3.13.1 Carbon fiber reinforced polymer (CFRP) laminate

Carbon fibre reinforced polymer (CFRP) as plate (3.20) is a composite material. A matrix and reinforcement make up the composite in this example. Carbon fibre is used as reinforcement in FRP, and this is what gives it its strength. To hold the reinforcements together, a polymer resin matrix, such as epoxy, is used as a binding agent. The material characteristics of CFRP are dependent on the two different parts that make up the structure. The use of carbon fibre reinforced polymer (CFRP) for structural members is an external strengthening method. The dry application procedure was employed to carry

out these strengthening methods, which made use of CFRP laminate and unidirectional woven carbon fabric. For carbon fibre production, crystal alignment gives a high strength-to-volume ratio to the fibre., As the crystal alignment offers the fibre an excellent strength-to-volume ratio, the long axis of the fibre is aligned with the carbon atoms in a roughly parallel fashion (in other words, it is strong for its size). Thousands of carbon fibres are woven together to make a tow, which may be used on its own or as part of a fabric. As well as the (Sika) Corporation. Look at plate (3.21 a). Physico-mechanical traits were evident in their appearance and behavior. Appendix-C. It had a tensile strength of 3500 MPa, a modulus of elasticity 230-GPa, and elongation of 1.70 percent when broken. A special epoxy called Sikadur-330 was used in conjunction with CFRP sheets. The epoxy was a two-component impregnation resin, with each component (A resin part and B hardener part)[83][84]. As A: B, the two components were blended at a ratio of 4:1. Sikadur-330's usual characteristics are shown in Appendix C.

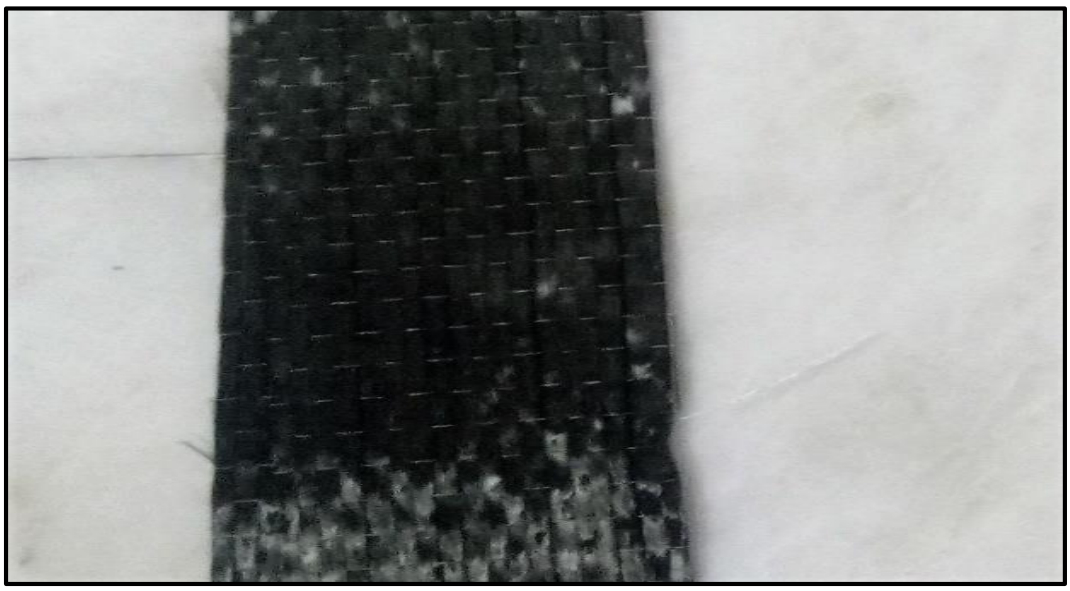

Plate (3.20): CFRP-laminates

3.13.1.1 Epoxy Sikadur-330 Preparation

Epoxy is a polymerizing that recovers if added with a catalytic or hardened agent. It is a multi-faceted polymer with many functions, including industries, pigment, varnish, adhesion, computers, construction materials, and automobile production. In this investigation, the CFRP sheet and the RC column are bonded by Epoxy as plate (3.21.a). For the assembly operation, two types of substances have been utilized. Of the CFRP to the concrete columns; Primer and Saturate. To ensure that the FRP composite is properly connected to the concrete surface, a low viscosity compound is employed as the primary component. Any holes on the concrete surface will affect their bonding efficiency. The base has two fluid components, a foundation, and a hardener as plates (3.21.b) and (3.21.c). When mixed, it creates a liquid substance used for closing the holes in the concrete surface.

Plate (3.21.a): Epoxy Sikadur-330 Preparation

Plate (3.21.b): type A

Plate (3.21.c): type B

Plate (3.21): Epoxy Sikadur-330 Preparation

3.13.2 Textile reinforced mortar (TRM) and bonding

the textile-reinforced mortars as plate (3.22) are now the new technology use as external strength in concrete members. These new materials are constructed of textiles which, impregnated with inorganic bindings such as cement-based mortars, constitute fabric meshes of long, Fiber rovings weaved or even unwoven. As part of the strengthening approach, high-tensile carbon fibres were inserted into cement-based mortars. The textiles in both orthogonal orientations have an equal amount of carbon fibres with 10 mm mesh carbon textile used in the strengthening of the tested specimens. The textiles are supplied and manufactured by the chinas company Shandong Jiangshan Fiber Technology. Two opposite orientations connected the textile rovings. Both the carbon rovings had a thickness of (0,4 mm) horizontal and vertical. The mesh measurements were (10 x 10) mm. The fibers had a tensile strength of 4900 MPa, a modulus of 230 GPa, and elongation at a break of 2.0%. All properties of the fabric were based on the manufacturer's product data sheet, Appendix-B.

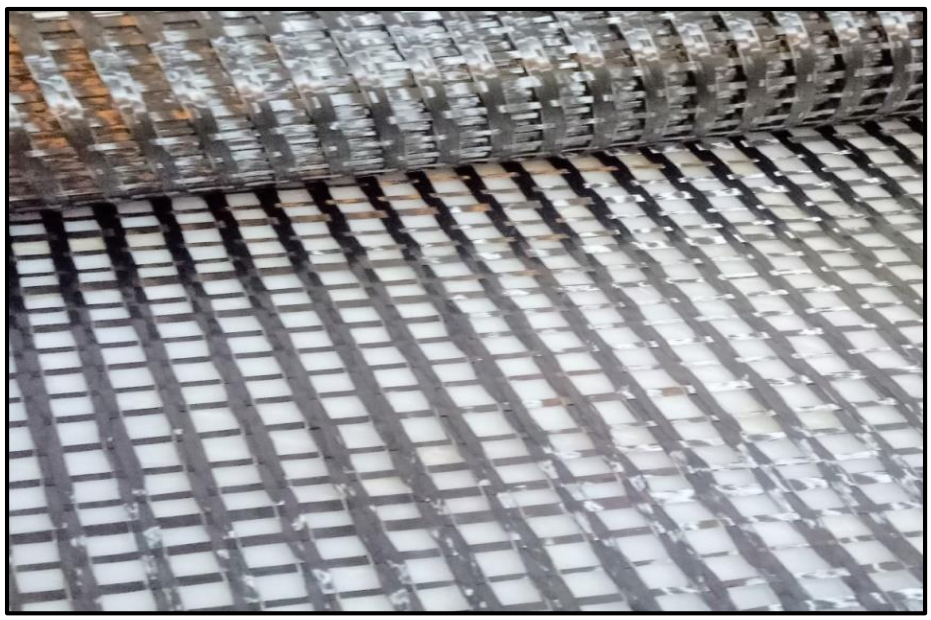

Plate (3.22) TRM sheet

3.13.2.1 Bonding materials (ReCon HS)

The good bonding between the TRM and concrete surface the cementitious materials were used. A commercial mortar was used in the TRM strengthening system known as (ReCon HS) as a plate (3.23). In the cementitious matrix, fibres and silica fume were added to a polymer-modified semi repair grout. It contains specially selected ingredients to provide high strength, fine, and smooth surfaces. This mortar is produced by Conmix company and commercially. As per the manufacturer datasheet, the mortar has a compressive strength of 75 MPa after 28 days of curing, as stated by ASTM C109[85], with a water to powder ratio W/P equal to the (0.14). The tensile strength of the mortar was 6 MPa at 28 days of casting, according to BS 6319-7. The manufacturing data sheet was listed in Appendix C.

Plate (3.23): (ReCon HS)

3.14 Configuration for Strengthened by (CFRPand TRM)

3.14.1 Strengthening by (CFRP)

The hollow concrete specimen confinement by one layer of an external laminate sheet of CFRP [86], with a different configuration, but with the same width. where the concentric and eccentric specimens strengthening as plate (3.24)

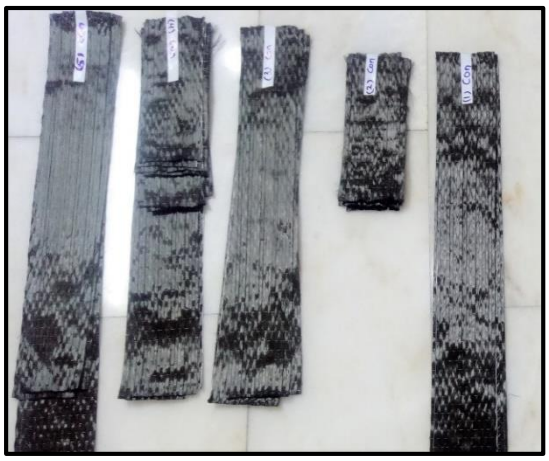

Plate (3.24.a):
(CFRP-Concentric configuration)

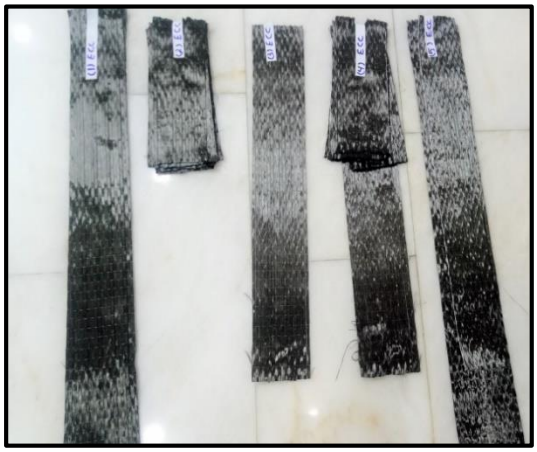

Plate (3.24.b):
(CFRP-Eccentric configuration)

Plate (3.24): (CFRP-Laminates)

The plate (3.24) above content the laminates of CFRP use to strength the concentric and eccentric hollow concrete columns where use (10) specimens, (5) specimens in concentric load and another (5) specimens in eccentric load. All the laminates have the same width and thickness. Where the width (100) mm and the thickness is about (0.167) mm. The specimens are first withdrawn from the treatment basin and allowed to dry for two days (dry treatment), following which the scraper is used to flush and rub the specimen (clear the specimen), and the corners of the column are rotated (rotation) for the region covered by the strengthening process (along the column at a distance of 600 mm). These ingredients are combined with a particular brush after they have been pre-

softened (one to a quarter) and are then applied using the epoxy materials; when the epoxy is finished, putty (mixed epoxy) is applied to the specimen created by CFRP. Overlapping CFRP is pressurized to prevent. air bubbles in this 100-mm-wide overlap region. According to the (ACI-code), you should then lift the specimens with a length of about five days. For all CFRP reinforced specimens, regardless of whether they are concentric or eccentrically loaded, the same procedure is used. As the plate (3.24) below: -

Plate (3.24.a): (Epoxy- for CFRP)

Plate (3.24.b): (particular brush)

Plate (3.24): (CFRP-strengthening)

3.14.2 Strengthening by (TRM)

The strengthening for specimens using the textile-reinforced mortar has the same procedure with the (CFRP) by preparing the TRM as the plate (3.25) for concentric and eccentric loading, but in the (TRM) use the (ReCon HS) to get good bonding between the (TRM) and surface of concrete[87]. At first preparing, all specimens required for this purpose, mix the (ReCon HS) with water according to the prepared proportions**.** And since the concrete's skin is smooth, so to reach a deep relationship between the (TRM) and concrete's surface. The smaller drill machine can be used to form grid grooves lines in the concrete as plate (24-a). After that, put the first layer of mortar; after that, employ the TRM show plate (24-b), followed by the second layer of (ReCon HS) illustrated as plate (24-c). leave the specimen 24 hr. approximately and then start the curing by water. All specimens strengthening with (TRM) have the same procedure in case the load is concentric or eccentric. As a plate (3.26) below:

Plate (3.25.a): (TRM-Concentric configuration)

Plate (3.25.b): (TRM-Eccentric configuration)

Plate (3.25): (TRM-Laminates)

Plate (3.26.a) (grid grooves lines)

Plate (3.26.b)
(TRM-strengthening)

Plate (3.26.c)
second LY.of mortar

Plate (3.26) (TRM-strengthening) procedure

Table (4) below shows the specimens with strengthening shape by using (CFRP-TRM)

Table (3.5): (CFRP-TRM. Cases)

Specimen	CFRP	TRM
CON-1 ECC-1	Three pieces of CFRP With a length of 750mm	Three pieces of TRM With a length of 750mm
CON-2 ECC-2	Eight pieces of CFRP With the length of 250mm	Eight pieces of TRM With the length of 250mm
CON-3	Four pieces of CFRP With the length of 600mm	Four pieces of TRM With the length of 600mm
ECC-3	One piece of CFRP With the length of 600mm	One piece of TRM With the length of 600mm
CON-4 ECC-4	Combined (2+3)	Combined (2+3)
CON-5 ECC-5	Combined (1+3)	Combined (1+3)

The labels (CON), (ECC) define the concentric and eccentric loading with the strengthening configuration, and (1, 2, 3, 4, 5) designates the numbers of cases.

3.15 Side opening specimens

All most the previous researchers did not study the hollow concrete column with side opening as the plate (3.27), in this research, is investigated the behavior of hollow concrete column with side opening. According to real functional services, it was located on the mould that produces square and round holes in specific positions. Present work (8) specimens, these specimens separate to another (4) specimens create as reference's specimens and have the two openings in one specimen (square or circular) opening located at the ends of the column, and remain, (4) specimens are strengthening specimens by (CFRP) as the figure below (3-27). The dimensions of side opening (50x50) mm and (50) mm for the square and a circular opening, respectively. These size dimensions of side opening according to ACI-code.

Plate (3.27): ((side opening)

3.16. Strain gauge for concrete (SGC)

Before installing the specimen in the machine for the test, fix the concrete strain gauge (SGC) [88][84], on the concrete surface with the position selected at the points need to read the straining of concrete. This work needs some of the materials using to these proposed as the plate (3.28.d). At first, and with the region needed to get the concrete deformations, the outer surface of the specimen is cleaned with a small scraper used for this purpose, and then a cloth is used for the purpose of removing dust from the specimen. Then the glue is added to the (SGC) so that this part is adjacent to the concrete surface, and then the paper is used and pressing on the (SGC) for one minute. Attention at this stage is not to damage the cable connected to the (SGC). This procedure will apply to the concentric and eccentric specimens as the plate (3.28.a) and (3.28.b) respectively.

Plate (3.28.d): ((SGC- accessories) (continue)

Plate (3.28.a): ((SGC-concentric specimen)

Plate (3.28.b): ((SGC-eccentric specimen)

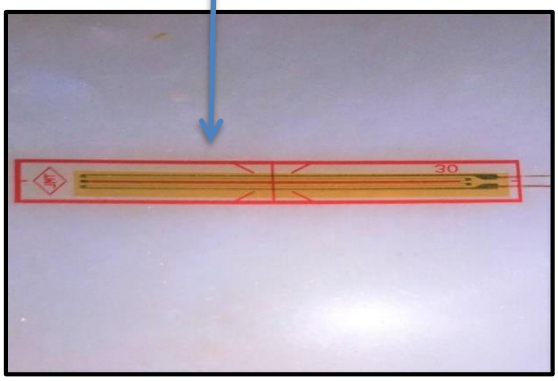

Plate (3.28.c): (concrete strain gauge (SGC))

Plate (3.28): installation the concrete strain gauge (SGC) for concentric and eccentric specimens (continued)

3.17 Instrumentation and Testing Procedure

3.17.1 Supports

The boundary conditions of the two ends of the hollow concrete column it is (pin-pin)[89]. By creating 4 boxes to describe the scenario. Two boxes for the specimen subject to concentric loading with dimension (160x160x80) mm, and another two boxes for the specimen subject to eccentric loading with dimension (280x160x80) mm as the plate (3.29). the top and bottom steel plate (loading zone) used with the thickness (20) mm to avoid unexpected failure at the top, and the side steel plate have the thickness (4) mm. by using the rode as a line load with the diameter (180) mm to represent the load case in the concentric or eccentric cases, as the Figure (3.4).

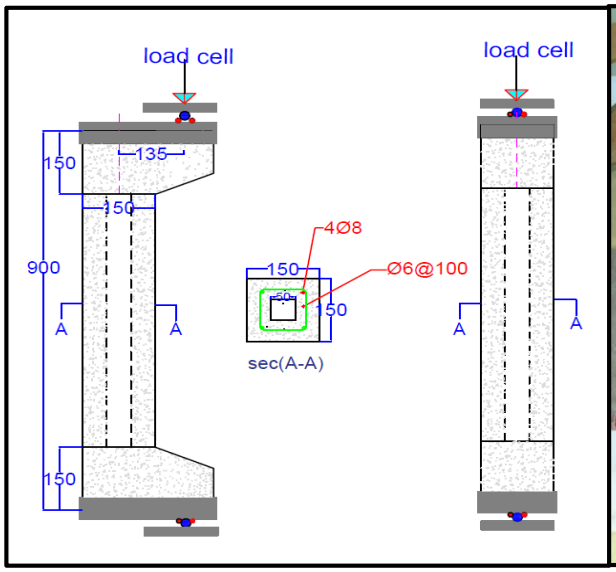

Fig. (3.4): model under CON. and ECC.

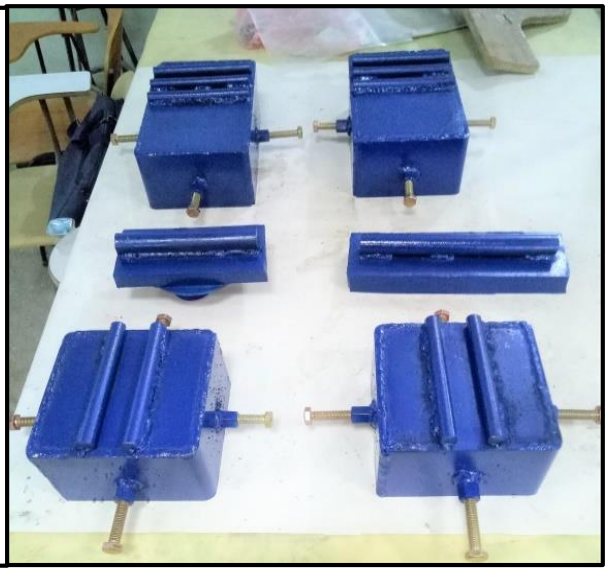

Plate (3.29): supports and line load

3.17.2 Machine test

All tested for hollow concrete column specimens were carried out in the structural laboratory of the civil engineering department at the University of Karbala. Were the test machine and computer are connected

by cables so that the loads can be conducted by the computer. This machine has (8) (USB) wires to connect the (strain gauge) for the concrete and the steel rebar. The lateral and vertical displacement take come by lateral variable displacement transmitted (LVDT)[90][91] , were these advises connected with the specimen and computer. All concrete moulds were subjected to two types of loading uniaxial compressive load and eccentric load using a test machine it is equivalent of 2000kN of force. A displacement rate of 0.5mm/min was used to produce the load. The top and bottom surfaces of the column were covered with thick sheets before testing to verify that the contact surface and applied load remained concentric. Fig (3-5) represent this machine test.

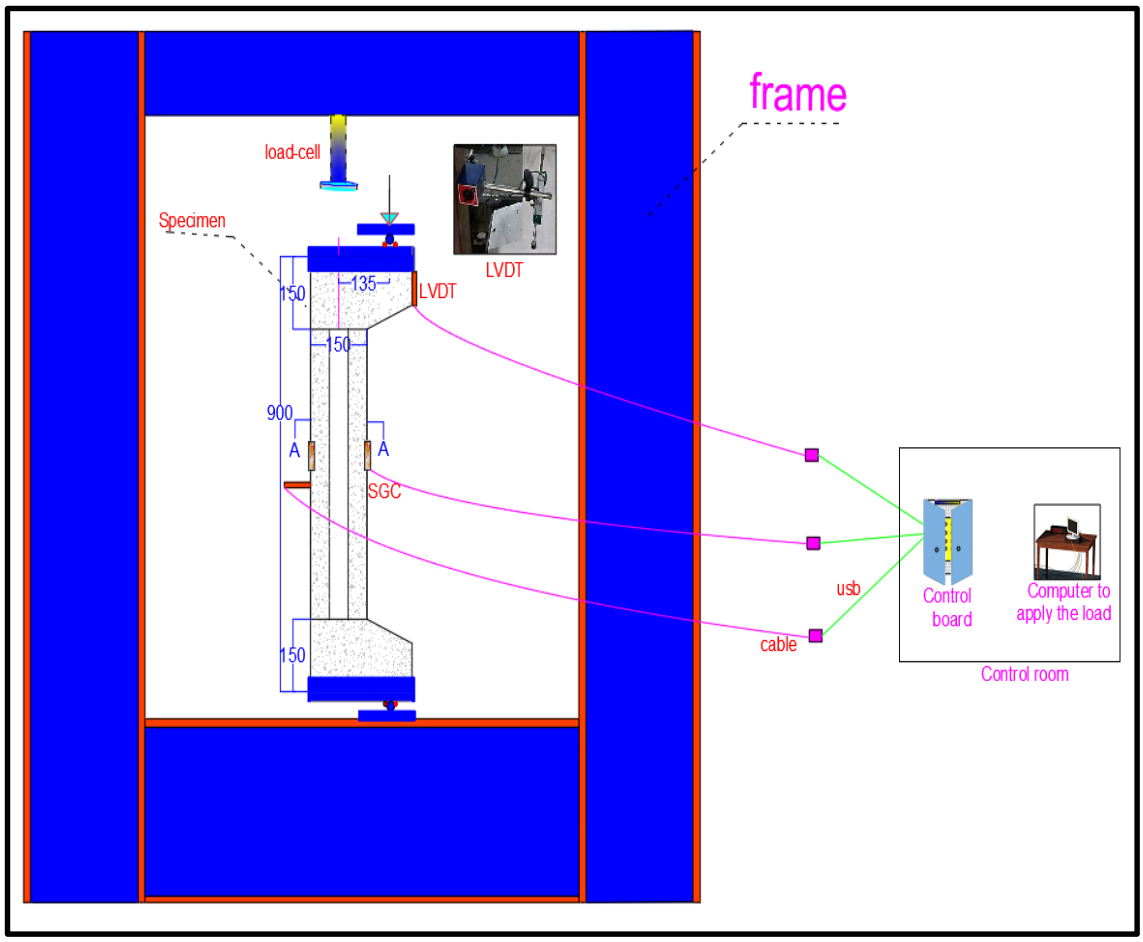

Fig. (3.5): Model under concentric and eccentric loading

3.18 Concentric and Eccentric loading test specimens

The number of specimens (32) tested up to failure with applied the line load at the center of a cross-section of the column for the specimens subjected to concentric load and applied the line load at the points from the center (e) of the column for the specimens subjected to eccentric load. The line load is applied via the load cell at the top end of the specimens.

3.18.1 Testing of control Specimens columns (CC-CO)

The control specimens have the (4) unconfined hollow RC columns divided into two specimens as concentric loading (solid, hollow) have the code by the following symbol (CC-CO-S),(CC-CO-H) respectively. The other specimens have the eccentric loading with eccentricity measured according to the aspect ratio (e/h) equal to (0.6h,0.9h) have the symbol (CC-ECC-60), (CC-ECC-90) respectively. (CC-CO-S),(CC-CO-H) underwent a concrete failure which took place at the surface and the bottom of the column as the plate (3.30.a)and (3.30.b), the increase of the load cause the buckled outward in the main reinforcement at the bottom, and then these steel rebar will cause damage to concrete. The solid specimen (CC-CO-S) have compressive strength (800) kN while these reading will reduce according to the hole in the hollow specimen (CC-CO-H) with compressive strength equal to the (610) kN. (CC-ECC-60), (CC-ECC-90) had a concrete failure due to the bending effect. However, the failure took place slightly away from the mid-height level with created the cracks on the tension side as the plate (3.30.c) and (3.30.d). The specimen has an aspect ratio (0.6h) carried a capacity more than the (0.9h). the case (CC-ECC-60) has the compressive strength equal to (150) kN and (68) kN for the (CC-ECC-90), So based on the above results, will utilize (0.9h) in strengthening specimens.

Plate. (3.30.a): (CC-CO-S)

Plate. (3.30.b): (CC-CO-H)

Plate. (3.30.c): (CC-ECC-60)

Plate. (3.30.d): (CC-ECC-90)

Plate. (3-30): Test of control Specimens columns

3.18.2 Testing of control Specimens columns Unconfined Columns with side opening (CC-CO-O)

Another control specimens have the (4) unconfined hollow columns with side opening, and this group is divided to the concentric loading and the eccentric loading with side opening (square and circular) as (CC-CON-SEQ-O),(CC-CON-CIR-O), (CC-ECC-SEQ-O), and (CC-ECC-CIR-O) as a plate (3.31).In this part of the research, reference specimens with side openings were examined, where two types of openings (circular and square) were used, and under the concentric and eccentric loading, the specimen (CC-CON-SEQ-O) gave a compressive load of about (430) KN, and for the case (CC-CON-CIR-O) have the compressive load equal to the (558)KN, the specimen with eccentric loading has the compressive load (64)KN for the specimen (CC-ECC-SEQ-O) and (65)KN for the specimen (CC-ECC-CIR-O).

Plate. (3.31.a): (CC-CON-SEQ-O)

Plate. (3.31.b): (CC-ECC-SEQ-O)

Plate. (3.31.c): (CC-CON-CIR-O)

Plate. (3.31.d): (CC-ECC-CIR-O)

Plate. (3.31): Test of control Specimens columns with side openings

3.19 Data Measurement during Tests

During the axial compression of the hollow RC columns, the external responses of the RC column such as the axial load (P), vertical displacement (v), and lateral displacement (x,y) values at the mid-height were automatically measured and recorded as a plate (32). Besides the external response of the hollow RC column, the readings from the axial and hoop strain values were also measured by the strain gauges attached to the steel reinforcement (SGS-for control specimens only) and recorded at were also recorded simultaneously with the external response of the hollow RC column. The axial load (P) was measured by the load cell of the (2000) kN compression machine. Since the upper plate is positioned according to the height of the tested specimen using the switch and does not move during the loading, the axial displacement and the lateral displacement of the hollow RC column is measured by a three LVDT device attached to the upper plate of the Loading machine assuming that the axial deformation(vertical displacement –Direction) and the two LVDT attached to the specimen at the mid-height with another direction (X, Y) to read the lateral displacement as in plate (3-32).

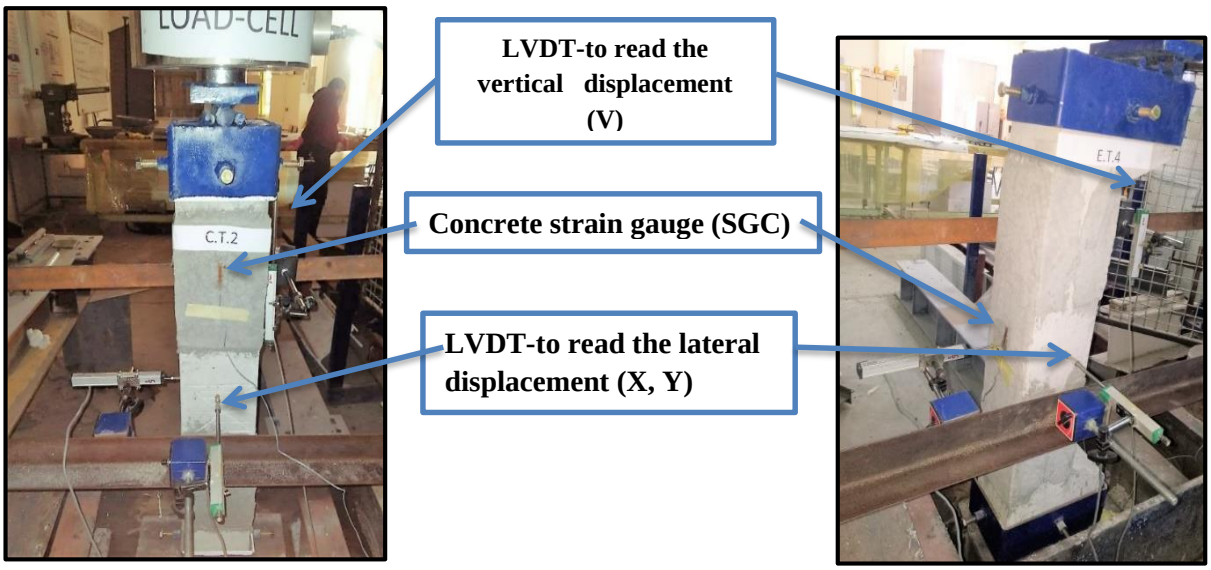

Plate. (3-32): SGC & LVDT

3.20 Stress-strain curve

When the load increases, the pressure on an unconfined concrete column increases. After the concrete column's yield level is attained via compression failure, the load decreases, the behavior of an RC concrete column covered with FRP, on the other hand, is unique. Confinement significantly increases the axial load due to warping resistance of the FRP. This rise continues until it achieves its maximum compressive strength (point D shown in Fig. (3.6). call it "Strain Hardening" when it happens. It's possible that if the confinement is not strong enough, then the columns will simply collapse under the imposed axial load. The relationship between stress and strain in any form of deformation can be regarded as stress-strain curves in this research. The stress calculated as the normal stress for the specimens has the concentric loading. In contrast, the stress with the specimens has the eccentric loading equal to the normal stress with the stress generated from the effect of the bending , see the equations below:

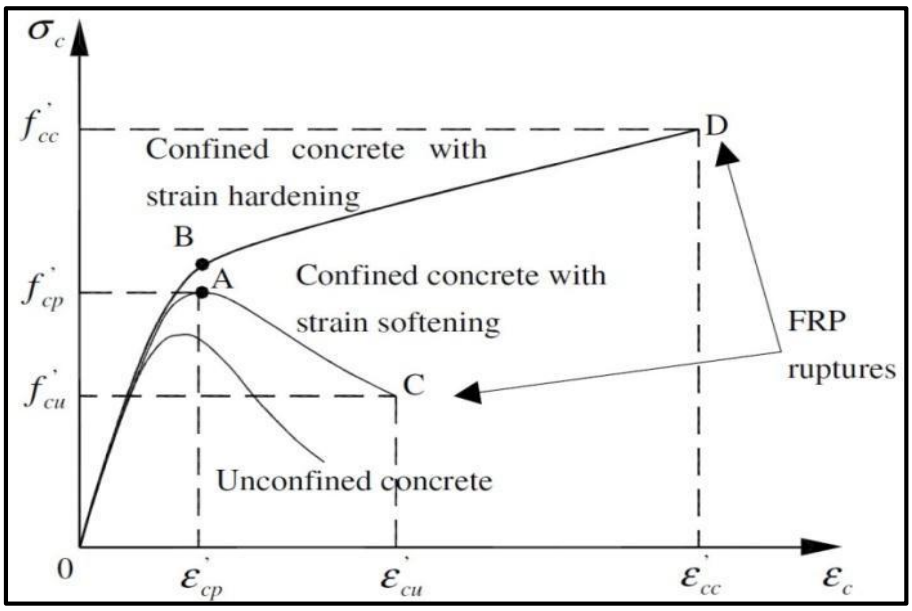

Fig. (3.6): stress-strain curve

For specimens that carry the concentric loading, the stress calculates as the equation (3-6) below:

$$f'_c = \frac{P}{A} \quad \text{---------- (3-6)}$$

where:

f'_c = compression stress (MPa)

P = load (N)

A = specimen cross-sectional area (mm^2).

For specimens subjected to the eccentric loading, the stress calculates as the below by Eq(3-7):

$$f'_c = \frac{P}{A} + \frac{M.C}{I} \quad \text{---------- (3-7)}$$

M = moment of neutral axis (N.mm)

C = perpendicular distance to the neutral axis (mm)

I = second moment area of neutral axis (mm^4)

3.21 max. crack width

Crack width was measured for specimens with eccentric loading using a micrometer, as shown in Plates (3-33). Were these specimens formed horizontal cracks on the tension face as the plate (3-34).

Plate. (3.33): MG10081-2 -micrometer

Plate. (3.34): Check the crack by using crack meter

3.22 Ductility

When looking at the behavior of FRP-wrapped columns, similarly important as a concrete column's strength is its ductility, which is influenced by its displacements at the point of failure and yield. The ductility of a solid material refers to its ability to deform under tensile stress. Tested the ductility and strength of CFRP-confined,partly degraded concrete columns. The confined concrete column ductility calculations are based on the load vs. displacement curve yield and failure point deformation measurements. The following equation can be used the equation (3-8) to calculate ductility (μΔ)[92][93]:

$$(\mu\Delta) = (\Delta u/\Delta y) \qquad \text{------- (3-8)}$$

In other words, the ratio between the ultimate displacement (Δu) corresponding to 85 % of the maximum load after peak strength and the yielding displacement (Δy).

All specimens were collected after examination as the following plates (3-35), (3-36) and (3-37).

plate. (3.35): Control specimens after failure

Plate. (3.36): Control specimens with side opening after failure

Plate. (3.37): All strengthening specimens after failure

Chapter Four: Experimental Results and Discussion

4.1 General

This chapter gives an overview and discussion of the results from the experimental test study reported in Chapter three. The prepared hollow RC columns are tested under axial compression with two types of loading (concentric and eccentric) with partial strengthening by (CFRP or TRM) laminates. All tests are conducted under displacement control with a 1mm/min displacement rate. Therefore, the summary for this section include as below: -

4.2 Specimens under concentric loading

In this case, will study the outcome of testing specimens carrying concentric loading and has a confinement by the CFRP or TRM.

4.2.1 Control columns under Concentric loading (CC-CO)

The experimental testing began with the unstrengthened columns. These groups were divided into four specimens of types , (CC-CO-S), (CC-CO-H).and the results were conducted as below:

4.2.1.1 Load vs. Displacement for specimens (CC-CO-S) and (CC-CO-H)

According to Figure.(4-1), the load vs. displacement curve for (CC-CO-S) starts from zero and travels upwards until it reaches a displacement of (1.2) mm. Where the failure load was (800) kN. The load vs. displacement curve for column (CC-CO-H) starts from zero and moves with an increased slope

until it reaches a final displacement equal to the (4.19) mm. with ultimate load reaching to the failed at (610) KN, as the figure. (4-2).

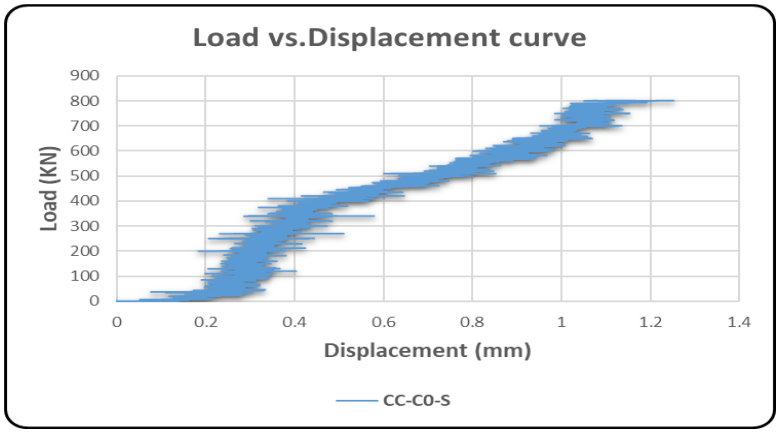

Fig. (4-1) Load-Displacement curve for (CC-CO-S)

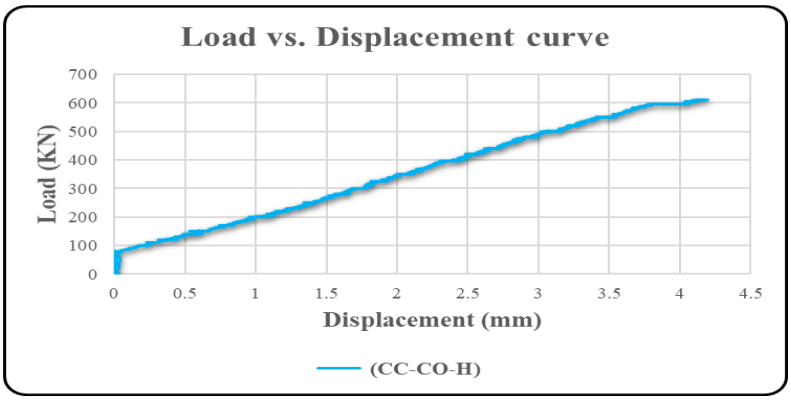

Fig. (4-2) Load-Displacement curve for (CC-CO-H)

4.2.1.2 Stress vs. Strain curves for control specimens

In this research, the (load vs. strain) curve for steel rebar by (SGS), fixed only in the control specimen (CC-CO-H) as the plate (4-1-a), in the previous chapter explained the prepared and fixation of the (SGS). This specimen (CC-CO-H) has the four steel strain gauge, three in the main steel rebar (SGS4), (SGS5), (SGS7), as the bottom, top, and middle, respectively. The (SGS6) for the stirrup. From figure (4-1-a), the strain gauge curve was reliable and objective in (SGS4) near the area of failure as the plate (4-1-b).

Plate. (4-1-a) Locations of SGS

Plate. (4-1-b) behavior of main rebar

Plate. (4-1) Strain gauge for steel rebar in control column

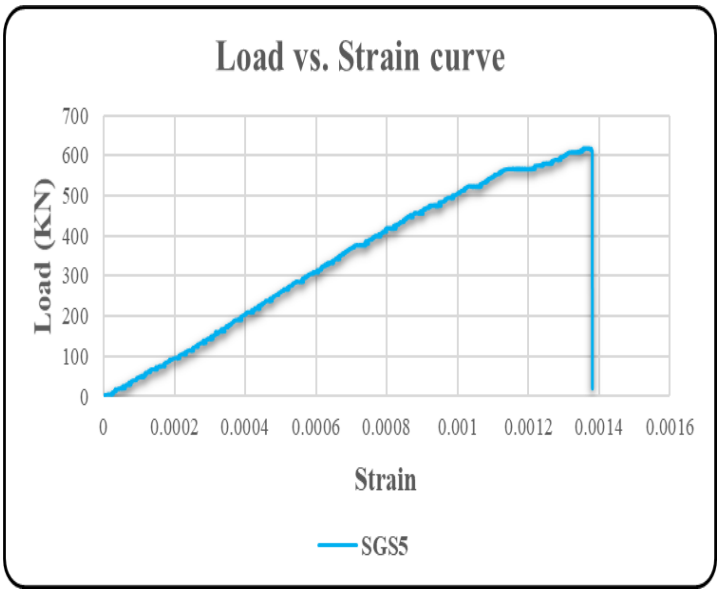

Fig. (4-3-a) Stress-Strain curve for SGS5

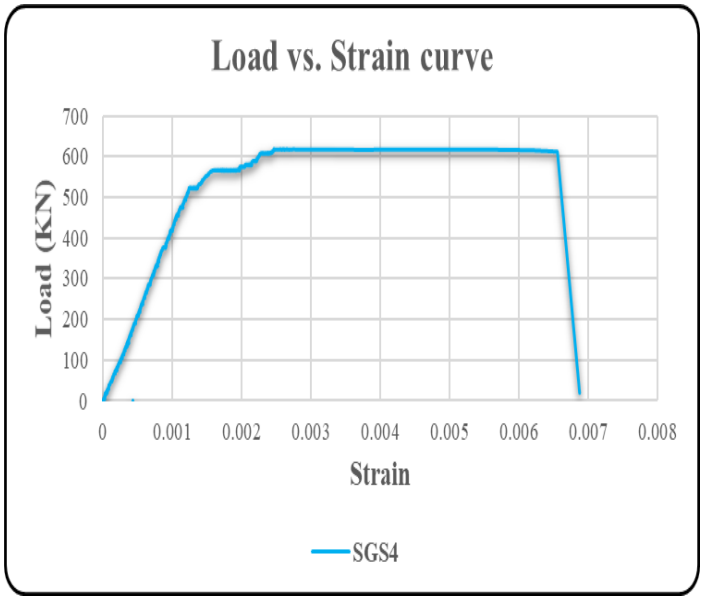

Fig. (4-3-b) Stress-Strain curve for SGS4

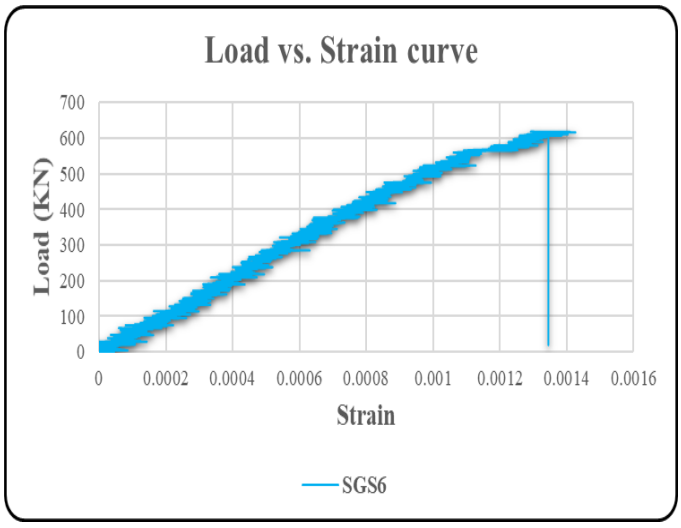

Fig. (4-3-c) Stress-Strain curve for SGS6

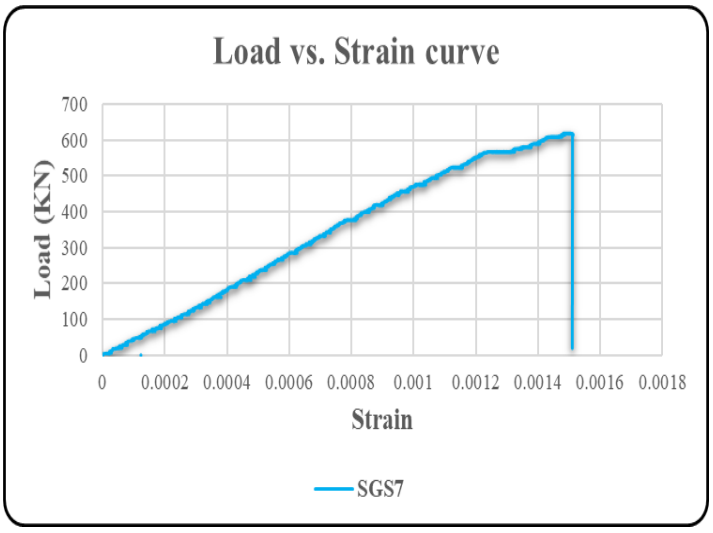

Fig. (4-3-d) Stress-Strain curve for SGS7

Fig. (4-3) Load-Strain curves for SGS in the control specimen for concentric load

For the concrete in the control specimen, the data are measured from the concrete strain gauge (SGC). These strain gauges are positioned on the specimen's outer concrete surfaces. Were data Illustrate via the figs. (4-4): -

- The control column (CC-CO-S) has the one concrete strain gauge (SGC) at the middle height of the specimen as the plate (4-2-a). Moreover, the specimen ((CC-CO-H) has three (SGC), these a three strain gauge fixed on the specimen with three locations (SGC1), (SGC2), (SGC3) at the top, middle height, and bottom, respectively. As the plate (4-2-b).
- The control column (CC-CO-S) have stress about (35) MPa and the strain equal to the (0.00143), and the (CC-CO-H) have the stress (28.8) MPa, and concrete strain (0.00138) for the both (SGC1, SGC2), was this reading to comparing between the cases, while the concrete strain (0.00182) for the (SGC3) near the failure position.

plate. (4-2-a) (CC-CO-S)

plate. (4-2-b) (CC-CO-H)

Plate. (4-2) Strain gauge for concrete in control column

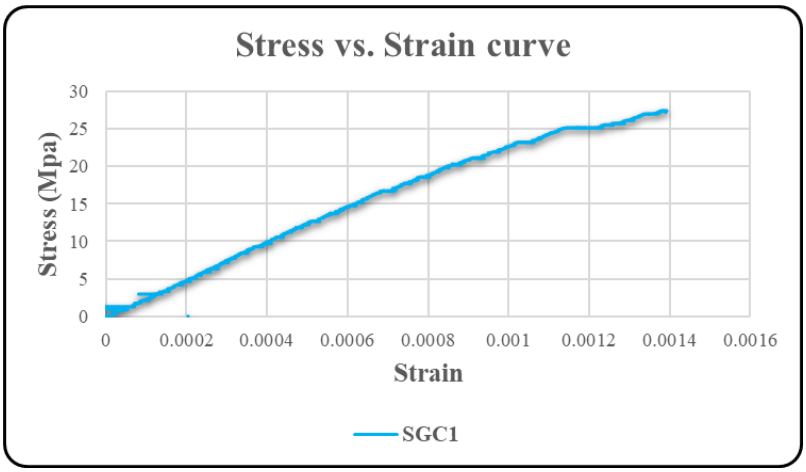

Fig. (4-4-a) Stress-Strain curve from SGC1

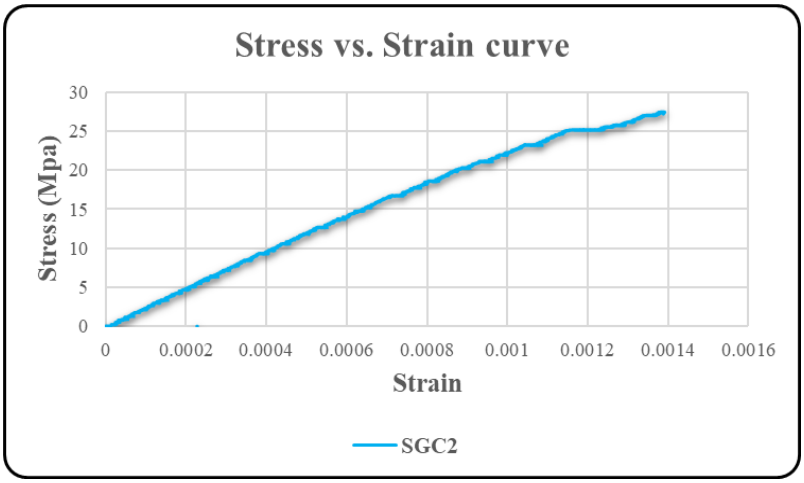

Fig. (4-4-b) Stress-Strain curve from SGC2

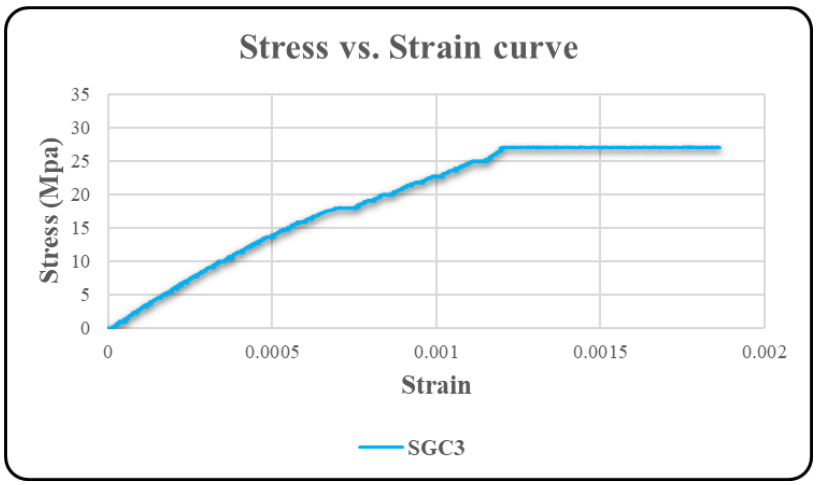

Fig. (4-4-c) Stress-Strain curve from SGC3

Fig. (4-4) Stress-Strain curve from SGC in control column (continue)

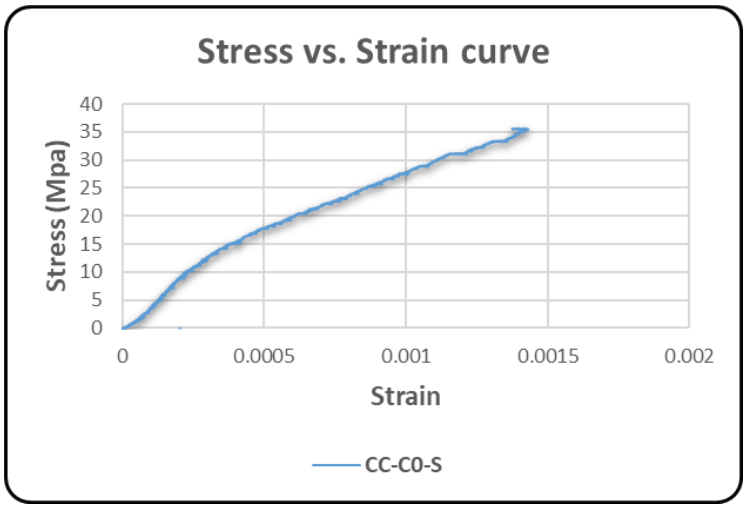

Fig. (4-4-d) Stress-Strain curve from SGC. Solid column

Fig. (4-4) Stress-Strain curve from SGC in control column (continued)

4.2.1.3 Mode of Failure for control specimens (CC-CO-S) and (CC-CO-H)

This group tested is (CC-CO-S) and (CC-CO-H). This group represents the columns without the wrap of CFRP or TRM. It can be noted that the mode of failure shared the same from one column to another. Look to the plate (4-3) and (4-4). These two failure cases are due to the generated plastic hinge near the bottom end. These columns failed because of two brittle mechanisms: steel reinforcement compressive bars buckled and the concrete cover spalls. Were explained in the stress-strain curve for concrete and steel in the specimen (CC-CO-H). From the steel strain gauge (SGS), the strain reaches the (0.0068), but the concrete strain is equal to the (0.0014) from the concrete strain gauge (SGC).

Plate. (4-3) Failure for (CC-CO-S)

Fig. (4-4) Failure for (CC-CO-H)

4.2.1.4 Ductility Index for the control specimens

Ductility defines as the ratio between the ultimate displacement (Δu) corresponding to 85 % of the maximum load after peak strength and the yielding displacement (Δy). Depending on the (load-displacement curve) to calculate the ductility by applying the equation below: -

Ductility=(Δu/Δy) ……..... eq. (3-4)

for the specimen (CC-CO-H), the ductility is equal to (1.1).

4.2.2 Specimens strengthening by CFRP and under concentric loading

This group has (5) cases with partials different form of CFRP configurations. illustrate the load vs. displacement as below and compare each result with the control case (CC-CO-H).

4.2.2.1 Load vs. Displacement

- The case **(CF1)** has the CFRP's three hoops in the top, middle, and bottom, as the plate (4-5). The load vs. displacement curve in fig (4-5) begins from (0,0) with total displacement equal to (**5.44) mm** when the maximum load was applied. This case failed at **(625) KN** with an increase in compressive strength about **(2.5) %** compared with the reference case (CC-CO-H).

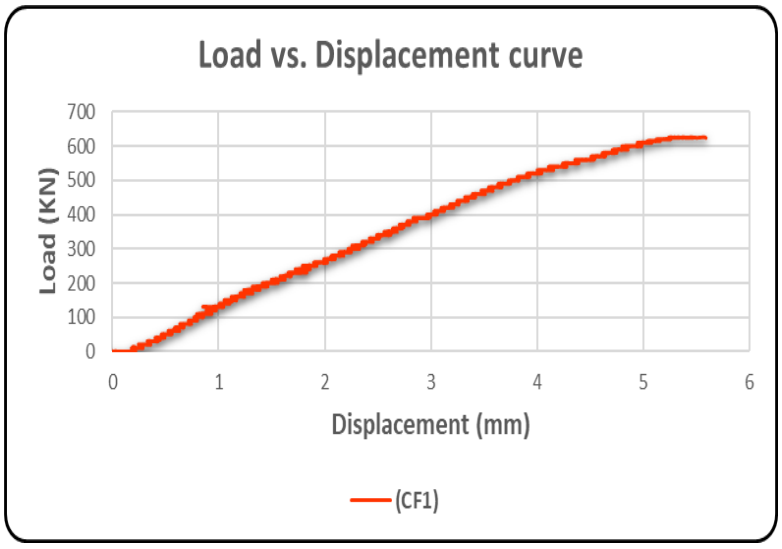

Fig. (4-5) Load-Displacement curve for (CF1)

Plate. (4-5) CF1

- The case **(CF2)** has two opposite (2X) shapes of CFRP at the top and bottom of the column as the plate (4-6). The load vs. displacement curve in fig (4-6) begins with a bit of concavity. When the load increases gradually, the maximum load reached (640.8) KN with maximum displacement equal to the **(5.26) mm**. This case has an increase in compressive strength of about **(5) %** compared with the reference case (CC-CO-H).

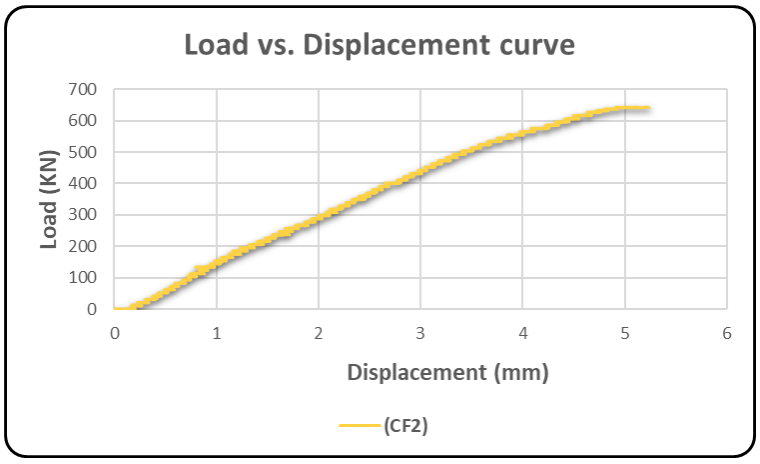

Fig. (4-6) Load-Displacement curve for (CF2)

Plate. (4-6) CF2

- The case **(CF3)** has the one vertical CFRP laminates on each column side as the plate (4-7). The load vs. displacement curve in fig (4-7), when the loading increases, the max load reaches the **(659.64) KN** with max. displacement equal to the **(6.17) mm**, this case has an increase in compressive strength of about **(8.1) %** compared with the reference case (CC-CO-H).

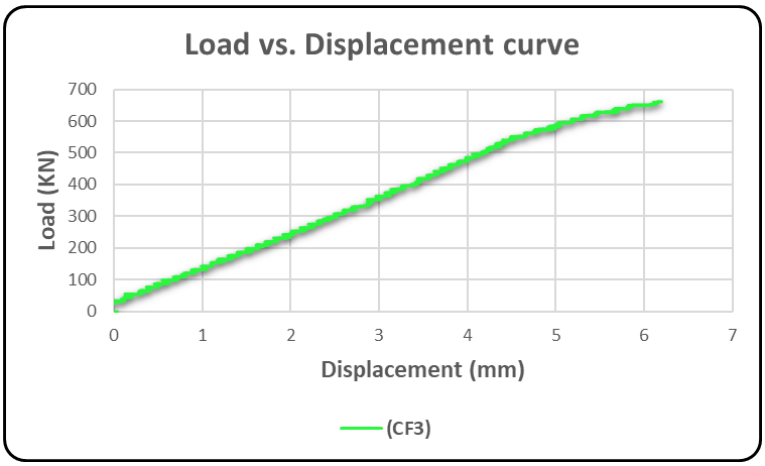

Fig. (4-7) Load-Displacement curve for (CF3)

Plate. (4-7) CF3

- The case **(CF4)** this specimen has the (four vertical) CFRP laminate on each column side and (2X-shape) of CFRP at top and bottom as the plate (4-8). In the load vs. displacement curve in fig (4-8), the max load reaches the (749.2) KN with max when the loading increases. Displacement equal to the **(4.85) mm**, this case has an increase in compressive strength of about **(22.8) %** compared with the reference case (CC-CO-H).

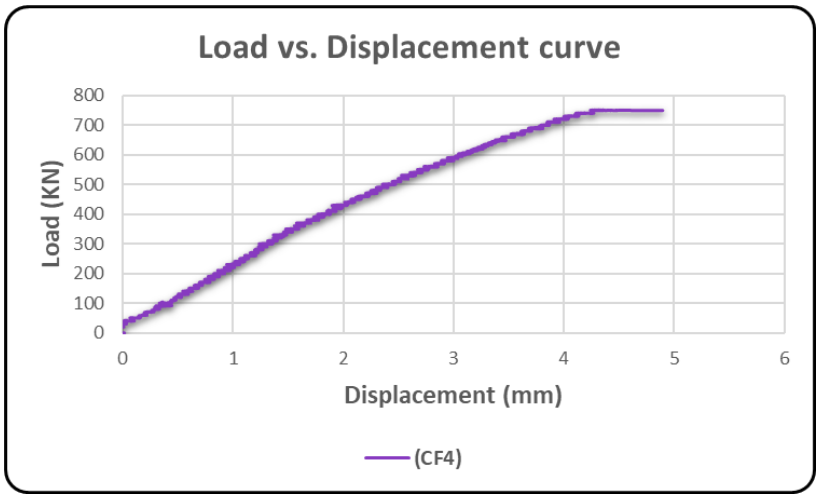

Fig. (4-8) Load-Displacement curve for (CF4)

Plate. (4-8) CF4

In the case **(CF5),** this specimen has the (4 vertical) CFRP laminate on each column side and (3hoop) of CFRP as the plate (4-9). The load vs. displacement curve in fig (4-9) has little concavity at first. When the loading increases, the max load reaches the **(689.5) KN** with max. displacement equal to the **(5.19) mm**. This case has an increase in compressive strength of about **(13) %** compared with the reference case (CC-CO-H).

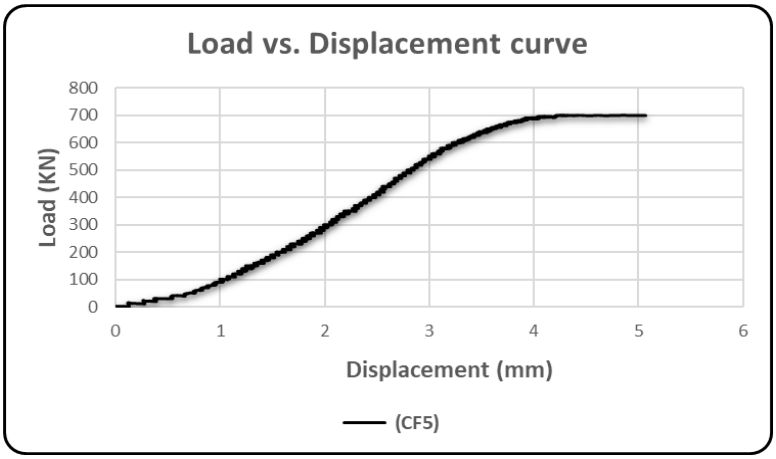

Fig. (4-9) Load-Displacement curve for (CF5)

Plate. (4-9) CF5

all results of displacement curve obtained from (LVDT) plotted in one graph with fig. (4-10)

The fig. (4-10) and table (4-1) show all results for all cases dealing with concentrically loading and strengthening partially by CFRP. the strengthening ratio in the table below calculated with respect to the control specimen (CC-CO-H).

Table. (4-1) results for control specimens and specimens that strengthening with CFRP and loaded concentrically

case	max.load(KN)	strain-concrete	axial-disp.(mm)	failure-location	axial-disp. at yeild(mm)	Ductility	strengthening(%)
CC-C0-S	800	0.00145	2	bottom	***	***	***
CC-CO-h	610	0.00138	4.19	bottom	3.91	1.1	***
CF1	625	0.0029	5.44	top	4.5	1.2	2.5
CF2	640.8	0.0022	5.26	top	4.78	1.1	5.0
CF3	659.64	0.00216	6.17	bottom	3.27	1.9	8.1
CF4	749.2	0.0017	4.85	top	4.14	1.2	22.8
CF5	689.5	0.0011	5.19	top	4.2	1.2	13.0

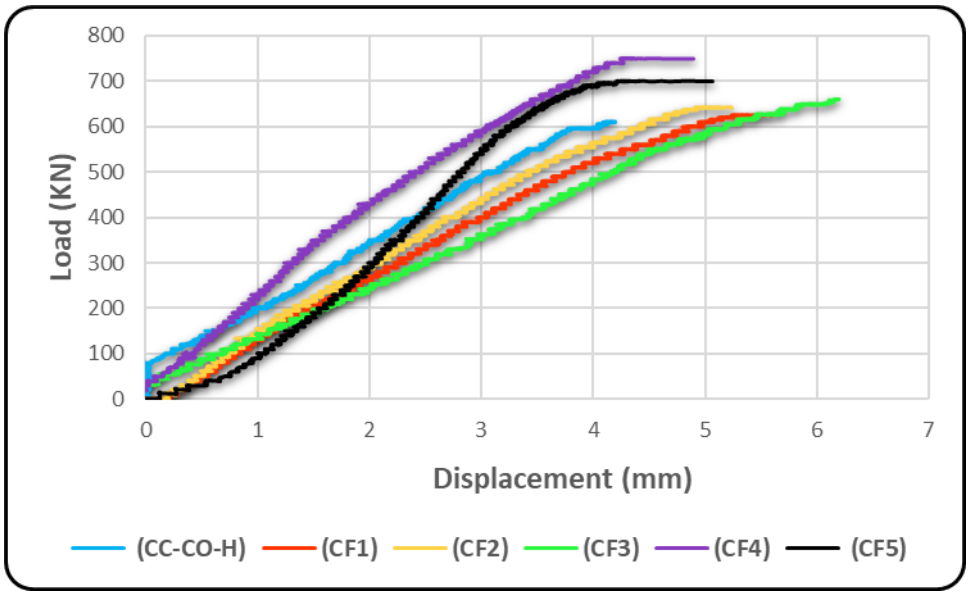

Fig. (4-10) Load-Displacement curves for (CF)

4.2.2.2 Stress vs. Strain for strengthening specimens (CF1, CF2, CF3, CF4, and CF5)

All cases with partially strengthening by CFRP and subjected to concentric loading contain one concrete strain gauge (SGC), positioned near the upper end of the column. Fig (4-11) and table (4-2) shows the results of these strain gauges.

Table. (4-2) Stress and strain obtained from SGC for strengthening by CFRP specimens under concentric loading

Case	Stress (MPa)	Strain
CF1	27.36	0.00304
CF2	28.04	0.00231
CF3	29.35	0.00127
CF4	33.08	0.00184
CF5	30.86	0.00113

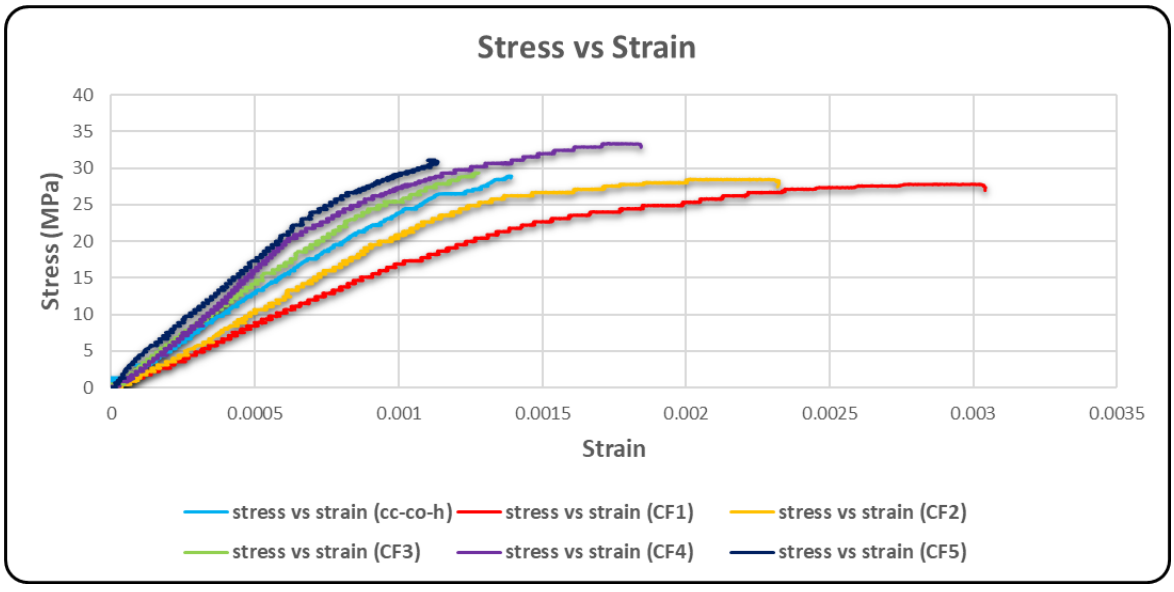

Fig. (4-11) Stress vs. Strain curves for CFRP cases

- These specimens have stressed more than or getting close to the (CC-CO-H), with a slight increase in strain.
- The max. stress founded in the case (CF4) (33.08) MPa, with an increase of about (14.86) % compared with the (CC-CO-H) have the stress (28.8) MPa.
- The max. strain occurred from the (CF1) (0.00304) with an increase (120.3) % compared with (0.00138) for the control specimen (CC-CO-H).

  From the stress-strain curves that can be seen, the shape of (CF2) same as (CF4) and (CF1, CF3, and CF5) have the same curve. This is related due to the effect of (X-shape) in case (CF2 and CF4) and the hoop laminates in case (CF1and CF5).

4.2.2.3 Mode of Failure for strengthening specimens (CF1, CF2, CF3, CF4, and CF5)

The specimen s with partials strengthening by CFRP laminates have the failure mode as below:

- In the case (CF1), the failure occurred in the top end of the column as the plate (4-10). this failure location differs from the control specimen (CC-CO-H)

Plate. (4-10-a) before failure for (CF1)

Plate. (4-10-b) after failure for (CF1)

Plate. (4-10) Failure mode for (CF1)

- In the case (CF2), the failure occurred in the top end of the column as the plate (4-11). This failure location differs from the control specimen (CC-CO-H), the failure occurred when the main rebar bent at the top end of the column.

Plate. (4-11-a) specimen (CF2) before testing

Fig. (4-11-b) specimen (CF2) after testing

Plate. (4-11) Failure mode for (CF2)

- While in the case (CF3), the failure occurred in the bottom end of the column as the plate (4-12). this failure location is similar to the control specimen (CC-CO-H).

plate. (4-12-a) specimen (CF3) before testing **plate. (4-12-b) specimen (CF3) after testing**

Plate. (4-12) Failure mode for (CF3)

- In the case (CF4), the failure occurred in the top end of the column as the plate (4-13). This failure location differs from the control specimen (CC-CO-H), the steel rebar near the hollow part buckled outward and then the concrete was damaged.

Plate. (4-13-a) specimen (CF4) before testing

Plate. (4-13-b) specimen (CF4) after testing

Plate. (4-13) Failure mode for (CF4)

- In the case (CF5), the failure occurred in the top end of the column as the plate (4-14). this failure location differs from the control specimen (CC-CO-H)

Plate. (4-14-a) specimen (CF5) before testing **Plate. (4-14-b) specimen (CF5) after testing**

Plate. (4-14) Failure mode for

According to the failure position, the specimens (CF1, CF2, CF4, and CF5) have failed due to the creation plastic hinge near the hollow part at the top

end of the concrete column as the plate (4-15), but specimen (CF3) have failure position near the bottom, this is caused to (CF3) did not have the hoop or bow laminates. Therefore, when the concentric loading increases during the test, these specimens (CF1, CF2, CF4, CF5) avoid the failure at the bottom as the (CC-CO-H). The mechanism of failure in specimens occurred when the main rebar reached the max. capacity then go to bent behavior outward direction then make the pressure on the concrete at this time, and so, the concrete expands and pushes outward and finally damaged, the CFRP will be ragged.

plate. (4-15) Failure mode for specimens that strengthening with CFRP and loaded concentrically

From the plate above the CFRP configuration with labels (CF1and CF5) containing a degree of concrete degradation less than other cases.

4.2.2.4 Ductility for specimens (CF1, CF2, CF3, CF4, and CF5)

These cases have the ductility the same as the control column or a little more than the control specimen where the case (CF3) has the excellent ductility value (1.9). all results of ductility were mentioned in the table (4-1)

4.2.3 Specimens strengthening by TRM and under concentric loading

This group has (5) cases with partials different form of TRM configurations. the load vs. displacement Can be illustrated as below. and comparing each result with the control case (CC-CO-H).

4.2.3.1 Load vs. Displacement

- The case **(CT1)** has the three hoops of TRM in the top, middle, and bottom as in plate (4-15). The load vs. displacement curve in fig (4-12) begins at (0) and increases in slope until it reaches a total displacement of **(6.11) mm** when the maximum load is applied. This case failed at **(620) kN** with an increase in compressive strength of about **(1.6) %** compared with the reference case (CC-CO-H).

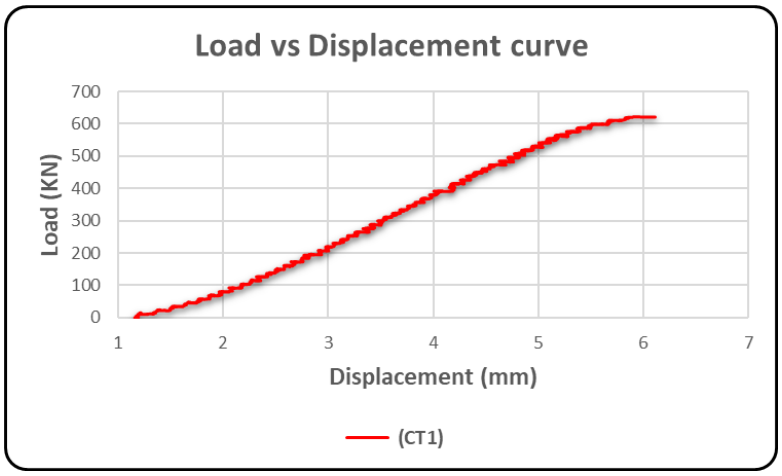

Fig. (4-12) Load-Displacement curve for (CT1)

Plate. (4-16) CT1

- The case **(CT2)** has the (2X) shape of TRM at the top and bottom of the column as the plate (4-17). Fig (4-13), begins with a little concavity when the load increases. Gradually, the max load reaches the **(635) KN** with max. Displacement equal to the **(8.65) mm**, this case has an increase in compressive strength of about **(4.1) %** compared with the reference case (CC-CO-H).

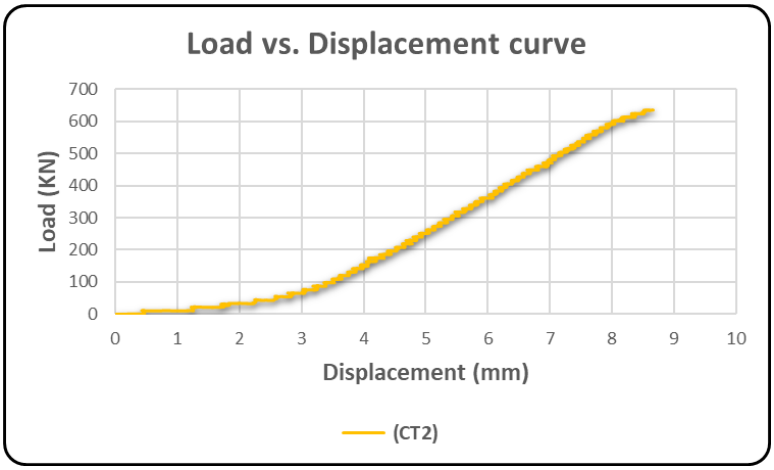

Fig. (4-13) Load-Displacement curve for (CT2)

Plate. (4-17) CT2

- The case **(CT3)** has one vertical TRM laminates on each column side as the plate (4-18). In the load vs. displacement curve in fig (4-14), when the loading increases, the max load reaches the **(627) KN** with max. displacement equal to the **(6.8) mm**, this case has an increase in compressive strength of about **(2.8) %** compared with the reference case (CC-CO-H).

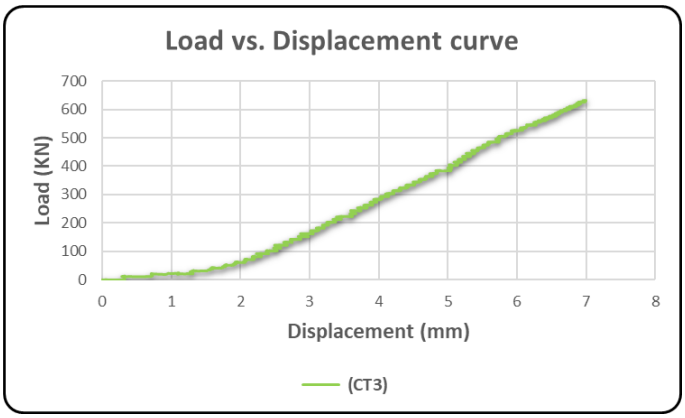

Fig. (4-14) Load-Displacement curve for (CT3)

Plate. (4-18) CT3

- In case **(CT4)** the specimen has the (four vertical) TRM laminate on each column side, and (2X-shape) of TRM at top and bottom as the plate (4-18). The load vs. displacement curve in fig (4-15), when the loading increases the max load reach to the **(654) KN** with max. Displacement equal to the **(10.67) mm**, this case has an increase in compressive strength of about **(7.2) %** compared with the reference case (CC-CO-H).

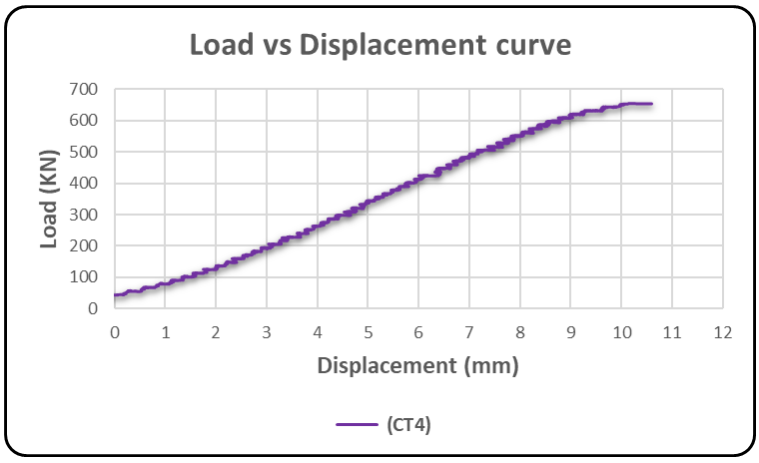

Fig. (4-15) Load-Displacement for (CT4)

Plate. (4-19) CT4

- In the case **(CT5),** this specimen has the (4 vertical) TRM laminate on each column side and (3hoop) of TRM as the plate (4-20). The load vs. displacement curve in fig (4-16) has little concavity at first. When the loading increases, the ultimate strength reaches the **(662) KN**. The displacement is equal to **(6.84) mm**. This case has an increase in compressive strength of about **(8.5) %** compared with the reference case (CC-CO-H).

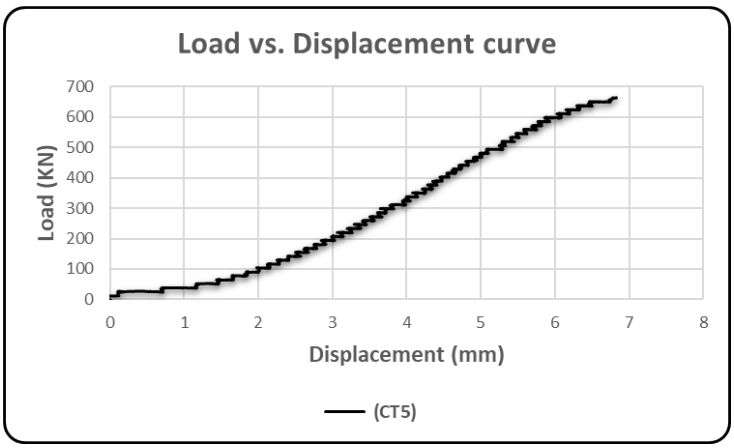

Fig. (4-16) Load-Displacement curve for (CT5)

Plate. (4-20) CT5

via fig (4-17) all cases that strengthened with TRM and loaded concentrically has the same behavior.

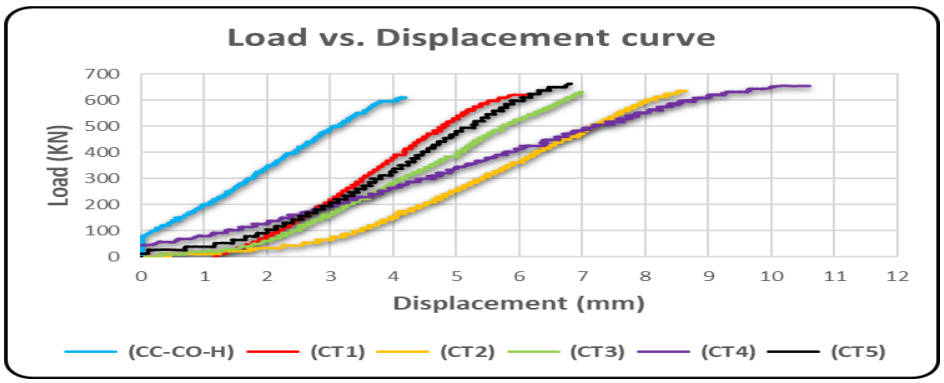

Fig. (4-17) Load-Displacement curves for (CT)

Table (4-3) illustrate all results for specimen s with strengthening by TRM under concentric loading.

Table. (4-3) results for control specimens and specimens that strengthening with TRM and loaded concentrically

case	max.load(KN)	strain-concrete	axial-disp.(mm)	failure-location	axial-disp. at yeild(mm)	Ductility	strengthening(%)
CC-C0-S	800	***	2	bottom	***	***	***
cc-co-h	610	0.00138	4.19	bottom	3.91	1.1	***
CT1	620	0.0013	6.11	top	5.7	1.1	1.6
CT2	635	0.0007	8.65	bottom	8.19	1.1	4.1
CT3	627	0.0015	6.9	top	6.4	1.1	2.8
CT4	654	0.0006	10.67	bottom	8.1	1.3	7.2
CT5	662	0.00069	6.84	bottom	6.3	1.1	8.5

4.2.3.2 Stress vs. Strain for strengthening specimen s (CT1, CT2, CT3, CT4, and CT5)

These cases have the same number and locations of the concrete strain gauge (SGC) for specimens strengthened by CFRP (CF). Fig (4-18) and table (4-4) Illustrates the data of (SGC).

Table. (4-4) Stress and strain obtained from SGC for strengthening by TRM specimens under concentric loading

Case	Stress (MPa)	Strain
CT1	27.35	0.00137
CT2	27.76	0.00073
CT3	28.13	0.0015
CT4	28.93	0.0007
CT5	29.42	0.0007

- The specimens confining partially by the TRM did not have more stress than the control specimen (CC-CO-H). Therefore, the max. stress consists of the case (CT5) with a value that reaches (29.42) MPa and the max. Strain obtains from the case (CT3) and the value equal (0.00150).
- The increase about the (2) % for the stress of specimen (CT5) compared with the un-confining specimen (CC-CO-H).
- The max. strain value obtained from the case (CT3) has the strain in concrete equal to the (0.0015) with enhancing in concrete deformation about (8.7) % in comparison with (CC-CO-H).
- (CT2, CT4, CT5) these specimens have the same behavior of (stress-strain) curves, also (CT2) have the stress little less than in cases (CT4, CT5). These specimens in (CT4 and CT5) did not have a good reading from concrete strain (SGC). This problem due to failure damage occurred far from the (SGC) location in these specimen s. These specimens failed by generating a plastic hinge near the bottom end. Moreover, the specimen s (CT1, CT3) have the same behavior, and a good strain reading was obtained from the (SGC).

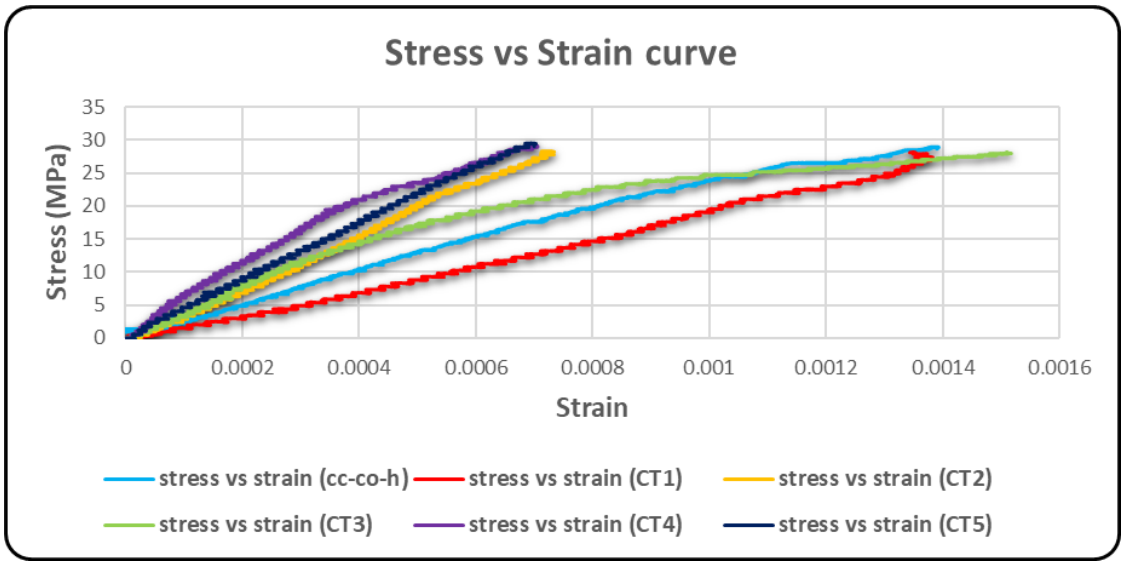

Fig. (4-18) Stress vs. Strain curves for TRM cases

4.2.3.3 Mode of Failure for strengthening specimens (CT1, CT2, CT3, CT4, and CT5)

In the case (CT1), the failure occurred in the top end of the column as the plate (4-21). this failure location differs from the control specimen (CC-CO-H)

Plate (4-21-a) specimen (CT1) before testing

plate (4-21-b) specimen (CT1) after testing

Plate (4-21) Failure mode for (CT1)

In the case (CT2), the failure occurred in the top end of the column as the plate (4-22). this failure location differs from the control specimen (CC-CO-H).

Plate (4-22-a) specimen (CT2) before testing

Plate (4-22-b) specimen (CT2) after testing

Plate (4-22) Failure mode for (CT2)

-in the case (CT3) has the failure occurred in the top end of the column as the plate (4-23). This failure location differs from the control specimen (CC-CO-H)

Plate (4-23-a) specimen (CT3) before testing

Plate (4-23-b) specimen (CT3) after testing

Plate (4-23) Failure mode for (CT3)

In the case (CT4), the failure occurred in the bottom end of the column as the plate (4-24). This failure location is similar to the control specimen (CC-CO-H)

Plate (4-24-a) specimen (CT4) before testing **Plate (4-24-b) specimen (CT4) after testing**

Plate (4-24) Failure mode for (CT4)

In the case (CT5), the failure occurred in the bottom end of the column as the plate (4-25). This failure location is similar to the control specimen (CC-CO-H)

Plate (4-25-a) specimen (CT5) before testing **Plate (4-25-b) specimen (CT5) after testing**

Plate (4-25) Failure mode for (CT5)

The specimens with labels (CT1, CT2, and CT3) have the same failure position. This failure is generated by creating the plastic hinge near the upper end of the column specimen, but the (CT4, and CT5) have the failure location near the lower end of the column. As a plate (4-26), the difference between these specimens is in the extent of the failure damage in the concrete of the specimen, where we notice in the specimen s (CT1, CT2, and CT3) that the damage is very clear in concrete, but it is less in the case (CT4, and CT5). The plate (4-26) below represent the failure in all cases and the (CT5) and (CT4) configuration illustrate the degradation in concrete less compared with other specimens.

4.2.3.4 Ductility for specimens (CT1, CT2, CT3, CT4, and CT5)

The max. value of ductility for these cases obtained from the case (CT4) equal to the (1.3). other ductility results for remain specimens inserted in previous time with table (4-4).

Plate (4-26): Failure mode for specimens that strengthened with TRM and loaded concentrically

4.3 Specimens under eccentric loading

This case has the specimens subjected to eccentric loading the work contain a control specimen s with two cases as below: -

4.3.1 Control columns under eccentric loading (CC-ECC)

In this case, the columns are subjected to eccentric loading with the eccentricity equal to the (0.6h) and (0.9h).

4.3.1.1 Load vs. Displacement for control specimens under eccentric load

The Column (CC-ECC-0.6h) has the load capacity reach to the (150) kN with displacement about (7.8) mm as the figure. (4-19). and for the Column (CC-ECC-0.9h) has the load vs. displacement curve rising from zero until it reaches a displacement of (5.59) mm. The curve undergoes increase in the slope until it reaches the ultimate load. The column eventually failed at (68.03) kN.as the figure (4-20)

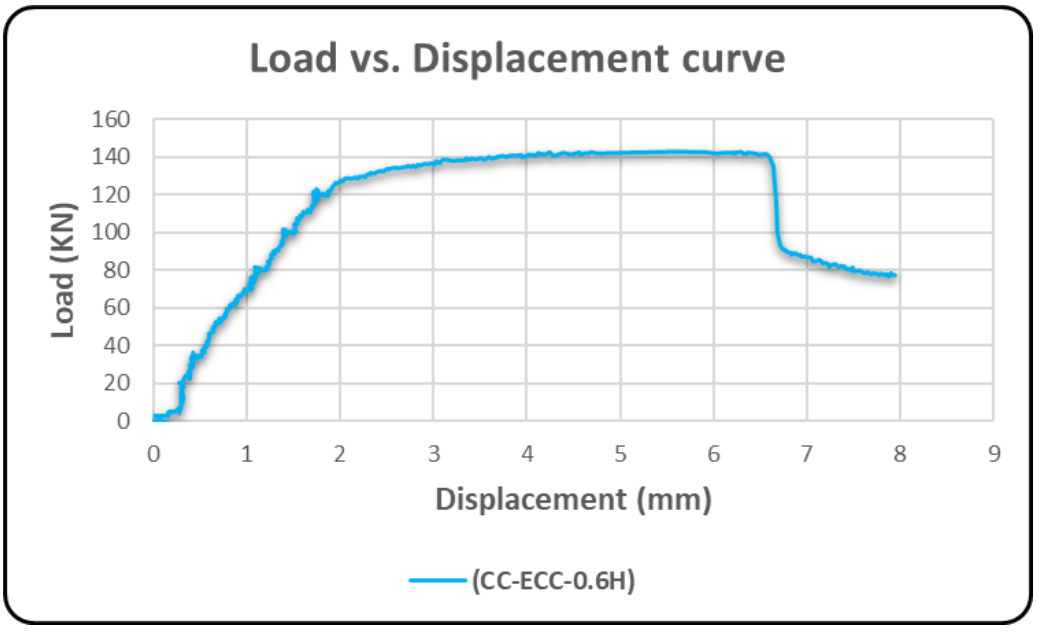

Fig. (4-19) Load-Displacement curve for (CC-ECC-0.6h)

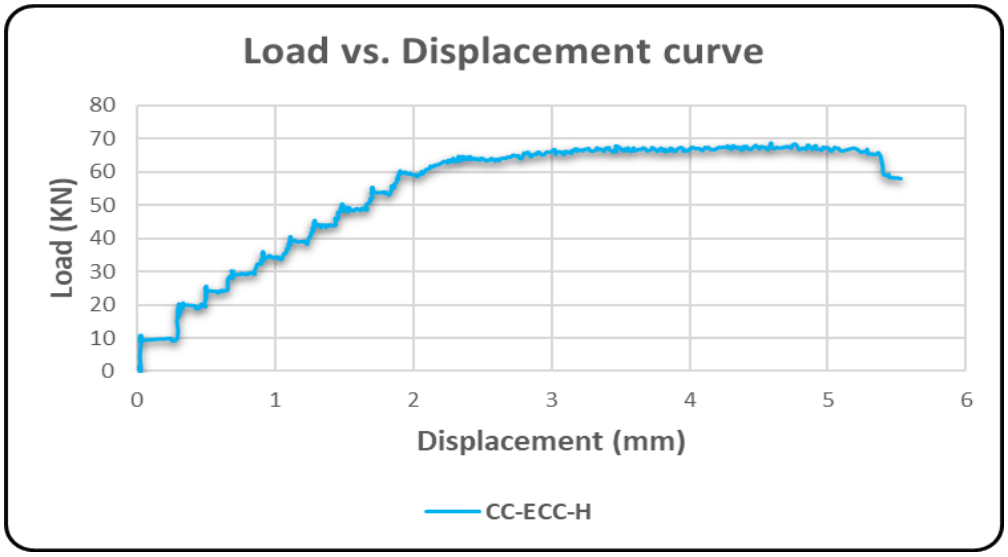

Fig. (4-20) Load-Displacement curve for (CC-ECC-0.9h)

4.3.1.2 Stress vs. Strain curves for control specimens under eccentric load

The control specimen with the label (CC-ECC-H), the eccentricity in this case equal to the (0.9h). To study the stress-strain curve in this specimen, put the (6) SGC divided into two groups, three in the tension face and another three in the compression face. The strain gauge in tension face has the labels (SGC1, SGC2, and SGC3), and the (SGC4, SGC5, and SGC6) for the compression face. Figure (4-21) illustrate the results of these SGC.

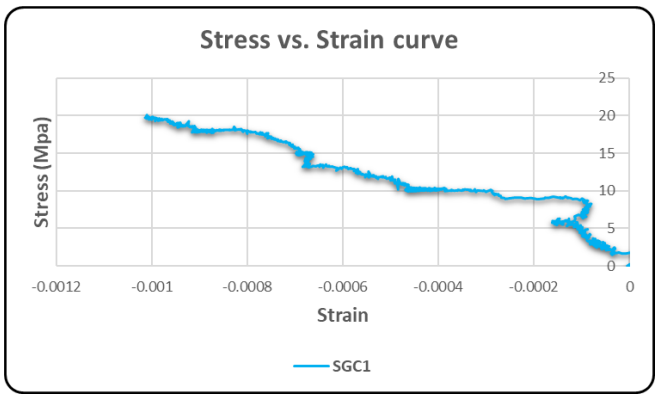

Fig. (4-21-a) stress-strain curve from (SGC1)

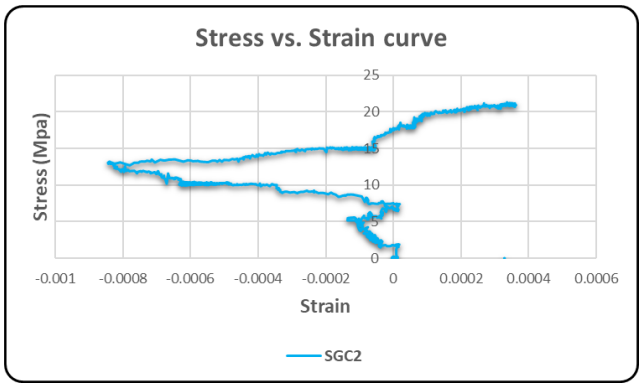

Fig. (4-21-b) stress-strain curve from (SGC2)

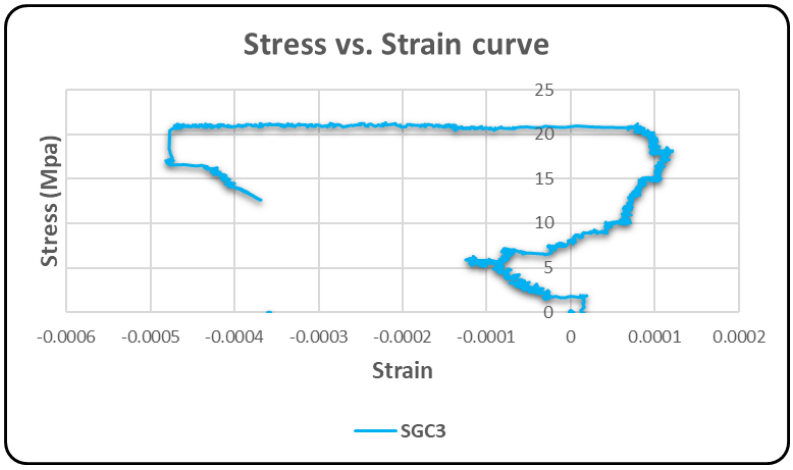

Fig. (4-21-c) stress-strain curve from (SGC3)

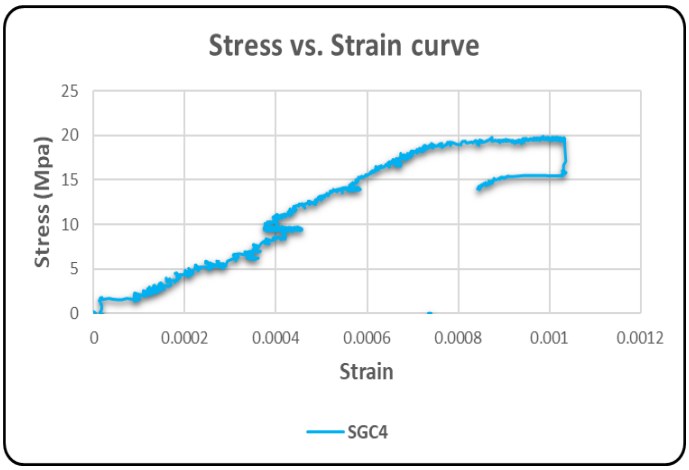

Fig. (4-21-d) stress-strain curve from (SGC4)

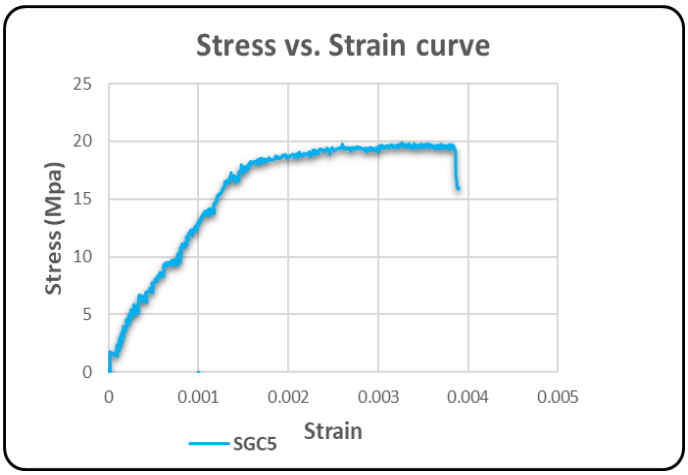

Fig. (4-21-e) stress-strain curve from (SGC5)

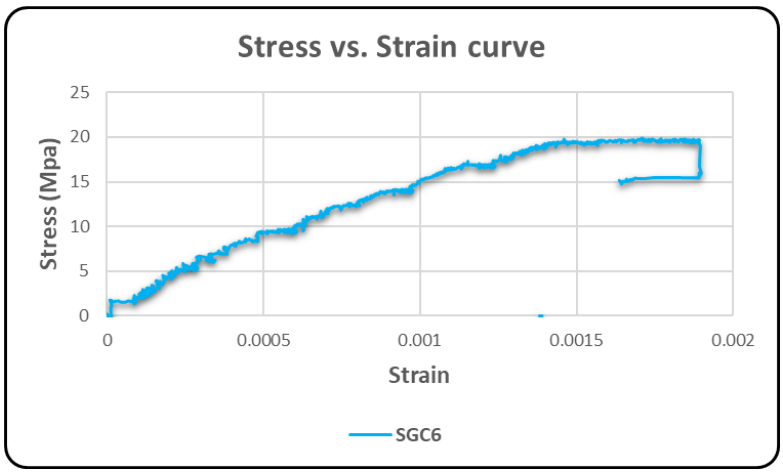

Fig. (4-21-f) stress-strain curve from (SGC6)

Fig. (4-21) Stress-Strain curves from SGC control specimens under eccentric load

- The data outcome from the (SGC1) had the concrete strain equal to the (-0.001), but the data from another strain gauge on the tension side did not have good reading due to the generated horizontal cracks and these cracks effect on the SGC reading, therefore neglecting the reading for (SGC2, SGC3) where the (SGC1) is located at the top end of the column.

The data for the compression side will stand from the (SGC4, SGC5, SGC6), the results found with (0.001,0.0038,0.0018) respectively. The strain (0.0038) from (SGC5) with stress equal to the (20) MPa, will compare with the other strengthening cases, the (SGC5) fixed at the middle height of the column.

4.3.1.3 Mode of Failure for control specimens under eccentric load (CC-ECC-H)

In the case (CC-ECC-H) contain the two unconfined specimens with a eccentricity equal to (135) mm from the center of the column for the specimen (0.9h) (CC-ECC-90), and (90) mm for the specimen (0.6h) (CC-ECC-60). The failure occurred due to the bending action as the plate (4-27), concrete failed in (CC-ECC-H), failure occurred somewhat above mid-height. Were the horizontal cracks formed at the tension face and the spalling in the concrete cover in the compression zone.

Plate. (4-27-a) Failure mode for (CC-ECC-0.9h)

Plate. (4-27-b) Failure mode for (CC-ECC-0.6h)

Plate (4-27) Failure mode for (CC-ECC-h)

4.3.1.4 Ductility Index for the control specimens

Max. Ductility obtained from the specimen (0.9h) (CC-ECC-90) the ductility equal to the (1.4).

4.3.1.5 Max. crack width for specimen (CC-ECC-H)

The horizontal tensional crack occurred due to the effect of the bent of the specimen. Because of the eccentricity, the stress will be formed as the tension face the surface concrete far from the load and compression area near the load. The max crack width (4) mm.

4.3.2 Specimens strengthening by CFRP under eccentric loading

This group has (5) specimens with partials different from CFRP configurations. Can illustrate the load vs. displacement as below and compare each result with the control case (CC-ECC-H).

4.3.2.1 Load vs. Displacement for strengthening specimens (EF1, EF2, EF3, EF4, and EF5)

- The case (EF1) has the CFRP's three hoop in the top, middle and bottom as the plate (4-28). The load vs. displacement curve in fig (4-22) begins at (0) and the total displacement equal to the (12.7) mm when the maximum load is applied. This case failed at (69.53) kN with an increase of about (2.2) % compared with the reference case (CC-ECC-H).

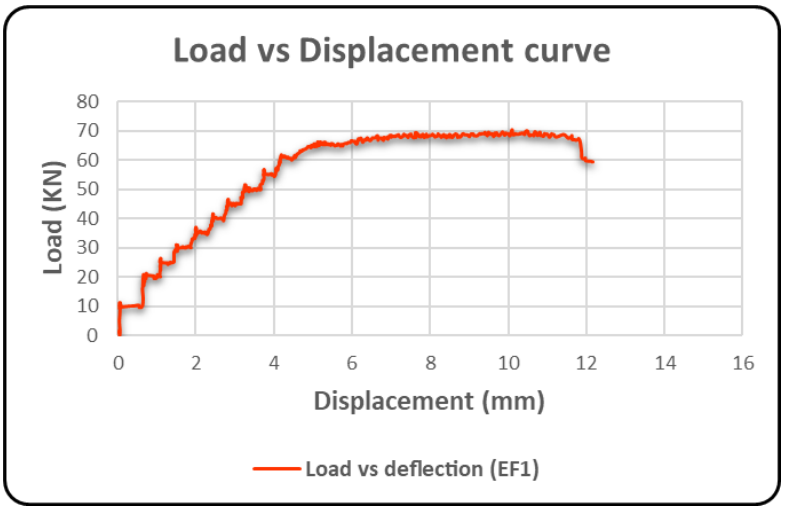

Fig. (4-22) Load-Axial displacement curve for (EF1)

Plate. (4-28) EF1

- The case (EF2) has the (2X) shape of CFRP at the top and bottom of the column as the plate (4-29). The load vs. displacement curve in fig (4-23), begins with little concavity. When the load increases Gradually, the max load reaches the (68.9) KN with max. displacement equal to (20.73) mm. This case has an increased compressive capacity of about (1.3) % compared with the reference case (CC-CO-H).

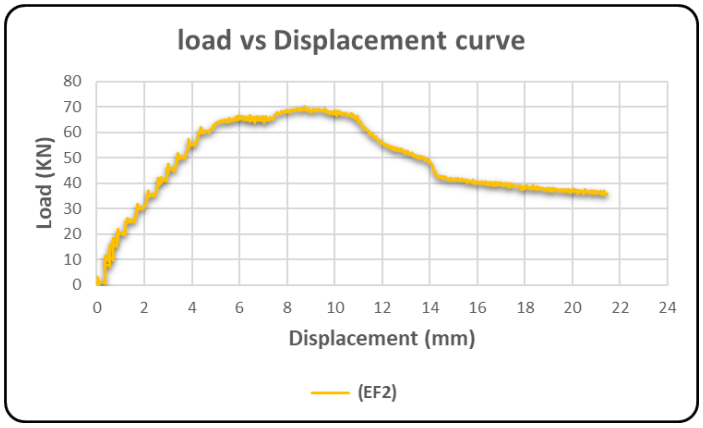

Fig. (4-23) Load-Axial displacement curve for (EF2)

Plate. (4-29) EF2

- The case (EF3) has the one vertical CFRP laminates on the tension side of the column as the plate (4-30). The load vs. displacement curve in fig (4-24) shows that the max load reaches (87.9) KN with max. displacement equal to the (8.62) mm, this case has an increase of about (29.2) % compared with the reference case (CC-CO-H).

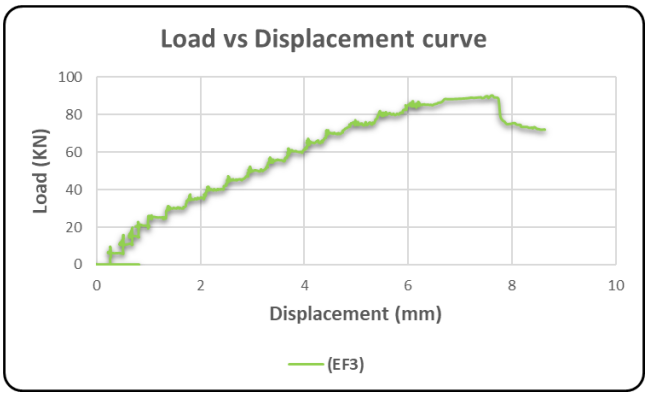

Fig. (4-24) Load-Axial displacement curve for (EF3)

Plate. (4-30) EF3

- In the case (EF4), this specimen has the (one vertical) CFRP laminate on the tension side and (2X-shape) of CFRP at the top and bottom as the plate (4-31). In the load vs. displacement curve in fig (4-25), the max load reaches (90.5) KN with max when the loading increases. Displacement equal to the (11.63) mm, this case has an increase of about (33) % compared with the reference case (CC-ECC-H).

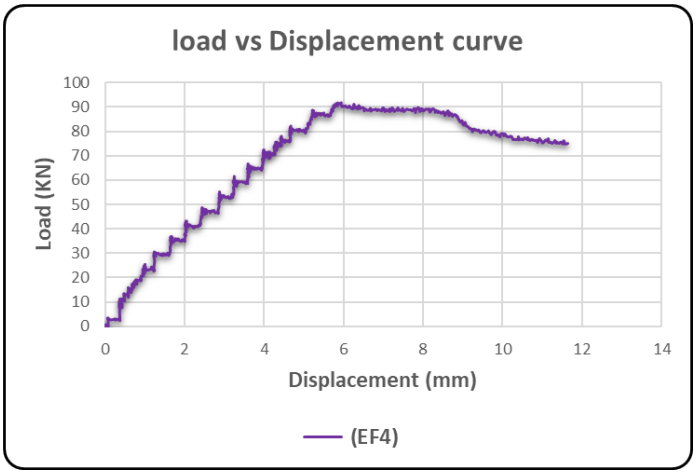

Fig. (4-25) Load-Axial displacement curve for (EF4)

Plate. (4-31) EF4

- In the case (EF5), this specimen has the (one vertical) CFRP laminate on the tension side and (3hoop) of CFRP as the plate (4-32). The load vs. displacement curve in fig (4-26) has little concavity at first; when the loading increases, the max load reaches the (94.8) KN with max. displacement equal to the (10.91) mm, this case has an increase of about (39.4) % compared with the reference case (CC-ECC-H).

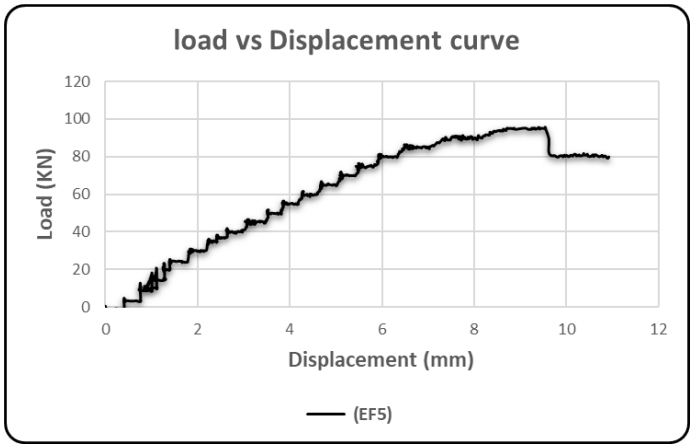

Fig. (4-26) Load-Axial displacement curve for (EF5)

Plate. (4-32) EF5

fig. (4-27) explain the behavior for all cases with eccentric loading, wherein the elastic stage all cases have the same behavior but the difference take place after plastic stage starting.

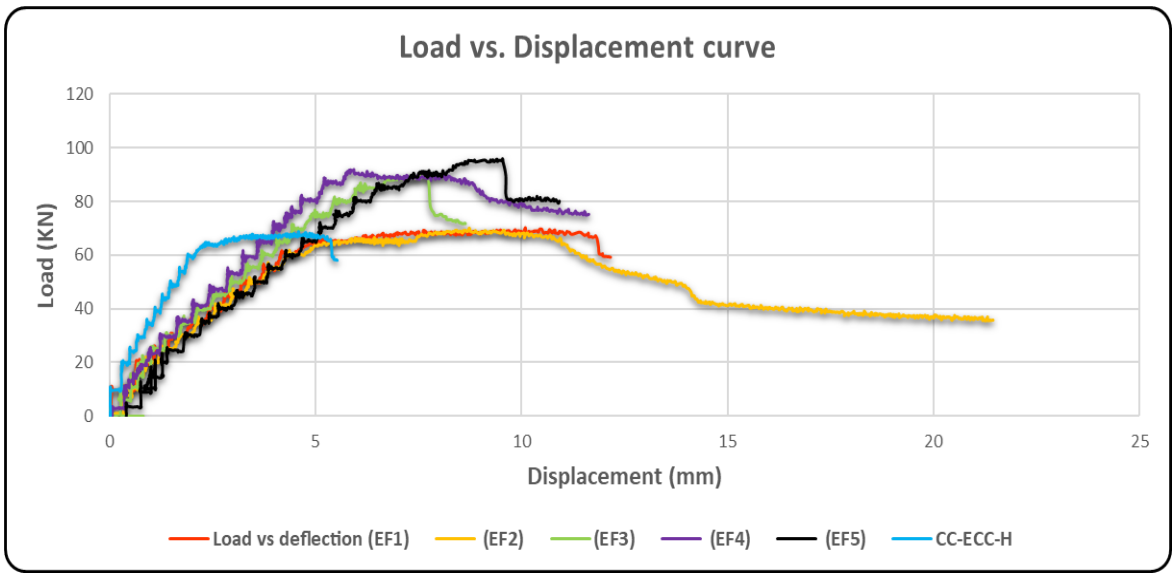

Fig. (4-27) Load-Axial displacement curves for control specimen and specimens that strengthened with CFRP under eccentric loading

The lateral displacement also generated and measured by (LVDT) for the middle height of the column. And the fig. (4-28) show the load with lateral displacement for all cases.

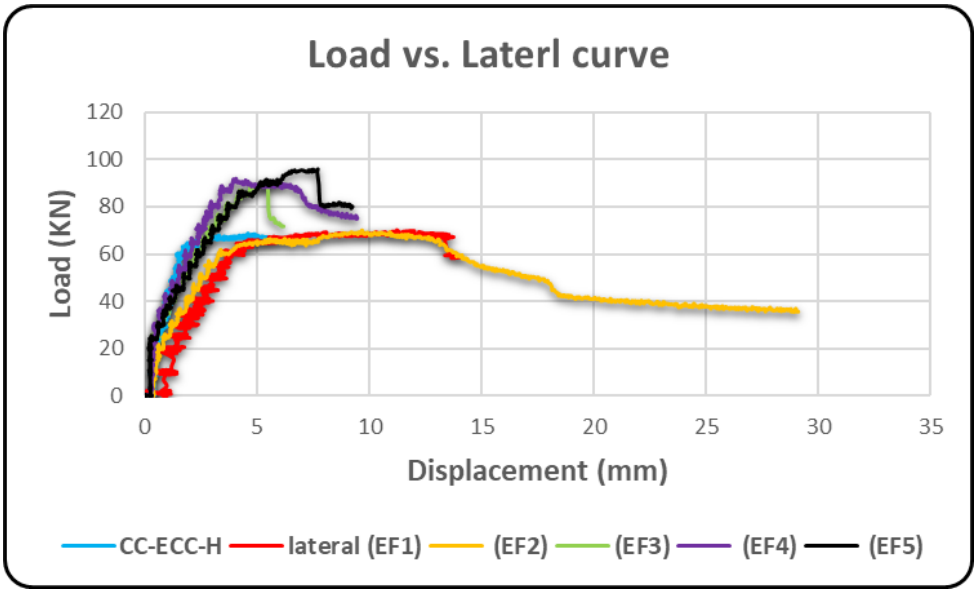

Fig. (4-28) Load-Lateral displacement curves for control specimen and specimens that strengthened with CFRP under eccentric loading

All the test results of eccentric column strengthening by CFRP reported in the table (4-5)

Table (4-5): results for control specimens and specimens that strengthening with CFRP and loaded eccentrically

case	max.load(KN)	strain-compression	strain-tension	axail-disp.(mm)	X-lateral (mm)	Y-lateral (mm)	axail-disp.at yeild (mm)	ductility	strengthening (%)
CC-ECC-0.9h	68.03	0.0038	N/A	5.59	5.7	0.1	4	1.4	***
EF1	69.53	0.0018	-0.0018	12.7	13.75	0.61	5.6	2.3	2.3
EF2	68.9	0.0036	-0.0199	21.44	28	-0.93	4	5.4	1.3
EF3	87.9	0.0017	-0.0039	8.62	5.94	-0.08	5.5	1.6	29.3
EF4	90.5	0.0013	-0.00316	11.63	9.26	-0.055	5.92	2.0	33.1
EF5	94.8	0.002	-0.0062	10.91	9.1	0.1	7.06	1.5	39.4

4.3.2.2 Stress vs. Strain for strengthening specimens (EF1, EF2, EF3, EF4, and EF5)

These specimens used two concrete strain gauges (SGC) located at the middle height of the concrete column on the tension and compression side. The results explain in fig (4-29). The stress calculated from eq (). This stress is created due to form a bent in the specimen because of the eccentricity (0.9h). also table (4-6) scheme all readings collected from SGC for specimens on compression and tension sides

Table (4-6): Stress and strain obtained from SGC for strengthening by CFRP specimens under eccentric loading

Case	Stress (MPa)	Strain
EF1	21.5	(C) 0.0018
		(T)-0.0018
EF2	23.1	(C) 0.0036
		(T)-0.0199
EF3	25.9	(C) 0.0017
		(T)-0.0039
EF4	27.2	(C) 0.0013
		(T)-0.00316
EF5	28.5	(C) 0.0020
		(T) -0.0062

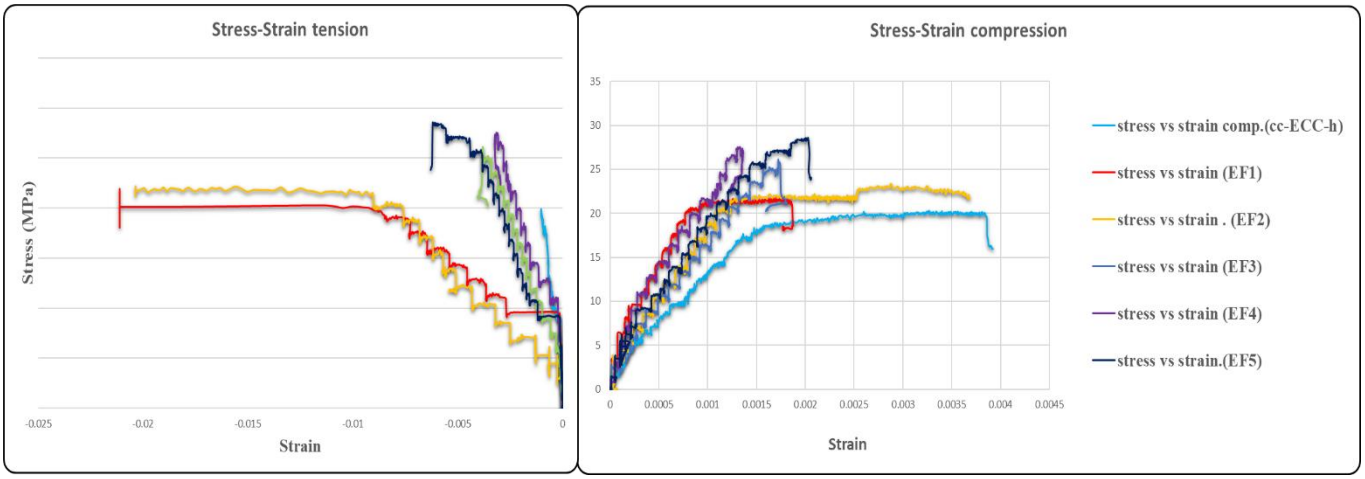

Fig. (4-29) Stress vs. Strain curves for (CC-ECC-h), EF1, EF2, EF3, EF4, and EF5)

- According to the results obtained from the concrete strain gauge (SGC) the significant value of compression and tension strain was obtained from the case (EF2) is (0.0036) and (-0.0199), respectively. The max. value of stress is founded from the case (EF5) with a value equal to the (28.5) MPa.

4.3.2.3 Mode of Failure for strengthening specimens (EF1, EF2, EF3, EF4, and EF5)

When the eccentricity developed, more ductile behavior was observed. The failure occurred in the middle height of the column. As a result of eccentricity, two types of stress are generated: tensile and compressive. The tensile side was found to have horizontal cracks. Also, the compression side has damage in concrete. The CFRP will increase the compressive strength and decrease the deterioration in concrete for the specimens as below: -

*For the case (EF1) and from the plate (4-33) note that the side exposed to the compressive stresses as in the plate (4-33-a), the behavior of the

specimen is similar to the reference specimen (CC-ECC-H), noting that the presence of (CFRP) has reduced the percentage of damaged concrete. Speaking with the side exposed to tensile stresses, generation of horizontal cracks is noted as the plate (4-33-b)

Plate (4-332-a) compression side for

Plate (4-33-b) tension side for EF1

Plate (4-33) Failure mode for EF1

*In the case of studying the failure mode of the (EF2) as the plate (4-34), the area of damage has increased in the part exposed to compressive stress compared with the reference specimen, this is caused due to effect of (X-

shape) of CFRP as the plate (4-34-a). And with the same specimen behavior but in the tension side, the horizontal crack will appear due to effect the tensile stresses as the plate (4-34-b)

Plate (4-34-a) compression side for EF2

Plate (4-34-b) tension side for EF2

Plate (4-34) Failure mode for EF2

In the specimen (EF3) as the plate (4-35) and in the compression side, no destroyed concrete surface was as the plate (4-35-a). Also, in the tension part, the horizontal cracks did not presences just in the top tension face as plate (4-35-b). This specimen (EF3) has the vertical CFRP laminate with a length equal to (600) mm.

Plate (4-35-a) compression side for EF3

Plate (4-35-b) tension side for EF3

Plate (4-35) Failure mode for EF3

According to the specimen (EF4) in the plate (4-36). Via the plate (4-36-a) the area of damage in concrete is decrease or eliminate compared with the reference specimen, and the horizontal crack formed in the bottom part of tension face as the plate (4-36-b)

Plate (4-36-a) compression side for EF4

Plate (4-36-b) tension side for EF4

Plate (4-36) Failure mode for EF4

In the specimen (EF5) as the plate (4-37), we notice that the damage is very little on both sides concerning the tensile or compressive stresses as the plates (4-37-a) and (4-37-b).

Plate (4-37-a) compression side for EF5

Plate (4-37-b) tension side for EF5

Plate (4-37) Failure mode for EF5

From the all cases failure mode above and the plate (4-38) below, it can be seen that the (EF5) has an excellent external partially strengthening by CFRP to carry the eccentric loading.

Plate (4-38) Failure mode for (EF1, EF2, EF3, EF4, and EF5)

4.3.2.4 Ductility

Maximum. ductility obtained from the specimen (EF2) was equal to (5.4) and has the label (EF2). This specimen has the partial strengthening by 2(X-shape) of CFRP at the top and bottom. Remain specimens less than (5.4)

4.3.2.5 Max. crack width for specimens (EF)

In this research, did not read the value and the width of the crack in the case of specimens subjected to concentric loading. Where the failure in this situation more brittle and go to more risk. While in the eccentric case, measured the width of crack was measured when the test finished. The table below (4-7) show the results of all cases (EF).

Table (4-7) results for (EF1, EF2, EF3, EF4, and EF5)

Case	max.load(KN)	M1=(P*e) (n.mm)	M2=(P*(e+d) (n.mm)	Stress1=(P/A) (Mpa)	Stress2=(M2*C/I) (Mpa)	Stress(S1+S2)	crack-width(mm)
CC-ECC-0.9h	68.03	9184050.0	9571821	3.0	17.0	20.0	***
EF1	69.53	9386550.0	10342587.5	3.1	18.4	21.5	0.4-mid
EF2	68.9	9301500.0	11230700	3.1	20.0	23.0	0.3-mid
EF3	87.9	11866500.0	12388626	3.9	22.0	25.9	0.1-top.side
EF4	90.5	12217500.0	13055530	4.0	23.2	27.2	0.05-top
EF5	94.8	12798000.0	13660680	4.2	24.3	28.5	0.15-top

4.3.3 Specimens strengthening by TRM and under eccentric loading

- The case (ET1) have the three hoop of TRM in the top, middle, and bottom of as the plate (4-39). The load vs. displacement curve in fig (4-30), begins at (0) and the total displacement equal to the (19.3) mm when the maximum load is applied. This case failed at (68.5) kN with an increase of about (0.7) % compared with the reference case (CC-ECC-H).

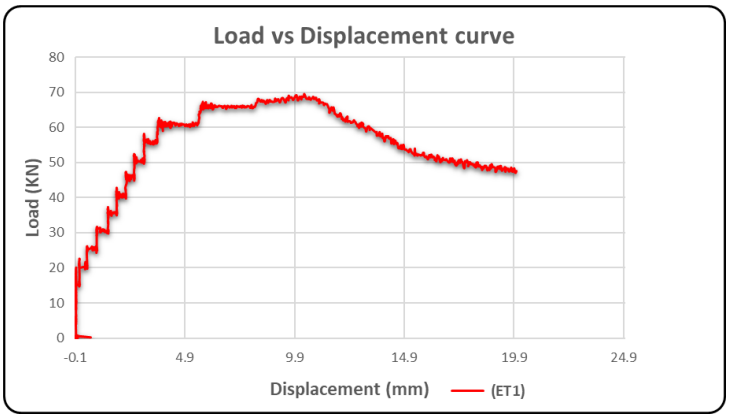

Fig. (4-30) Load-Displacement curve for (ET1)

Plate (4-39) ET1

- The case (ET2) has the (2X) shape of TRM at the top and bottom of the column as the plate (4-40). In fig (4-31), when the load increases gradually, the max load reaches the (70.7) KN with max. displacement equal to the (9.11) mm. This case has an increased compressive capacity of about (4) % compared with the reference case (CC-ECC-H).

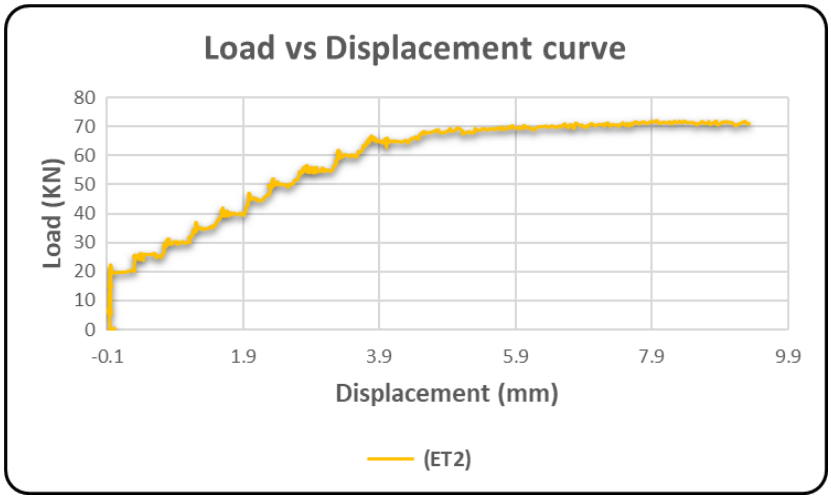

Fig. (4-31) Load-Displacement curve for (ET2)

Plate (4-40) ET2

- The case (ET3) has the one vertical TRM laminates on the tension side of the column as the plate (4-41). In the load vs. displacement curve in fig (4-32), when the loading increases, the max load reach to the (82.64) KN with max. displacement equal to the (15.6) mm, this case has an increase of about (21.5) % compared with the reference case (CC-ECC-H).

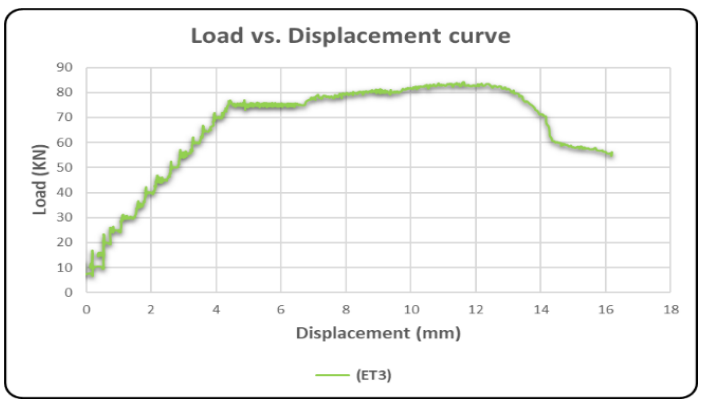

Fig. (4-32) Load-Displacement curve for (ET3)

Plate (4-41) ET3

- In the case (ET4), this specimen has the one vertical TRM laminate on the tension side and (2X-shape) of TRM at the top and bottom as the plate (4-42). The load vs. displacement curve in fig (4-33), when the loading increases the max load reach to (84.4) KN with max. displacement equal to the (12.35) mm, this case has an increase of about (24.1) % compared with the reference case (CC-ECC-H).

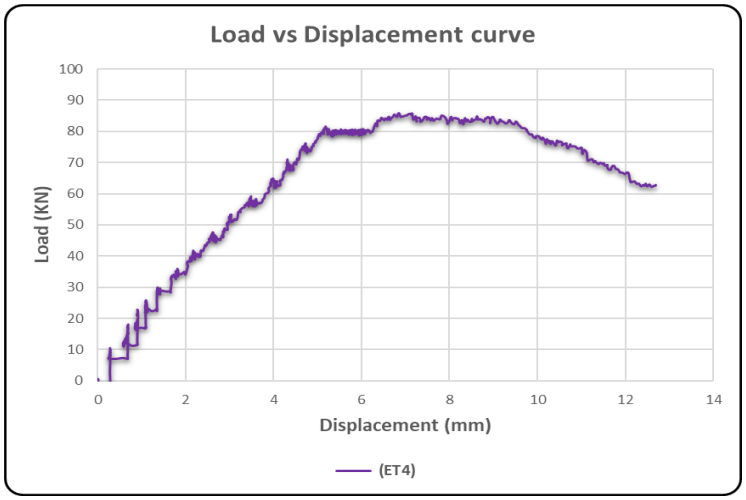

Fig. (4-33) Load-Displacement curve for (ET4)

Plate (4-42) ET4

- In the case (ET5), this specimen has the one vertical TRM laminate on the tension side and (3hoop) of TRM as the plate (4-43). The load vs. displacement curve in fig (4-34), when the loading increases, the max load reaches the (86.5) KN with max. displacement equal to the (19.15) mm, this case has an increase of about (27.2) % compared with the reference case (CC-ECC-H).

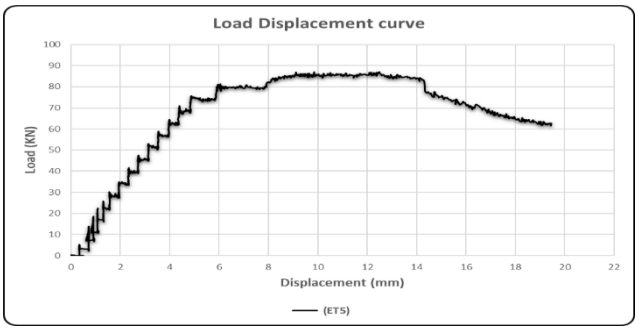

Fig. (4-34) Load-Displacement curve for (ET5)

Plate (4-43) ET5

The results for specimens with strengthening by TRM are grouped into the table (4-8)

Table (4-8): results for control specimens and specimens that strengthening with TRM and loaded eccentrically

case	max.load(KN)	strain-compression	strain-tension	axail-disp.(mm)	X-lateral (mm)	Y-lateral (mm)	axail-disp.at yeild (mm)	ductility	strengthening (%)
CC-ECC-0.9h	68.03	0.0038	N/A	5.59	5.7	0.1	4	1.4	***
ET1	68.5	0.0012	-0.0043	20	19.7	-1.7	4.2	4.8	0.7
ET2	70.7	0.0037	N	9.11	10.67	-1.62	3.9	2.3	4.0
ET3	82.64	0.003	-0.02	16.1	17.75	-1.04	4.32	3.7	21.5
ET4	84.4	0.005	-0.02	12.68	10.73	-0.06	5.22	2.4	24.1
ET5	86.5	0.00059	-0.0113	19.46	17.08	1.5	5.8	3.4	27.2

the fig. (4-35) and (4-36) illustrate the all load with axial displacement curves and (load with lateral curve for all cases strengthening by TRM.

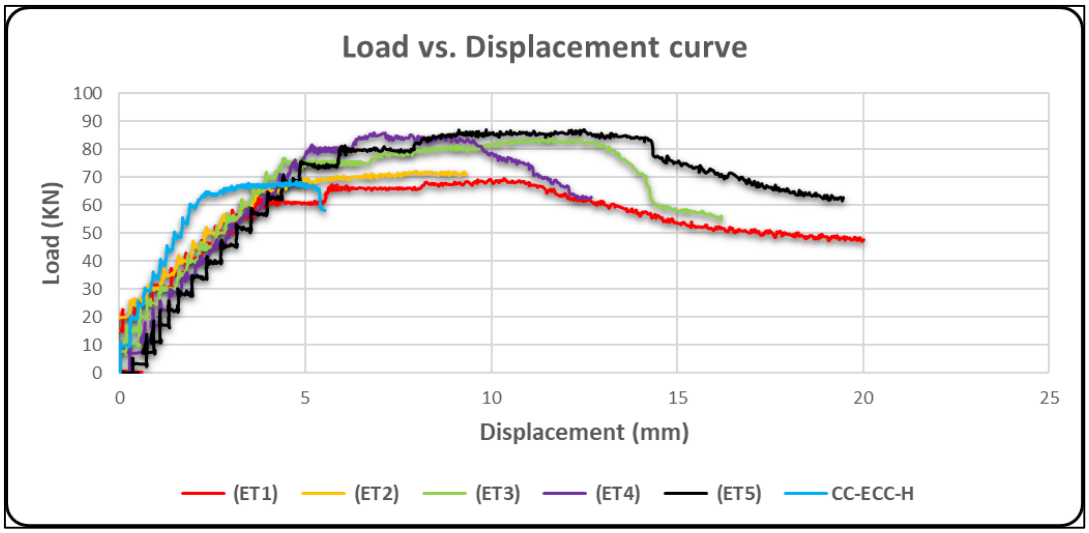

Fig. (4-35): Loads vs. Displacement curve for (CC-ECC-H, ET1, ET2, ET3, ET4, andET5)

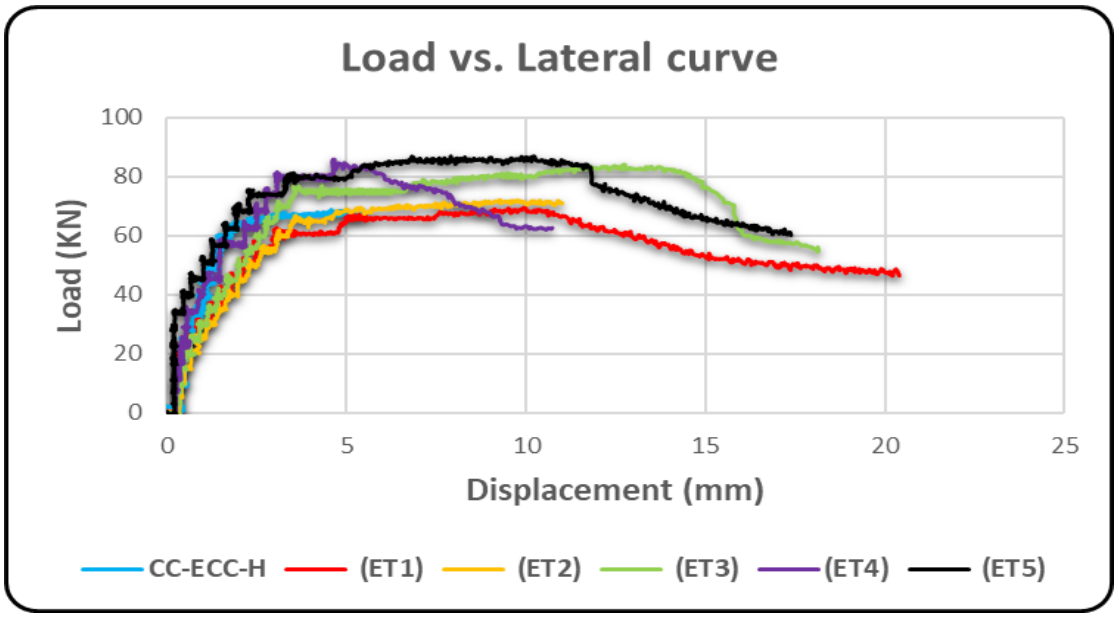

Fig. (4-36): Loads vs. Lateral displacement curve for (CC-ECC-H, ET1, ET2, ET3, ET4, andET5)

4.3.3.2 Stress vs. Strain for concrete in strengthening specimens (ET1, ET2, ET3, ET4, and ET5)

This specimen used two strain concrete gauges (SGC) located at the middle height of the concrete column on the tension and the compression side. The results explain in fig (4-37) and table (4-9). The stress calculated from eq (). This stress created due to form the bent in the specimen because the eccentricity (0.9h)

Table (4-9): Stress and strain obtained from SGC for strengthening by TRM specimens under eccentric loading

Case	Stress (MPa)	Strain
ET1	21.9	(C) 0.0012
		(T) -0.0043
ET2	21.5	(C) 0.0037
		(T) N/A
ET3	26.1	(C) 0.003
		(T)-0.02
ET4	25.6	(C) 0.005
		(T)-0.02
ET5	27.2	(C) 0.00059
		(T) -0.011

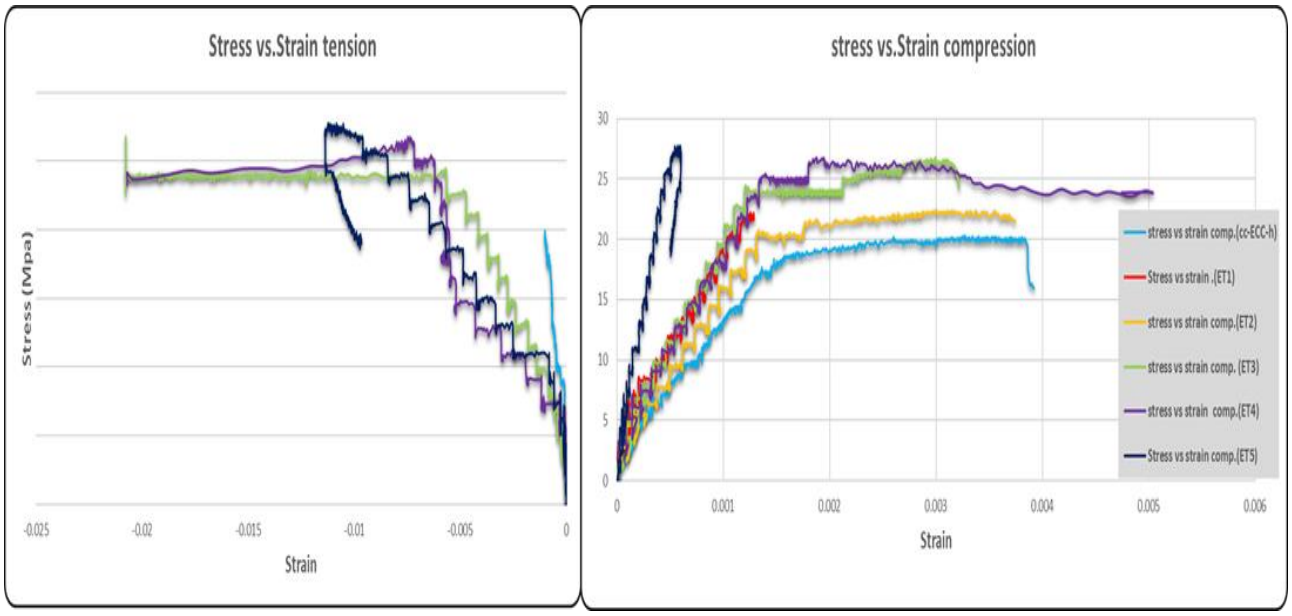

Fig. (4-37) Stress vs. Strain curves for (CC-ECC-h), ET1, ET2, ET3, ET4, and ET5)

4.3.3.3 Mode of failure for specimens (ET1, ET2, ET3, ET4, and ET5)

These specimens strengthened by (TRM) laminates subjected to eccentric loading have the behavior and failure mode same as the specimen s in (CFRP) under the same type of loading. The horizontal crack created in the tension face is due to the bent in the specimen because of the buckling outward in main rebar and crushing in the concrete in compression side.

in the case (ET1) as the plate (4-44), concerning the area exposed to compression stresses, a slight damage of concrete column is noted (the reason may be due to the use of mortar in TRM) as it works to block the view, as the plate (4-44-a). As for the part exposed to tensile stresses, the specimen was affected by these stresses by forming horizontal cracks on this side, see plate (4-44-b). The crack width is greater than the same configuration but uses CFRP laminates.

Plate (4-44-a) Compression side for ET1

Plate (4-44-b) Tension side for ET1

Plate (4-44) Failure mode for ET1

Regarding the specimen (ET2) with the plate (4-45), where no damage was observed in the concrete for the part subjected to compressive stresses as the plate (4-45-a).and for the tension face, the cracks generated as the plate (4-45-a).

Plate (4-45-a) Compression side for ET2

Plate (4-45-b) Tension side for ET2

Plate (4-45)Failure mode for ET2

The plate (4-46) this specimen (ET3) showed a clear effect of tensile stresses through the generation of many horizontal cracks along the specimen as the plate (4-46-a). Likewise, the part exposed to compressive stresses was clearly concrete damage in the middle area, as the plate(4-46-b).

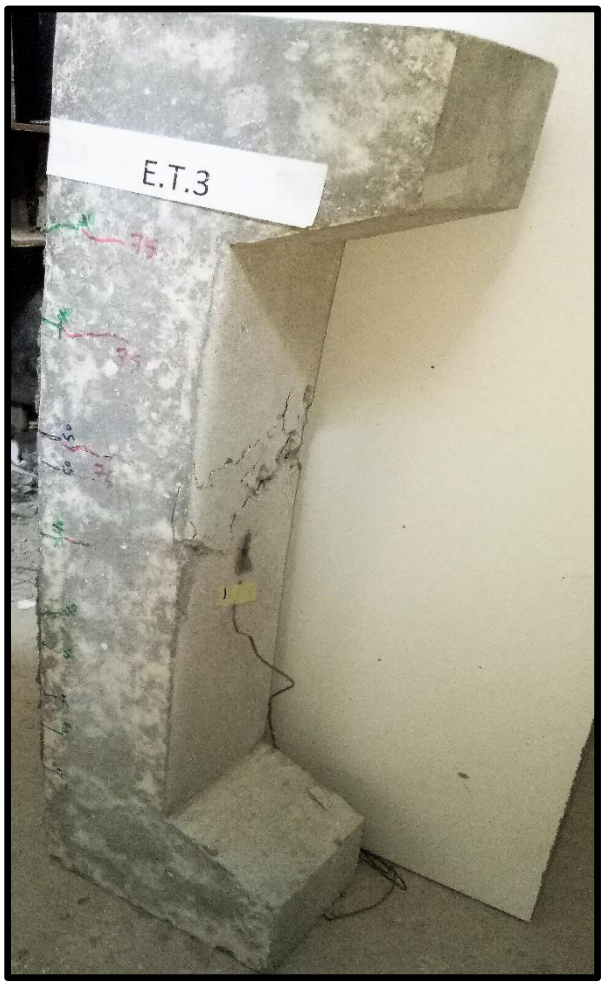

Plate (4-46-a) Compression side for ET3 **Plate (4-46-b) Tension side for ET3**

Plate (4-46) Failure mode for ET3

for the plate (4-47) explain the mode of failure for the case (ET4) which showed cracks on the part exposed to tensile stresses as the pate (4-47-a).and with the compression stress a few the lost in concrete as the plate (4-47-b).

Plate (4-47-b) Compression side for ET4

Plate (4-47-a) Tension side for ET4

Plate (4-47) Failure mode for ET4

For the specimen (ET5) and with the plate (4-48), the cracks are evident in the upper part of the side exposed to tensile stresses and clearly in part near the upper third part of the column as the plate (4-48-a). For the compression face, the specimen showed the concrete failure near the corner as the plate (4-48-b).

Plate (4-48-a) Compression side for ET5

Plate (4-48-b) Tension side for ET5

Plate (4-48) Failure mode for ET5

plate (4-49) illustrate all tension cracks for all cases

Plate (4-49) Failure mode for ET

4.3.3.4 Ductility

Max. ductility obtained from the specimen (ET1) is equal to (4.8). This specimen has the partial strengthening by 3(hoop) of TRM at the top, middle, and bottom. Remain specimens less than (ET1), and the values were inserted with table (4-8)

4.3.3.5 Max. crack width for specimens for (ET1, ET2, ET3, ET4, andET5)

In these cases, the crack width did not have good reading for strengthening by TRM due to the cementitious materials used as mortar in TRM.

All results for stress in cases are reported in the table (4-10). Moreover, the crack width mentioned in this table is for the mortar TRM and not for the concrete of the column.

Table (4-10) bending moment and stresses for (CC-ECC-H, ET1, ET2, ET3, ET4, andET5)

Case	max.load(KN)	M1=(P*e) (n.mm)	M2=(P*(e+d) (n.mm)	Stress1=(P/A) (Mpa)	Stress2=(M2*C/I) (Mpa)	Stress(S1+S2)	crack-width(mm)
CC-ECC-0.9h	68.03	9184050.0	9571821	3	17	20	***
ET1	68.5	9247500.0	10596950	3.0	18.8	21.9	6
ET2	70.7	9544500.0	10298869	3.1	18.3	21.5	2.8
ET3	82.64	11156400.0	12623260	3.7	22.4	26.1	3
ET4	84.4	11394000.0	12299612	3.8	21.9	25.6	2
ET5	86.5	11677500.0	13154920	3.8	23.4	27.2	3

4.4 Comparison between specimens with CFRP and TRM

For the specimens under concentric loading the figures below illustrated the comparison for (stress vs. strain) curve and the (load vs. Displacement) curve for the two cases CFRP and TRM.

4.4.1 Comparison between specimens with concentric loading

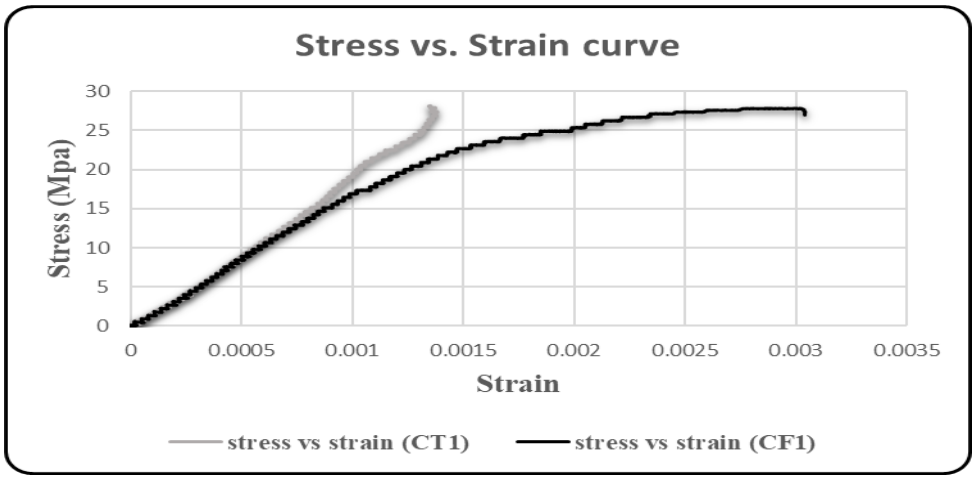

Fig. (4-38): Stress vs. Strain curve for (CF1 and CT1)

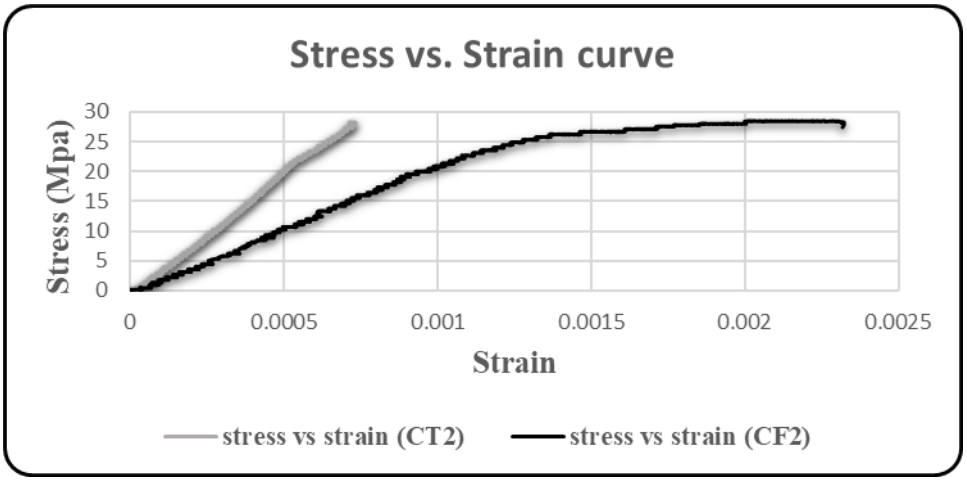

Fig. (4-39): Stress vs. Strain curve for (CF2 and CT2)

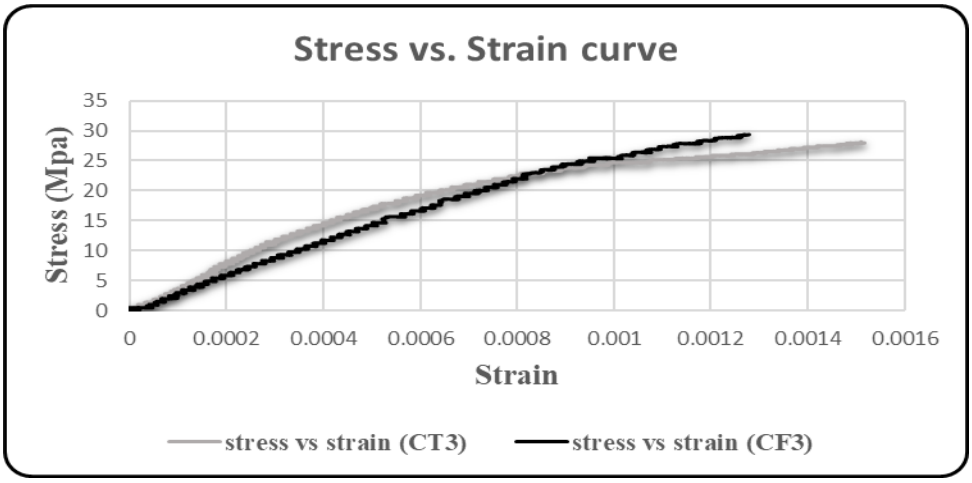

Fig. (4-40): Stress vs. Strain curve for (CF3 and CT3)

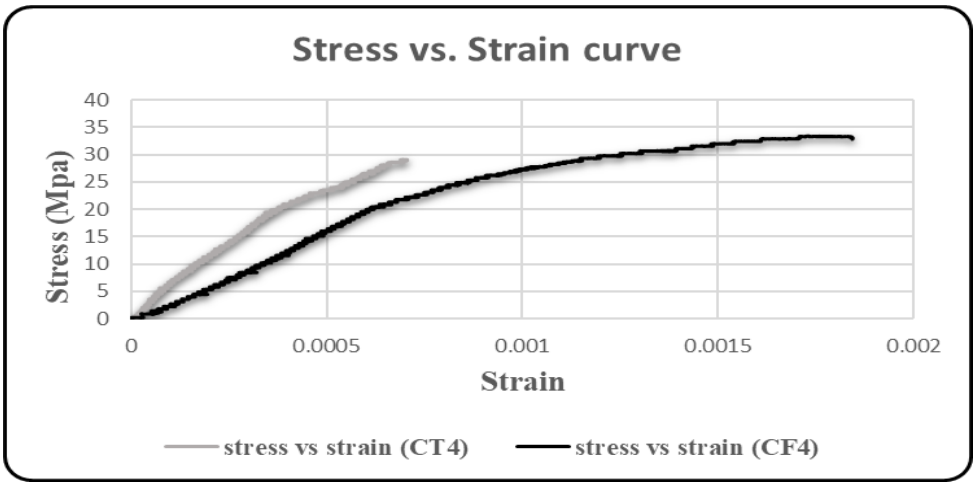

Fig. (4-41): Stress vs. Strain curve for (CF4 and CT4)

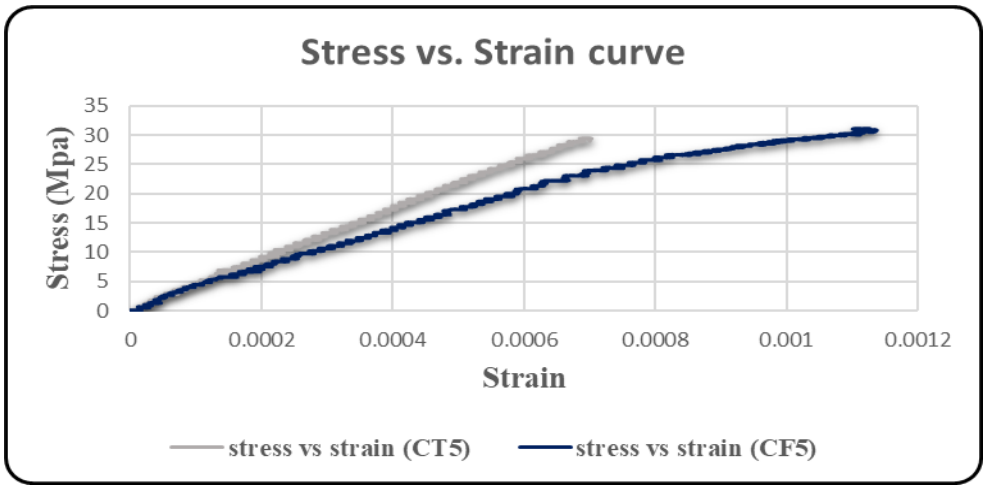

Fig. (4-42): Stress vs. Strain curve for (CF5 and CT5)

From the figures with (stress vs. strain) curves above, the strain in specimens with strengthening by CFRP more than the TRM except for the specimen (CT3) and also the behavior of slightly elastic stage has the same response for two models.

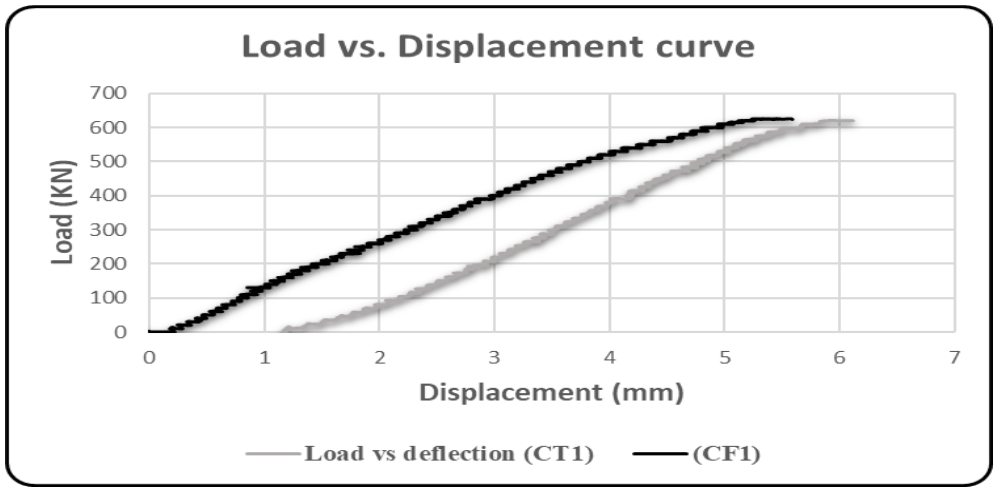

Fig. (4-43): Load vs. Axial displacement curve for (CF1 and CT1)

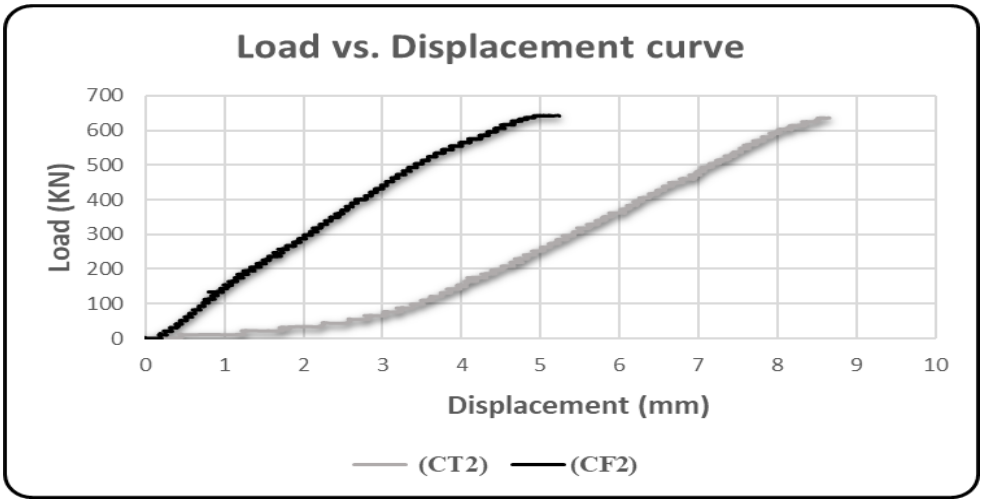

Fig. (4-44): Load vs. Axial displacement curve for (CF2 and CT2)

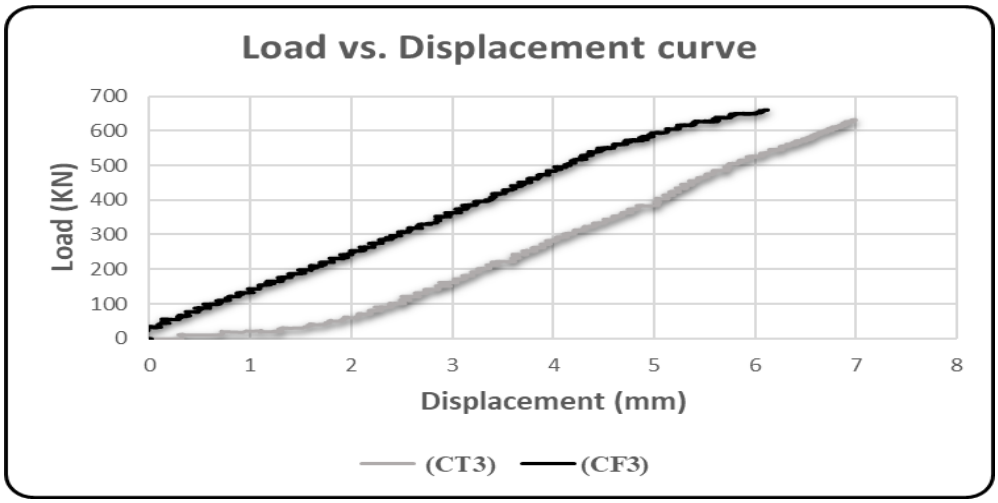

Fig. (4-45): Load vs. Axial displacement curve for (CF3 and CT3)

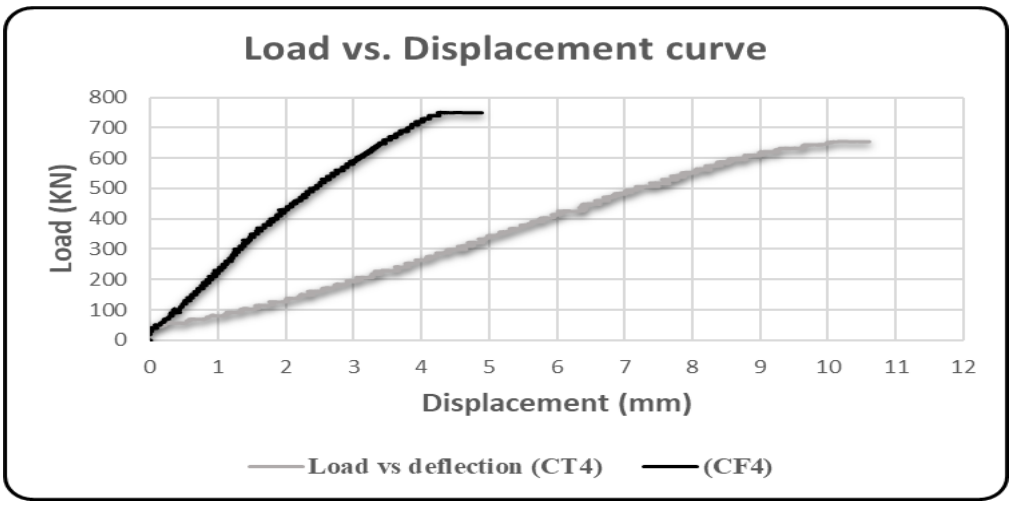

Fig. (4-46): Load vs. Axial displacement curve for (CF4 and CT4)

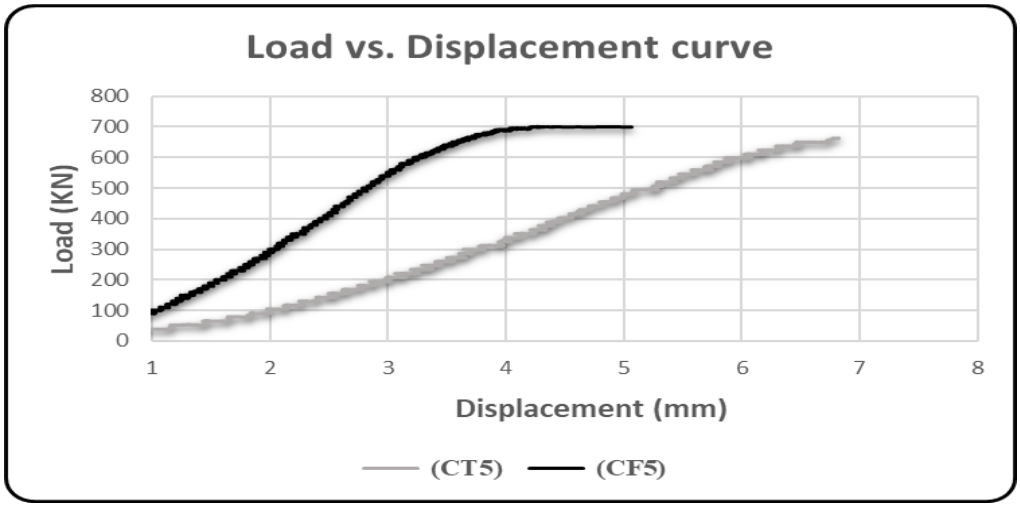

Fig. (4-47): Load vs. Axial displacement curve for (CF5 and CT5)

From the figures above with the (load vs. Axial displacement) curves the specimens with CFRP has the compressive strength more than the TRM, but with respect to the displacement the specimens with TRM more than the CFRP.

4.4.2 Comparison between specimens with eccentric loading

Also for specimens with strengthening by CFRP or TRM under subjected to the eccentric loading, the comparison between the specimens is as below:

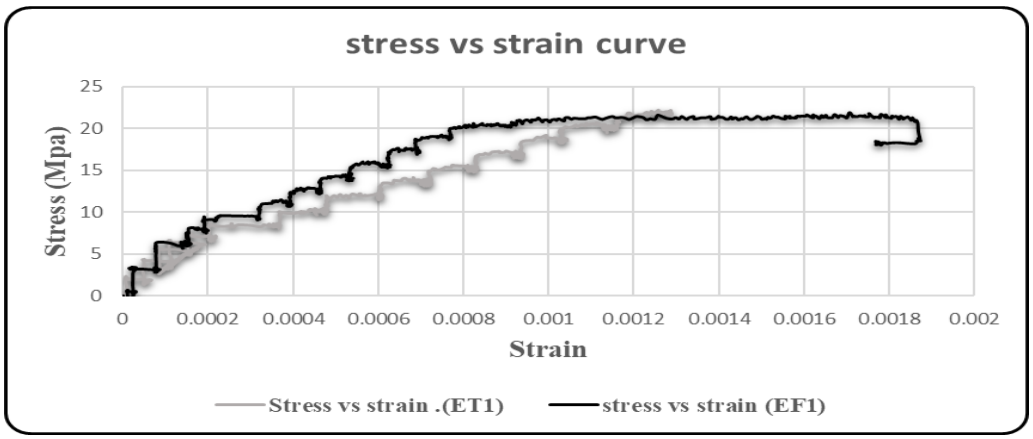

Fig. (4-48): Stress vs. Strain curve for (EF1 and ET1)

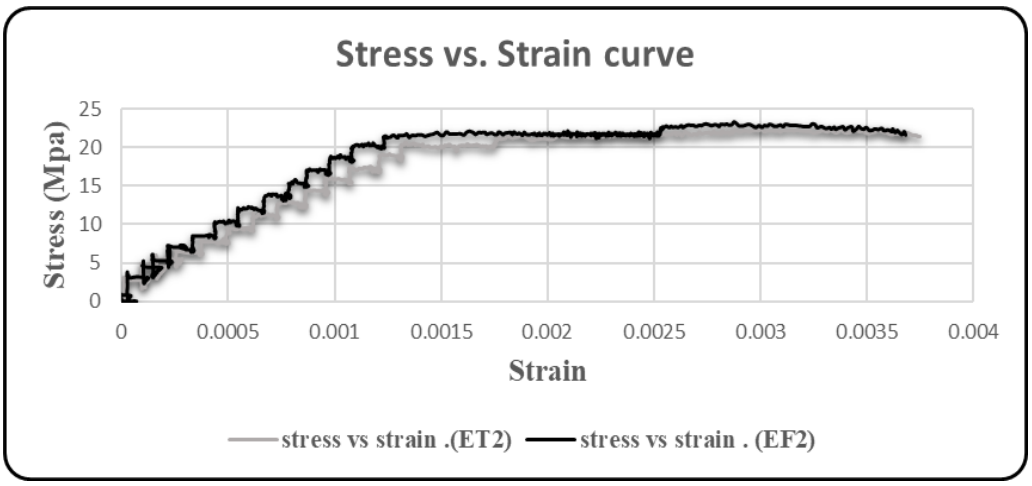

Fig. (4-49): Stress vs. Strain curve for (EF2 and ET2)

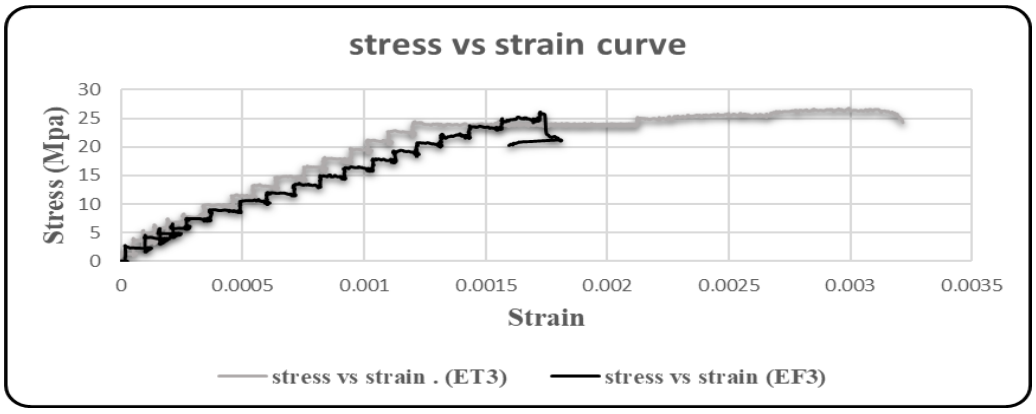

Fig. (4-50): Stress vs. Strain curve for (EF3 and ET3)

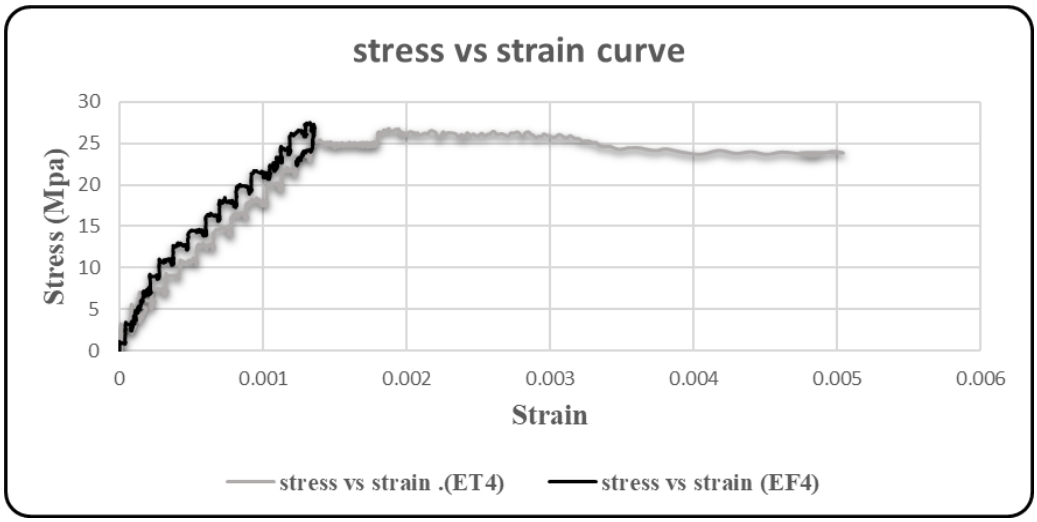

Fig. (4-51): Stress vs. Strain curve for (EF4 and ET4)

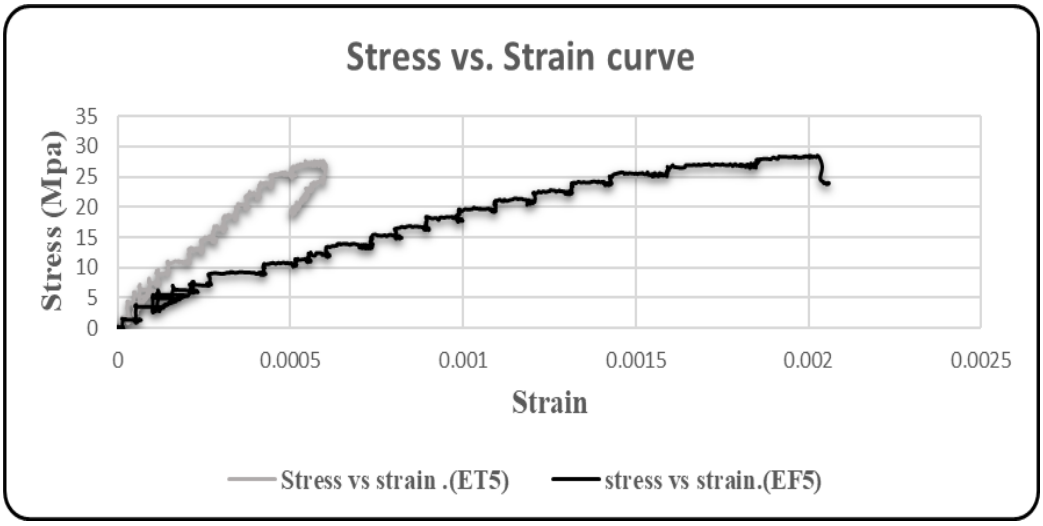

Fig. (4-52): Stress vs. Strain curve for (EF5 and ET5)

From the figures above with the (Stress vs. Strain) curves the specimens with CFRP has the stress more than the TRM, but the max. strain obtained from (ET4) with value (0.005).

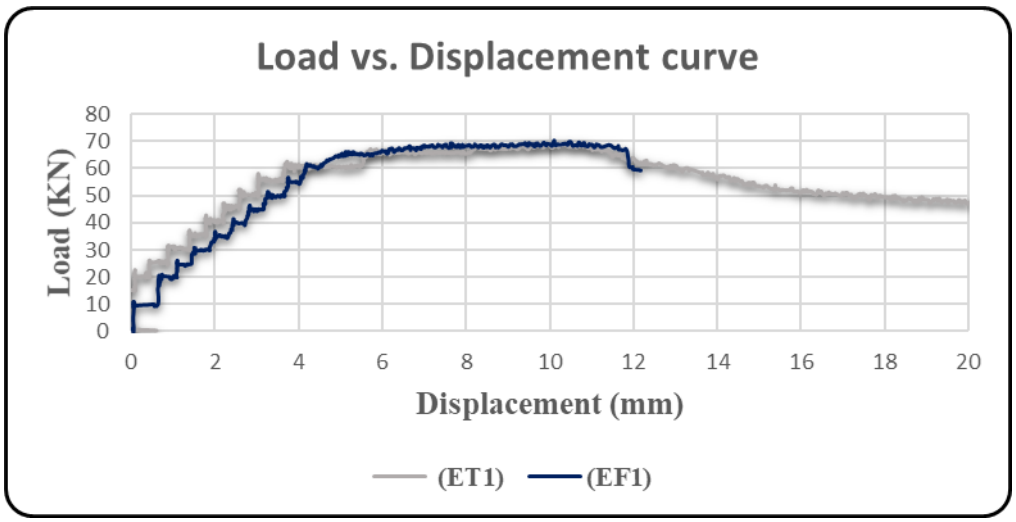

Fig. (4-53): Load vs. Axial displacement curve for (EF1 and ET1)

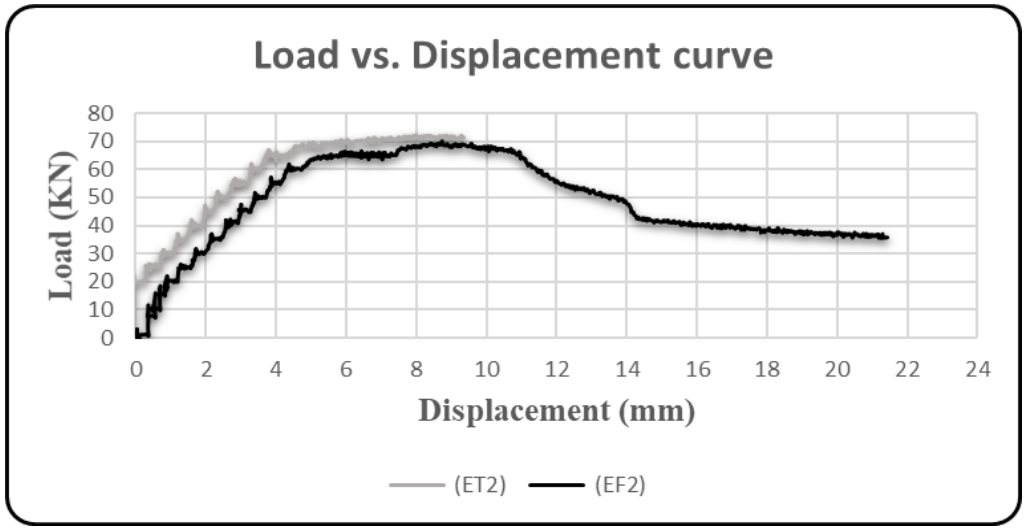

Fig. (4-54): Load vs. Axial displacement curve for (EF2 and ET2)

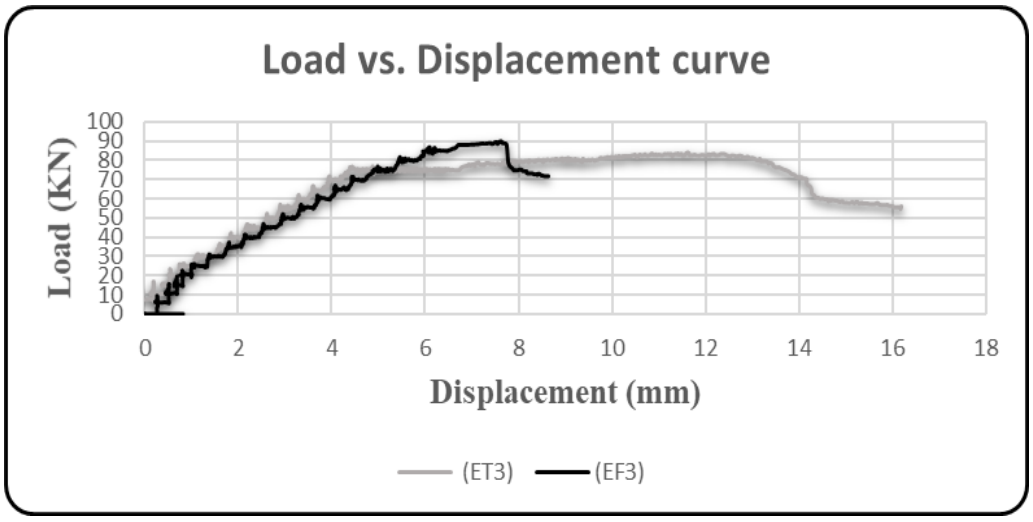

Fig. (4-55): Load vs. Axial displacement curve for (EF3 and ET3)

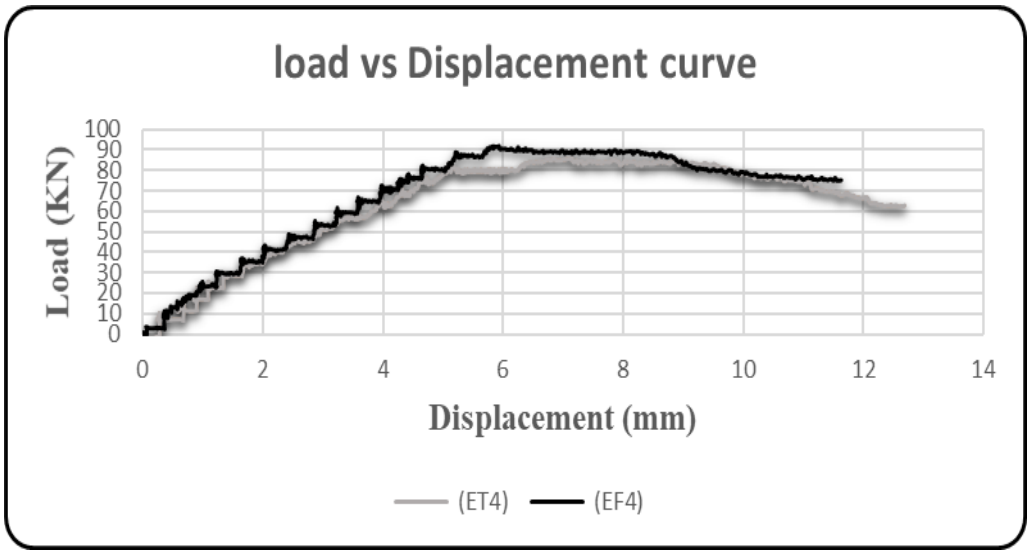

Fig. (4-56): Load vs. Axial displacement curve for (EF4 and ET4)

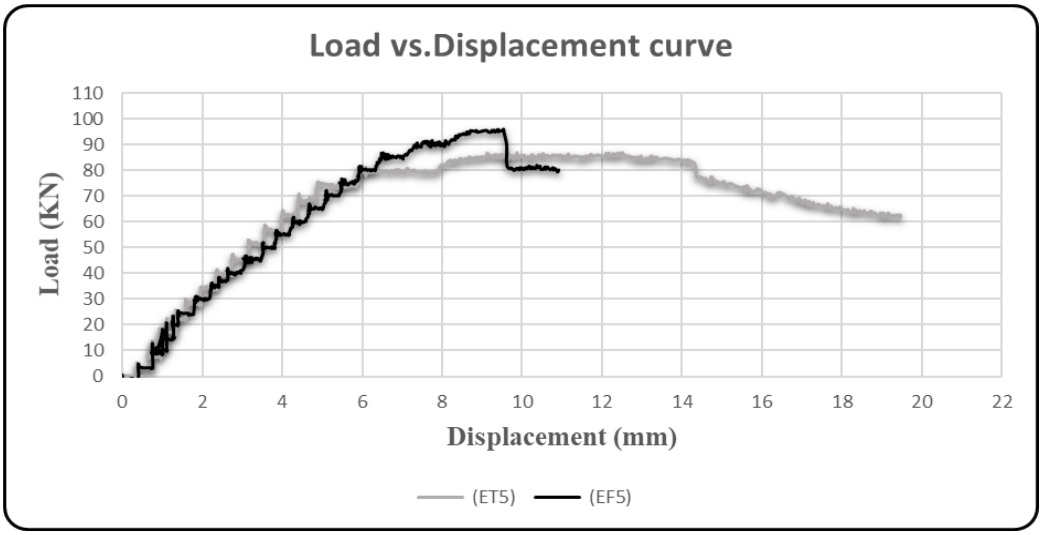

Fig. (4-56. a): Load vs. Axial displacement curve for (EF5 and ET5)

For the (load vs. displacement) curves the two specimens slightly have the same response for the elastic stage, and related to the axial displacement the specimens with TRM has the max displacement compared with CFRP, except the (EF2).

**From these comparisons above the CFRP its come out a good result for the compressive strength, therefore if the criterion of strengthening depending on the compressive strength the CFRP its good idea. and with displacement and strain the TRM had a good result.

4.5 Specimens with Side Opening

In this research, and also to the addition studying the effect of partial reinforcement of the hollow concrete column using two materials (CFRP or TRM). Furthermore, the behavior of the same column is studied with the addition of side openings at the two ends of the column subjected to concentric or eccentric loading, with two side holes (square or circular). as in Fig. (4-57) and fig.(4-58).

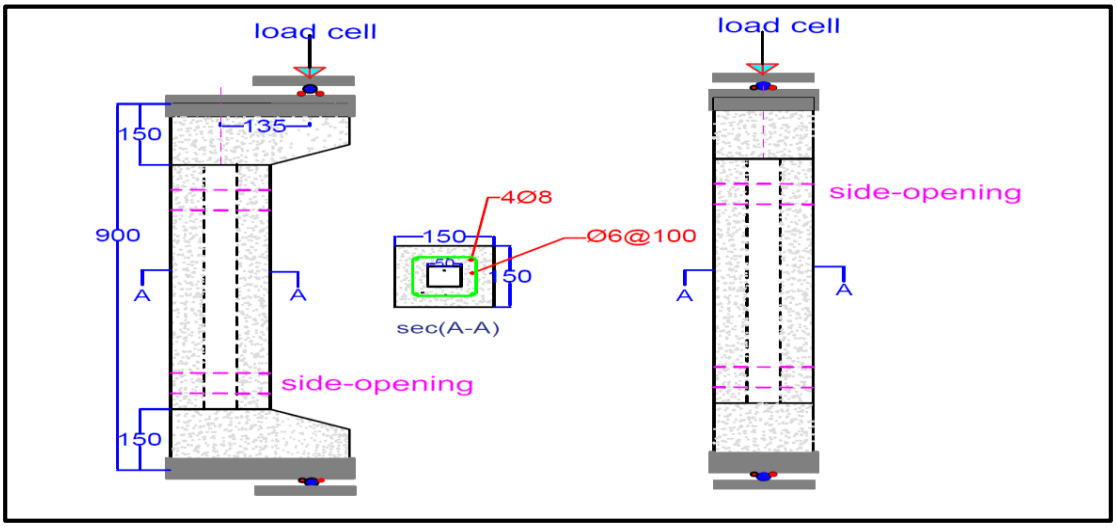

Fig. (4-57) Specimens with Side Opening

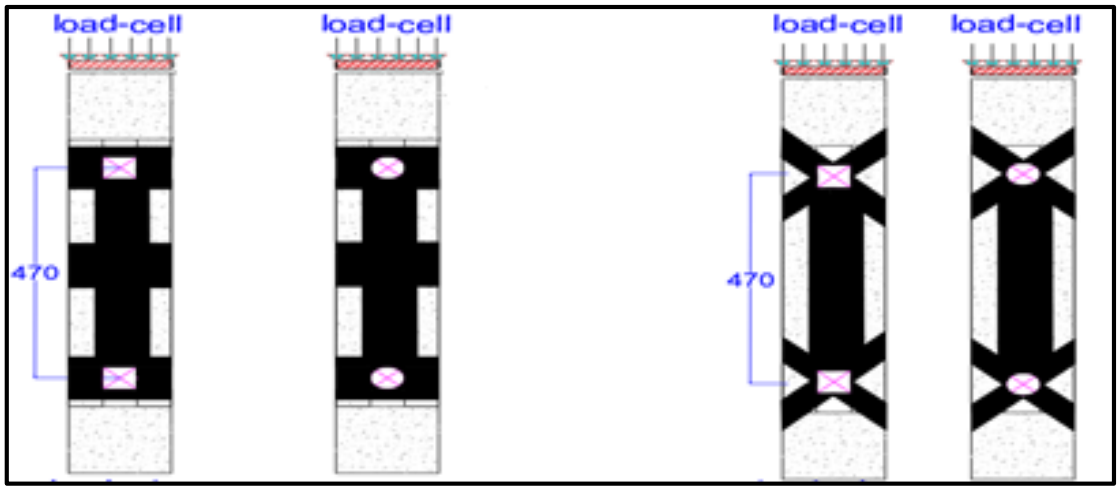

Fig. (4-58-a) strengthened specimen with side opening under eccentric loading

Fig. (4-58-b) strengthened specimen with side opening under concentric loading

Fig. (4-58) Strengthening for side openings

Where in this research (8) specimens are examined, these specimens are divided into two groups. The first one has (4) specimens, and they are considered reference specimens that contain circular or square holes without external strengthening and under the influence of concentric or eccentric loading. In contrast, the remaining columns contain the same side openings and the same effect of loads with addition of Partial strengthening of the specimens using (CFRP),and with depended on the results obtained from the specimens previously examined in this research, which do not contain side openings. in this case of side openings, the form of strengthening (CF4) was adopted for specimens with concentric loading, while the strengthening has the label (EF5) was adopted for specimens under eccentric loading, as shown in fig (4-58).

4.5.1 Control columns with side openings and under concentric loading

4.5.1.1 Load vs. Displacement for control column with side openings and under concentrically loading

According to Fig.(4-59), the load vs. displacement curve for the specimen with circular side opening (CC-CON-CIR-O) starts from zero and travels upwards until it reaches a displacement of (8.78) mm. where the max. load reach to the(555) kN. with decreased about (-9) % comparing with the control specimens without side open (CC-CON-H) (610) kN. and for specimen has the square side opening(CC-CON-Squ-O) the displacement reach to the (4.36) mm with the max. load capacity reach to the (430)kN as the fig. (4-60), with decreased about the (-29.5)% compare with the (CC-CO-H).

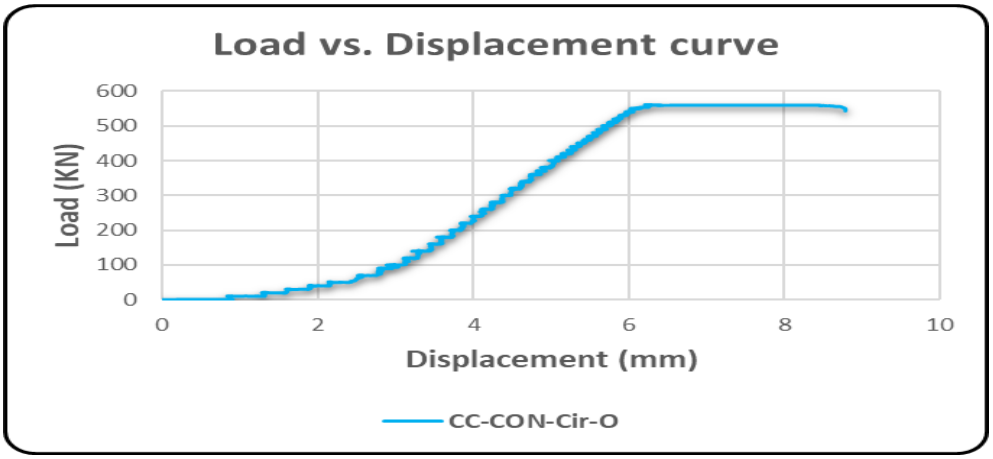

Fig. (4-59) Load-Displacement curve for (CC-CON-Cir-O)

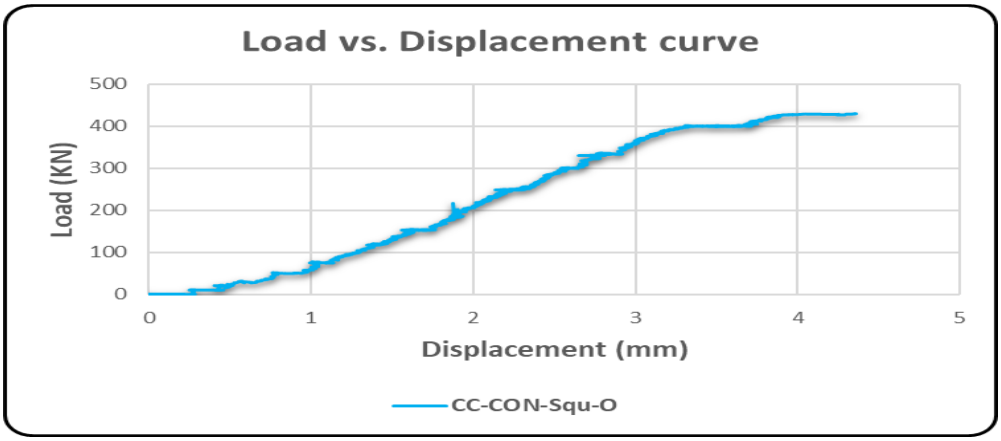

Fig. (4-60) Load-Displacement curve for (CC-CON-Squ-O)

4.5.1.2 Stress vs. Strain curves for control specimens with side openings and under concentric loading

In this specimens fixed only one strain gauge (SGC) near the top opening side for the circular side opening as the plate (4-50). the stress reach to the (24.6) MPa, and the strain obtained from the (SGC1) equal to the (0.0017) as the fig. (4-61). and for the square side opening fixed three (SGC) as the plate (4-51),the strain obtained from these three strain gauge equal to the (SGC1=0.00132,SGC2=0.0008,and SGC3=0.00088) and the stress reach to the (19.11)MPa, as the fig. (4-42)

plate. (4-51) Locations of SGC for (CC-CON-Squ-O) plate. (4-50) Locations of SGC for (CC-CON-Cir-O)

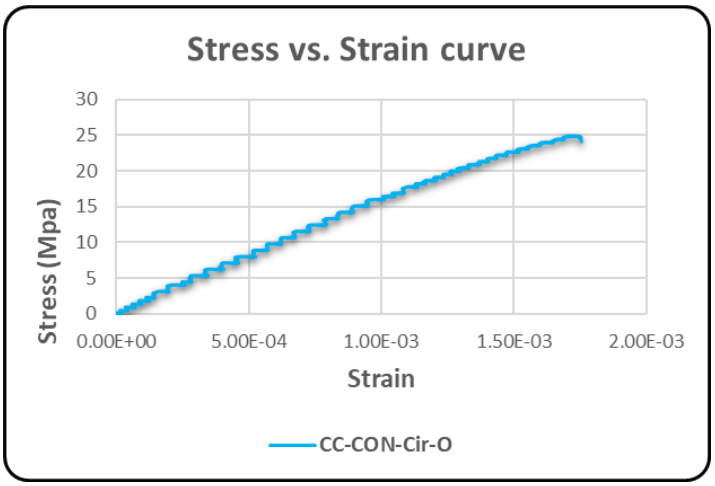

Fig. (4-61) Stress-strain curve (CC-CON-Cir-O)

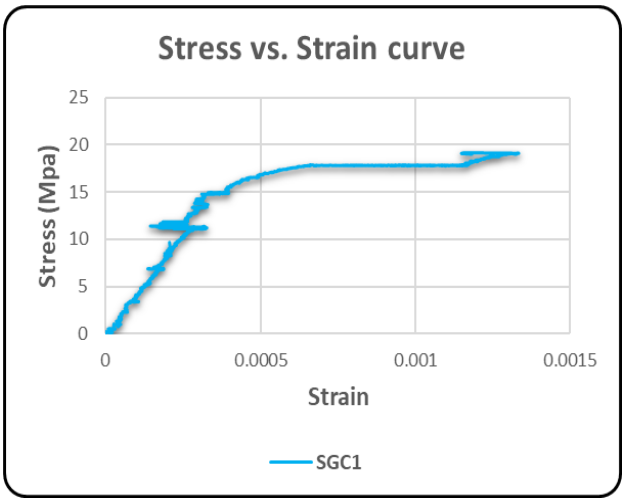

Fig. (4-62-a) Stress-strain curve obtained from SGC1)

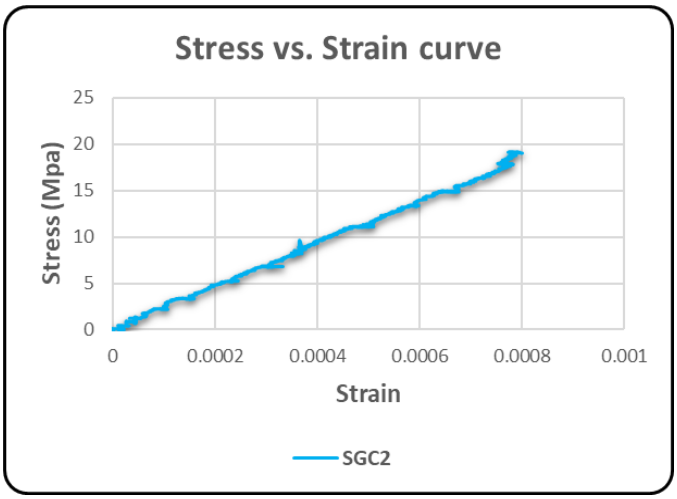

Fig. (4-62-b) Stress-strain curve obtained from (SGC2)

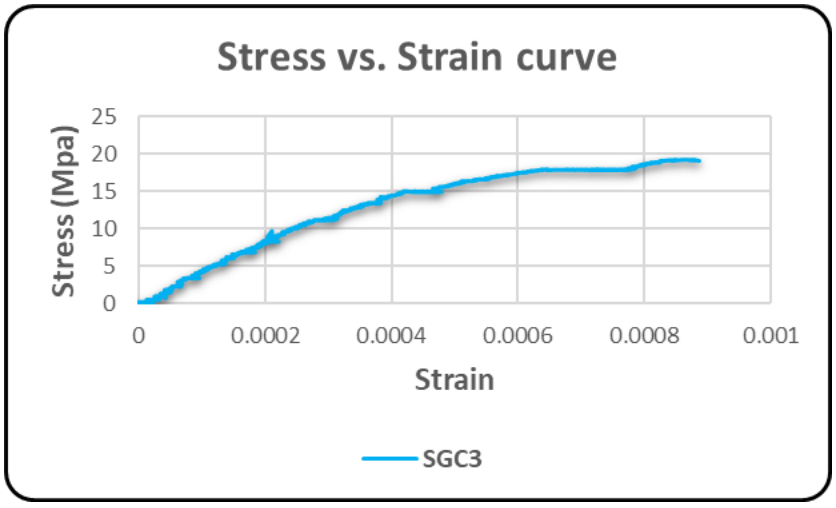

Fig. (4-62-c) Stress-strain curve obtained from (SGC3)

Fig. (4-62) Stress-strain curve for (CC-CON-Squ-O)

4.5.1.3 Mode of Failure for control specimens with side openings and under concentric load

For the specimen has the circular side opening the mode of failure as the plate (4-52) this failure occurred by generating plastic hinge near the circular opening at the bottom end as the plate (4-52-a) and (4-52-b). Where the main rebar buckled due to increase the concentric loading and then the concrete cover spalling out. And for the specimen with square opening, the plastic hinge creation near the side opening at the top end, as the plate (4-53)

plate. (4-52-a) plastic hinge near the circular open

plate. (4-52-b) buckling in main rebar for (CC-CON-Cir-O)

plate. (4-52) Failure mode for (CC-CON-Cir-O)

plate. (4-53) Failure mode for (CC-CON-Squ-O)

4.5.1.4 Ductility for control specimens with side openings and under concentric load

The circular side opening increase the ductility with value about (1.5) and the specimen with square side opening has the ductility equal to the (1.3), and the ductility for the specimen without side opening has the value about (1.1).

4.5.2 Specimens with side openings that strengthening by CFRP and under concentric loading

These specimens have the side openings (square or circular) subjected to the concentric loading. The strengthening for this specimens same the case (CF4) with the labels (CF-Cir-O) and (CF-Squ-O) for circular and square side openings respectively, as the plate (4-54)

Plate (4-54) Specimens (CF-Cir-O), (CF-Squ-O)

4.5.2.1 Load vs. Displacement for specimens (CF-Cir-O),and (CF-Squ-O)

In figures (4-63) and (4-64) illustrate the load vs. displacement curves for the specimens (CF-Cir-O),and (CF-Squ-O) respectively , when the load starting applied the curve begin from (0) and increases in slope until it reaches a total displacement. the specimen has the label(CF-Cir-O) this specimen failed at the compression load equal to (660) kN with the displacement equal to (7.86) mm. At the failure point this specimen has increased about the (18.9) % comparing with the control (CC-CON-Cir-O). And for the specimen (CF-Squ-O) ,the max load capacity equal to the (560.3) kN with additional in capacity reached to the (30.3) %compared with the (CC-CON-SQU-O). The max. displacement has the value equal to the (6.06) mm.

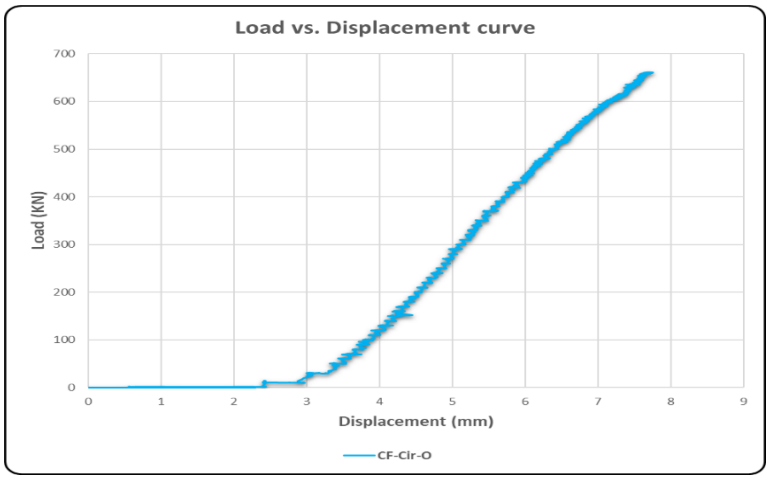

Fig. (4-63) Load-Displacement curve (CF-Cir-O)

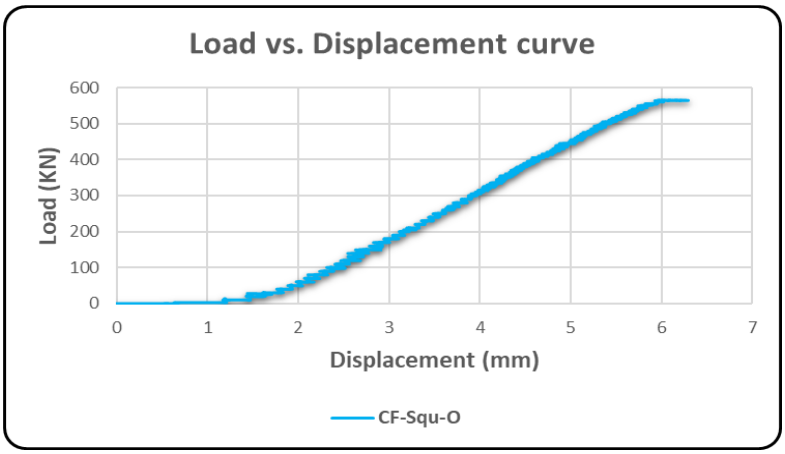

Fig. (4-64) Load-Displacement curve (CF-Squ-O)

4.5.2.2 Stress vs. Strain curves for specimens(CF-Cir-O),and (CF-Squ-O)

For the specimen (CF-Cir-O) two strain gauge (SGC)are fixed,the first near the circular opening at the top (SGC1) and another one at the middle height of column (SGC3) as the plate (4-55). the stress reach to the (29.33) MPa, and the strain obtained from (SGC1) equal to (0.00168) and for (SGC3) the strain reach to the (0.0018). and for the (CF-Squ-O) fixed three (SGC) as the plate (4-56). The strain obtained from these three strain gauge equal to the (SGC1=0.00326, SGC2=0.00164, and SGC3=0.002) and the stress reach to the (25.1) MPa. the figures (4-65) for circular side openings and (4-66) for the square side openings below show the stress strain curves for this specimens .

plate. (4-55) Locations of SGC for (CF-Cir-O)

plate. (4-56) Locations of SGC for (CF-Squ-O)

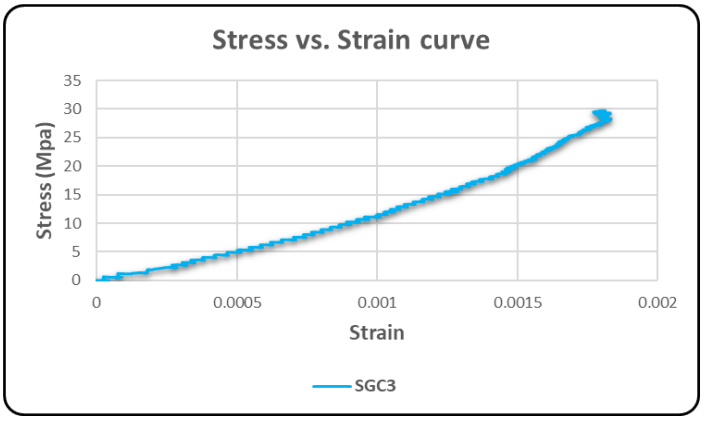

Fig. (4-65-a) Stress-strain curve (SGC3)

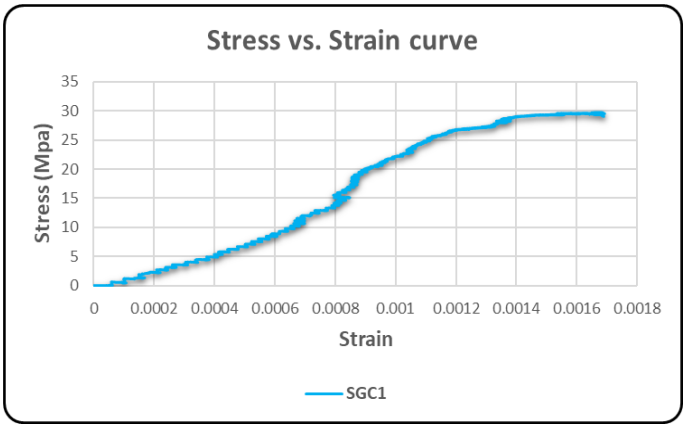

Fig. (4-65-b) Stress-strain curve (SGC1)

Fig. (4-65) Stress-strain curve (CF-Cir-O)

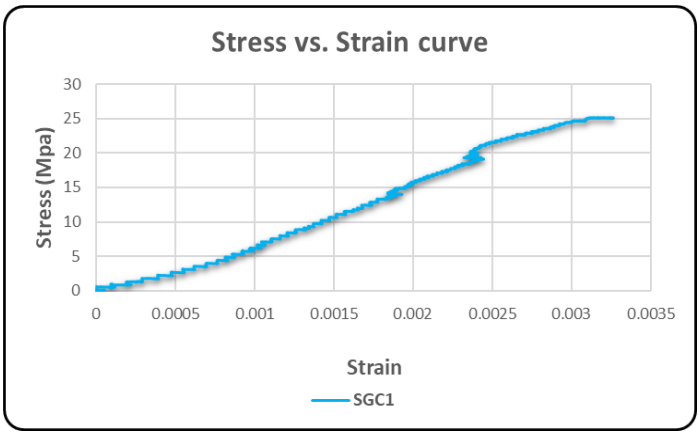

Fig. (4-66-a) Stress-strain curve (SGC1)

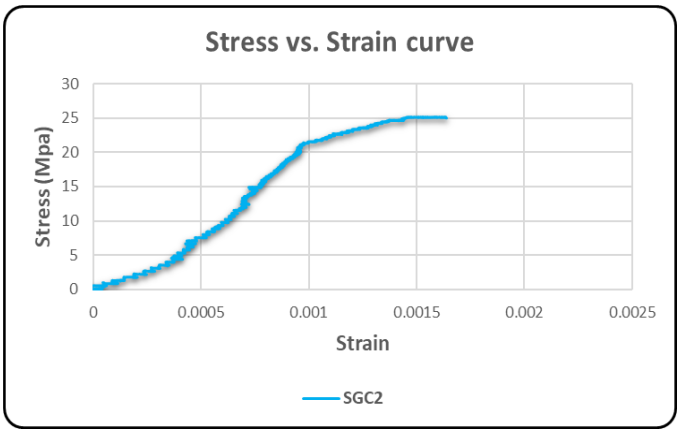

Fig. (4-66-b) Stress-strain curve (SGC2)

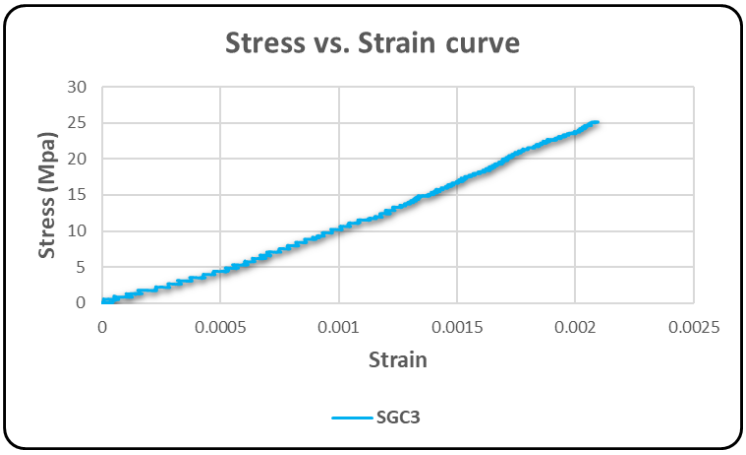

Fig. (4-66-c) Stress-strain curve (SGC3)

Fig. (4-66) Stress-strain curve (CF-Squ-O)

From the figures above the strain in concrete and comparing the reading between specimens in control and the strengthening columns, the strain increased in the specimen (CF-Squ-O), but in the (CF-Cir-O) the increase had more marginal.

4.5.2.3 Mode of Failure for specimens (CF-Cir-O),and (CF-Squ-O)

The two specimens (CF-Cir-O) and (CF-Squ-O) failed due to generating the plastic hinge near the side opening at top end of column. as the plate (4-57). Where the main rebar buckled due to increase the concentric loading and then the concrete cover spalling out. The configuration of the CFRP has the increase in load capacity for the column under concentric loading but also the concrete affected more than comparing with the control specimens.

plate. (4-57) Failure mode for (CF-Cir-O) and (CF-Squ-O)

4.5.2.4 Ductility for the specimens(CF-Cir-O),and (CF-Squ-O)

Depending on the (stress- strain) curve to compute the ductility [1], for these specimens (CF-Cir-O) and (CF-Squ-O). The circular side opening increase the ductility with value about (2.1) and the specimen with square side opening has the ductility equal to the (1.64), and the ductility for the control specimens without strengthening equal to the (1.5) and (1.3) for the circular and the square side openings, respectively.

4.5.3 Control columns with side openings and under eccentric loading

The specimens under eccentric loading with the circular and square side openings at the ends of the column, with the labels (CC-ECC-Cir-O) and (CC-ECC-Squ-O), respectively.as the plate (4-58)and (4-59)

plate. (4-58) (CC-ECC-Squ-O)

plate. (4-59) (CC-ECC-Cir-O)

4.5.3.1 Load vs. Displacement curves for control speicmens with side openings and under eccentric loading

For the specimen with circular side opening (CC-ECC-Cir-O) and under eccentric loading the max. load capacity reached to the value (65.8) kN with the displacement equal to the (11.4) mm as the fig.(4-67) , and for the specimen has the square side opening (CC-ECC-Squ-O) the load equal to the (64.8)kN with the axail displacement equal to the (12.84)mm as the fig.(4-48). And also the reducing in compressive load comparing with specimen under eccentric loading and without side opening (CC-ECC-0.9H) (68.03) kN very little. But the vertical displacement it has doubled, where the displacement equal to the (5.59) mm for the (CC-ECC-0.9H).

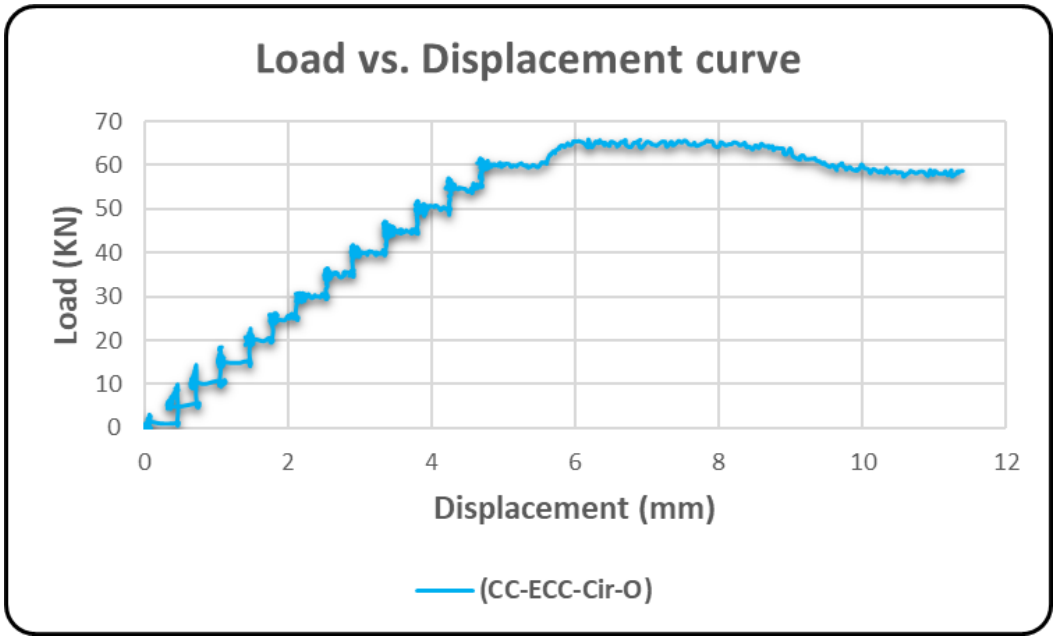

Fig. (4-67) Load –Axail displacement curve for (CC-ECC-Cir-O)

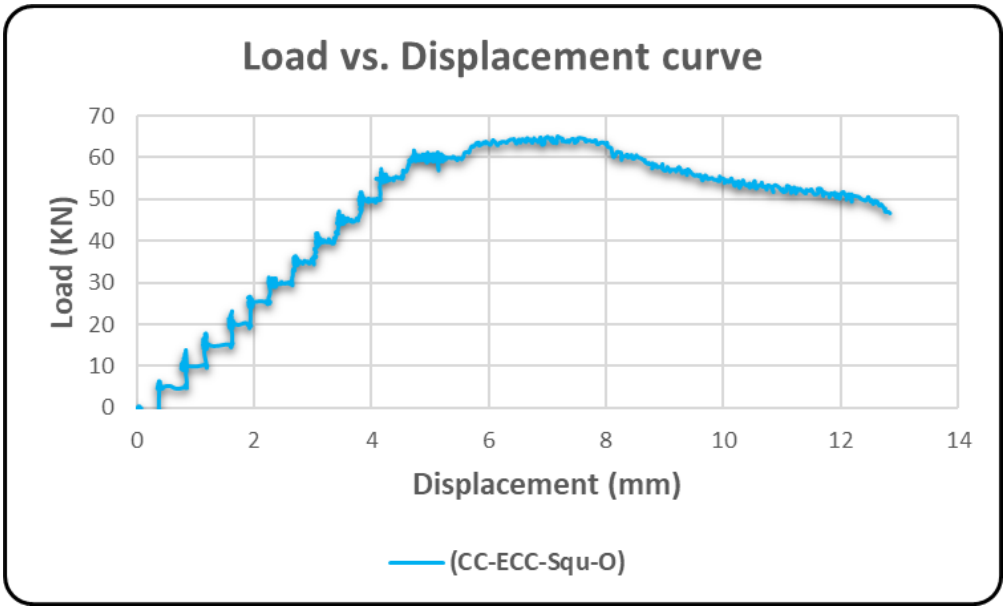

Fig. (4-68) Load –Axail displacement curve for (CC-ECC-Squ-O)

4.5.3.2 Stress vs. Strain curves for control specimens speicmens with side openings and under eccentric loading

To evaluate the strain in concrete for the specimen (CC-ECC-Cir-O), used the concrete strain gauge (SGC) in the different positions on the tension and compression sides as the (SGC1) in the compression face, and (SGC2) in the tension face, the strain equal to the (0.00138) from the (SGC1) and (-0.02) for the (SGC2) as the fig.(4-69).

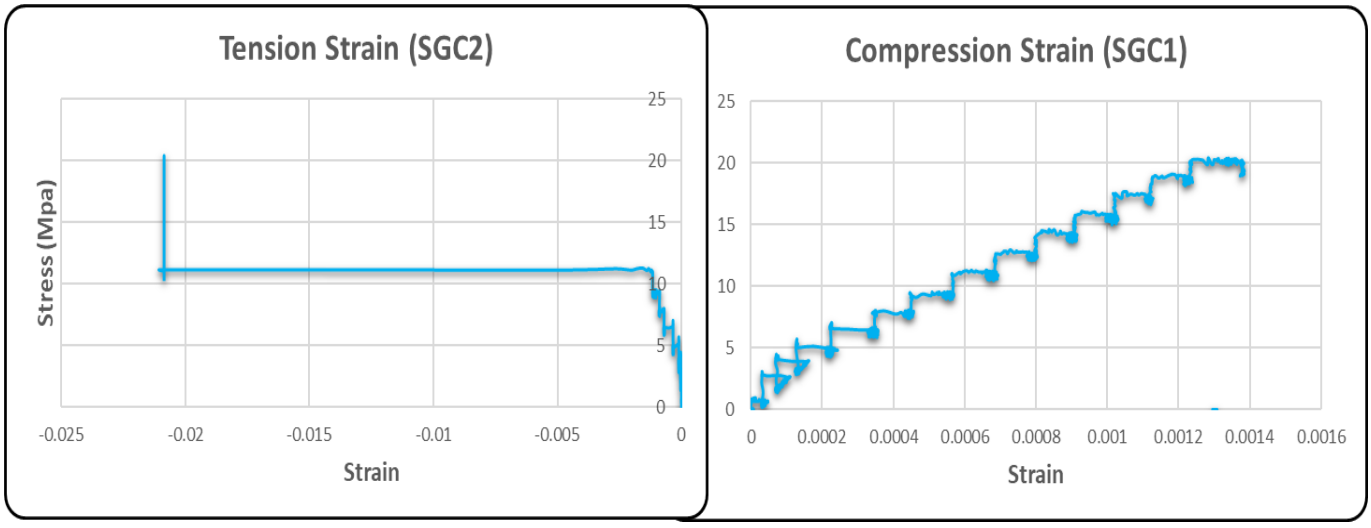

Fig. (4-69) Stress-Strain curve for (CC-ECC-Cir-O)

Also for the specimen (CC-ECC-Squ-O) , six strain gauge divided to two groups three on the tension face (SGC1,2,and 3) and remain part on the compression face (SGC4,5,6) located at the top and middle and bottomof column for both groups. The figures (4-70) below explain these stress-strain curve obtained from the SGC.

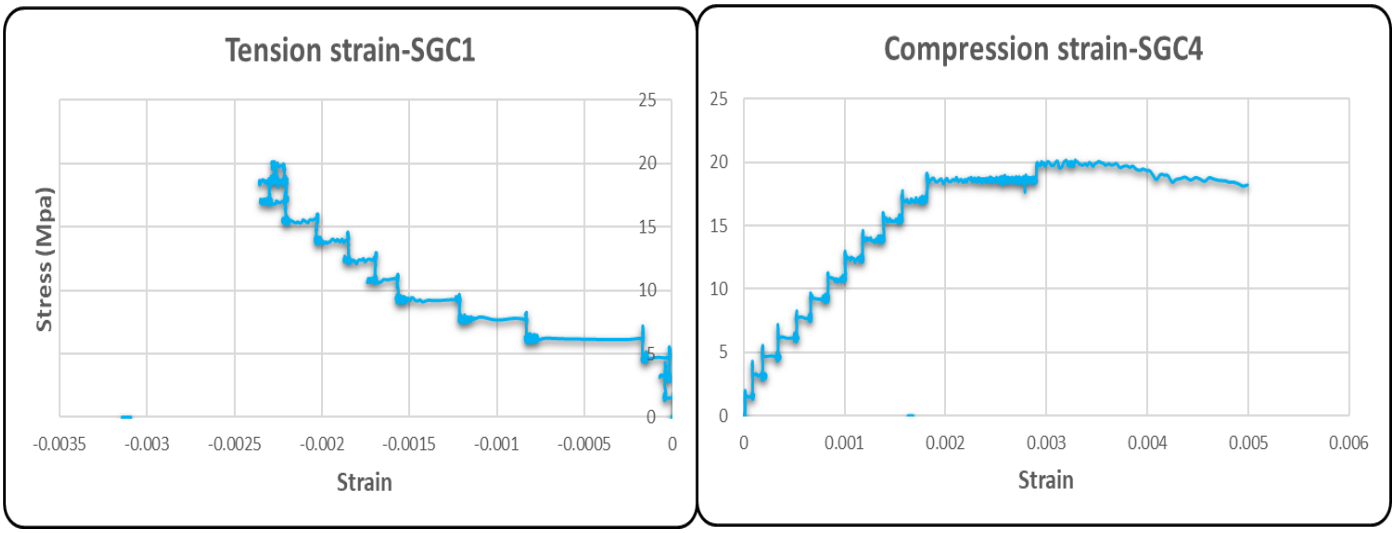

Fig. (4-70-a) Stress-Strain curve for (SGC1 and SGC4)

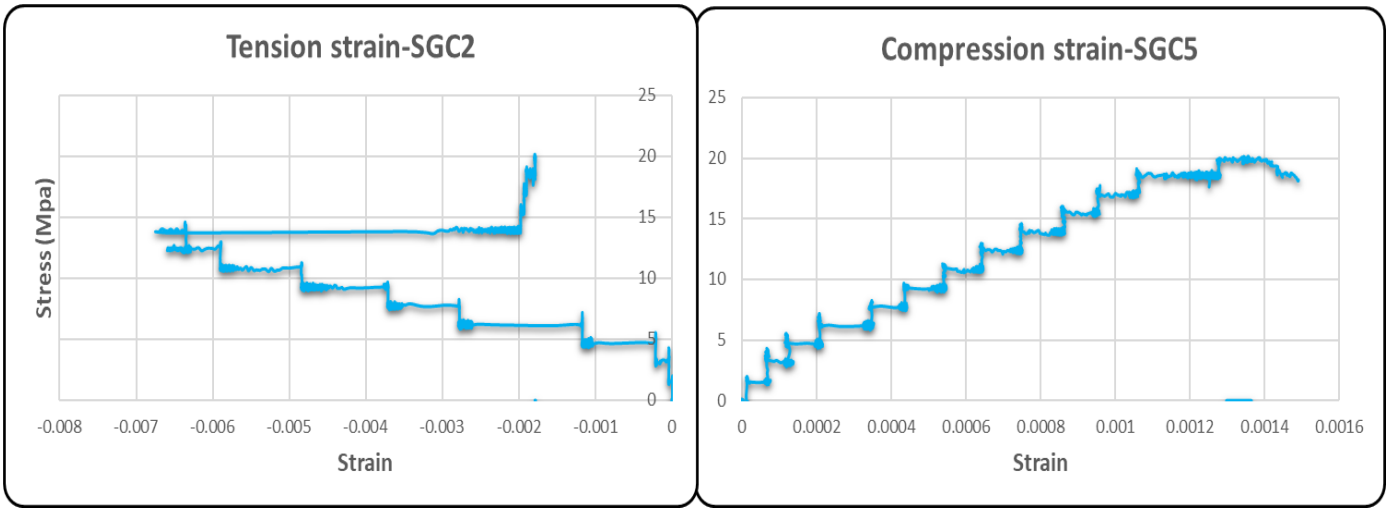

Fig. (4-70-b) Stress-Strain curve for (SGC2 and SGC5)

Fig. (4-70) Stress-Strain curve for (CC-ECC-Squ-O) (continue)

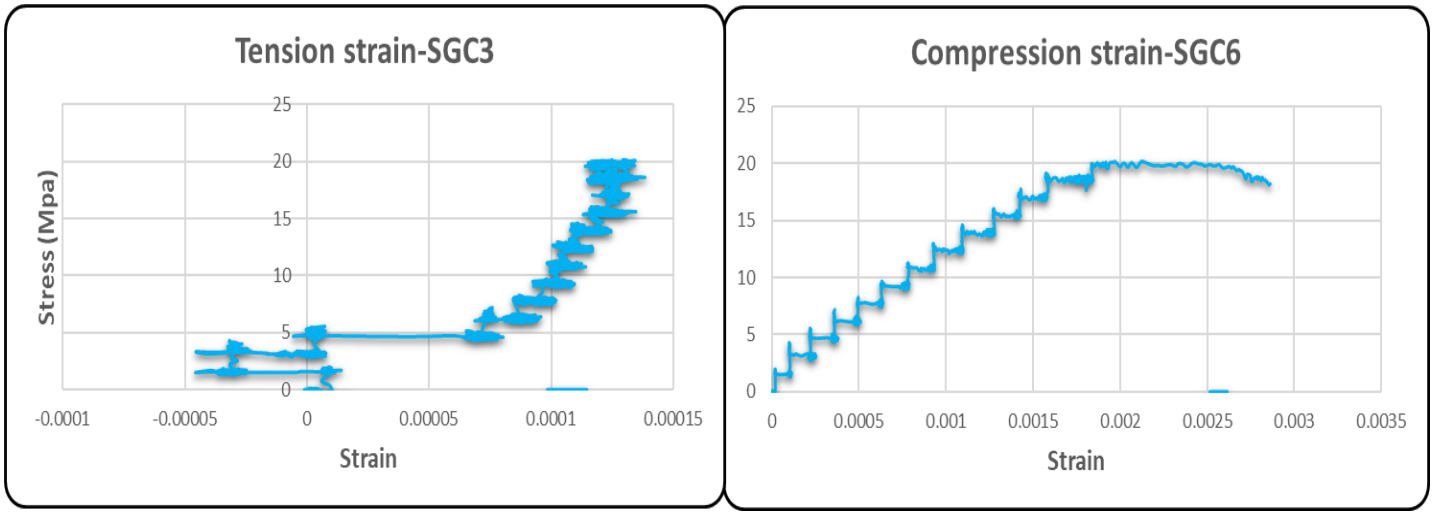

Fig. (4-70-c) Stress-Strain curve for (SGC3 and SGC6)

Fig. (4-70) Stress-Strain curve for (CC-ECC-Squ-O) (continued)

The reading of the strain concrete in tension face equal to the (SGC1=-0.003,SGC2=-0.0067) and for the SGC3 did not have reading .and for the compression face the (SGC4=0.005,SGC5=0.0015,and SGC6=0.0028) .

4.5.3.3 Mode of Failure for control speicmens with side openings and under eccentric loading

In the case (**CC-ECC-Cir-O)** when the eccentric load applied the horizontal crack will have developed at the circular side open at the top where the cracks start from the inner face of the circular hole also more cracks will generate with increase loading as the plate (4-60).and for the compression face the area of concrete damage will have developed at the top near the circular open as the plate (4-61).And for the specimen (CC-ECC-Squ-O) the failure also generate at the top side opening and the crack initiated from the corner of square open as the plates (4-62),(4-63) for tension and compression face respectively .

plate. (4-62) Tension Face of (CC-ECC-Squ-O)

plate. (4-60) Tension Face of(CC-ECC-Cir-O)

plate. (4-63) Compression Face(CC-ECC-Squ-O)

plate. (4-61) Compression Face(CC-ECC-Cir-O)

The concrete damage in compression zone will have changed from the middle in the control specimens without side opening **(**CC-ECC-H) to the top at the side opening in the two cases (CC-ECC-Cir-O) and (CC-ECC-Squ-O).

4.5.3.4 Ductility for the specimens with side openings and under eccentric loading

By using the load vs displacement curve calculate the ductility for the two cases is calculated. The specimen with circular opening has the ductility equal to the (2.3) while the specimen with the square side opening has the ductility reach to the (2.5), these two specimens have the ductility more than the control specimens (1.4).

4.5.4 Specimens with side openings that strengthend by CFRP and under eccentric loading

This specimens have the side openings (square or circular) and subjected to the eccentric loading. According to the results of specimens without opening and carry the eccentric loading, this specimen with label (EF5) has a good performance comparing with the control specimen. The labels (EF-Cir-O),and (EF-Squ-O) for circular and square side opening respectively, as the plate (4-64).

plate. (4-64) Strenfthening specimens with labels (EF-Cir-O) and (EF-Squ-O)

4.5.4.1 Load vs. Displacement curve for specimens with side openings that strengthend by CFRP and under eccentric loading

For the specimen with circular side opening (EF-Cir-O) and under eccentric loading, the max. load capacity reached to the value (80.1) kN with the axail displacement equal to the (10.84) mm as in fig (4-71). and for the specimen has the square side openings (EF-Squ-O), the load equal to the (75.38) kN with the vertical displacement equal to the (12) mm as in fig.(4-72). the increased in load capacity obtained from the case (EF-Cir-O) equal to the (21.73) % comparing with (CC-ECC-Cir-O) ,and the increases equal to the (16.32)% in specimen (EF-Squ-O) with respect to (CC-ECC-Squ-O).

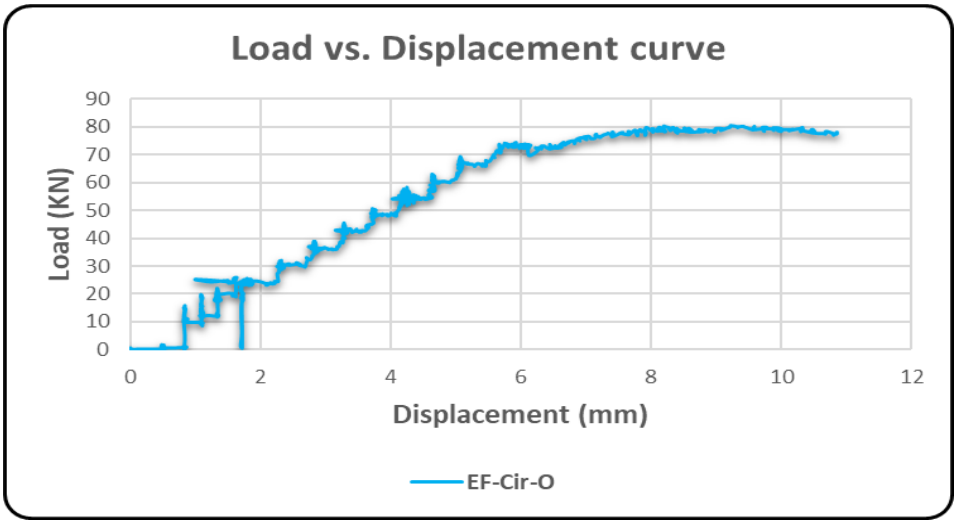

Fig. (4-71) Load Displacement curve (EF-Cir-O)

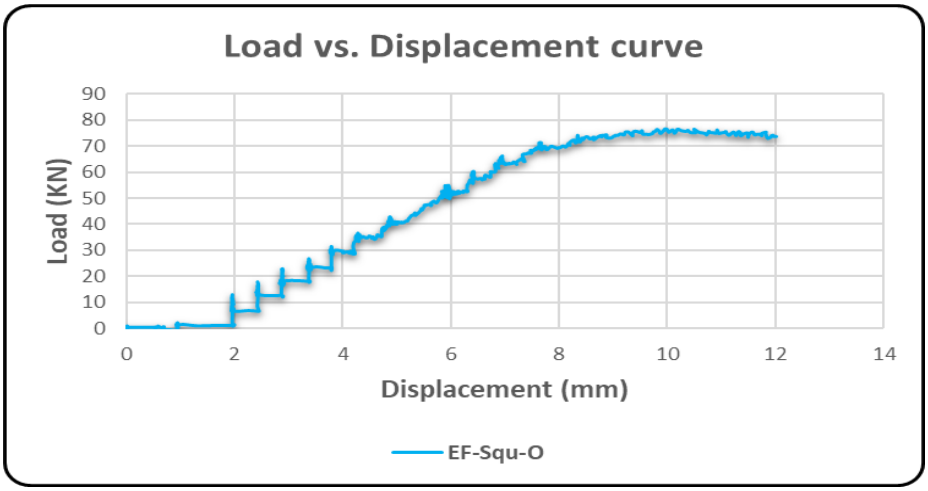

Fig. (4-72) Load Displacement curve (EF-Squ-O)

4.5.4.2 Stress vs. Strain curves for specimens with side openings that strengthend by CFRP and under eccentric loading

In the specimen (EF-Cir-O) , three concrete strain gauge two on the compression side and one on the tension side at middle height of column as in plate (4-65). The reading obtained from (SGC1=0.0085) near the circular opening at the top and the (SGC3=0.002). and the strain in concrete in tension face obtained from (SGC2=-0.0036). and for the specimen (EF-Squ-O), three strain gauge on the compression face and one on the tension face as the plate (4-66). the reading of the compression face equal to the (SGC2=0.003), (SGC3=0.0046),and (SGC4=0.0018), and for the tension

face equal to the (SGC1=-0.005). The max strain in concrete on compression face gained from the (EF-Cir-O) with the (SGC1=0.0085). the figures (4-73) below explain the curves for stress –strain curves for this two specimens.

plate. (4-65) Locations of SGC for (EF-Cir-O)

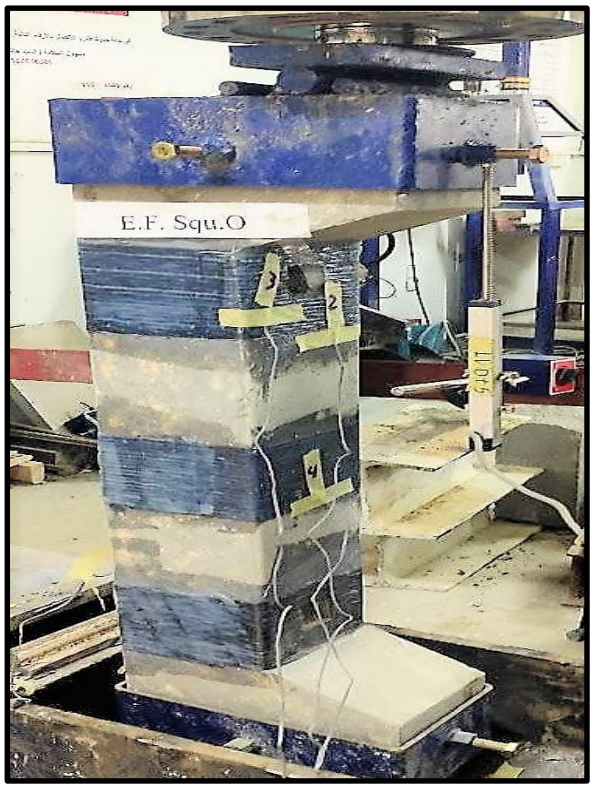

plate. (4-66) Locations of SGC for (EF-Squ-O)

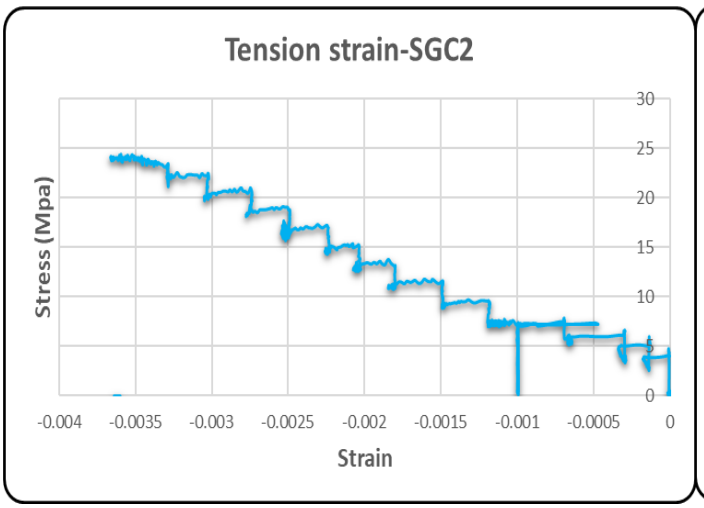

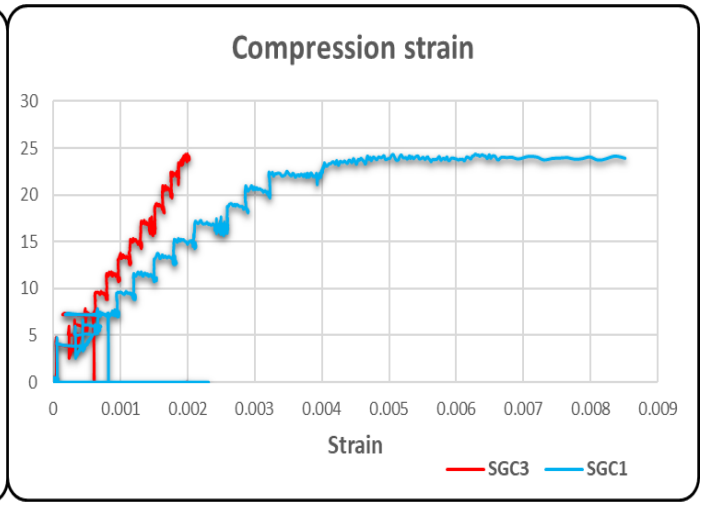

Fig. (4-73-a) Stress-Strain curve for (EF-Cir-O)

Fig. (4-73) Stress-Strain curve for (EF-Squ-O) and (EF-Cir-O) (continue)

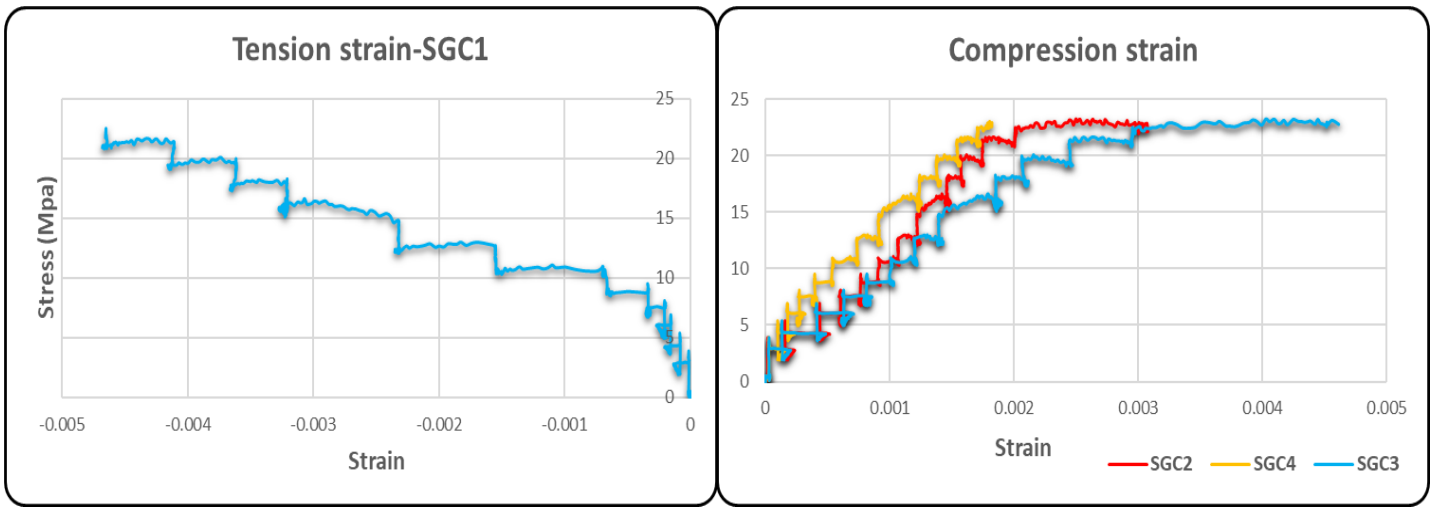

Fig. (4-73-b) Stress-Strain curve for(EF-Squ-O)

Fig. (4-73) Stress-Strain curve for (EF-Squ-O) and (EF-Cir-O) (continued)

4.5.4.3 Mode of Failure for specimens with side openings that strengthend by CFRP and under eccentric loading

In the case (EF-Cir-O) and (EF-Squ-O) The CFRP confining in two models delayed the longitudinal main rebar buckling at the top and disallowed external concrete cover spall out as the control specimens (CC-ECC-CIR-O) and (CC-ECC-SQU-O), when the eccentric load applied the horizontal crack will have developed at the circular side open at the top where the cracks start from the inner face of the circular hole and square hole also more cracks will generating with increase loading. But the CFRP blocking vision of this cracks on the tension face for two cases, as the plate (4-67-a) and (4-67-b).and for the two cases, the compression side did not exhibit the damage in concrete. or the crushing in concrete very slightly comparing with control specimens.as the plates (4-68-a)(4-68-b).

plate. (4-67-a) Tension Face of (EF-Cir-O)

plate. (4-67-b) Compression Face of(EF-Cir-O)

plate. (4-67) Failure mode for (EF-Cir-O)

plate. (4-68-a) Tension Face of (EF-Squ-O)

plate. (4-67-b) Compression Face of (EF-Squ-O)

plate. (4-68) Failure mode for (EF-Squ-O)

Plate. (4-69-a) cracks in (EF-Squ-O)

Plate. (4-69-b) cracks in (EF-Cir-O)

Plate. (4-69) Cracks in at top end for (EF-Cir-O) and (EF-Squ-O)

From the plate (4-69) showed the cracks inside the hole for the tension face.

4.5.4.4 Ductility for the specimens (EF-Cir-O) and (EF-Squ-O)

By using the load vs displacement curve to compute the ductility for the two cases. The cases (EF-Cir-O) and (EF-Squ-O) have the ductility equal to the (2.2) and (2.5) respectively, the ductility in two specimens did not show more value with the control specimens.

4.5.4.5 Crack width for specimens (EF-Cir-O) and (EF-Squ-O)

Table (4-11) illustrated the cracks width and load capacity for intervals time during the test for the cases (CC-ECC-Cir-O) and (CC-ECC-Squ-O) with two locations near the side open at top and the middle height of column. Also the max crack width equal to the (4) mm and (3) mm for specimens (CC-ECC-Squ-O) and (CC-ECC-Cir-O) as the plates (4-70), where the reading of this cracks takes after complete the test.

Table. (4-11) max. width of tip crack in (CC-ECC-Cir-O) and (CC-ECC-Squ-o)

specimens	Loading (kN)	Cracks width (mm)	Location
CC-ECC-Cir-O	15	0.05	***Close to the open at top***
	35	0.16	
	50	3	
CC-ECC-Squ-O	15	0.03	***Close to the open at top***
	45	0.2	
	60	4	
CC-ECC-Cir-O	20	0.07	***At the middle***
	35	0.1	
	50	0.15	
CC-ECC-Squ-O	20	0.05	***At the middle***
	45	0.2	
	60	0.25	

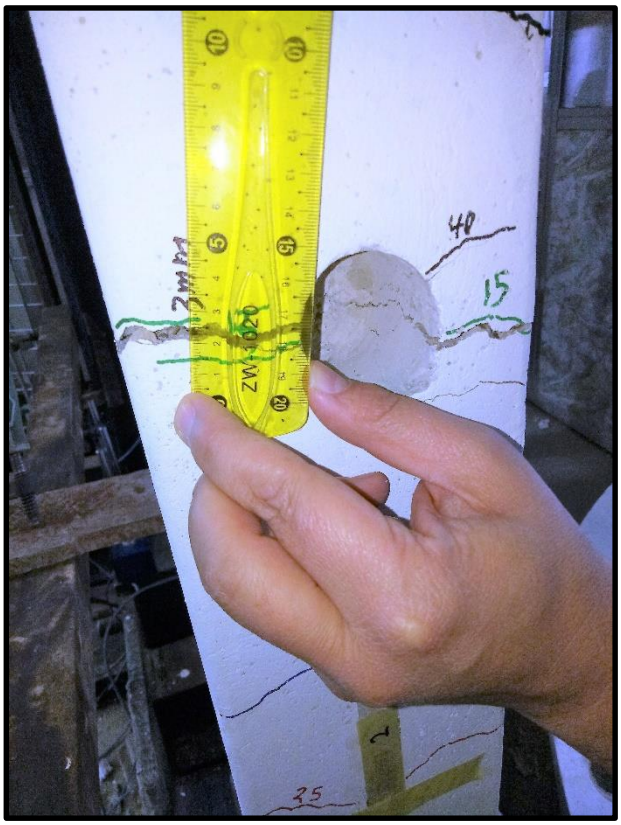

plate. (4-70-a) max.of tip crack in (CC-ECC-Cir-O) **plate. (4-70-b) max.of tip crack in (CC-ECC-Squ-O)**

plate. (4-70)max.of tip crack in (CC-ECC-Squ-O) and (CC-ECC-Cir-O)

And for the specimens strengthening by CFRP (EF-Cir-O) and (EF-Squ-O), The first crack did not appear in the case (EF-Cir-O) as the control specimen, while the initiated cracks begin from the inner surface of circular opening with load reach to (20) kN .and the final crack at max load measured after complete the test (3) mm.

(EF-Squ-O) the first crack starting from the load (15) kN in the inner wall of the side open as the control specimen. The final crack equal to the (4) mm.

2.2.5 Comparison between strengthened specimens with side opens

For the specimens under concentric loading the figures below illustrated the comparison for (stress vs. strain) curve and the (load vs. Displacement) curve for the two cases CFRP and TRM.

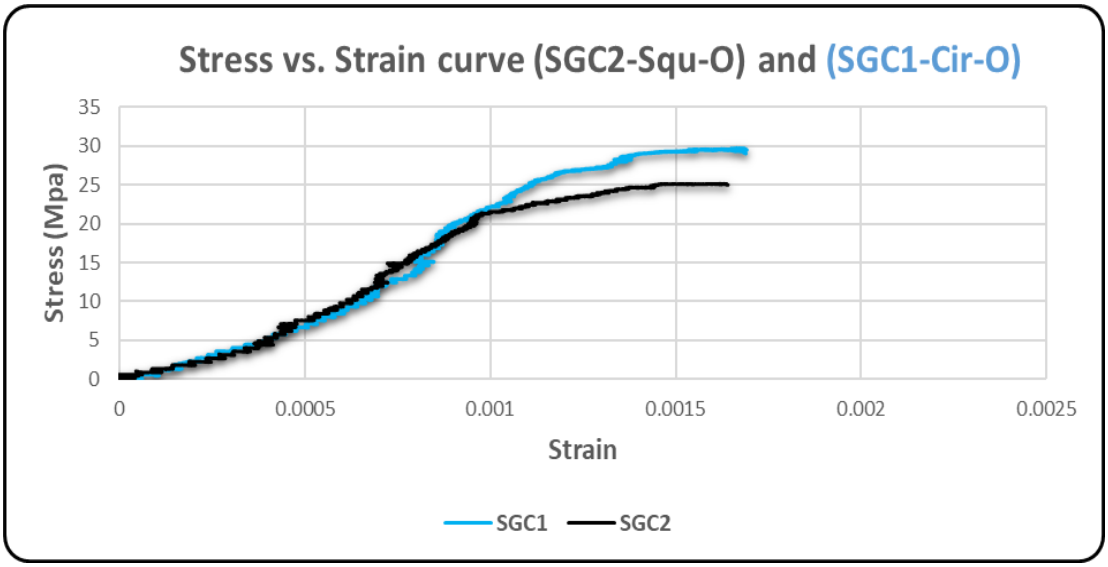

Fig. (4-74) Stress-Strain curve for (CF-Squ-O) and (CF-Cir-O)

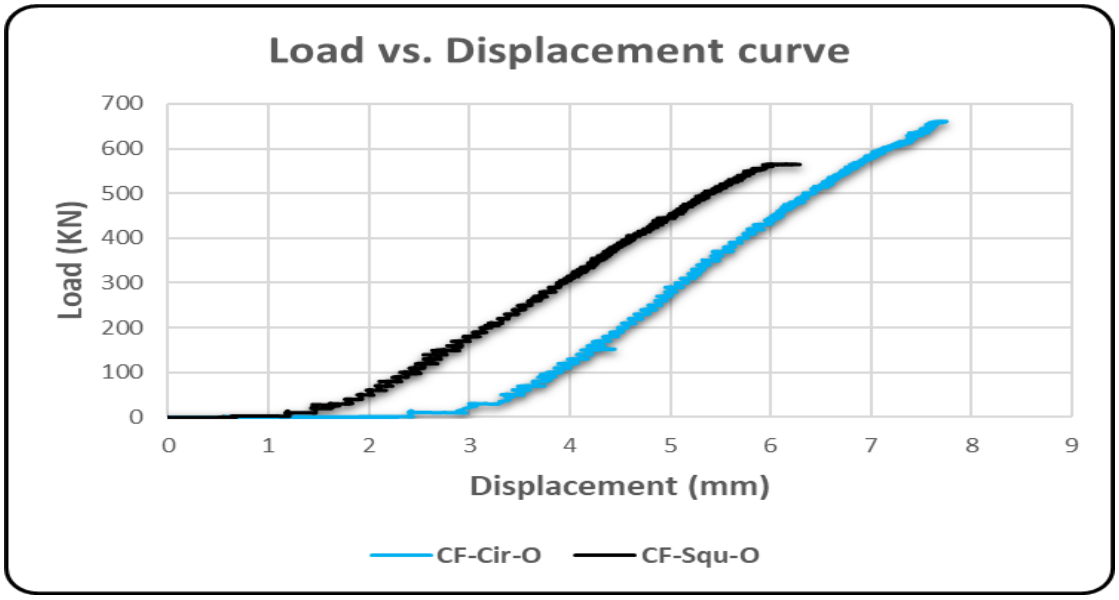

Fig. (4-75) Load-Displacement curve for (CF-Squ-O) and (CF-Cir-O)

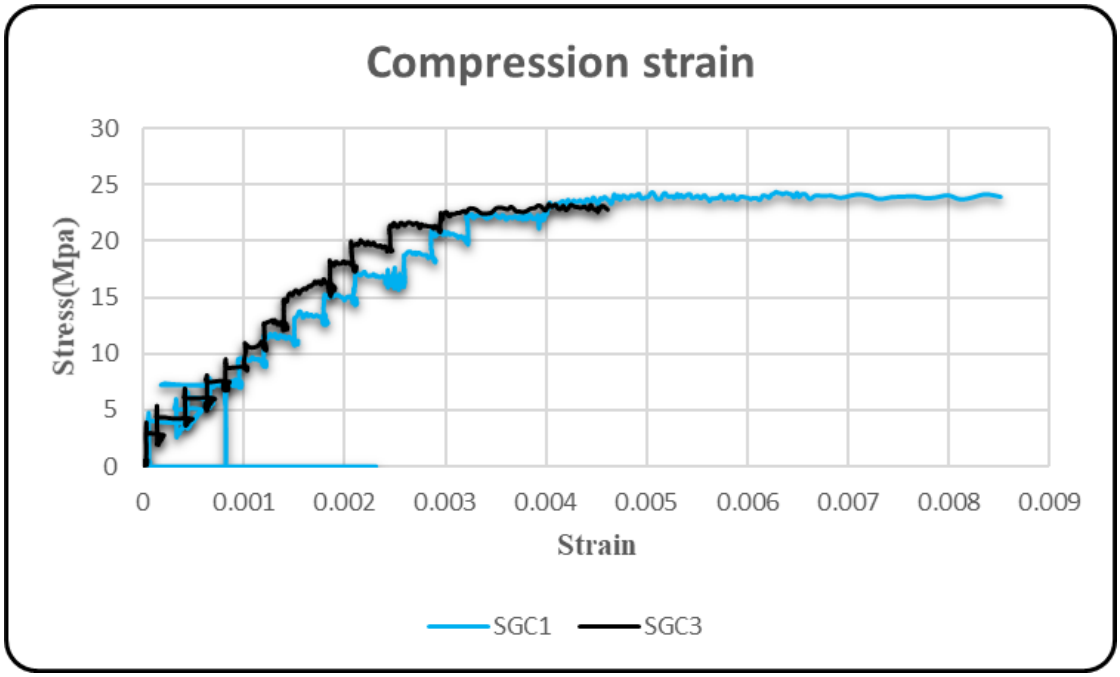

Fig. (4-76) Stress-Strain curve for (EF-Squ-O) and (EF-Cir-O)

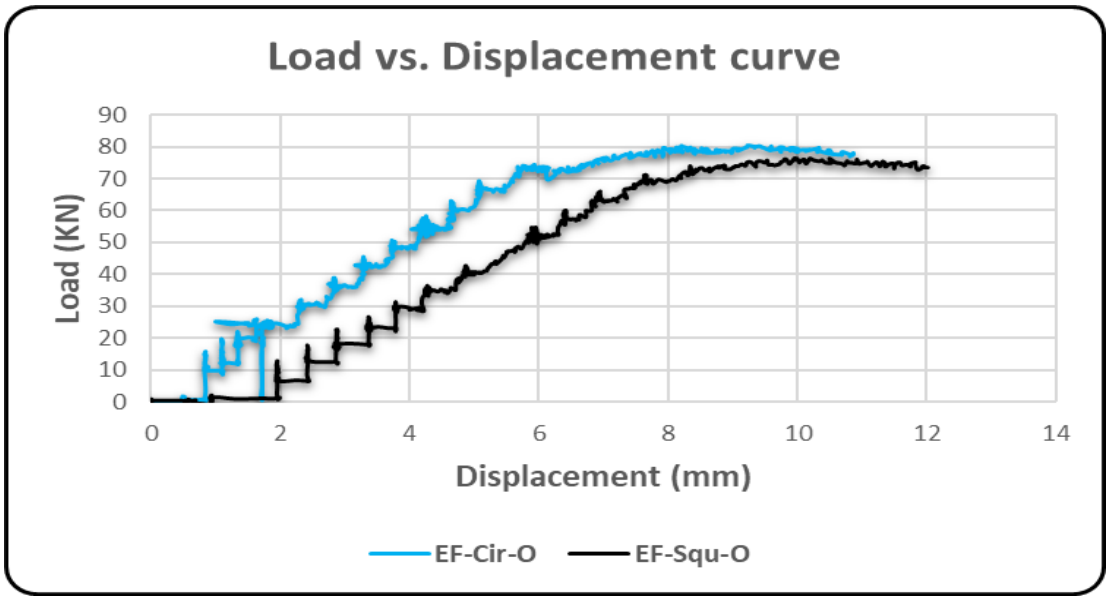

Fig. (4-77) Load-Displacement curve for (EF-Squ-O) and (EF-Cir-O)

*From these comparsons above , and for the specimens subjected to concentric loading, the load capacicity for (CF-Cir-O) more than the (CF-Squ-O),also the behaviore of curves obtained from (SGC) near the top opening for the circular and square open showed the same respons for elastic stage and then increase in stresses when the plastic stage begined as in figures. (4-74)and (4-75).

*And with respect to the eccentric loading ,the load capacity didn't showed the more diffrences between the speicemens (EF-Cir-O) and (EF-Squ-O),and for the readings obtained from the (SGC) on the compression face and also near the side open at the top edge (EF-Cir-O) gaveed the strain about twicing the ((EF-Squ-O),as the figures (4-76)and (4-77).

CHAPTER 5: FINITE ELEMENT ANALYSIS

5.1 Introduction

By using F.E computer program with commercial ABAQUS/Standard 2019 that is an advanced three dimensional finite element computer program, is adopted to perform a nonlinear finite element analysis to analyze the behavior of hollow concrete columns strengthening by carbon fiber and textile mortar (CFRP-TRM) that were conducted experimentally in the current study. In this section, the experimental laboratory works a study is presented among the differences between the outcomes of the three dimensional nonlinear finite element (FE) study and the outcomes of the laboratory work to confirm the appropriateness of elements types, material properties, the convergence study, and the real constants of the representing hollow concrete models, with the different configurations of external strengthening by using the two materials (CFRP-TRM), loading conditions including the boundary conditions (pin-pin) at the top and bottom of the column, and the static of (concentric and eccentric) line load.

5.2 Modeling of hollow concrete column

This section presents detailed date regarding the simulation of the geometry along with the boundary of the supporting and loading conditions of the tested column models. also the simulation for (CFRP or TRM).

5.2.1 Parts and Assembly

Generally, five parts were involved in the modeling the column models. Those parts were concrete column, main reinforcement of the rebar, transvers of reinforcement for stirrups rebar, carbon fiber reinforced polymer (CFRP), textile reinforced mortar (TRM), two boxes from steel plate for the supporting conditions and steel rode for the line load in the two load cases (CON and ECC). Each one of those parts was firstly drawn, and then different parts were assembled and merged to produce the modelling column specimens. Figures (5-1-a) and (5-1-c) exhibit prototype models that tested under the effects of concentric (CON.), and eccentric (ECC.) loading, respectively. In additionally, modeling the (CFRP and TRM) as the figures (5-1-d), (5-1-e), respectively and the fig(5-1-b) explain the hollow part inside the column. the features of the rebars modelling are illustrated in fig. (5-2)

In meshing the hollow concrete columns, solid brick components were employed. to achieve a sufficient 3D final element evaluation stress distribution. ABAQUS provides a variety of solid brick elements for meshing purposes. Linear Hexahedral elements with reduced integration (C3D8R) that is an 8-node linear brick with reduced integration and hourglass control. Also, a 2-node linear 3-D truss (T3D2) was adopted for meshing steel rebar for main and stirrups of reinforcement. To model CFRP and TRM material use shell element type (S4R),and elastic data with laminate type and Hashing's damage criterion is selected. The failure can be obtained through the force-displacement diagram.

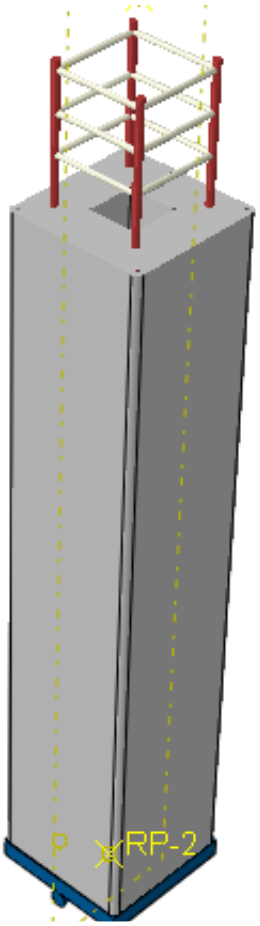

(5-1-a) model for concentric

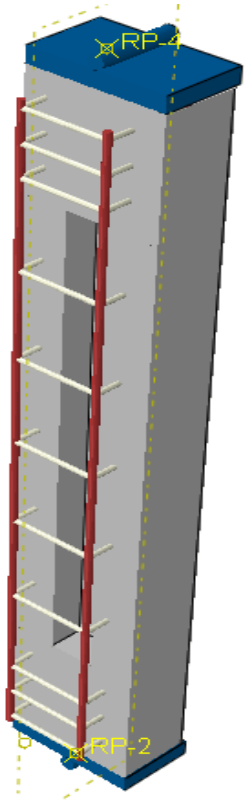

(5-1-b) Hollow part

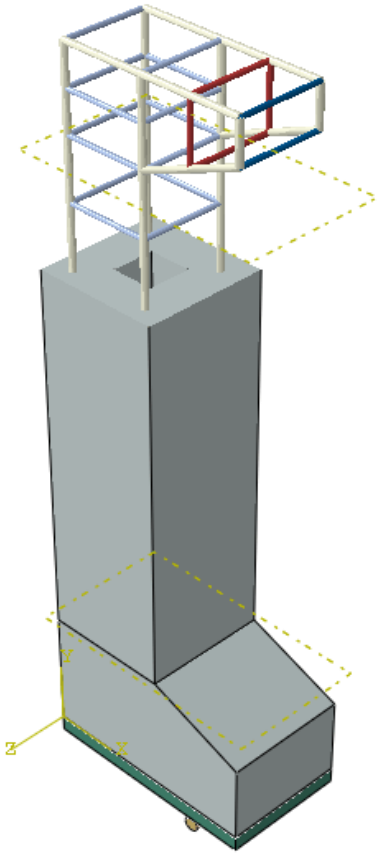

(5-1-c) model for eccentric

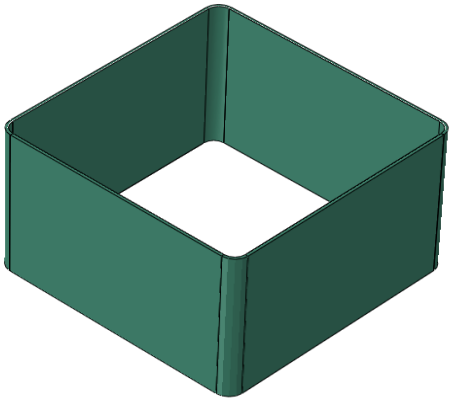

(5-1-d) CFRP-Laminate for case (CF1or EF1)

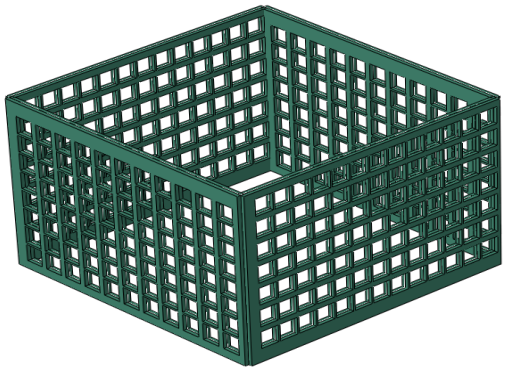

(5-1-e) TRM-Laminate for case (CT1 or ET1)

(5-1) Modeling of Parts by ABAQUS

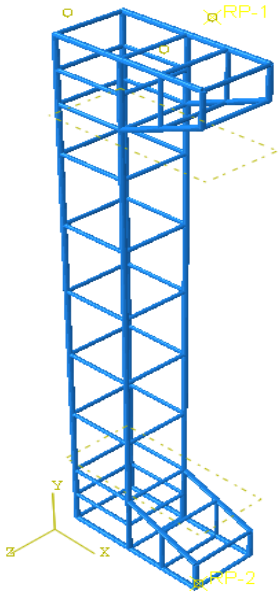

(5-2-a) ECC- rebar configuration in Abaqus

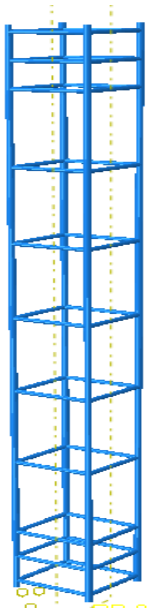

(5-2-b) CON- rebar configuration in Abaqus

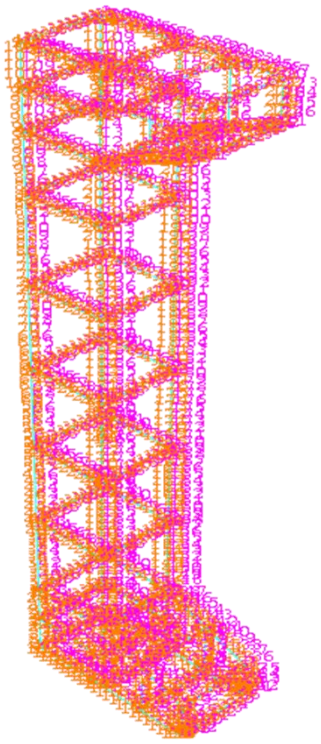

(5-2-c) Mesh whole rebar

(5-2-d) Mesh main rebar

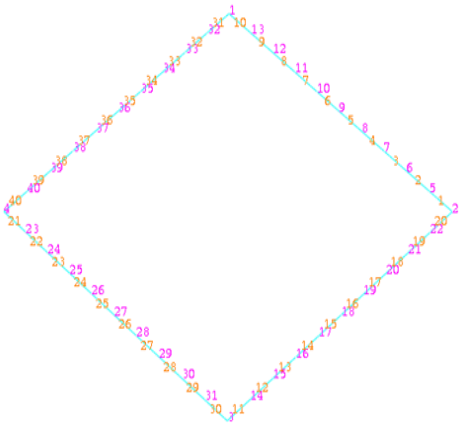

(5-2-e) Mesh stirrups rebar

Figures (5-2) rebar configuration in ABAQUS

5.2.2 Interaction

After the assembly operation completed, then the interactions between these components will create as: hollow concrete columns and steel rebar, the top and bottom concrete column and the bearing load plates, also between the external surface of the concrete side and the internal surface of the (CFRP.TRM). The type of interaction between the concrete and steel rebar its (embedded region).and the connections between the two ends and supports its (surface to surface contact). The final interaction between the (CFRP, TRM) and the external surface of concrete will come out by the (tie), these interactions between the materials have the were linked with different forms of constraint based on experimental results for the production of a progressive composites system., as shown in Figure (5-3). In this study, a tie constraint was chosen to connect the bearing steel plate (loading plates) and the concrete at the top and bottom head of column. Another tie constraint was used as a constrain between the concrete column and the steel rode (supports).

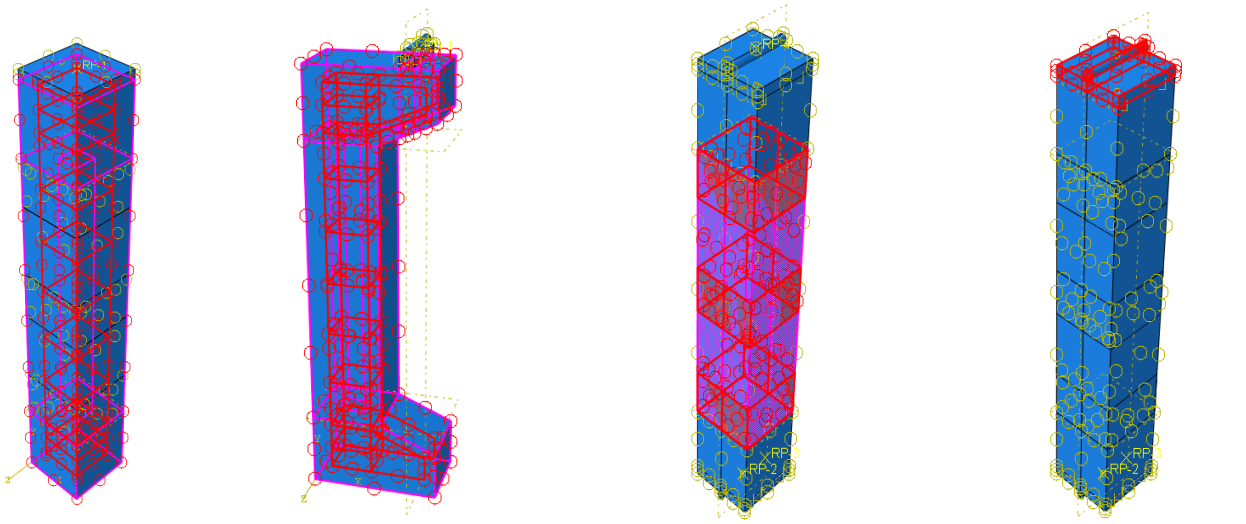

(5-3-a) for concentric (5-3-b) for eccentric (5-3-c) for (CFRP or TRM) (5-3-d) for Load plate

Figures (5-3) Interactions

5.2.3 Boundary Conditions and loading

To emulate the setting of the experimental program, boundary conditions were carefully determined. At the top and bottom of the column, simply supported (pin-pin) criteria were given. The two references points created to simulated the boundary conditions at top and the bottom. After creation the references points then simulate the boundary conditions for the two type of loading in concentric or eccentric loading as fig (5-4). Displacements were constrained in supports for both the x- and z-axes at top and bottom ends, while permitted in the y-axis at the top. In this experimental work the static load come out as the line loading. In which the line load represented the concentric and eccentric loading. It took 20mm away from the center of each concentric column, and this displacement was applied to the top of each column at 135mm (0.9h) intervals along its axis, depending on how much eccentricity was desired.

.

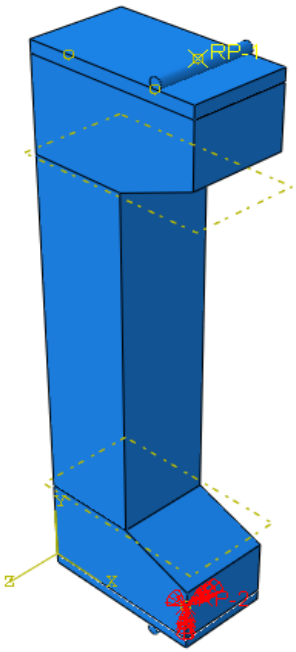

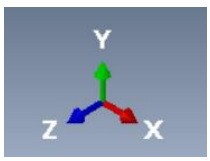

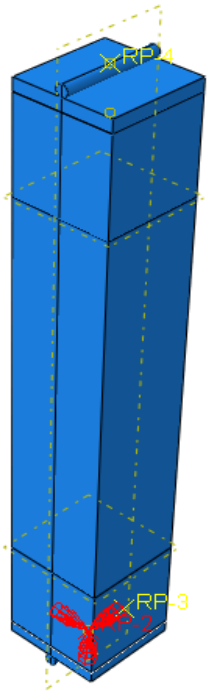

Boundary condition at top

UX = UZ =0

UY ≠ 0

Boundary condition at bottom

UX = UY = UZ = 0

Figures (5-4-a) boundary Conditions for ECC. models

Figures (5-4-b) boundary Conditions for CON. models

Figures (5-4) boundary Conditions

5.3 Convergence Study

Mesh size selection is a crucial stage in finite element modeling. Before beginning the study, an appropriate pre-analysis of several mesh sizes was done to establish the optimal size that provides the requisite accuracy based on the level of analysis complexities. A convergence analysis was conducted on hollow concrete column models. A good convergence of findings is attained when the column is partition into a sufficient number of components. This is essentially accomplished when the mesh is reduced the size of the object has a minor impact on the outcome. The convergence research for hollow column models was assessed as a result of the influence of changing the element size from (50 mm to 10 mm) on the final loading capacity. As illustrated in Figure. (5-5). In compared to the experimental results, using a mesh size of (10 mm) as the fig(5-5-f) resulted in more precise displacement.

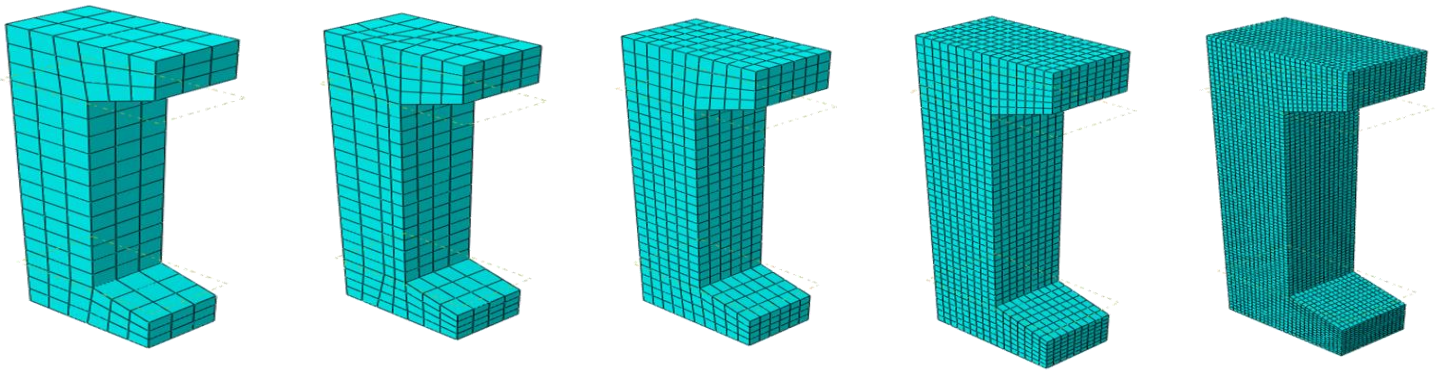

(5-5-a) Mesh -50 (5-5-b) Mesh -40 (5-5-c) Mesh -30 (5-5-d) Mesh -20 (5-5-e) Mesh -10

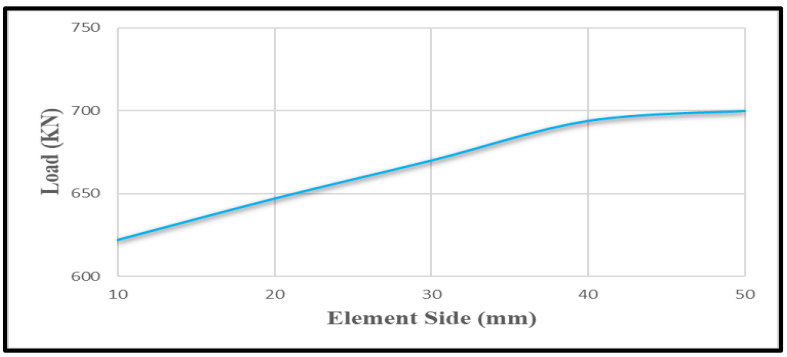

Figures (5-5-f) The convergence study

Figures (5-5) Mesh Size

5.4 Comparison Study between the Results of the Experimental Program and FEM Analysis

This section provides a comparison of the findings of the experimental study with the data of the nonlinear Finite element analysis. The nonlinear FE analysis was conducted for all hollow concrete column models divided to concentric and eccentric loading by considering the types of concrete (NSC), steel rebar with two dimeters (8 and 6), with use two types for external strengthening (CFRP and TRM) with five configuration of strengthening for each part as figures (5-6-1) for concentric loading and (5-6-2) for models with eccentric loading. Same models with strengthening by (TRM) under concentric and eccentric loading as the figures (5-7-1) and(5-7-2).

The structural behavior of hollow concrete column models developed using nonlinear FE analysis coincided well with the structural performance gained through the experimental investigation. The compared study covered the load to the displacement curve, mode of failure, and plastic strain.

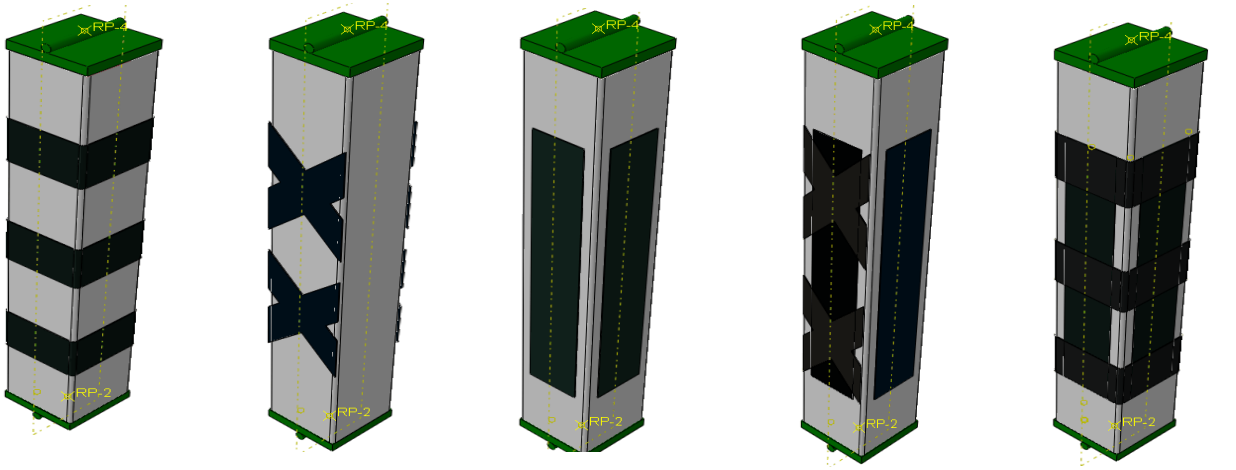

(5-6-1-a) –(CF1) (5-6-1-b) –(CF2) (5-6-1-c) –(CF3) (5-6-1-d) –(CF4) (5-6-1-e) –(CF5)

Figures (5-6-1) Strengthening Specimens by CFRP under Concentric

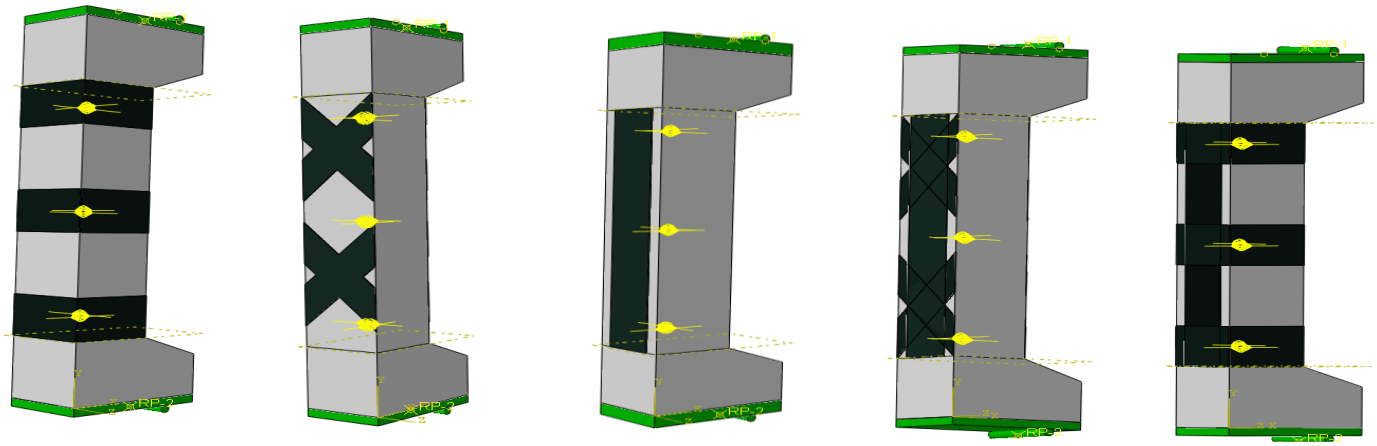

(5-6-2-a) –(EF1) (5-6-2-b) –(EF2) (5-6-2-c) –(EF3) (5-6-2-d) –(EF4) (5-6-2-e) –(EF5)

Figures (5-6-2) Strengthening Specimens by CFRP under Eccentric

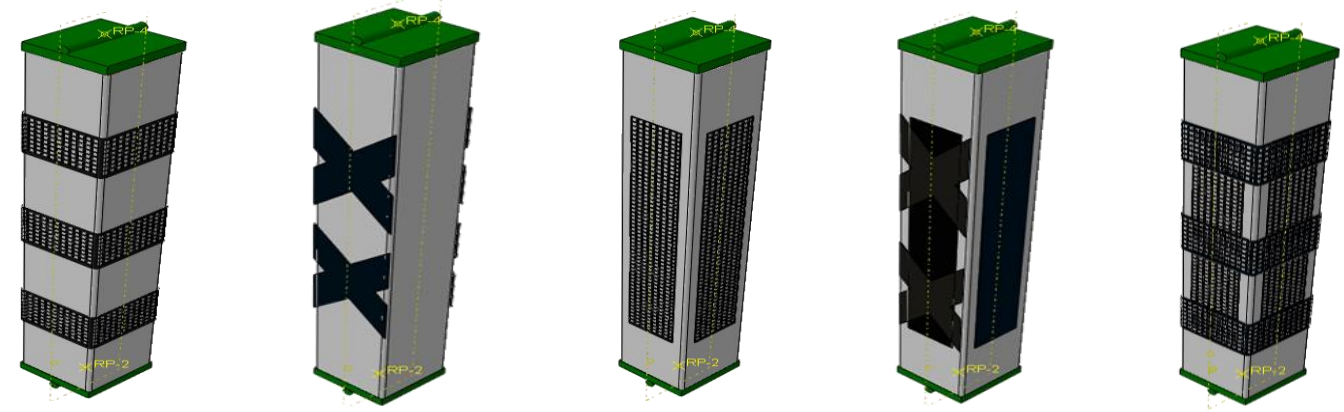

(5-7-1-a) –(CT1) (5-7-1-b) –(CT2) (5-7-1-c) –(CT3) (5-7-1-d) –(CT4) (5-7-1-e) –(CT5)

Figures (5-7-1) Strengthening Specimens by TRM under Concentric Loading

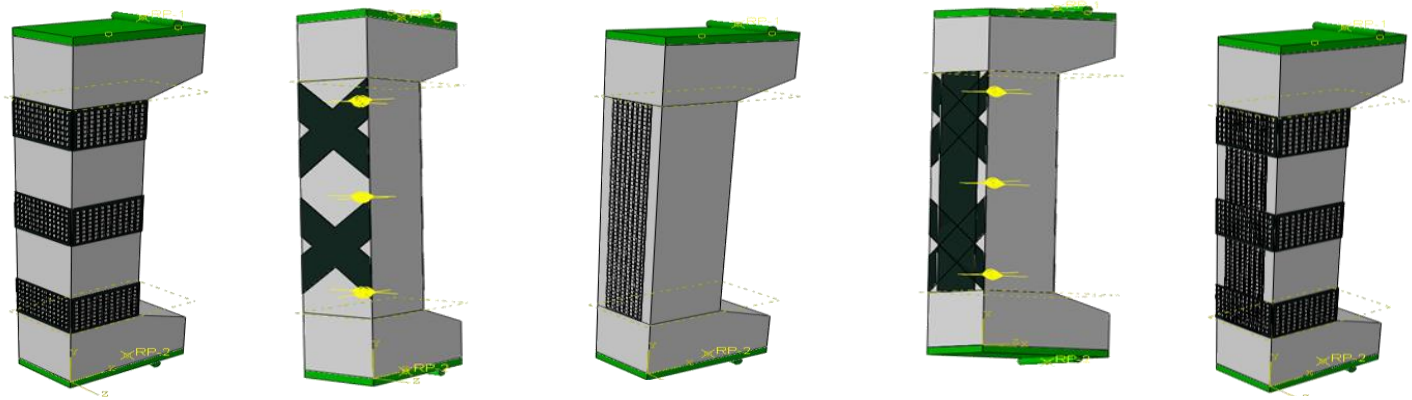

(5-7-2-a) –(ET1) (5-7-2-b) –(ET2) (5-7-2-c) –(ET3) (5-7-2-d) –(ET4) (5-7-2-e) –(ET5)

Figures (5-7-2) Strengthening Specimens by TRM under Eccentric Loading

5.4.1 Comparison between the results of the experimental program and FEM Analysis for specimens with concentric load

Table (5-1) illustrates the comparison of the ultimate loads and displacement from computed finite element models and experimental testing. The FEA and experimental findings were performed to validate association.

Table (5-1) Ultimate load comparison between the Experimental and the FE for Concrete columns under concentric lodging

Model ID	P_{ult_lab} (kN)	P_{ult_FE} (kN)	$(\frac{P_{ult_{FE}} - P_{ult\_lab}}{P_{ult\_lab}}) * 100$
CC-CO-H	610	648.2	6.2
C.F1	625	676.2	8.2
C.F2	640.8	673.1	5
C.F3	659.64	721	9.35
C.F4	749.2	779.4	4
C.F5	689.5	749.7	8.7
C.T1	620	674.2	8.7
C.T2	635	639.3	0.67
C.T3	627	648.2	3.4
C.T4	654	686.1	4.9
C.T5	662	671.6	1.45
Average			5.5

Table (5-1) above clearly indicates that all of the numerical values of axial compressive load of the tested specimens were more than the experimental values.

5.4.1.1 Load-displacement curves for specimens strengthened by CFRP and loaded concentrically

Figures from (5-8) to (5-12), compare test and numerical findings in terms of load-displacement curves for specimens with concentrically condition. In terms of ultimate load capacity and displacement, the analytical results for the investigated specimens correspond well with the experimental results. The FEA findings additionally show a failure point, but the experimental load-displacement curves didn't contain this point,

although with a smaller difference. Several factors are indicated in finite element analysis as the hypotheses for the increased stiffness in elastic stage. Some of these concepts have been observed:

1. The FEA hypothesized that the concrete was a homogeneous material, but the actuality that it was heterogeneous.
2. In the FEA, a perfect connection was assumed between the steel rebar and the concrete, as well as between the TRM textile and the mortar and the concrete surface. The assumption, however, would not remain true in the physical specimen.
3. The boundary conditions and supports in FEM was simulated as the perfect situation (pin-pin) at two ends, but in the laboratory these simulations did not accurate have the hundred percent.

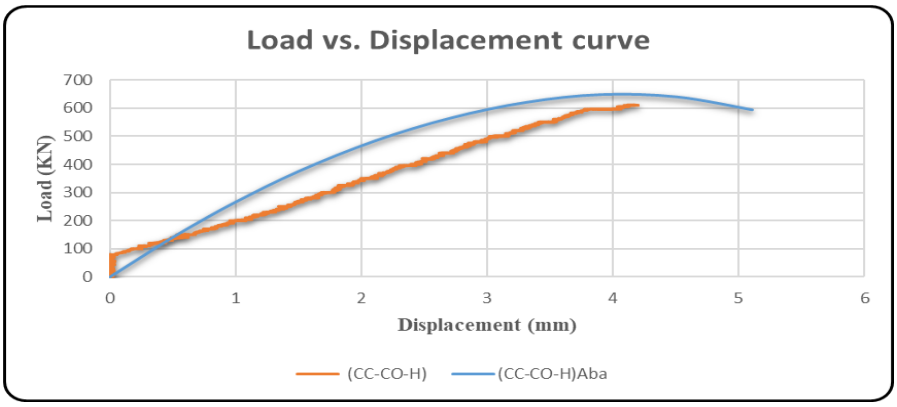

Fig. (5-8) Experimental and Numerical Load vs. Displacement curve for (CC-CO-H).

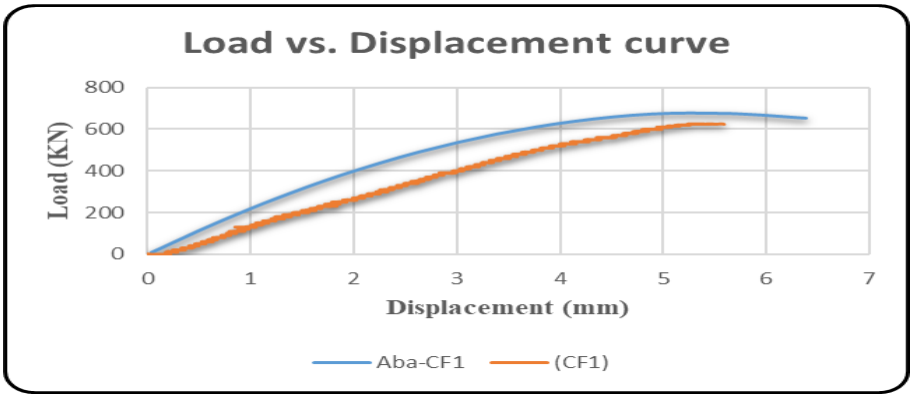

Fig. (5-9) Experimental and Numerical Load vs. Displacement curve for (CF1).

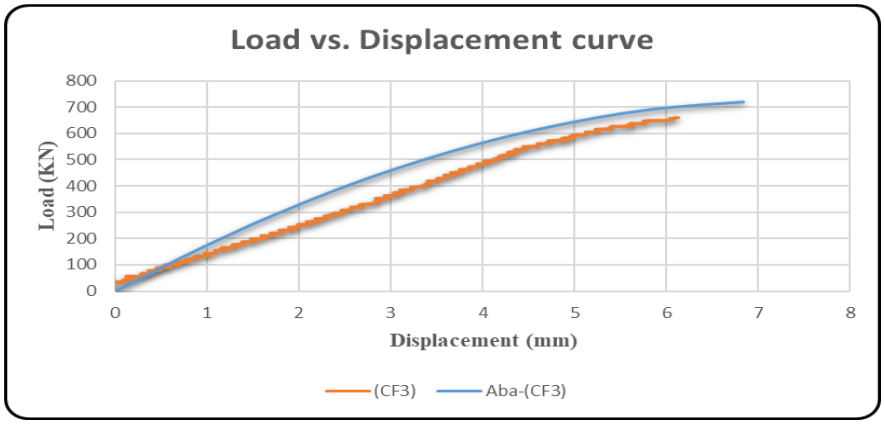

Fig. (5-10) Experimental and Numerical Load vs. Displacement curve for (CF3).

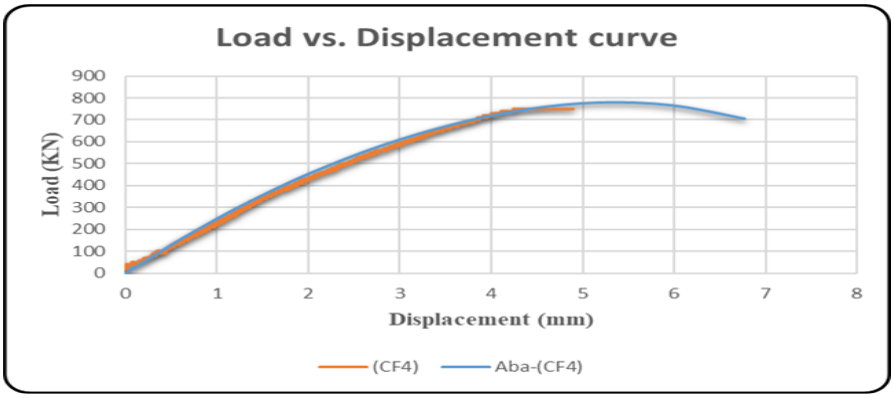

Fig. (5-11) Experimental and Numerical Load vs. Displacement curve for (CF4).

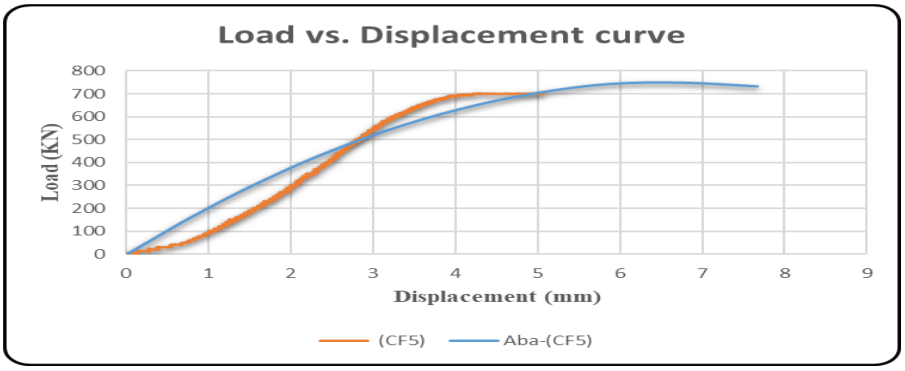

Fig. (5-12) Experimental and Numerical Load vs. Displacement curve for (CF5).

5.4.1.2 Failure mode and von-misses stresses for concentric specimens

Figures (5-13) to (5-16) to demonstrate how much the loaded specimens have warped after failing in both tests and numerical simulations. According to the position and angle of their failure surfaces, the two forms are very similar. The comparison between the outcomes is given a true satisfaction. von-mises stress, from the ABAQUS program funded the stress at the max elastic stage and the stress when the curve started dropped. This information will be important for calculating the column's plastic dissipation energy while formulating analytic solutions to the problem. obtained this parameter from the plastic strain (PE) [1],in ABAQUS, where these plastic strain depended on the damage occurred in the concrete. For the specimens with strengthen by CFRP. The max. plastic strain obtained from the cases reported in the table (5-2) below

Table (5-2) models with plastic strain

Model	Plastic strain
CC-CO-H	$1.386*10^{-2}$
CF1	$1.487*10^{-2}$
CF4	$3.486*10^{-2}$
CF5	$1.124*10^{-2}$

(5-13- a) failure mode of column (CC-CO-H) in laboratory

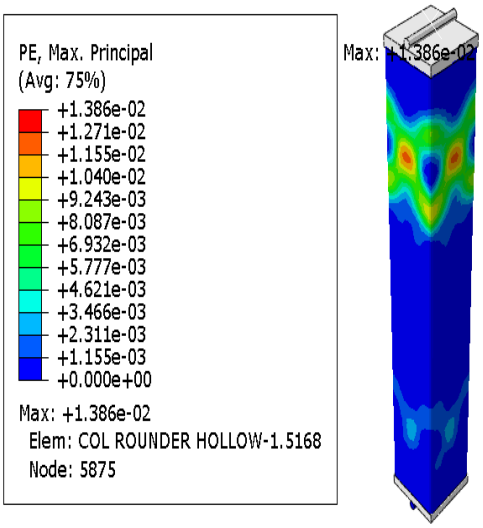

(5-13-b) failure mode of column (CF1) in ABAQUS

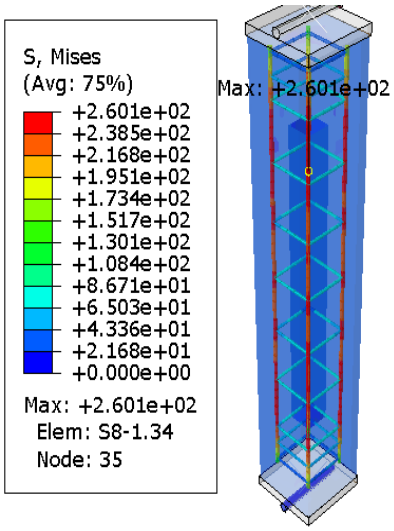

(5-13-c) von-misses stress at max. elastic

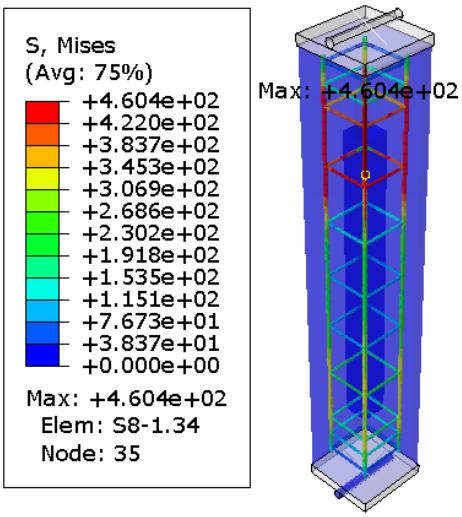

(5-13 d) von-misses stress at failure

Fig. (5-13) Comparison between the experimental and FE for (CC-ECC-H).

(5-14 a) failure mode of column (CF1) in laboratory

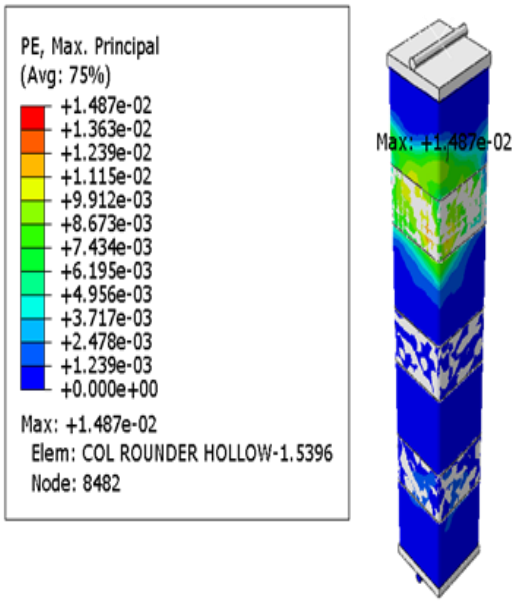

(5-14-b) failure mode of column (CF1) in ABAQUS

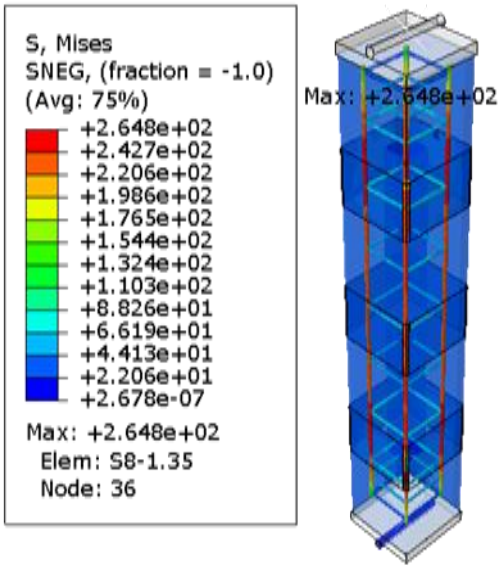

(5-14-c) von-misses stress at max. elastic

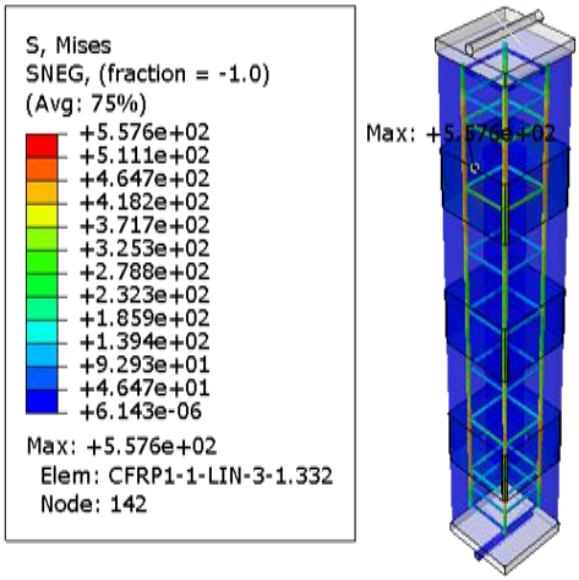

(5-14- d) von-misses stress at failure

Fig. (5-14) Comparison between the experimental and FE for (CF1).

(5-15-a) failure mode of column (CF4) in laboratory

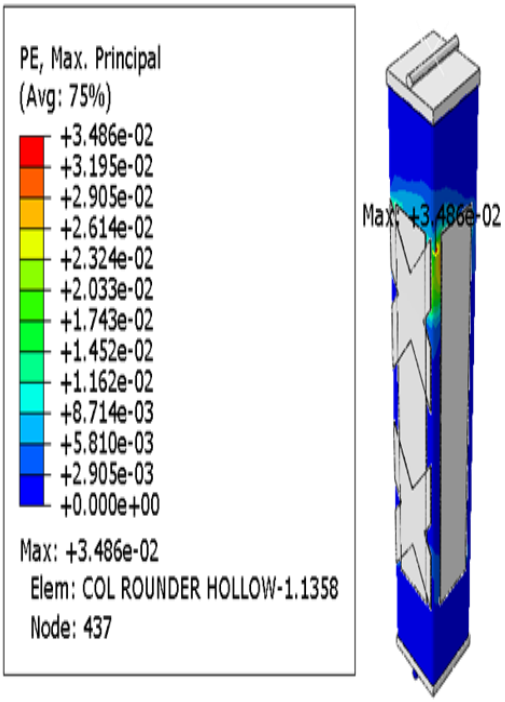

(5-15-b) failure mode of column (CF4) in ABAQUS

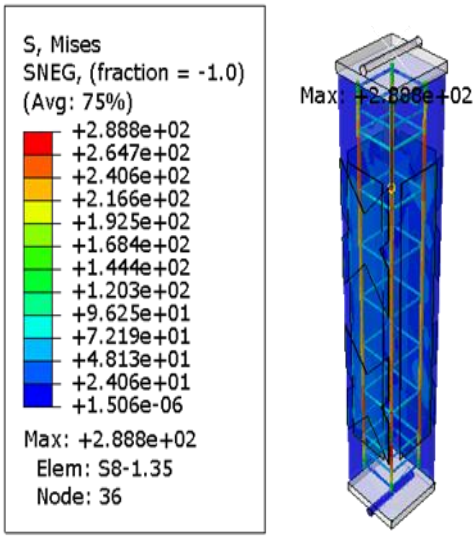

(5-15-c) von-misses stress at max. elastic

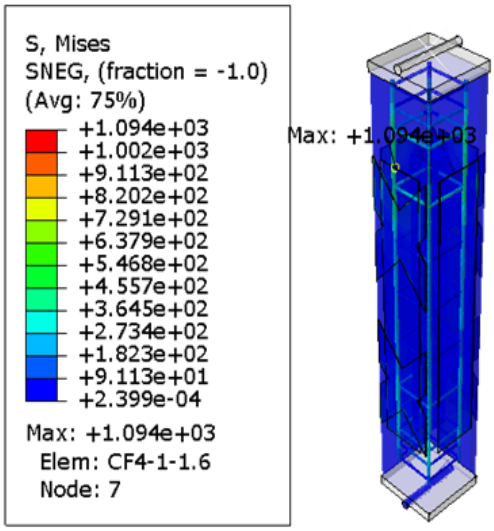

(5-15-d) von-misses stress at failure

Fig. (5-15) Comparison between the experimental and FE for (CF4).

(5-16- a) failure mode of column (CF5) in laboratory

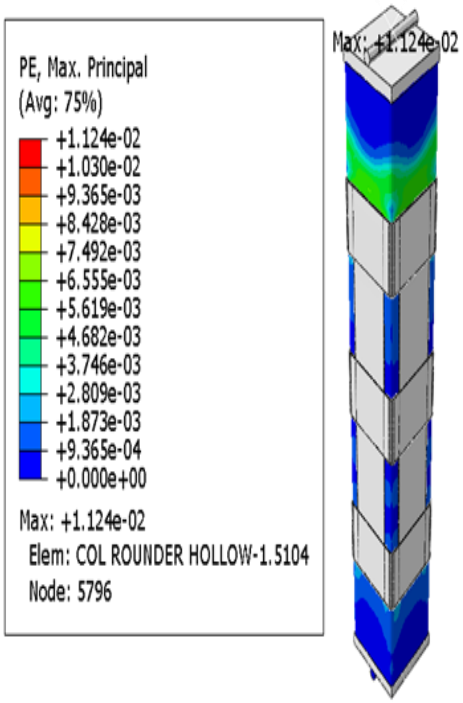

(5-16-b) failure mode of column (CF5) in ABAQUS

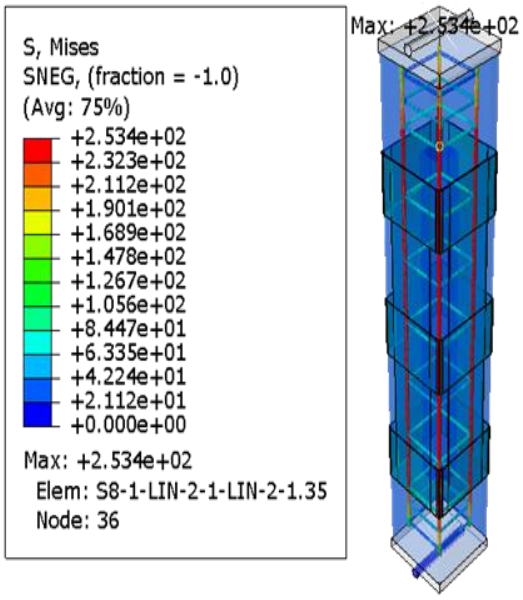

(5-16-c) von-misses stress at max. elastic

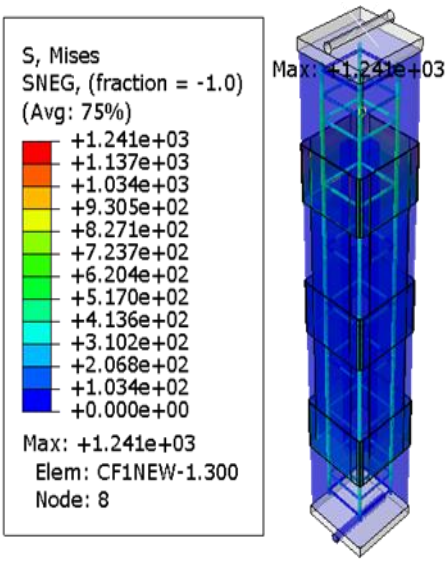

(5-16- d) von-misses stress at failure

Fig. (5-16) Comparison between the experimental and FE for (CF5).

From the figures above and with respect to the von-misses stresses, the contributions of the CFRP started when the elastic stage finished. And the max. von-misses stresses obtained from the case (CF5) with value reached to the ($1.24*10^{3)}$ MPa, With percentage of the contributions near to the (31.79) % from the strength of the CFRP laminate.

5.4.2 Comparison between the results of the experimental program and FEM Analysis for specimens with eccentric load

Table (5-3) illustrates the comparison of the ultimate loads and displacement from computed finite element models and experimental testing. The eccentricity fixed with distance equal to the (0.9h) for all models as the experimental cases.

Table (5-3) ultimate load comparison between the experimental and the FE for concrete columns under eccentric lodging

Model ID	P_{ult_lab} (kN)	P_{ult_FE} (kN)	$(\frac{P_{ult_{FE}} - P_{ult\_lab}}{P_{ult\_lab}}) * 100$
CC-ECC-H	68.03	71.7	5.4
E.F1	69.53	78.1	12.3
E.F2	68.9	78.1	13.3
E.F3	87.9	98.18	11.6
E.F4	90.5	102.8	13.6
E.F5	94.8	110.8	16.9
E.T1	68.5	77.35	12.9
E.T2	70.7	78.9	9.78
E.T3	82.64	87.05	11.59
E.T4	84.4	86.79	2.8
E.T5	86.5	90.79	4.95
Average			10.46

5.4.2.1 Load-displacement curves for specimens loaded eccentrically

For model specimens, vertical displacement is calculated at the position of the line load was measured at the top end of column same with experimental column and at the tension face of the column model. The load-displacement curves plot for all columns got from the numerical analysis and together with the experimental results as shown in Figures (5-17) to Figure (5-20). At the early stages of loading, the column models are free from any cracks and the relation between the load and the displacements is linear. With increasing of the applied load, the first crack is happening, the slope of the load-displacement curve decrease, the relation between the load and the displacements convert to nonlinear and it continues until the buckling is happen.

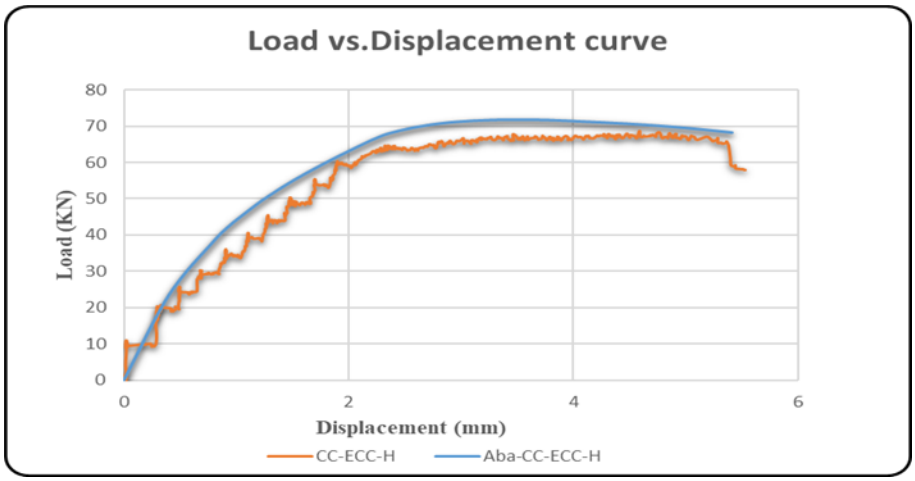

Fig. (5-17) Experimental and Numerical Load vs. Displacement curve for (CC-ECC-H).

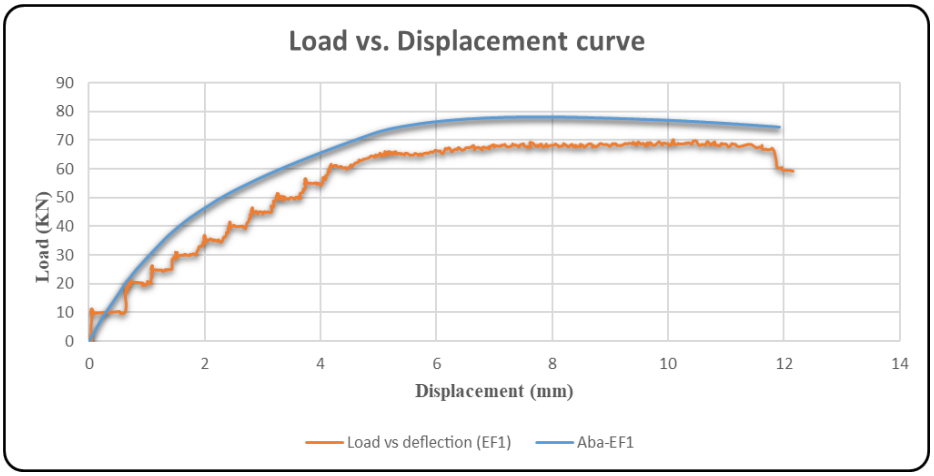

Fig. (5-18) Experimental and Numerical Load vs. Displacement curve for (EF1).

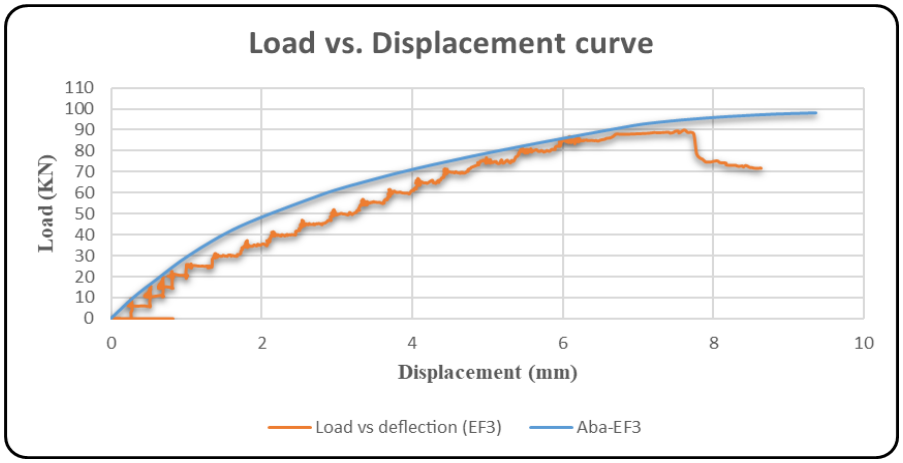

Fig. (5-19) Experimental and Numerical Load vs. Displacement curve for (EF3).

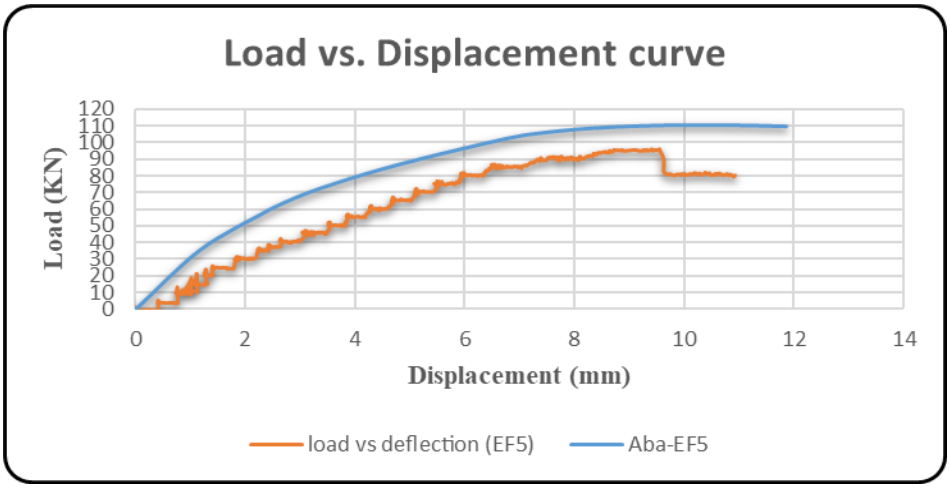

Fig. (5-20) Experimental and Numerical Load vs. Displacement curve for (EF5).

5.4.2.2 Failure mode and von-misses stresses for eccentric specimens

At the ultimate stage, damage has occurred for both experimental and numerical tested columns. Depending on the CDP theory that if the plastic strain (PE) exceeds zero, the concrete will have cracked, then the maximum plastic principal strain was used in the current study as a proxy for the creation of cracks. The cracks are considered to be vertical orient toward the principal plastic strain. The figures (5-21) to (5-23) show the mode failure for these specimens.

(5-21- a) failure mode of column (CC-ECC-H) in laboratory

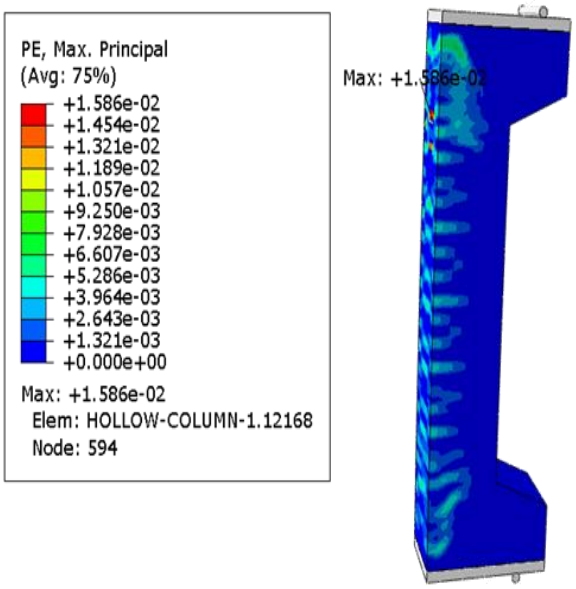

(5-21-b) failure mode of column (CC-ECC-H) in ABAQUS

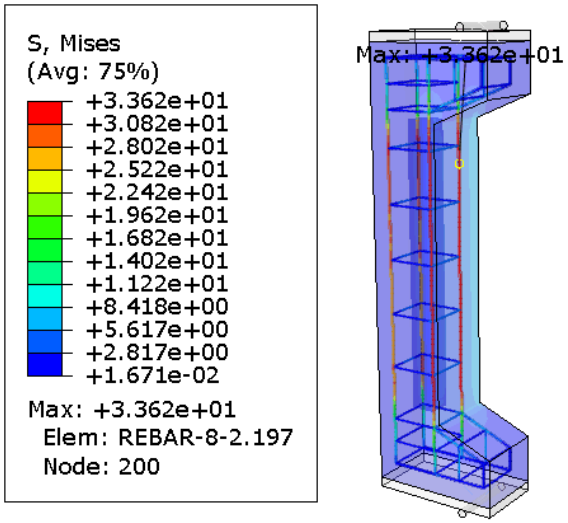

(5-21-c) von-misses stress at max. elastic

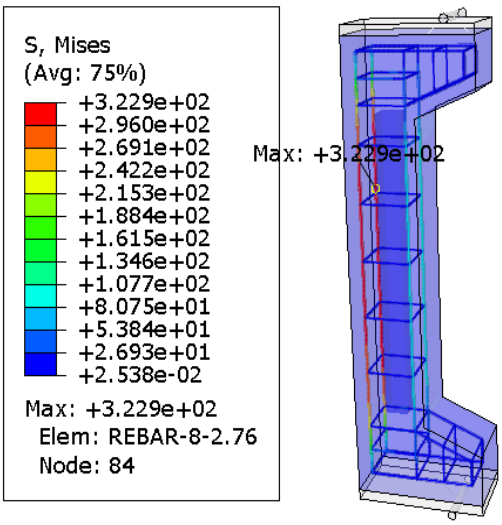

(5-21- d) von-misses stress at failure

Fig. (5-21) Comparison between the experimental and FE for (CC-ECC-H).

(5-22- a) failure mode of column (EF1) in laboratory

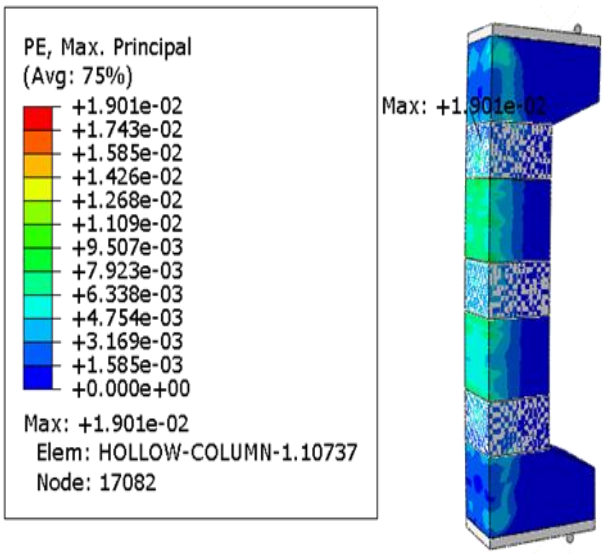

(5-22-b) failure mode of column (EF1) in ABAQUS

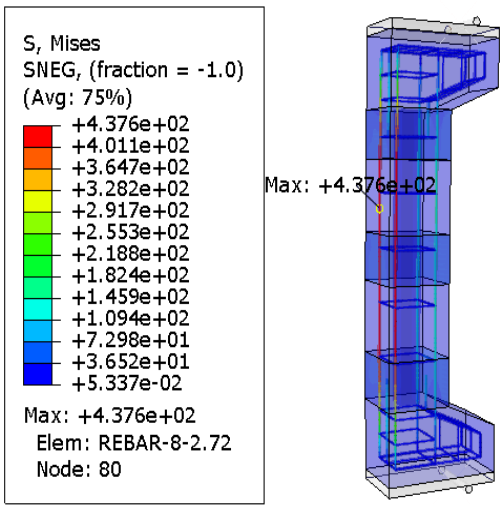

(5-22- c) von-misses stress at max. elastic

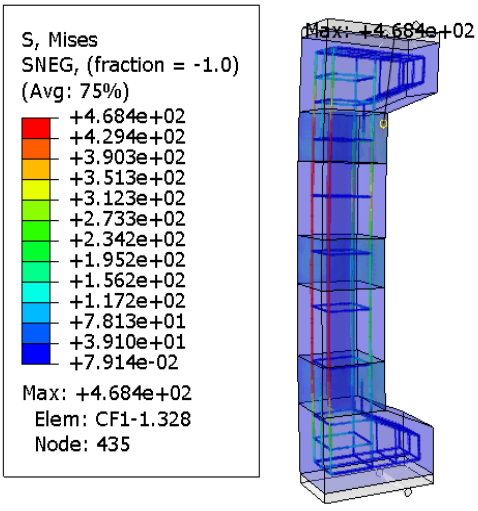

(5-22- d) von-misses stress at failure

Fig. (5-22) Comparison between the experimental and FE for (EF1).

(5-23- a) failure mode of column (EF5) in laboratory

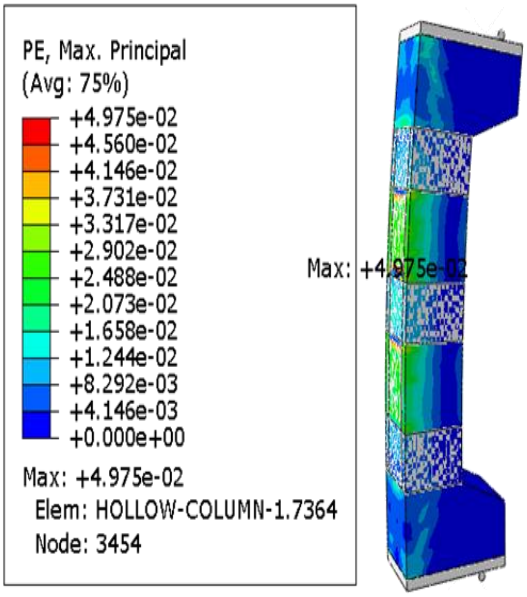

(5-23-b) failure mode of column (EF5) in ABAQUS

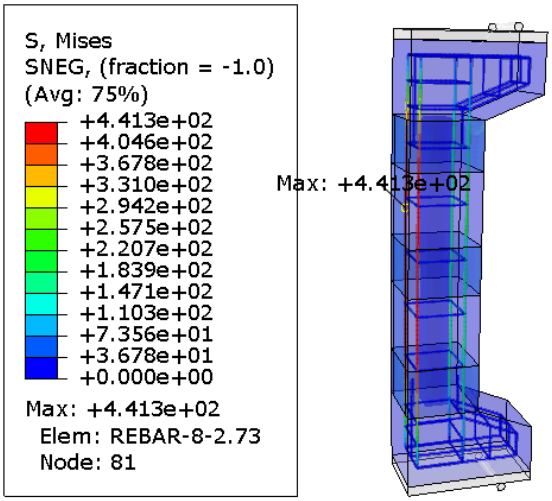

(5-23-c) von-misses stress at max. elastic

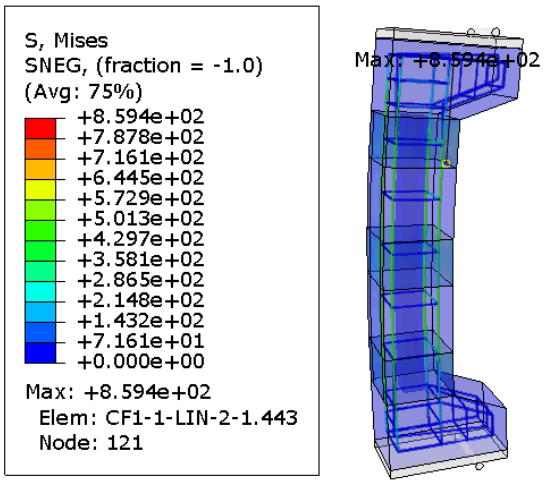

(5-23- d) von-misses stress at failure

Fig. (5-23) Comparison between the experimental and FE for (EF5).

From the figures above and with respect to the von-misses stresses, the contributions of the CFRP started when the elastic stage finished. And the max. von-misses stresses obtained from the case (EF5) with value reached to the ($8.59x10^{2}$) MPa, with percentage of the contributions near to the (22) % from the strength of the CFRP laminate. The max. plastic strain obtained from the modeling in the ABAQUS reported in the table (5-4) below

Table. (5-4) plastic strain from FE for (CC-ECC-H, EF1, EF5).

Model	Plastic strain
CC-ECC-H	$1.586x10^{-2}$
EF1	$1.901x10^{-2}$
EF5	$4.975x10^{-2}$

5.5 Case study specimens with side openings

For the specimens with consist the side opening, the modeling in ABAQUS with figure (5-24) for specimens unstrengthen and subjected to concentric and eccentric loading, and the mesh as in the figure (5-25).

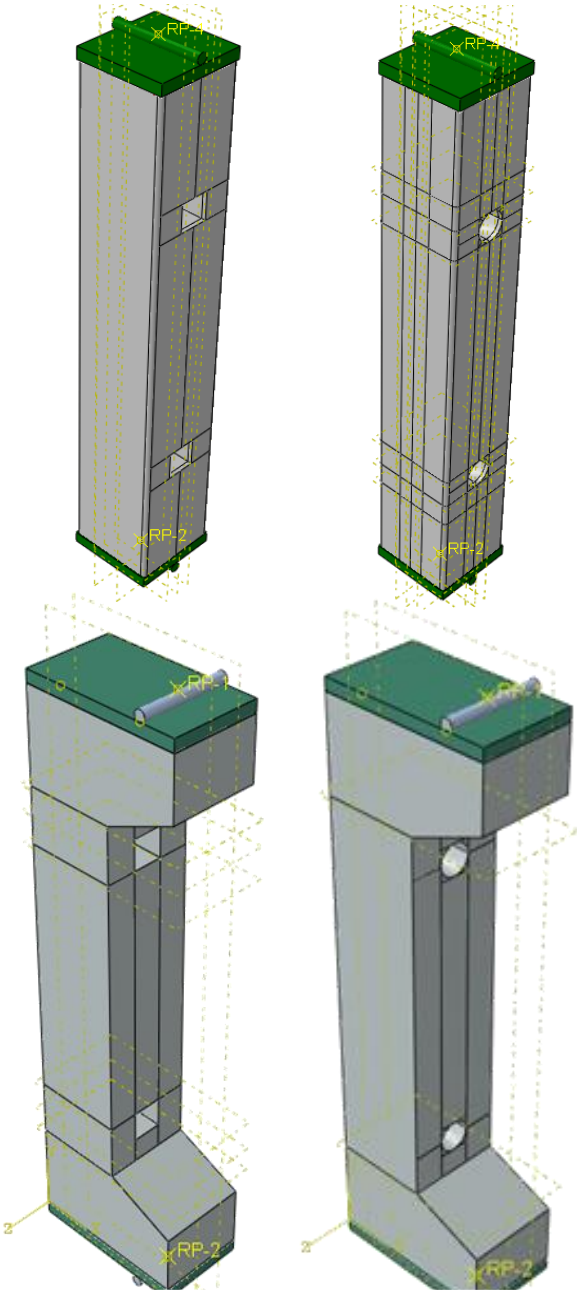

Fig. (5-24) Modeling of side opening with CON. & E

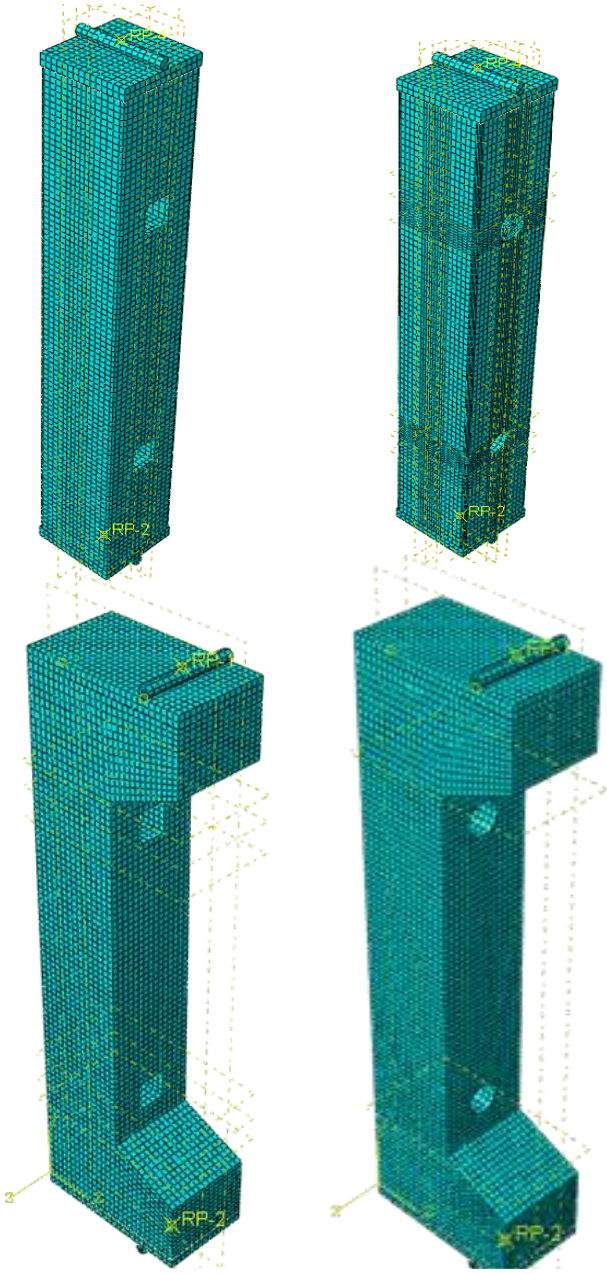

Fig. (5-25) Mesh of side opening

5.5.1 Load-displacement curves for control columns with side openings

The load-displacement curve plots for columns got from the numerical analysis and together with the experimental results as shown in figure (5-26) to figure (5-29) For model specimens. a good agreement was obtained between the experimental and FEA results.

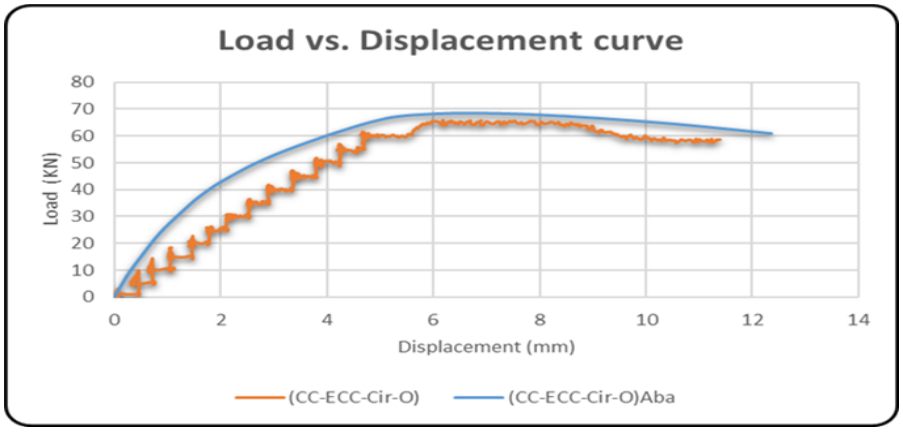

Fig. (5-26) Experimental and Numerical Load vs. Displacement curve for (CC-ECC-Cir-O).

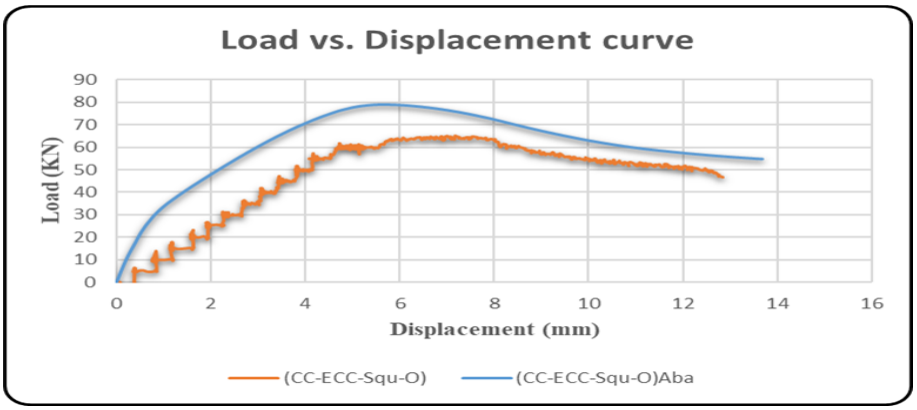

Fig. (5-27) Experimental and Numerical Load vs. Displacement curve for (CC-ECC-Squ-O).

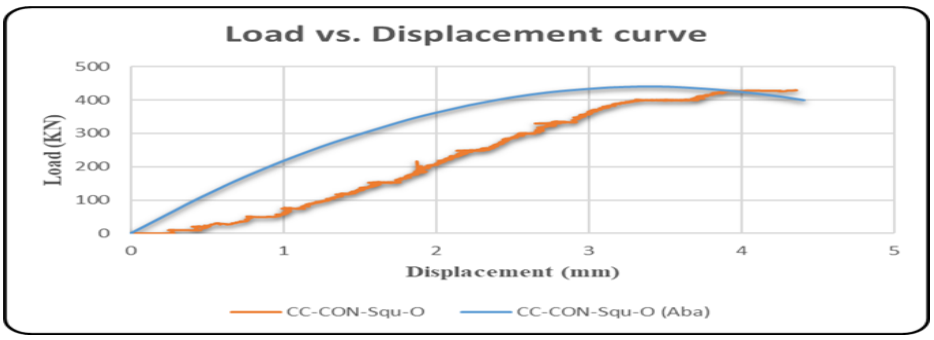

Fig. (5-28) Experimental and Numerical Load vs. Displacement curve for (CC-CON-Squ-O).

5.5.2 Failure mode and von-misses stresses control columns with openings

(5-29-a) failure mode of column (ECC-Cir-O) in laboratory

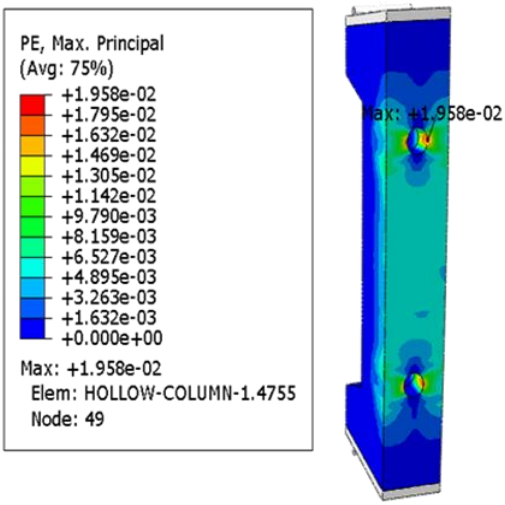

(5-29-b) failure mode of column (ECC-Cir-O) in FE

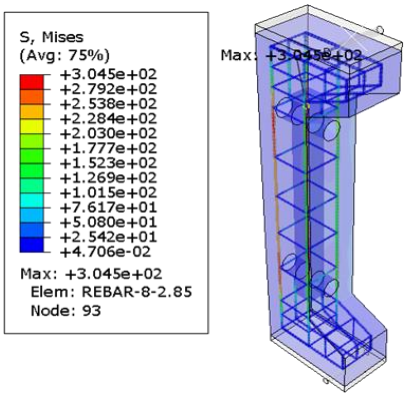

(5-29-c) von-misses stress at max. elastic

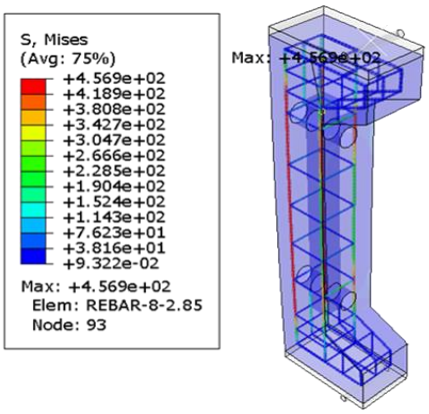

(5-29- d) von-misses stress at failure stage

Fig. (5-29) Comparison between the experimental and FE for (CC-ECC-Cir-O).

(5-30-a) failure mode of column (ECC-Squ-O) in laboratory

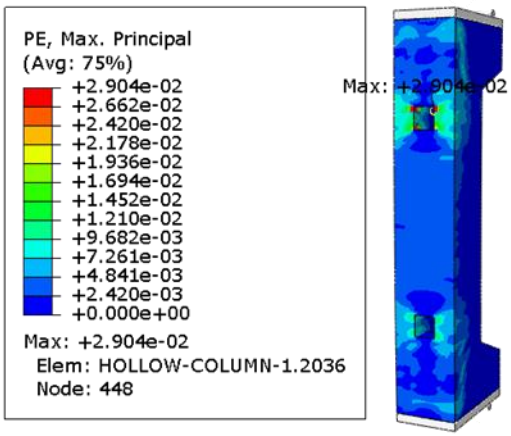

(5-30-b) failure mode of column (ECC-Squ-O) in FE

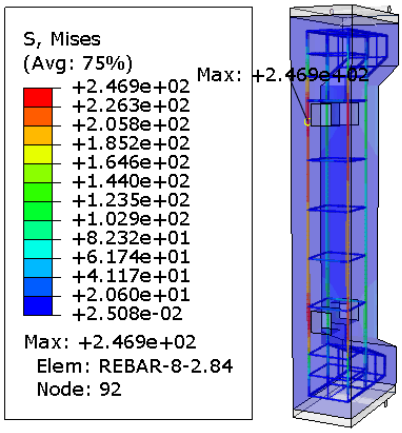

(5-30-c) von-misses stress at max. elastic

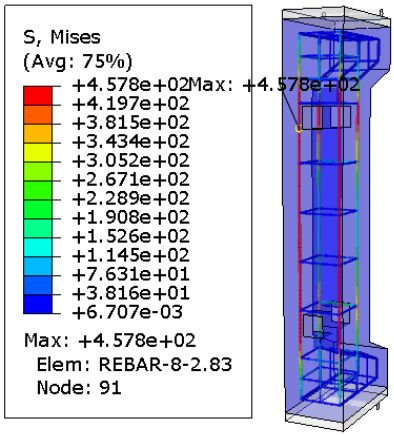

(5-30- d) von-misses stress at failure stage

Fig. (5-30) Comparison between the experimental and FE for (CC-ECC- Squ -O).

(5-31-a) failure mode of column (CC-CO-Squ-O) in laboratory

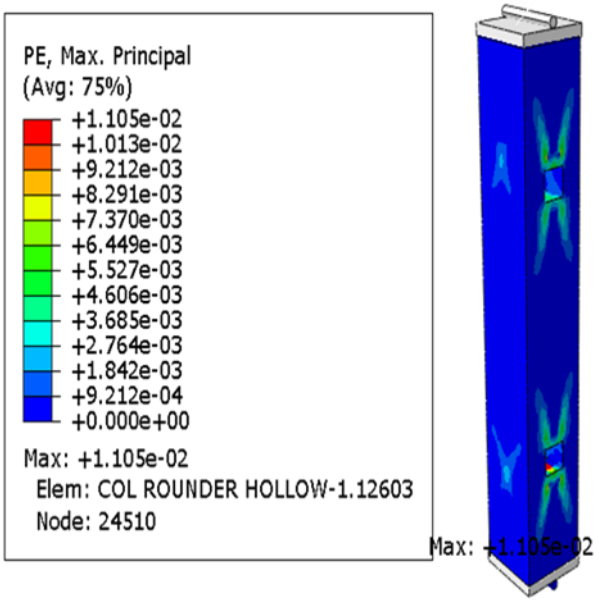

(5-31-b) failure mode of column (CC-CO-Squ-O) in FE

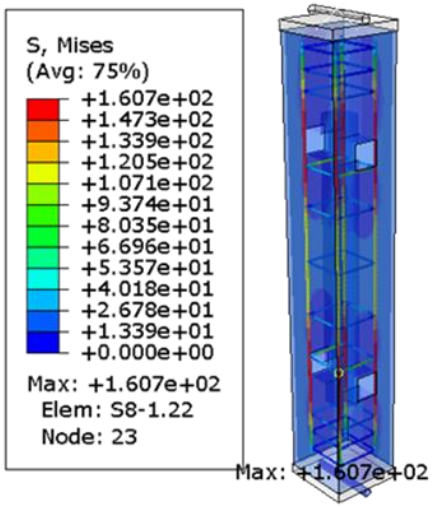

(5-31-c) von-misses stress at max. elastic

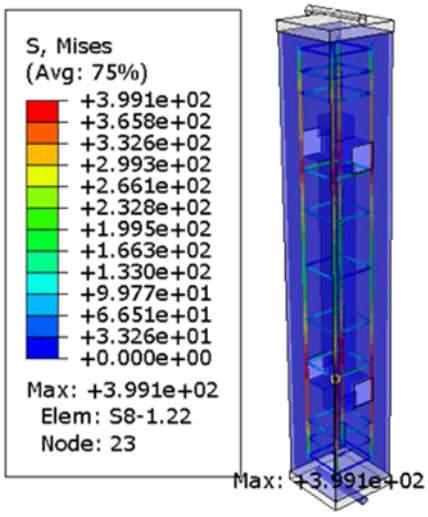

(5-31- d) von-misses stress at failure stage

Fig. (5-31) Comparison between the experimental and FE for (CC-CO-Squ -O).

From the results related to control specimens with side openings the good coincide between the FEM and the experimental work for the failure position has been occurred. For specimen with circular side open gathered value of the plastic strain less than the square open for as the figures (5-29-b) and (5-30-b).

5.5.3 Strengthening specimens with side openings

5.5.3.1 Load-displacement curves for strengthening columns with side openings

with the side opening and subjected to the eccentric loading the figures (5-30) illustrated the comparing between the FEM, and laboratory test for the load vs. displacement curve

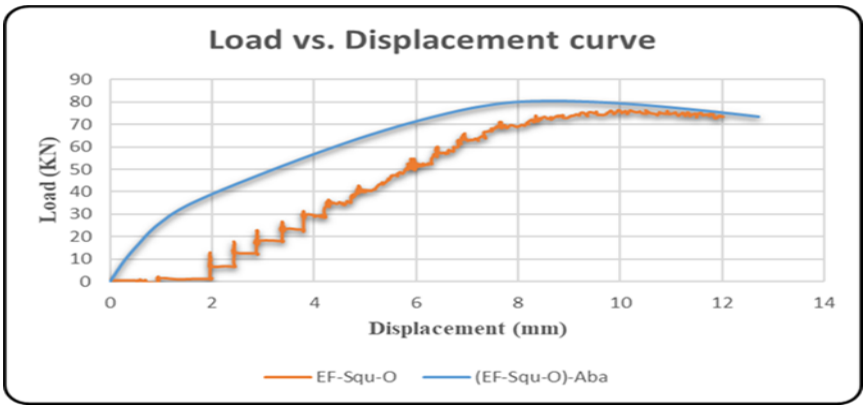

Fig. (5-32) Experimental and Numerical Load vs. Displacement curve for (EF-Squ-O).

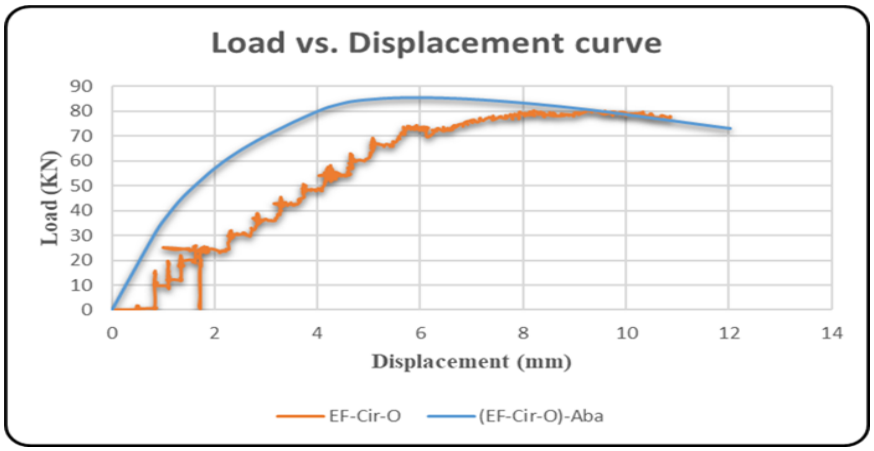

Fig. (5-33) Experimental and Numerical Load vs. Displacement curve for (EF-Cir-O).

5.5.3.2 Failure mode and von-misses stresses for strengthening specimens and with side openings

(5-34-a) failure mode of column (EF-Squ-O) in laboratory

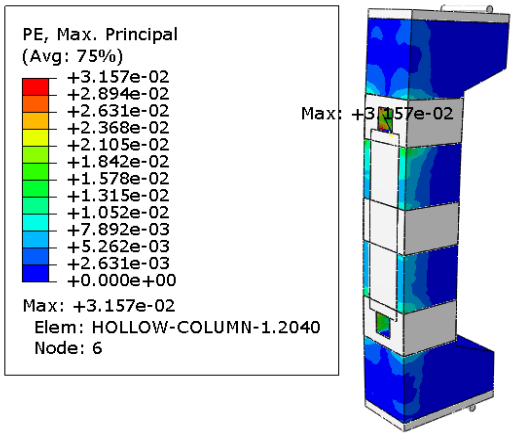

(5-34-b) failure mode of column (EF-Squ-O) in FE

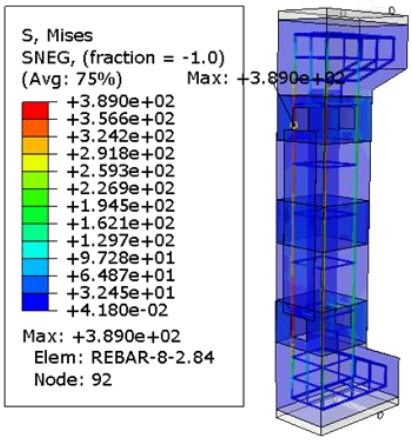

(5-34-c) von-misses stress at max. elastic

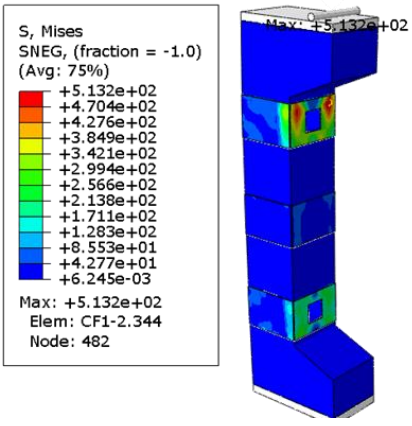

(5-34- d) von-misses stress at failure stage

Fig. (5-34) Comparison between the experimental and FE for (EF- Squ -O).

(5-35-a) failure mode of column (EF-Cir-O) in laboratory

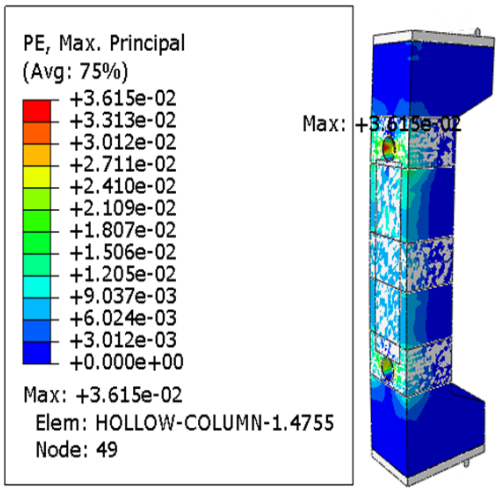

(5-35-b) failure mode of column (EF-Cir-O) in FE

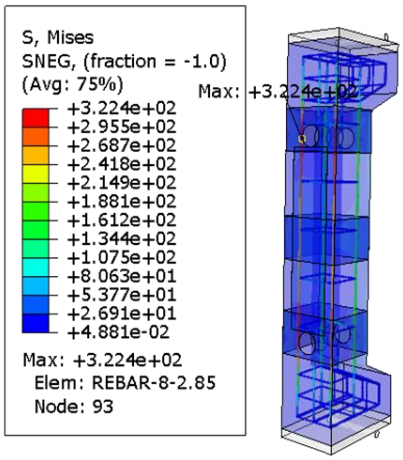

(5-35-c) von-misses stress at max. elastic

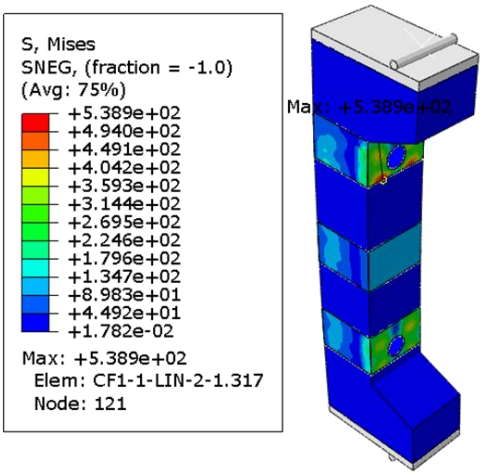

(5-35- d) von-misses stress at failure stage

Fig. (5-35) Comparison between the experimental and FE for (EF- Cir -O).

From the previous figures above the specimens with strengthening by CFRP the maximum. von-misses stress obtained from the case (EF-Cir-O) with value reached to the ($5.389x10^2$) MPa, while the sample (EF-Squ-O) has the stress equal to the ($5.132x10^2$) MPa.

(5-36-a) failure mode of column (CF-Squ-O) in laboratory

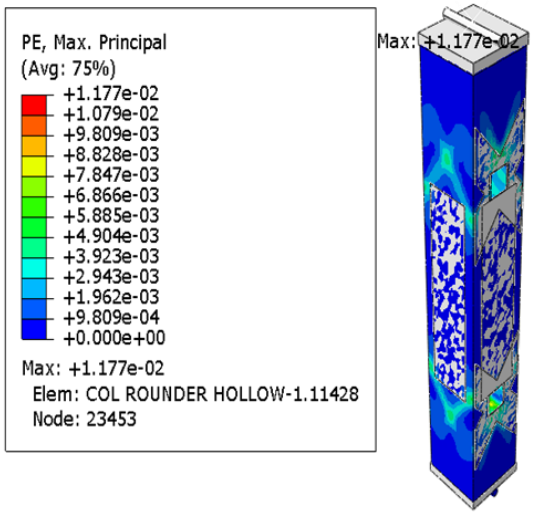

(5-36-b) failure mode of column (CF-Squ-O) in FE

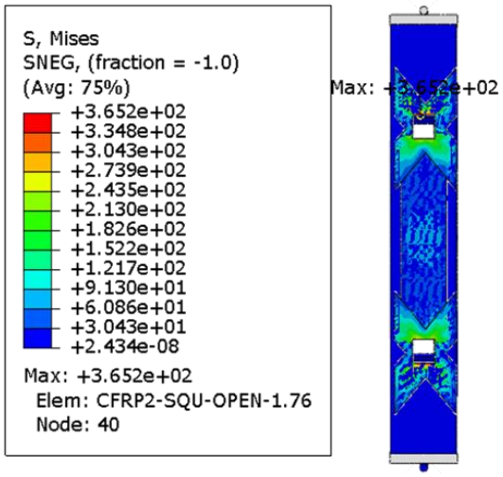

(5-36-c) von-misses stress at max. elastic

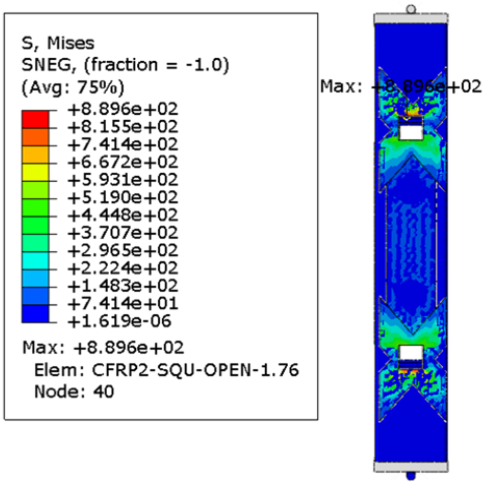

(5-36- d) von-misses stress at failure stage

Fig. (5-36) Comparison between the experimental and FE for (CF- Squ -O).

From the figures (5-31), and for the concentric loading the specimen (CC-CO-Squ-O) has the maximum. von-misses stress equal to the ($3.99x10^2$) MPa. and for the strengthening sample (C.F-Squ-O) the stresses rise to the ($8.89x10^2$) as the fig (5-36). Also for this case the contribution of the CFRP starting from the elastic stage as the fig (5-36-c,d).

All results conducted from the ABAQUS and related to the side opening were tabulated in the table (5-5).

Table (5-5) ultimate load comparison between the experimental and the FE for concrete columns with side openings

Model ID	P_{ult_lab} (kN)	P_{ult_FE} (kN)	$(\frac{P_{ult_{FE}} - P_{ult\_lab}}{P_{ult\_lab}}) * 100$
CC-CO-Squ-O	430	441.2	2.6
CC-CO-Cir-O	555	580.4	4.5
CC-ECC-Squ-O	64.8	70.1	8.1
CC-ECC-Cir-O	65.8	68.5	4.1
C.F-Squ-O	661	557.47	15.6
C.F-Cir-O	560.3	659.71	17.7
E.F-Squ-O	75.38	80.49	6.7
E.F-Cir-O	80.1	85.66	6.9
Average			8.27

5.6 Specimens strengthening by TRM and under loaded concentrically

in this part study the compression between the specimens with strengthening by TRM in experimental and FEM, under the effect of two types of load concentric and eccentric loading.

5.6.1 Load-displacement curves for specimens strengthening by TRM and under loaded concentrically

Figure (5-37) to Figure (5-44) compared the load-displacement curve for columns got from the numerical analysis and together with the experimental results For model specimens under concentric loading. A good agreement was obtained between the experimental and FEA results. Also comparing between the finite element and laboratory work for failure location.

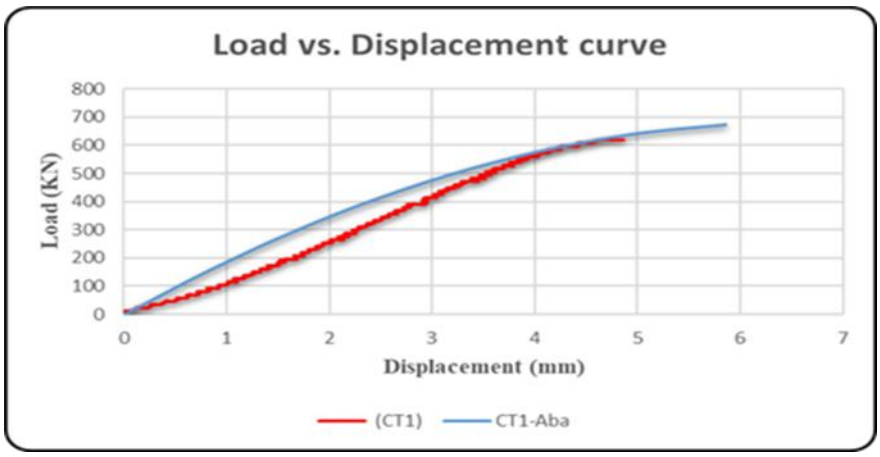

Fig. (5-37) Experimental and Numerical Load vs. Displacement curve for (CT1).

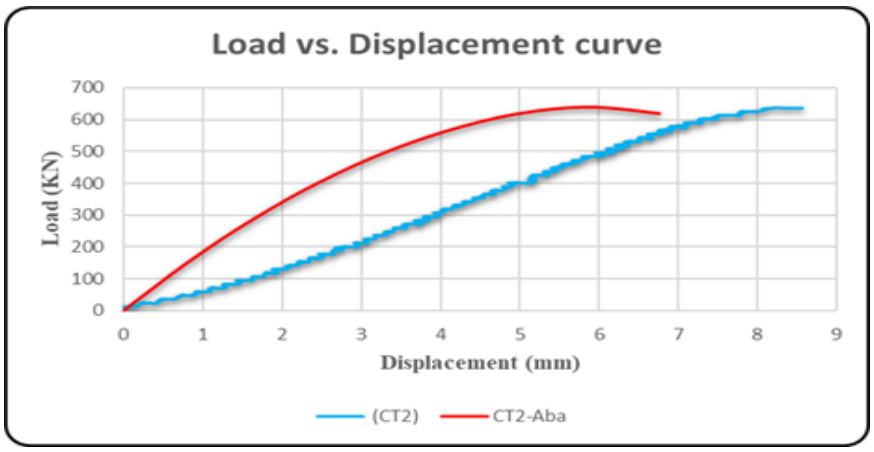

Fig. (5-38) Experimental and Numerical Load vs. Displacement curve for (CT2).

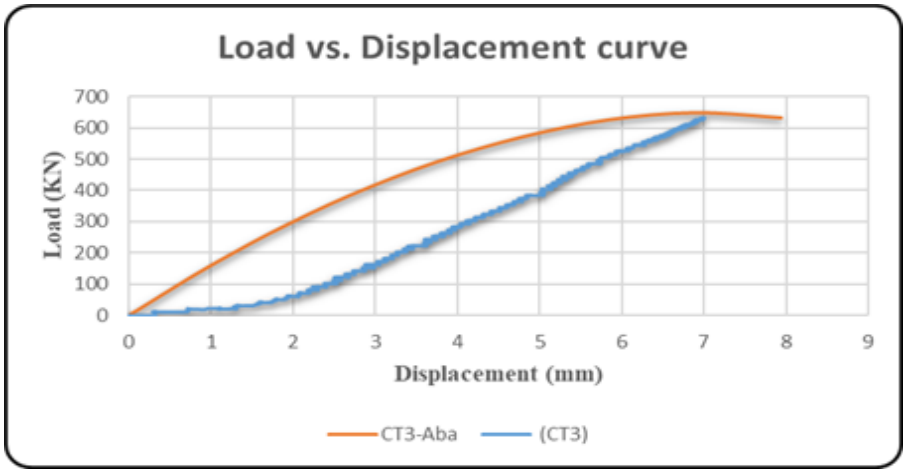

Fig. (5-39) Experimental and Numerical Load vs. Displacement curve for (CT3).

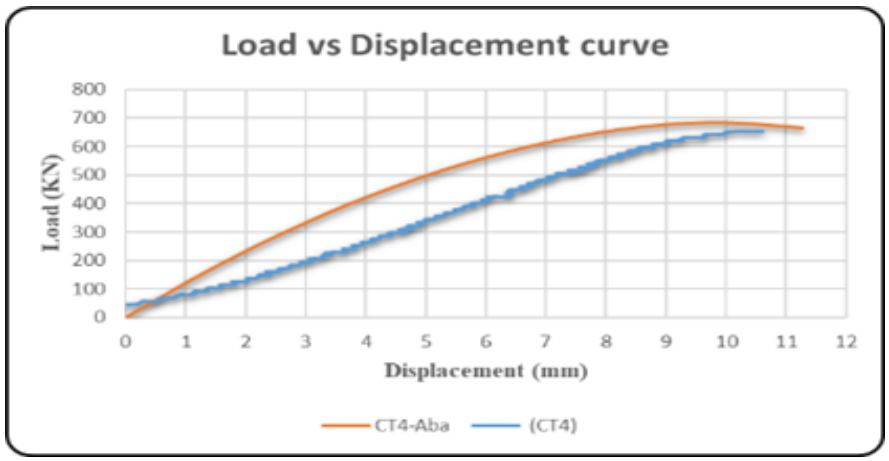

Fig. (5-40) Experimental and Numerical Load vs. Displacement curve for (CT4).

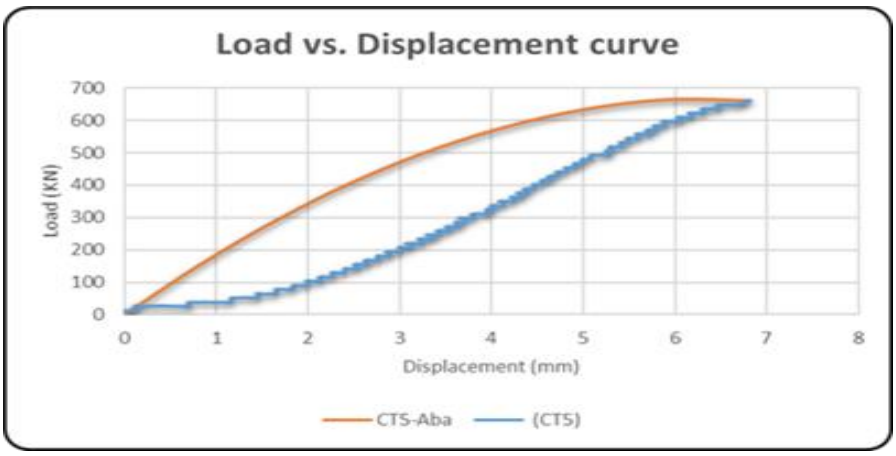

Fig. (5-41) Experimental and Numerical Load vs. Displacement curve for (CT5).

5.6.2 Failure mode and von-misses stresses for strengthening specimens by TRM and under loaded concentrically

(5-42-a) failure mode of column (CT1) in laboratory

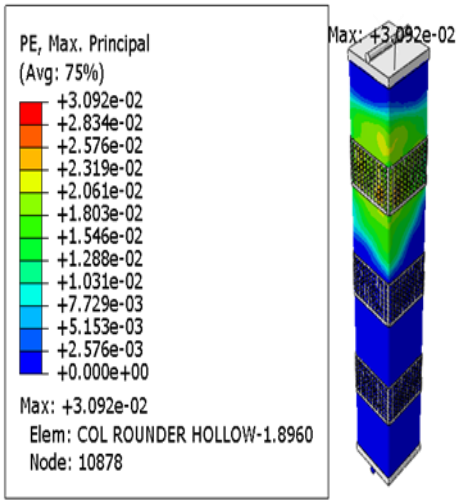

(5-42-b) failure mode of column (CT1) in FE

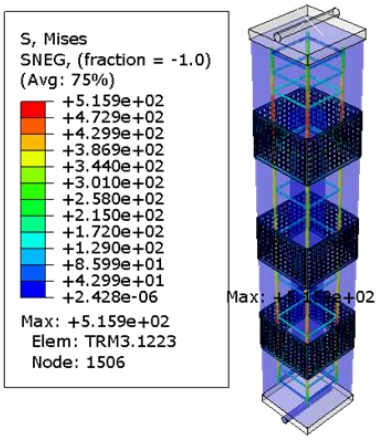

(5-42-c) von-misses stress at max. elastic stage

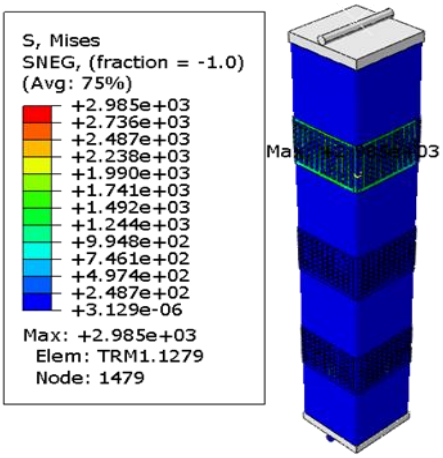

(5-42- d) von-misses stress at failure stage

Fig. (5-42) Comparison between the experimental and FE for (CT1).

(5-43-a) failure mode of column (CT3) in laboratory

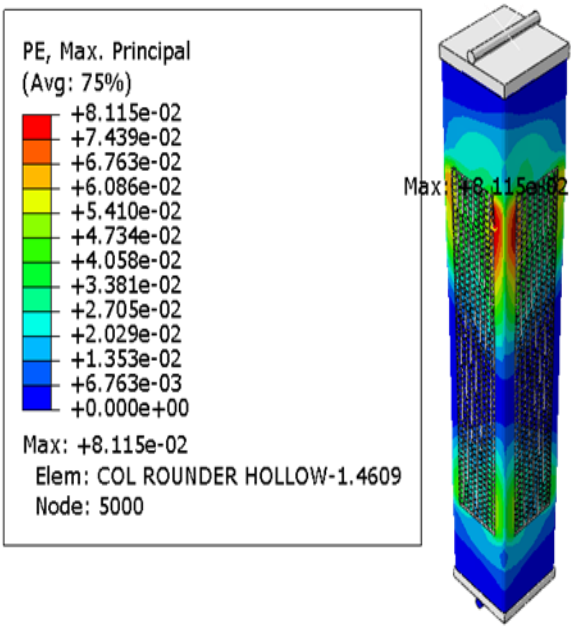

(5-43-b) failure mode of column (CT3) in FE

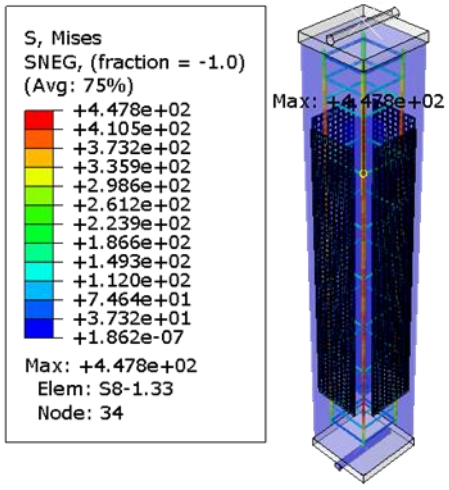

(5-43-c) von-misses stress at max. elastic stage

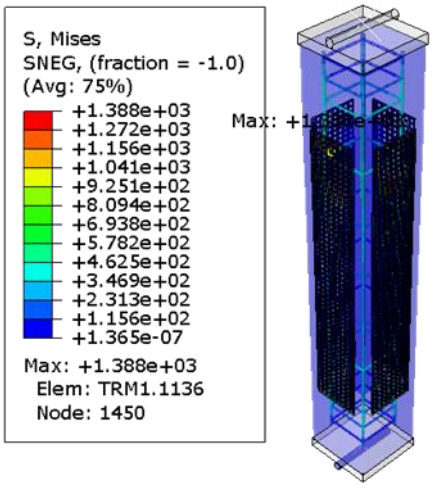

(5-43- d) von-misses stress at failure stage

Fig. (5-43) Comparison between the experimental and FE for (CT3).

(5-44-a) failure mode of column (CT5) in laboratory

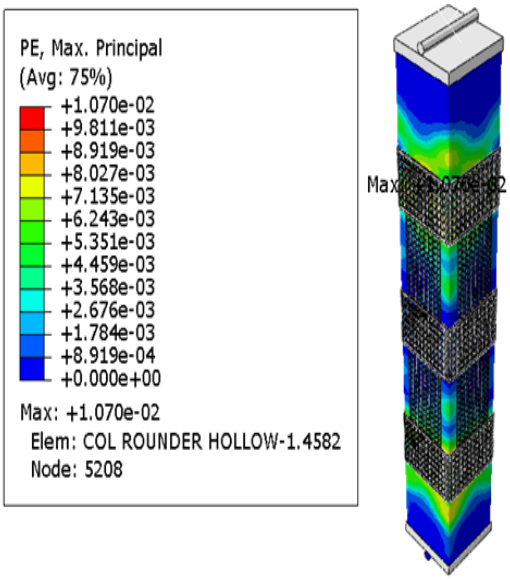

(5-44-b) failure mode of column (CT5) in FE

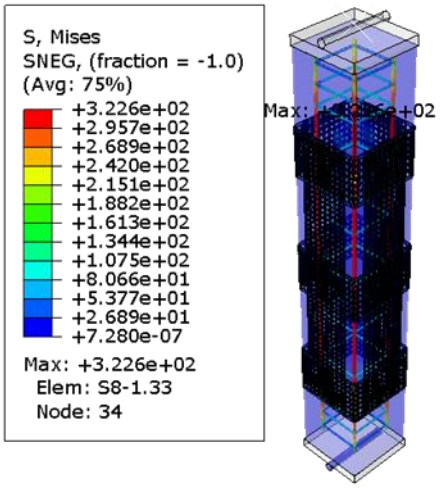

(5-44-c) von-misses stress at max.

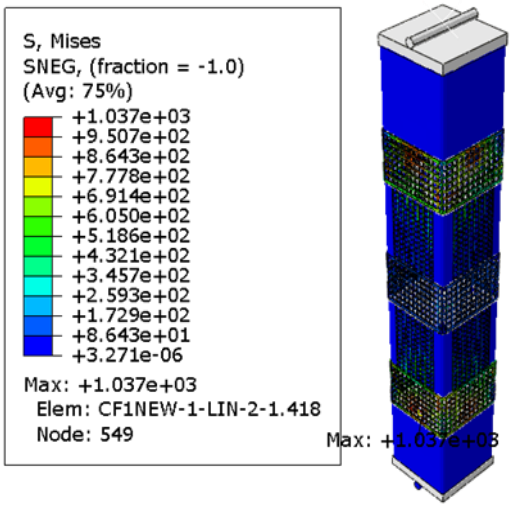

(5-44- d) von-misses stress at failure stage

Fig. (5-44) Comparison between the experimental and FE for (CT5).

From the figures (5-42) and (5-43) for the models (CT1) and (CT3), respectively, good agreement between the FE and the experimental test with the failure location. The maximum von-misses stress obtained by model (CT5) with value near to the ($1.037x10^{3}$) MPa. also the max. plastic strain (PE) reading in the (CT3) with value ($8.11x10^{-2}$).

5.7 Eccentric loading for specimens strengthening by TRM and under eccentric load

For the specimens subjected to eccentric loading and strengthening by TRM, ABAQUS utilizing to comparing between the experimental and FEM as below:

5.7.1 Load-displacement curves for specimens strengthening by TRM and under eccentric load

For model specimens, vertical displacement is measured at the position of the line load was measured at the top end of column same with experimental column and at the tension face of the column model. The load-displacement curves plot for all columns got from the numerical analysis and together with the experimental results as shown in figure (5-45) to figure (5-23). At the early stages of loading, the column models are free from any cracks and the relation between the load and the displacements is linear. With increasing of the applied load, the first crack is happening, the slope of the load-displacement curve decrease, the relation between the load and the displacements convert to nonlinear and it continues until the buckling is happen.

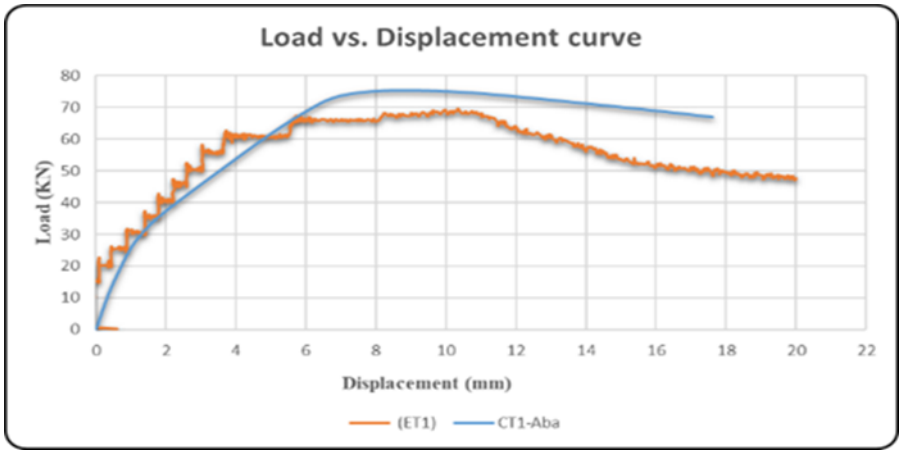

Fig. (5-45) Experimental and Numerical Load vs. Displacement curve for (ET1).

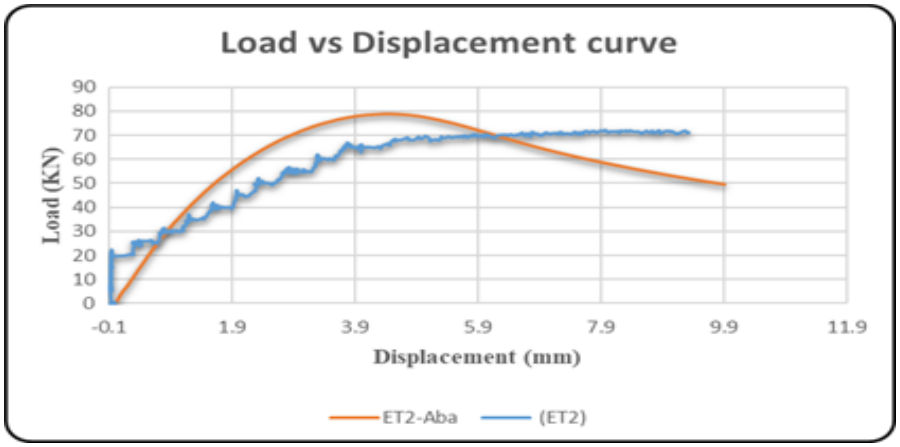

Fig. (5-46) Experimental and Numerical Load vs. Displacement curve for (ET2).

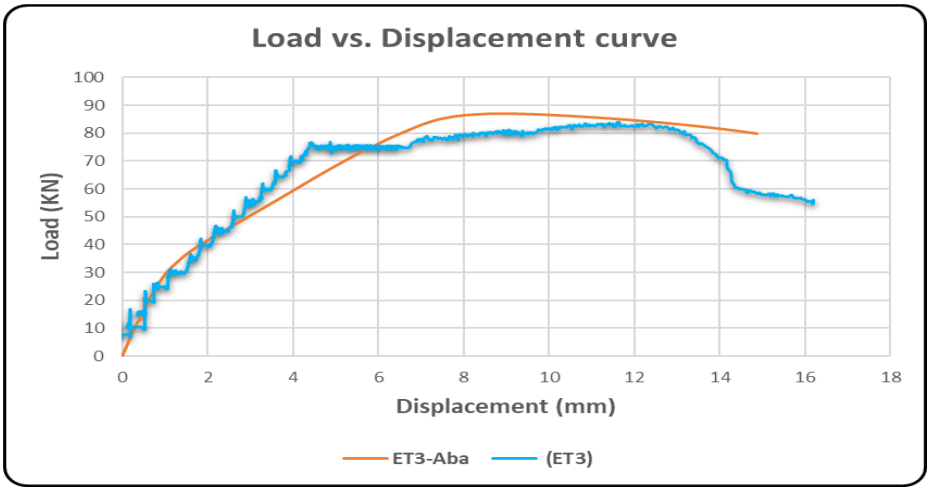

Fig. (5-47) Experimental and Numerical Load vs. Displacement curve for (ET3).

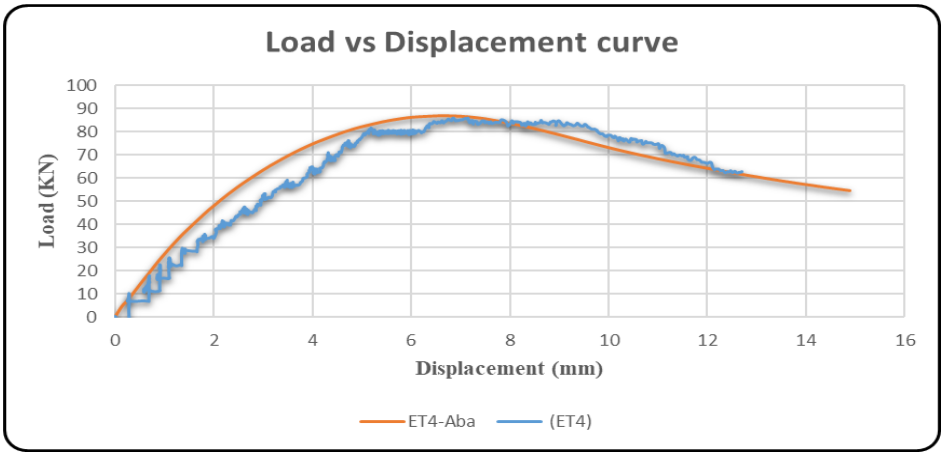

Fig. (5-48) Experimental and Numerical Load vs. Displacement curve for (ET4).

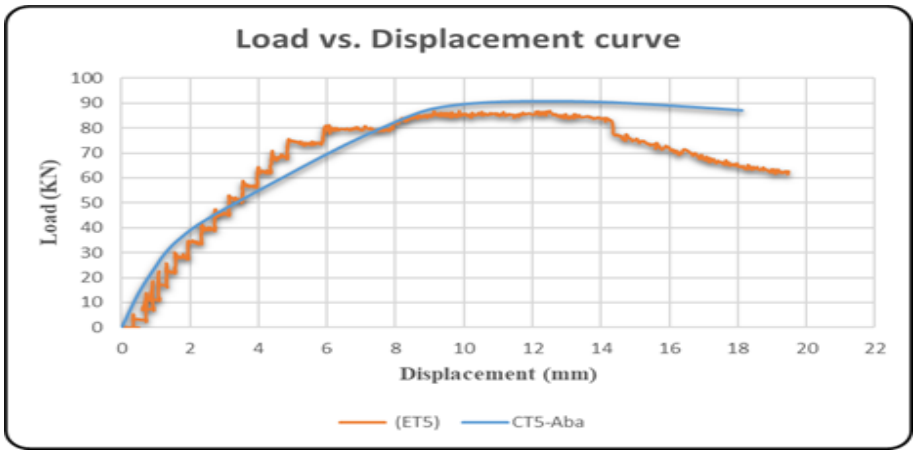

Fig. (5-49) Experimental and Numerical Load vs. Displacement curve for (ET5).

5.7.2 Failure mode and von-misses stresses for strengthening specimens by TRM and under loaded eccentrically

(5-50-a) failure mode of column (ET1) in laboratory

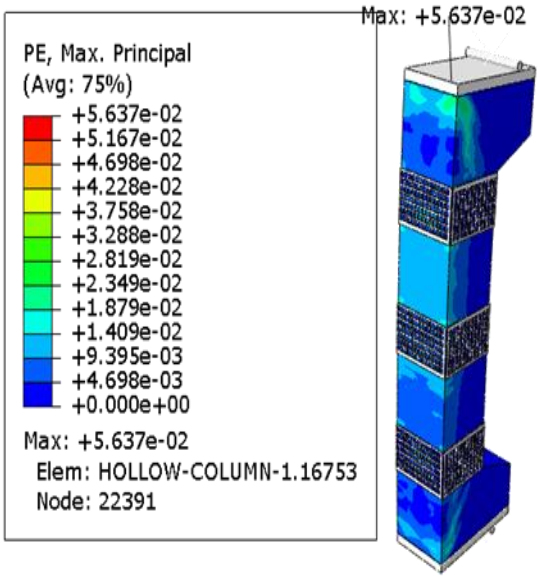

(5-50-b) failure mode of column (ET1) in FE

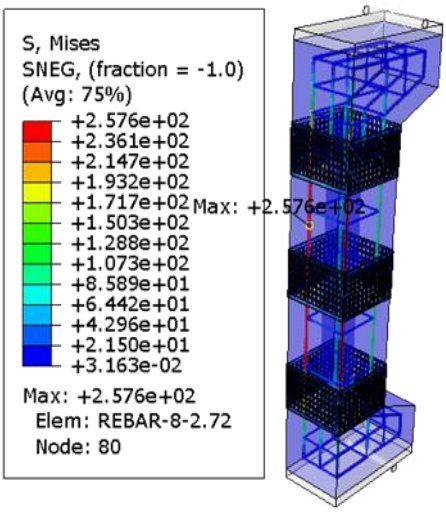

(5-50-c) von-misses stress at max. elastic

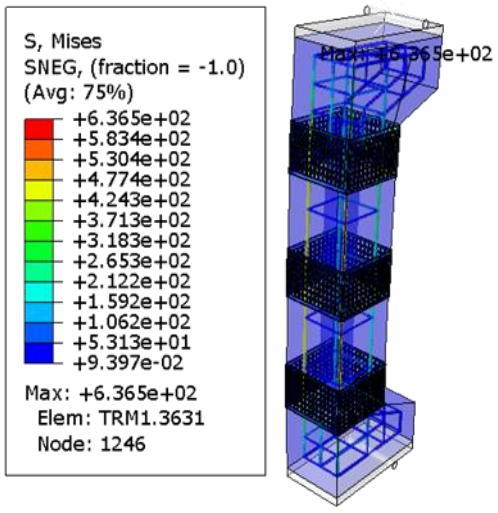

(5-50- d) von-misses stress at failure stage

Fig. (5-50) Comparison between the experimental and FE for (ET1).

(5-51-a) failure mode of column (ET3) in laboratory

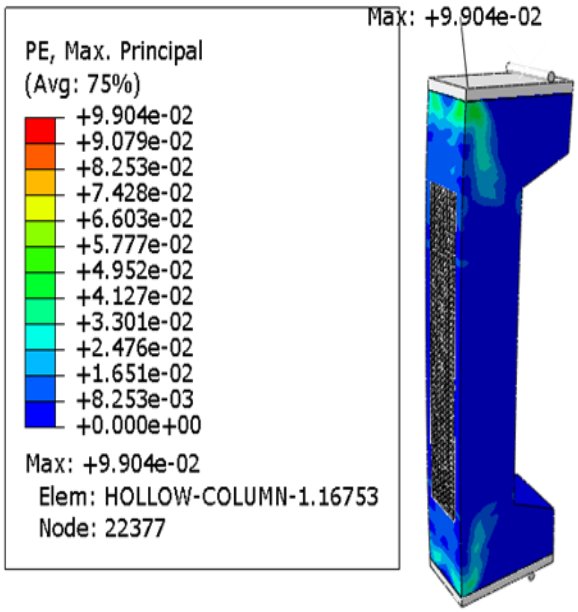

(5-51-b) failure mode of column (ET3) in FE

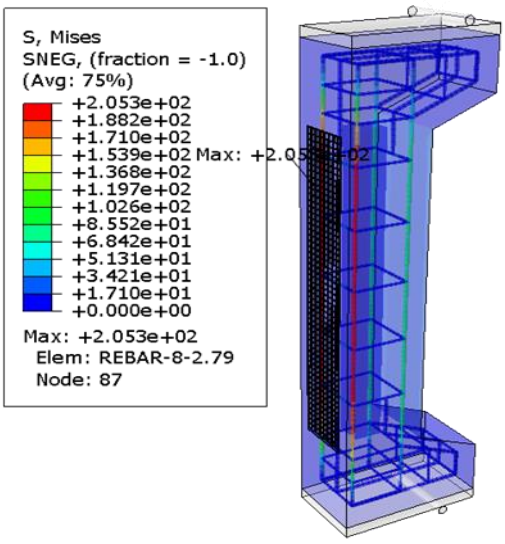

(5-51-c) von-misses stress at max. elastic

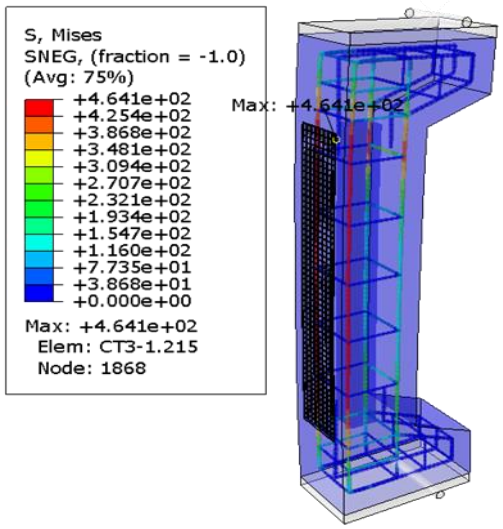

(5-51- d) von-misses stress at failure stage

Fig. (5-51) Comparison between the experimental and FE for (ET3).

(5-52-a) failure mode of column (ET5) in laboratory

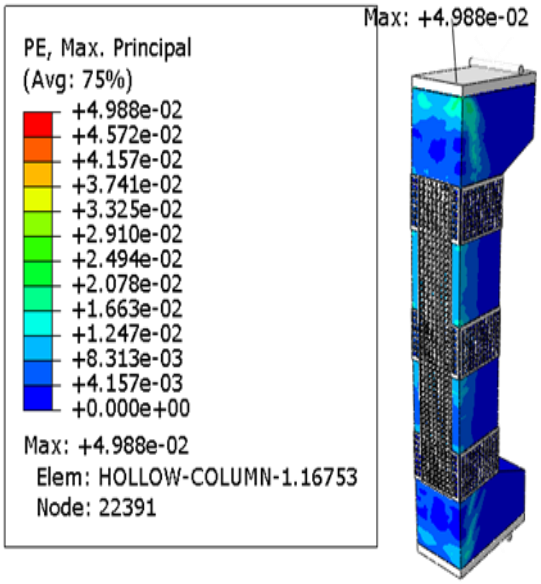

(5-52-b) failure mode of column (ET5) in FE

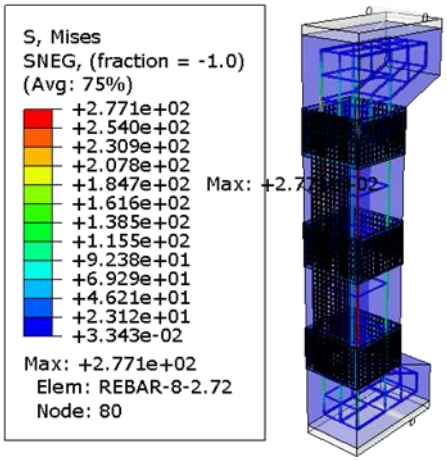

(5-52-c) von-misses stress at max. elastic

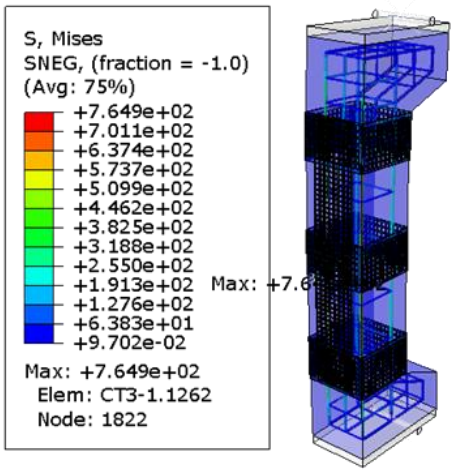

(5-52- d) von-misses stress at failure stage

Fig. (5-52) Comparison between the experimental and FE for (ET5).

From the figures (5-51-b) the plastic strain reach to the ($9.9x10^{-2}$) for model (ET3). and the maximum von-misses stresses equal to the ($7.64x10^{2}$) MPa from the (ET5) as the figure(5-52-d).

Chapter 6: Conclusions

The experimental results of this study have shown that the concentric and eccentric loading and deformation capacities of hollow RC columns are increased considerably after strengthening with partial confinement by using carbon fibre polymer (CFRP) or textile reinforce mortar (TRM).

however, the effect on the axial load capacity diminishes as the loading eccentricity increases. Prediction of the behavior of strengthening hollow RC columns were proven quite difficult as the tests in laboratory on the specimen columns exhibited many unexpected factors such as the failure location as generate the plastic hinge in the top or bottom when the load applied concentrically or formed two parts when specimens subjected two eccentric loading by creation the tension face and compression zone, for two cases of strengthening (CFRP or TRM) ,this differs due to the nonhomogeneity in the concrete.

The experimental and the modelling study were aimed to demonstrate and predict the behavior of the isolated hollow RC columns with pin ended connections with a confinement by CFRP or TRM materials. In reality many unforeseen factors such as the non-homogeneous nature of the concrete, existence of weak planes throughout the volume of the column specimens, uneven confinement of the FRP due to workmanship errors, possible errors in applying the boundary conditions at two ends. In spite of all the factors mentioned above, the specimens under concentric loading with CFRP or TRM confinement, failed with more dangerous during the test where the failure has the brittle behavior in the (strengthening or unstrengthening) cases.

From the above, the work is divided to two groups, first group have the specimens subjected to concentric loading and another group the specimens subjected to eccentric loading.

First group composed the (12) cases, these cases have the two cases without strengthening (solid or hollow) casting as the reference specimens with the labels (CC-CO-S) and (CC-CO-H). And five specimens strengthening partially by CFRP with labels (CF1, CF2, CF3, CF4, and CF5) and remain five strengthening with TRM as the (CT1, CT2, CT3, CT4, and CT5). the second group have the same details for the first group but the load carried eccentrically and the references specimens not containing the solid column, use two cases of hollow column with two eccentricity distance as (0.6h and 0.9h) with labels as (CC-ECC-0.6h) and (CC-ECC-0.9h). After complete the test of control specimens and analysis the results, the eccentricity fixed for the strengthening cases with (0.9h) about (135) mm from the center of column. However, for the specimens strengthening by CFRP the labels (EF1, EF2, EF3, EF4, and EF5).and when the apply the TRM have the labels (ET1, ET2, ET3, ET4, and ET5).

And also created the eight specimens with two type of side opening (circular or square) at the ends of column. divided the specimens into two groups. The first group has four specimens with control columns without strengthening and the side openings have the labels (CC-CON-Cir-O) for the case subjected to concentric loading with circular side openings at both edges, (CC-CON-Squ-O) for the case subjected to concentric loading and square opening at the top and bottom, (CC-ECC-Cir-O) for the case subjected to eccentric loading and circular open at the top and bottom , (CC-ECC-Squ-O) for the case subjected to eccentric loading and square open at the top and bottom. And remain group have the specimens with strengthening by CFRP with the same configuration in the (CF4) for specimens subjected concentric loading with labels (CF-Cir-O) and (CF-Squ-O) for the specimen with circular side opening and square side opening, respectively. And another specimens subjected to eccentric loading have the strengthening configuration with in (EF5) and has the labels (EF-Cir-O) and (EF-Squ-O) for the specimen with circular side opening and square side opening, respectively

The selection of the cases in CFRP configuration same with (CF4, EF5) in the specimens with side opening depending on the results come out from the first stage of specimens.

The structural performance of each model was investigated by evaluating the ultimate loading capacity, curves of load vs. displacement, curve of load vs. strain, stress vs. strain curves, ductility, and failure mode. This chapter offers conclusions that based on the results of the experimental program and the numerical study along with suggestions for future works.

6.1 Specimens under Concentric Loading

Study the behavior of unstocky concrete column, confining with partially CFRP or TRM laminates with (5) different configurations. (12) specimens exposed to concentric loading were tested. Deboning between the layers of CFRP confinement and the concrete column was detected by clicking noises in RC columns confined by CFRP composites prior to their final failure. However, they were not abrupt. For the TRM the mortar make work as the covering for the specimen.

6.1.1 Specimens with Concentric Loading with CFRP

1- The max. compressive strength obtained from (CF4) with an increase of about (22.8) % compared with (CC-CO-H).This specimen (CF4) have the (four vertical) CFRP laminate on each column side and (2X-shape) of CFRP at the top and bottom.

2-The failure position changed from the bottom as in the reference specimens(CC-CO-H) and (CC-CO-S), to the top end of the column (CF1, CF2, CF4, and CF5), due to the development of the plastic hinge near the hollow part, except the (CF3) have the same behavior as the reference specimens. This specimen has this response maybe because it did not have the (hoop or X) shape as the other specimen.

3-According to the ductility, the specimen (CF3) with four vertical CFRP laminates on each column side has a good value of ductility equal to (1.9).

4-The two specimens (CF4 and CF5) have a good load capacity (749.2) and (689.5) kN, respectively, but the ductility is not enhanced.

5- (CF1) have a concrete strain (0.0029), and the specimens (CF4 and CF5) have (0.0017and 0.001) respectively.

6- The drop in concrete strain and ductility obtained by (SGC) for the two specimens (CF4 and CF5) owing to partial confinement by CFRP. Furthermore, the failure of the interior hollow section of the concrete column might explain the problem.

•The results showed changing behavior and the failure position between the control column and the strengthening specimens.

•Also, the strengthening with the partially confining of (CFRP) has a good performance for the compressive capacity and the ductility.

• The CFRP increased the confinement of the column and then delayed the failure of the specimen .in other words, it changed the failure in the column from the brittle failure (sudden failure) to the semi-brittle failure.

6.1.2 Specimens with Concentric Loading with TRM:-

1- The specimen with the case (CT5) has the max. value of compressive strength about (662) kN and the increase about to the (8.5) % compared with the control specimen (CC-CO-H) have the compressive strength about to the (610) kN. Case (CT5) have partially TRM strengthening and composed from (1) vertical segments on each face of the column and the confining by (3) hoop segments at the top, middle, and bottom, this increase in the compressive stress occurred in the case (CT5) due to confinement effect of the confinement of by TRM.

2- According to the ductility, the max. Value (1.3) obtained from the case (CT4), where this case has the partially confining by TRM with (1) vertical segments at each face and (2X) shape at the top and bottom laminates.
3- For deals with (stress-strain) curve the max. stress value reaches to the (29.4) MPa from the case (CT5) with increase near to the (2) % comparing with the unconfined specimen (CC-CO-H), have the stress about (28.8) MPa.
4- The max. Strain occurred with the case (CT3) have the value (0.0015) obtained from the (SGC), this case has the TRM configuration as the (1) vertical TRM segments on each face of the column, the increase in concrete deformation for this case (CT3) about the (8.7) % compared with the control specimen (CC-CO-H) have the strain (0.00138).
5- The sound at the failure in the case (CC-CO-H) is more than the case (CC-CO-S). due to dispersed energy formed in the hollow inside the column.
6- The specimens partially coated by TRM have a sound failure less than the control column, caused by the mortar used to block the specimen and covering, so the TRM is the shell around the column. Therefore, the amount of splitting concrete is small when it fails. This situation happened with cases (CT4, CT5).
7- The specimens (CT1 and CT3) mechanism of failure occurred due to buckling the main rebar at the top and then concrete damaged, but when increased the confinement as the (CT4 and CT5) the behavior and failure location changed, also the specimen (CT2) has the failure location same the specimens (CT4, CT5). However, it contains a large amount of fragmented concrete. This difference in behavior between specimens is due to different TRM configurations and locations.

6.2 Specimens under Eccentric Loading

Experimental measurements of eccentric static loads and their distribution over these columns are being studied. Unstocky concrete column behavior with partial composite laminates CFRP and TRM confined in five forms is examined, were tested (12) specimens subjected to eccentric loading. Moreover, the following conclusions can be drawn:

6.2.1 Specimens with Eccentric Loading with CFRP

1- The failure mode reaches the ductile failure for the specimen without being confined by CFRP (CC-ECC-H). The horizontal cracks grow up at the middle height of the hollow column on the tension face, and by increasing load, the horizontal crack width and new cracks will be increasing. Also, the concrete at the compression side will be pressing and damaged. The specimen with no full confinements (EF) gives the impression of failure more ductility than the (CC-ECC-H).

2- Concerning compressive strength, the case (EF5) has the value (94.8) kN, with increase about (39.4) % compared with the reference specimen (CC-ECC-H). This case has the vertical laminate of CFRP on the tension side and three hoops of CFRP laminate.

3- All failures mode with eccentric load has the behavior of horizontal crack on the tension face of the intermediate length of the specimen, with smash concrete for the opposite side, except the specimen (EF5) these tension cracks did not appear.

3- The ductility reached the max. value (5.4) in the case (EF2), also this case has the max axial and lateral displacement (21.44,28) mm, respectively. This case has the (2X-shape) at the top and bottom.

4- The stress vs. strain curve has the same behavior for all cases in the elastic stage.

5- Strain in compression side, the significant value obtained from the case (EF2) (0.0036), also have the max value in the tension side (-0.0199). This tension strain value is due to the developed horizontal crack at the (SGC) position.

7- For this study, the configuration in the specimen (EF5) has a good performance concerning the strength capacity.

8- The specimens with vertical laminate in the tension side did not have concrete damage on the compression side as (EF3and EF5)

6.2.2 Specimens with Eccentric Loading with TRM: -

This group contain five configurations of the external partials strengthening with use TRM, the following conclusions can be drawn:

1-With respect to compressive strength the max. load capacity equal (86.5) kN for the (ET5) with increase in compressive about (27.2) comparing with control specimen(CC-ECC-H).

2- The cracks formed on the side subjected to tensile stress, as well as the part exposed to pressure, as is the case in specimens reinforced with CFRP, but it cannot be relied on more clearly and that is because the mortar blocks the view.

3- The ductility reached the max. Value (4.8) in the case (ET1), also this case has the max Vertical and lateral displacement (20,19.7) mm, respectively.

4- The max. reading obtained from SGC equal to (0.005) with compression strain for specimen (ET4), and for tensile strain all specimens more than the CFRP specimens, also mortar maybe effect on this reading.

• The results showed the change of the behavior for the failure position between the control column and the strengthening specimens.

• Also, the strengthening with the partially confining of (CFRP) has a good performance concerning the compressive capacity and the ductility.

6.3 Specimens with side opening

6.3.1 Specimens with side opening and under concentric loading

For the specimens without strengthening the results showed: -

1- when the specimens subjected to concentric loading the load decreasing about (-9) % for specimen with the circular side opening. And the percentage of decreasing rising to the (-29.5) % for specimens with square side opening. These decreasing in compression load compared with the control specimen (CC-CO-H), this is due to the reducing in the concrete part.

2- the value of the load capacity in specimen with circular hole more than that with square opening, this due to the effect of the Sharpe edge in the square side open.

3- The failure occurred in the bottom when the specimen has the circular opening and the plastic hinge generated in the area of the hole. but with the specimen has the square side openings the plastic hinge formed near the square hole at the top end.

4- For this cases the ductility calculated depended on the figures of (load vs. strain curve) obtained the SGC.So the max value obtained from the specimen with circular side openings.

5- The strain in concrete measured by using (SGC) marginal change comparing with the control specimens for the specimen has the circular or square side open.

6.3.2 Specimens with side opening and under concentric loading

For the specimens strengthening the outcomes showed

1- Partial strengthening using CFRP gives a percentage increase in compressive capacity up to limits (19.1 and 30.3) %, for specimens (CF-CIR-O and CF-SQU-O) comparing with (CC-CO-CIR-O and CC-CO-SQU-O), respectively.

2- By generated the plastic hinge at the top for the two models the failure occurred in the area of the side hole. and the main rebar bent at this zone (side open).

3- The ductility computed depending on the (stress- strain) curves for specimens (CF-Cir-O) and (CF-Squ-O), The circular side opening has the ductility with value about (2.1) and the specimen with square side opening has the ductility equal to the (1.64).

6.3.3 Specimens with side opening and under eccentric loading

1- When the specimen subjected to eccentric loading and also has the side opening, the capacity of the load decreased with marginal value due to the effect of presence side opening for both cases circular or squared, this is because the eccentric loading applied perpendicular on the axes of the side opening.

2- the increased in load capacity obtained from the case (EF-Cir-O) equal to the (21.73) % comparing with (CC-ECC-Cir-O), and the increases equal to the (16.32) % in specimen (EF-Squ-O) with respect to (CC-ECC-Squ-O).

3- The failure occurred by developed the tension cracks near the side opening at the top of column. when the eccentric loading increased the horizontal cracks

generated at the inner face of the side opening for the both cases circular or square opening.

4- Max. value for concrete strain gauge (SGC) obtained from the case (EF-Cir-O) with the value reached to (0.0085), this value for the SGC near the circular opening at the top edge.
5- The crack width reduced due to effect of the CFRP for the (EF-Cir-O) or (EF-Squ-O).

6.4 Conclusions from Finite Element Analysis

1- In terms of compressive strength, load displacement curves, and failure mechanism, the model built by the ABAQUS software predicts a reasonable simulation for the true behavior of hollow concrete columns with an acceptable level of accuracy.
2- The three-dimensional finite element model by ABAQUS/Standard was capable to simulate the structural behavior of hollow concrete column strengthened parially by CFRP or TRM and subjected to concentric and eccentric loading with an average variation ratio equal to (5.5)% and (10.46)% respectivaly for the ultimate loading capacity.the average of side opening equal to (8.27)% for the two models simulation and the two types of loadings.

3- As a consequence, the suggested model is dependable and can be implemented with confidence, as shown by the high agreement between the analytical findings and the experimental values.
4- In addition, the cohesive model demonstrated a high degree of accuracy in simulating the binding behavior between the CFRP sheet and the TRM and concrete substrate. It was determined that the failure mechanism and the estimated ultimate load were the most closely linked with the testing outcomes.

5- Simulation for the models with side opening has a good result in terms of failure position, by generated internal cracks at the hole (circular or square).

6.5 Possible Areas for Future Research

The possible future research areas are suggested as follows:

1. The effect of column length can be investigated by testing taller columns, as the model proposed already gives the predicted loading lines for any given length.

2. The effect of hollow core diameter can be investigated in larger cross-sections.

3. A similar study to this study can be done on the rectangular cross-sectioned hollow RC columns to see the effects of the same variables used in this study.

4. For the textile mortar (TRM) apply this technology in the same cross-section of the hollow column with rehabilitation column.

5. For the side opening study the effect of the repeated load on the two cases.

APPENDIX-A

A-1 Design of Concrete Columns

According to the ACI-Code 318-18, the design calculations are induced, as follows:

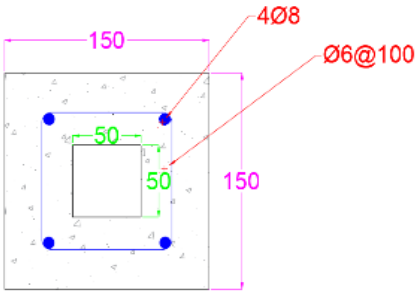

- **Longitudinal Reinforcement**

A_g= (150*150) -(50*50) =20000 mm^2

$A_{st}=4*\frac{\pi}{4}*(8)^2=201.06\ mm^2$

$$\rho = \frac{A_{st}}{A_g} = \frac{201.06}{20000} = 0.010$$

$0.01 \leq \rho \leq 0.08$ (ok) *ACI Code 10.9.1 specifies that reinforcement ratio between (1-8)%*

- **Clear Spacing of Longitudinal Reinforcement** *ACI Code 7.6.3*

The greatest of $\begin{Bmatrix} 40\ mm \\ 1.5 * d_b \\ \frac{4}{3} * d_{agg.} \end{Bmatrix}$= 40 mm

- **Length development**

Ld=$\left(\frac{fy\ \psi_t\ \psi_e}{2.1\ \lambda\ \sqrt{f_c'}}\right) d_b$

Ld=$\left(\frac{500.7*1*1}{2.1\ *1*\ \sqrt{30}}\right) * 8 = 348mm$

- **Lap Splice**

the greatest of $\begin{Bmatrix} 300\ mm \\ 1.30 * Ld \end{Bmatrix}$

$=\begin{Bmatrix} 300\ mm \\ 1.30 * 348 \end{Bmatrix}$= 453 mm

- **Max Spacing of Transverse Reinforcement** *ACI Code 7.10.5.2*

Max Spacing $\begin{Bmatrix} 16\ d_b \\ 48\ d_{tie} \\ least\ dimension \end{Bmatrix} = 125\ mm$ use 100 mm, and 50 mm at top and bottom. use A_{st}= (0.01×20000) =200 mm^2 Pu= [0.85$fc'(Ag-A_{st})$ +$fyAst$]

- Pu= [0.85×30× (20000−200) +500.7×200] =605 kN. load in the experimental test reach to the (610) KN for the control specimen.

APPENDIX-B

APPENDIX-B MATERIAL PROPERTIES

B.1 Cement

Table B-1 Chemical composition and main compounds of cement.

No.	Chemical Composition		% by (weight)	Limits of IQS No. 5/1984
1	Lime	CaO	62.79	---
2	Silica	SiO_2	20.58	---
3	Alumina	Al_2O_3	5.6	---
4	Iron Oxide	Fe_2O_3	3.28	---
5	Magnesia	MgO	1.77	≤ 5
6	Sulfate trioxide	SO_3	2.35	< 2.8 if C3A > 5
7	Free lime	f.CaO	0.9	---
8	Loss on ignition	L.O.I	1.94	≤4
9	Insoluble residue	I.R	0.86	≤1.5
10	Lime saturation factor	L.S.F	0.9	(0.66 – 1.02)
Compound composition				
11	Tri-calcium aluminates	C_3A	9.4	---
12	Tri-calcium silicate	C_3S	50.55	---
13	Di-calcium silicate	C_2S	23.22	---
14	Tetra-calcium aluminates ferrite	C_4AF	10.5	---
Tested by the factory.				

Table B-2 Mechanical composition of cement.

Mechanical Properties	Test Result	Limits of IQS No. 5/1984
Fineness (m^2/kg)	395	> 230
Initial Setting time (min)	150	> 45
Final Setting time (hr)	3:27	< 10
Compressive strength (MPa)		
2 days	25.3	> 15
28 days	43.1	> 23
Tested by the factory.		

B.2 Fine Aggregate

Table B-3 Grading of the fine sand.

Sieve Size (mm)	Cumulative Passing %	Limits of IQS No.45/1984, Zone 2
4.75	99	90-100
2.36	83	75-100
1.18	70	55-90
0.6	58	35-59
0.3	26	8-30
0.15	5	0-10
Tested by the Laboratories of the Engineering College/ University of Karbala.		

Table B-4 Physical Properties of the Fine Aggregate

Physical Properties	Test Result	Limits of IQS No.45/1984
Specific gravity	***	-
Fineness modulus	***	-
Sulfate content SO_3	0.1%	≤0.5%
Absorption	2.1 %	5
Tested by the Laboratories of the Engineering College/ University of Karbala		

B.3 Coarse Aggregate

Table B-5 Mechanical and chemical properties of coarse aggregate.

Properties	Test Result	Limits of IQS No.45/1984
Sulfate content SO_3	0.062%	≤0.1%
Clay content	0.3%	≤ 2%
Tested by the Structural Laboratories of the Engineering College/ University of Karbala.		

Table B-6 Grading of the coarse aggregate.

Sieve Size(mm)	Passing %	
	Coarse aggregate	Limits of IQS No.45/1984 (2.36-9.5)mm
12.5	100	100
10	100	85-100
4.75	10	0-30
2.36	2	0-10
Tested by the Structural Laboratories of the Engineering College/ University of Karbala.		

Table B-7 Rebar test (8&6) mm

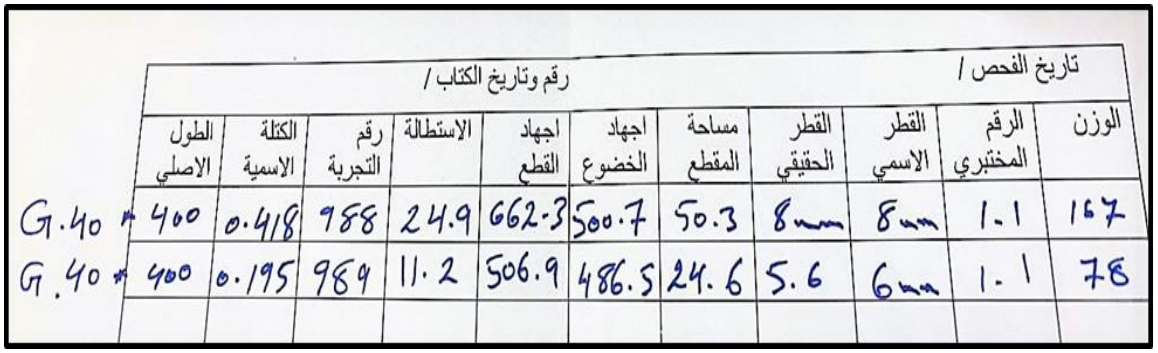

رقم وتاريخ الكتاب /									تاريخ الفحص /	
الطول الاصلي	الكتلة الاسمية	رقم التجربة	الاستطالة	اجهاد القطع	اجهاد الخضوع	مساحة المقطع	القطر الحقيقي	القطر الاسمي	الرقم المختبري	الوزن
G.40 * 400	0.418	988	24.9	662.3	500.7	50.3	8mm	8mm	1.1	167
G.40 * 400	0.195	989	11.2	506.9	486.5	24.6	5.6	6mm	1.1	78

Tested by the Mechanical Laboratories of the Engineering College/ University of Karbala.

B.4 Carbon Fiber Textile

Table B-8 Properties of carbon fiber textile (data provided by the manufacture)

Property*	**Unit**	**Value**
Mass per unit length	g/km	820
Fiber density	g/cm^3	1.82
Thickness of rovings	Mm	0.4
Width of rovings (weft)	Mm	4
Width of rovings (warp)	Mm	10*10 (double) (mm)
Fiber tensile strength	MPa	4900
Fiber elastic modulus	GPa	230
Fracture strain	Mm	2

APPENDIX-C

APPENDIX-C MATERIAL DATASHEETS

C.1 Superplasticizer (Sika Viscocrete 5930L)

Construction

Product Data Sheet
Edition 02/2016/025
Version 02
Sika® ViscoCrete® 5930-L

Sika ViscoCrete® 5930-L

High Performance Super plasticizer Concrete Admixture

Product Description

Sika ViscoCrete® 5930-L is a third generation super plasticizer for concrete and mortar. It meets the requirements for super plasticizer according to ASTM-C- 494 Types G and F and BS EN 934 part 2: 2001.

Uses:

Sika ViscoCrete® 5930-L is suitable for the production of concrete.
Sika ViscoCrete® 5930-L facilitates extreme water reduction, excellent flow ability at the same time optimal cohesion and highest self-compacting behavior.
Sika ViscoCrete® 5930-L is used for the following types of concrete:
-Precast concrete.
-Ready Mix Concretes.
-Concrete with highest water reduction (up to 30%).
-High strength concrete.
-Hot weather Concrete.
-Self compacting concrete.
-High water reduction, excellent flowability, coupled with high early strengths, have a
-positive influence on the above mentioned applications.

Advantages

Sika ViscoCrete® 5930-L acts by different mechanisms. Through surfaces adsorption and sterical separation effect on the cement particles, In parallel to the hydration process, the following properties are obtained:
-Strong self-compacting behavior. Therefore suitable for the production of self compacting concrete.
-Extremely high water reduction (resulting in high density and strengths).
-Excellent flowability (resulting in highly reduced placing - and compacting efforts)
-Increase high early strengths development.
-Improved shrinkage- and creep behavior.
-Reduced rate of carbonation of the concrete.
-Improved Water Impermeability.
Sika ViscoCrete® 5930-L does not contain chloride or other, steel corrosion promoting ingredients, It may therefore be used without any restrictions for reinforced and prestressed concrete construction.

Technical Data

Basis	Aqueous solution of modified polycarboxylate
Appearance	Brownish liquid
Density	1.1 kg/lt. ± 0.01
PH	6-8

Packaging

1000 Kg (IBC) /200Kg/20kg/5 Kg Jerry cans
Bulk Tanks packing available upon request

Storage/ Shelf Life

In unopened, undamaged original container, protected from direct sunlight and frost at temperatures between + 5 °C and + 35°C. Shelf life at least 12 months from date of production

Application

Dosage	Recommended dosage: For soft plastic concrete: 0.4 - 1 % liter by weight of cement For flowing and self-compacting concrete (S.C.C.) 1.2 - 2 % liter by weight of Cement.
Addition	Sika ViscoCrete® 5930-L is added to the gauging water or simultaneously with it Poured into the concrete mixer. For optimum utilization of the high water reduction We recommend through mixing at a minimal wet mixing time of 60 seconds. The addition of the remaining gauging water - to fine tune concrete consistency - May only be started after 2/3 of wet mixing time, to avoid surplus water in the Concrete.
Concrete Placing	With the use of Sika ViscoCrete® 5930-L concrete of highest quality is being produced. The standard rules of good concreting practice (production as well as placing) Must also be observed Sika ViscoCrete® 5930-L concrete. Fresh concrete must be cured properly.
Frozen Sika ViscoCrete® -5930L	Frozen Sika ViscoCrete® 5930-L may be used after It has been slowly thawed at room temperature and intensively mixed
Combinations	Sika ViscoCrete® 5930-L may be combined with the following Sika products: Sika Pump®. Sika Rapid®. Sika Ferrogard®-901. Sikafume®. Sika Retarder® Pre-trials are recommended if combinations with the above products are being Made. Please consult our technical service.
Important Flowing Concrete S.C.C	Sika ViscoCrete® 5930-L is also used to produce flowing and self-compacting Concrete (S.C.C.) for these, special mix designs are required, contact our Technical Service division.

Safety Instructions

Ecology	Do not dispose of into water or soil, but according to local regulations.
Transport	Non-hazardous.
Safety Precautions	In contact with skin, wash off with soap & water. In contact with eyes or mucous Membrane, rinse immediately with clean warm water and seek medical attention without delay.
Toxicity	Non-Toxic under relevant health and safety codes.

Legal notes

Sika Iraq L.L.C
Southern industrial area-Makhmour road
PO Box 33-0884
ERBIL
IRAQ

Phone 00964/7480501393
00964/662603381
info.iraq@eg.sika.com
www.sika.com

C.2 Cement Mortar (Recon HS)

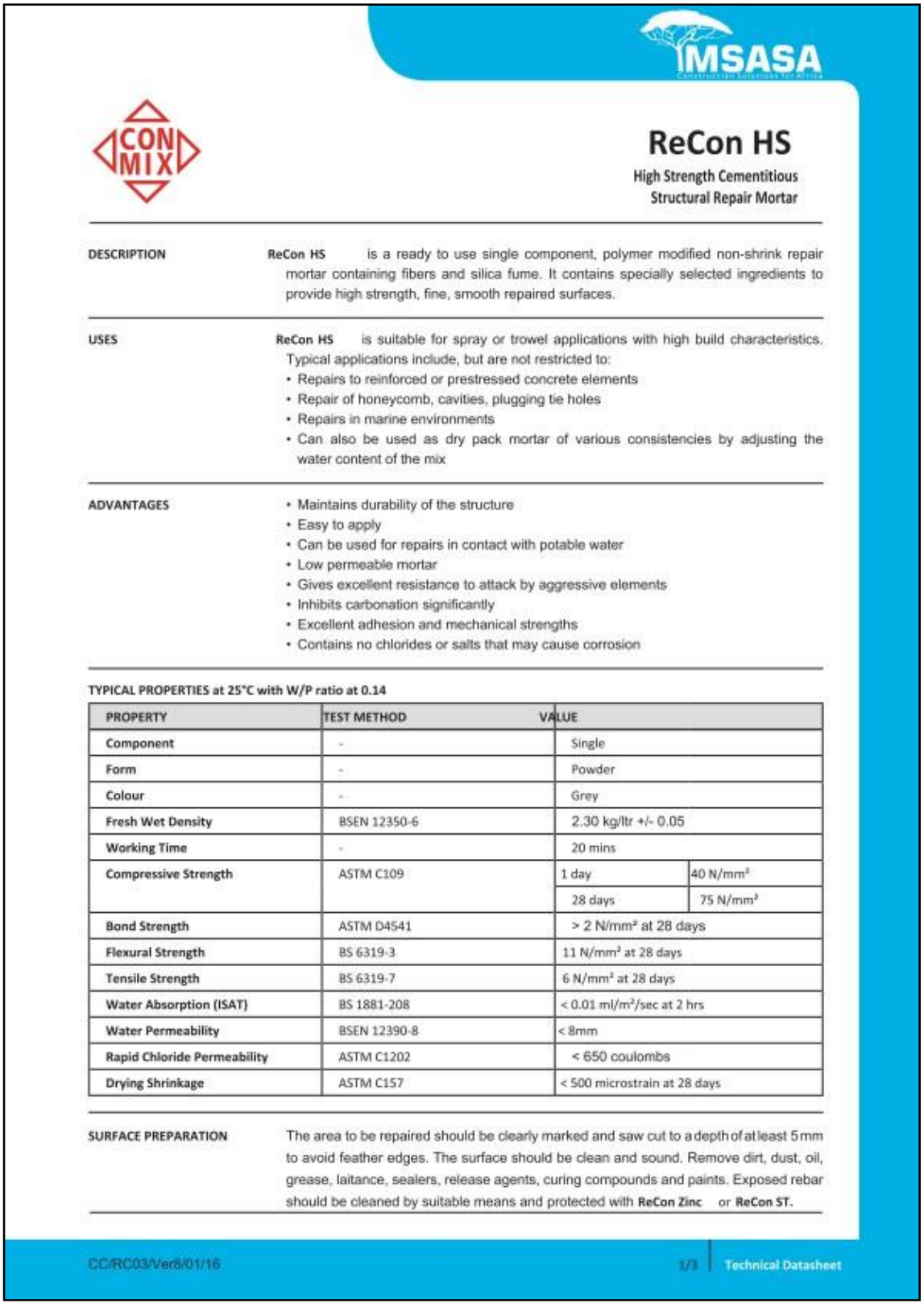

MSASA

CON MIX

ReCon HS

High Strength Cementitious Structural Repair Mortar

DESCRIPTION

ReCon HS is a ready to use single component, polymer modified non-shrink repair mortar containing fibers and silica fume. It contains specially selected ingredients to provide high strength, fine, smooth repaired surfaces.

USES

ReCon HS is suitable for spray or trowel applications with high build characteristics. Typical applications include, but are not restricted to:

- Repairs to reinforced or prestressed concrete elements
- Repair of honeycomb, cavities, plugging tie holes
- Repairs in marine environments
- Can also be used as dry pack mortar of various consistencies by adjusting the water content of the mix

ADVANTAGES

- Maintains durability of the structure
- Easy to apply
- Can be used for repairs in contact with potable water
- Low permeable mortar
- Gives excellent resistance to attack by aggressive elements
- Inhibits carbonation significantly
- Excellent adhesion and mechanical strengths
- Contains no chlorides or salts that may cause corrosion

TYPICAL PROPERTIES at 25°C with W/P ratio at 0.14

PROPERTY	TEST METHOD	VALUE	
Component	-	Single	
Form	-	Powder	
Colour	-	Grey	
Fresh Wet Density	BSEN 12350-6	2.30 kg/ltr +/- 0.05	
Working Time	-	20 mins	
Compressive Strength	ASTM C109	1 day	40 N/mm²
		28 days	75 N/mm²
Bond Strength	ASTM D4541	> 2 N/mm² at 28 days	
Flexural Strength	BS 6319-3	11 N/mm² at 28 days	
Tensile Strength	BS 6319-7	6 N/mm² at 28 days	
Water Absorption (ISAT)	BS 1881-208	< 0.01 ml/m²/sec at 2 hrs	
Water Permeability	BSEN 12390-8	< 8mm	
Rapid Chloride Permeability	ASTM C1202	< 650 coulombs	
Drying Shrinkage	ASTM C157	< 500 microstrain at 28 days	

SURFACE PREPARATION

The area to be repaired should be clearly marked and saw cut to a depth of at least 5 mm to avoid feather edges. The surface should be clean and sound. Remove dirt, dust, oil, grease, laitance, sealers, release agents, curing compounds and paints. Exposed rebar should be cleaned by suitable means and protected with **ReCon Zinc** or **ReCon ST.**

CC/RC03/Ver8/01/16 1/3 Technical Datasheet

C.3 Carbon Fiber Sheet (SikaWrap 300C)

BUILDING TRUST

PRODUCT DATA SHEET

SikaWrap®-300 C

WOVEN UNIDIRECTIONAL CARBON FIBRE FABRIC, DESIGNED FOR STRUCTURAL STRENGTHENING APPLICATIONS AS PART OF THE SIKA® STRENGTHENING SYSTEM.

DESCRIPTION

SikaWrap®-300 C is a unidirectional woven carbon fibre fabric with mid-range strengths, designed for installation using the dry or wet application process.

USES

SikaWrap®-300 C may only be used by experienced professionals.

Structural strengthening of reinforced concrete, masonry, brickwork and timber elements or structures, to increase flexural and shear loading capacity for:

- Improved seismic performance of masonry walls
- Replacing missing steel reinforcement
- Increasing the strength and ductility of columns
- Increasing the loading capacity of structural elements
- Enabling changes in use / alterations and refurbishment
- Correcting structural design and / or construction defects
- Increasing resistance to seismic movement
- Improving service life and durability
- Structural upgrading to comply with current standards

CHARACTERISTICS / ADVANTAGES

- Multifunctional fabric for use in many different strengthening applications
- Flexible and accommodating to different surface planes and geometry (beams, columns, chimneys, piles, walls, soffits, silos etc.)
- Low density for minimal additional weight
- Extremely cost effective in comparison to traditional strengthening techniques

APPROVALS / CERTIFICATES

- Poland: Technical Approval ITB AT-15-5604/2011: Zestaw wyrobów Sika CarboDur do wzmacniania i napraw konstrukcji betonowych
- Poland: Technical Approval IBDiM Nr AT/2008-03-0336/1 „Płaskowniki. pręty, kształtki i maty kompozytowe do wzmacniania betonu o nazwie handlowej: Zestaw materiałów Sika CarboDur® do wzmacniania konstrukcji obiektów mostowych
- USA: ACI 440.2R-08, Guide for the Design and construction of Externally Bonded FRP Systems for strengthening concrete structures, July 2008
- UK: Concrete Society Technical Report No. 55, Design guidance for strengthening concrete structures using fibre composite material, 2012.

PRODUCT INFORMATION

Construction	Fibre orientation	0° (unidirectional)
	Warp	Black carbon fibres 99 %
	Weft	White thermoplastic heat-set fibres 1 %
Fibre Type	Selected mid-range strength carbon fibres	

Packaging		**Fabric length per roll**	**Fabric width**
	10 rolls in cardboard box	≥ 50 m	100 mm
	4 rolls in cardboard box	≥ 50 m	300 mm
	2 rolls in cardboard box	≥ 50 m	600 mm
Shelf life	24 months from date of production		
Storage conditions	Store in undamaged, original sealed packaging, in dry conditions at temperatures between +5 °C and +35 °C. Protect from direct sunlight.		
Dry Fibre Density	1.82 g/cm³		
Dry Fibre Thickness	0.167 mm (based on fibre content)		
Area Density	304 g/m² ±10 g/m² (carbon fibres only)		
Dry Fibre Tensile Strength	4 000 N/mm²		(ISO 10618)
Dry Fibre Modulus of Elasticity in Tension	230 000 N/mm²		(ISO 10618)
Dry Fibre Elongation at Break	1.7 %		(ISO 10618)

TECHNICAL INFORMATION

Laminate Nominal Thickness	0.167 mm		
Laminate Nominal Cross Section	167 mm² per m width		
Laminate Tensile Strength	**Average** 3 500 N/mm²	**Characteristic** 3 200 kN/mm²	(EN 2561*) (ASTM D 3039*)
Laminate Modulus of Elasticity in Tension	**Average** 225 kN/mm²	**Characteristic** 220 kN/mm²	(EN 2561*)
	Average 220 kN/mm²	**Characteristic** 210 kN/mm²	(ASTM D 3039*)
	* modification: sample with 50 mm Values in the longitudinal direction of the fibres Single layer, minimum 27 samples per test series		
Laminate Elongation at Break in Tension	1.56 % 1.59 %		(based on EN 2561) (based on ASTM D 3039)
Tensile Resistance	**Average** 585 N/mm	**Characterstic** 534 N/mm	(based on EN 2561) (based on ASTM D 3039)
Tensile Stiffness	**Average** 37.6 MN/m 37.6 kN/m per ‰ elongation	**Characteristic** 36.7 MN/m 36.7 kN/m per ‰ elongation	(based on EN 2561)
	Average 36.7 MN/m 36.7 kN/m per ‰ elongation	**Characteristic** 35.1 MN/m 35.1 kN/m per ‰ elongation	(based no ASTM D 3039)

C.4 Epoxy Resin (Sikadur 330)

BUILDING TRUST

PRODUCT DATA SHEET

Sikadur®-330

2-COMPONENT EPOXY IMPREGNATION RESIN

PRODUCT DESCRIPTION

Sikadur®-330 is a 2-component, thixotropic epoxy based impregnating resin and adhesive.

USES

Sikadur®-330 may only be used by experienced professionals.
Sikadur®-330 is used as:
- Impregnation resin for SikaWrap® fabric reinforcement for the dry application method
- Primer resin for the wet application system
- Structural adhesive for bonding Sika® CarboDur® plates into slits

CHARACTERISTICS / ADVANTAGES

- Easy mix and application by trowel and impregnation roller
- Manufactured for manual saturation methods
- Excellent application behaviour to vertical and overhead surfaces
- Good adhesion to many substrates
- High mechanical properties
- No separate primer required

APPROVALS / STANDARDS

- Adhesive for structural bonding tested according to EN 1504-4, provided with the CE-mark

PRODUCT INFORMATION

Chemical Base	Epoxy resin	
Packaging	5 kg (A+B)	Pre-batched unit
Colour	Component A: white paste Component B: grey paste Components A + B mixed: light grey paste	
Shelf Life	24 months from date of production	
Storage Conditions	Store in original, unopened, sealed and undamaged packaging in dry conditions at temperatures between +5 °C and +30 °C. Protect from direct sunlight.	
Density	1.30 ± 0.1 kg/l (component A+B mixed) (at +23 °C)	
Viscosity	Shear rate: 50 /s	
	Temperature	**Viscosity**
	+10 °C	~10 000 mPas
	+23 °C	~6 000 mPas
	+35 °C	~5 000 mPas

TECHNICAL INFORMATION

Flexural E-Modulus	~ 3 800 N/mm² (7 days at +23 °C)	(DIN EN 1465)
Tensile Strength	~ 30 N/mm² (7 days at +23°C)	(ISO 527)
Tensile Modulus of Elasticity	~ 4 500 N/mm² (7 days at +23 °C)	(ISO 527)
Elongation at Break	0.9 % (7 days at +23 °C)	(ISO 527)
Tensile Adhesion Strength	Concrete fracture (> 4 N/mm²) on sandblasted substrate	(EN ISO 4624)
Coefficient of Thermal Expansion	4.5×10^{-5} 1/K (Temperature range –10 °C – +40 °C)	(EN 1770)

Glass Transition Temperature (EN 12614)

Curing time	Curing temperature	TG
30 days	+30 °C	+58 °C

Heat Deflection Temperature (ASTM D 648)

Curing time	Curing temperature	HDT
7 days	+10 °C	+36 °C
7 days	+23 °C	+47 °C
7 days	+35 °C	+53 °C

Resistant to continuous exposure up to +45 °C.

Service Temperature	–40 °C to +45 °C

SYSTEM INFORMATION

System Structure	Substrate primer - Sikadur®-330. Impregnating / laminating resin - Sikadur®-330. Structural strengthening fabric - SikaWrap® type to suit requirements.

APPLICATION INFORMATION

Mixing Ratio	Component A : component B = 4 : 1 by weight When using bulk material the exact mixing ratio must be safeguarded by accurately weighing and dosing each component.
Consumption	See the "Method Statement for SikaWrap® manual dry application" Ref 850 41 02. Guide: 0.7 - 1.5 kg/m²
Ambient Air Temperature	+10 °C min. / +35 °C max.
Dew Point	Beware of condensation. Substrate temperature during application must be at least 3 °C above dew point.
Substrate Temperature	+10 °C min. / +35 °C max.
Substrate Moisture Content	< 4 % pbw

Pot Life (EN ISO 9514)

Temperature	Pot life	Open time
+10 °C	~90 minutes (5 kg)	~90 minutes
+23 °C	~60 minutes (5 kg)	~60 minutes
+35 °C	~30 minutes (5 kg)	~30 minutes

The pot life begins when the resin and hardener are mixed. It is shorter at high temperatures and longer at low temperatures. The greater the quantity mixed, the shorter the pot life. To obtain longer workability at high temperatures, the mixed adhesive may be divided into portions. Another method is to chill components A+B before mixing them (not below +5 °C).

APPLICATION INSTRUCTIONS

SUBSTRATE QUALITY